THE DEVELOPMENT OF Manganese ALLOYS EXHIBITING HIGH DAMPING CAPACITY.

BY J.A. HEDLEY B.Sc., M.Sc., A.I.M.

Thesis submitted for the
Ph.D. Degree in the
University of London.

ABSTRACT

Certain manganese-copper alloys exhibit a unique combination of high damping properties with sufficient mechanical properties to allow their use in structural, load-bearing applications. The dramatic fall in damping properties as the material temperature rises above room temperature precludes the use of the alloys in applications which generate much heat. The work reported in this thesis was initiated with the aim of identifying those microstructural features which are responsible for the high damping properties. It was anticipated that these features could then be duplicated and encorporated in an alloy system with improved elevated temperature capabilities.

The experimental approach has concentrated on the use of electron microscope, X-ray diffraction and neutron diffraction methods. It has been possible to show that all those alloys which develop the high damping property are antiferromagnetic. The antiferromagnetic interaction between neighbouring atoms is probably the driving force which leads to a martensitic transformation from a cubic to a tetragonal structure. A direct consequence of the martensitic transformation is a microstructure consisting of many microtwin boundaries which are also antiferromagnetic domain boundaries. It is the reversible motion of these boundaries under an oscillating stress which is responsible for the high hysteretic loss. The decline in damping properties to a very low level can be directly correlated with the antiferromagnetic Néel temperature and the martensitic transformation temperature.

Attention was then turned to alternative alloys based on manganese and in the manganese-nickel system an alloy was found with outstandingly better high temperature-damping properties than

previously reported for manganese-copper alloys. The simple binary alloy exhibited poor ancillary properties and an alloy development programme was therefore initiated which led to specific alloy compositions possessing a variety of different property combinations.

CONTENTS.

		Page.
	CHAPTER 1.	
	INTRODUCTION	1
1.1	INTRODUCTION INCLUDING A SUMMARY OF THE THESIS.	1
1.2	THE Mn-Cu SYSTEM-CHEMICAL AND MAGNETIC STRUCTURES.	5
1.3	THE fcc/fct TRANSFORMATION.	7
1.4	ANTIFERROMAGNETIC BEHAVIOUR.	11
1.5	DAMPING CAPACITY.	15
	CHAPTER 2.	
	EXPERIMENTAL PROCEDURE FOR Mn-Cu ALLOYS	20
2.1	PREPARATION OF Mn-Cu ALLOYS.	20
2.2	METALLOGRAPHY OF Mn-Cu ALLOYS.	20
2.3	ELECTRON MICROSCOPY.	21
2.4	X-RAY CRYSTALLOGRAPHY.	21
	2.4.1 Selection of a suitable X-radiation.	21
	2.4.1.1 Axial ratio measurement.	21
	2.4.1.2 Atomic ordering.	22
	2.4.1.3 Peak to background ratio.	23
	2.4.2 Determination of the axial ratio.	24
	2.4.3 Heating, cooling and straining the sample during X-ray examination.	25
2.5	NEUTRON DIFFRACTION EXAMINATION.	26
2.6	DAMPING CAPACITY DETERMINATION.	26
	CHAPTER 3.	
	RESULTS ON Mn-Cu ALLOYS.	29
3.1	ELECTRON MICROSCOPY.	29
	3.1.1 Structure formed on quenching samples into water.	29
	3.1.2 Microtwin boundaries.	29
	3.1.3 The precipitation of αMn.	31

3.1.4 Tweed and related structures. 32
3.1.4.1 Diffraction contrast associated with alloys containing 57% or more Mn. 32
3.1.4.2 Diffraction contrast associated with alloys containing 50% or less Mn. 33
3.2 X-RAY DIFFRACTION RESULTS. 34
3.3 NEUTRON DIFFRACTION RESULTS. 36
3.4 DAMPING CAPACITY MEASUREMENTS. 37

CHAPTER 4.
DISCUSSION ON Mn-Cu ALLOYS. 39
4.1 ELECTRON MICROSCOPY. 39
4.2 NEUTRON DIFFRACTION. 40
4.3 X-RAY CRYSTALLOGRAPHY. 42
4.4 THE DAMPING MECHANISM. 45
4.4.1 Structural considerations. 45
4.4.2 The application of the damping mechanism to the damping capacity results. 47
4.5 THE $\gamma \rightarrow \gamma + \alpha$ REACTION. 51
4.5.1 Introduction. 51
4.5.2 The electron microscope evidence. 55
4.5.3 The neutron diffraction evidence. 59
4.6 CRITERIA NECESSARY FOR THE DEVELOPMENT OF HIGH DAMPING PROPERTIES. 63

CHAPTER 5.
THE SELECTION OF ALTERNATIVE ALLOYS. 66
5.1 SUMMARY OF PUBLISHED WORK. 66
5.2 THE THERMAL EQUILIBRIUM DIAGRAMS OF Mn-Fe AND Mn-Ni. 68
5.2.1 The Mn-Fe system. 68
5.2.2 The thermal equilibrium diagram for Mn-Ni. 68
5.3 EXPERIMENTAL PROCEDURE. 69
5.3.1 Alloy preparation. 69

5.3.2 Metallography. 70
5.3.3 X-ray crystallography. 71
5.3.4 Electron microscopy. 72
5.3.5 Heat treatment procedure. 72
5.3.6 Damping Capacity. 73
5.4 THE Mn-Fe SYSTEM. 73
5.4.1 Results. 73
5.4.1.1 Artefact structures. 73
5.4.1.2 Structural studies. 74
5.4.2 Discussion. 75
5.5 Mn-Ni ALLOYS. 75
5.5.1 Results. 75
5.5.1.1 Artefact structures. 75
5.5.1.2 Alloys based on the precipitation of the intermetallic compound Mn-Ni. 75
5.5.1.3 85%Mn-15%Ni alloy. 77
5.5.1.4 80%Mn-20%Ni alloy. 79
5.5.1.5 90%Mn-10%Ni alloy. 80
5.5.1.6 95%Mn-5%Ni alloy. 80
5.5.2 Discussion. 80
5.5.2.1 Alloys based on the intermetallic compound MnNi. 80
5.5.2.2 High Mn alloys in the Mn-Ni system. 81

CHAPTER 6.

THE Mn-Fe-Ni SYSTEM. 84
6.1 INTRODUCTION. 84
6.2 RESULTS. 84
6.3 DISCUSSION. 85

CHAPTER 7.

THE Mn-Fe-Cu SYSTEM. 86
7.1 INTRODUCTION. 86
7.2 RESULTS. 86

7.3 DISCUSSION. 88

CHAPTER 8.

THE Mn-Ni-Cu SYSTEM. 89

8.1 INTRODUCTION. 89

8.2 RESULTS. 89

8.2.1 Alloys T12(45%Mn-10%Ni-45%Cu), T13(55%Mn-10%Ni-35%Cu) and T14(65%Mn-10%Ni-25%Cu). 89

8.2.2 Alloy T22(60%Mn-5%Ni-35%Cu). 90

8.2.3 Alloy T21(70%Mn-5%Ni-25%Cu). 90

8.2.4 Alloy T15(80%Mn-15%Ni-5%Cu). 90

8.2.5 Alloy T16(80%Mn-5%Ni-15%Cu). 91

8.2.6 Alloy T24(85%Mn-10%Ni-5%Cu). 93

8.2.7 Alloy T23(85%Mn-5%Ni-10%Cu). 94

8.3 DISCUSSION. THE TERNARY SYSTEM Mn-Ni-Cu. 94

CHAPTER 9.

OTHER ALLOY ADDITIONS. 97

9.1 INTRODUCTION. 97

9.2 RESULTS AND DISCUSSION. 98

9.2.1 The ternary system Mn-Cu-Zn. 98

9.2.1.1 Alloy T27(70%Mn-5%Zn-25%Cu). 98

9.2.1.2 Alloy T30(70%Mn-20%Cu-10%Zn). 99

9.2.1.3 Alloy T28(80%Mn-15%Cu-5%Zn). 99

9.2.1.4 Alloy T29(85%Mn-10%Cu-5%Zn). 100

9.2.2 Alloys containing Be. 100

9.2.2.1 Alloy Q31(80%Mn-14.4%Cu-5%Ni-0.6%Be). 100

9.2.2.2 Alloy T32(60%Mn-38.4%Cu-1.6%Be). 101

9.2.2.3 Alloy Q41(80%Mn-14.8%Cu-5%Ni-0.2%Be). 101

9.2.3 Alloys containing Si. 102

9.2.3.1 Alloy Q33(80%Mn-14%Cu-5%Ni-1%Si). 102

9.2.4 Alloys containing Al. 103

9.2.5 Alloy T20(85%Mn-14%Ni-1%C), alloy Q39(80%Mn-10%Cu-5%Ni-5%Fe) and R40(80%Mn-10%Cu-5%Fe-0.1%C-5%Ni). 104

CHAPTER 10.

GENERAL DISCUSSION AND CONCLUSIONS. 106

10.1 THE DAMPING MECHANISM. 106

10.1.1 The effect of various additions on the $\gamma \rightarrow \gamma + \alpha$ reaction. 106

10.1.2 The effect of the various additions on the fcc/fct transformation temperature. 108

10.1.3 Damping properties at room temperature. 109

10.1.4 Damping properties at elevated temperatures. 110

10.2 HAVE THE AIMS OF THE RESEARCH PROGRAMME BEEN MET? 112

ACKNOWLEDGEMENTS. 114

LIST OF FIGURES.

Fig. 1. The Mn-Cu thermal equilibrium diagram with superimposed Néel temperatures and fcc/fct transformation temperatures.

Fig. 2. Antiferromagnetic structure approached by the γMn fct phase of the Mn-Cu system at large Mn compositions. The Magnetic moments alternatively point up and down at distances of c/2 along the 'c' axis.

Fig. 3. Relationships between the axial ratio and the angular difference between the cubic and tetragonal components of the {200} and {220} reflections.

Fig. 4. A 57%Mn-43%Cu alloy, solution treated for 2 hours at 850°C and water quenched. Shows dislocation features, typical of any annealed metal. x 55,000.

Fig. 5. A 57%Mn-43%Cu alloy, solution treated for 2 hours at 850°C, water quenched and heat treated for 7 hours at 400°C. Shows a high density of boundaries. x 30,000.

Fig. 6. A 57%Mn-43%Cu alloy, solution treated for 2 hours at 850°C, water quenched and heat treated for 6 hours at 400°C. Shows boundaries lying edge-on in a [100] oriented foil. x 37,000.

Fig. 7. A 57%Mn-43%Cu alloy, solution treated for 2 hours at 850°C, water quenched and heat treated for 6 hours at 400°C. Shows the initiation of microtwins at dislocations. x 21,000.

Fig. 8. Same area as in Fig. 7, showing further microtwin propagation. x 21,000.

Fig. 9. A 57%Mn-43%Cu alloy, solution treated for 2 hours at 850°C, water quenched and heat treated for 6 hours at 400°C. Shows a substructure of microtwins with larger stable microtwins. x 37,000.

Fig.10. A 57%Mn-43%Cu alloy, solution treated for 2 hours at 850°C, water quenched and heat treated for 6 hours at 400°C. Shows the lengthwise growth of microtwins within a large stable microtwin. x 18,000.

Fig.11. A 57%Mn-43%Cu alloy, solution treated for 2 hours at 850°C, water quenched and heat treated for 6 hours at 400°C. Shows the growth of microtwins in one orientation at the expense of microtwins in another orientation. x 28,000.

Fig.12. A 57%Mn-43%Cu alloy, solution treated for 2 hours at 850°C, water quenched, heat treated for 6 hours at 400°C and reduced 6% in thickness by cold rolling. Microtwin movement has been reduced or prevented by the dislocation tangles. x 29,000.

Fig.13. A 57%Mn-43%Cu alloy, solution treated for 2 hours at 850°C and furnace cooled. Shows the fine nature of the microtwin distribution formed on slow cooling. x 37,600.

Fig.14. A 57%Mn-43%Cu alloy, solution treated for 2 hours at 850°C, water quenched and heat treated for 24 hours at 400°C. Shows microtwins terminating at an αMn particle. x 41,000.

Fig.15. A 57%Mn-43%Cu alloy, solution treated for 2 hours at 850°C and furnace cooled. Shows the striated structure known as "basket-weave" or "tweed". A fine substructure consisting of closely-spaced streaks lies within the striations. Magnification not known. Approx. x 180,000.

Fig.16. A 57%Mn-43%Cu alloy, solution treated for 2 hours at 850°C, water quenched and heat treated for 6 hours at 400°C. Shows the unidirectional component of the tweed pattern with a $\{111\}$ type reflection operating. x 42,000.

Fig.17. A 57%Mn-43%Cu alloy, solution treated for 2 hours at 850°C, water quenched and heat treated for 6 hours at 400°C. Shows tweed striations lying in two directions with a $\{220\}$ reflection operating. x 59,000.

Fig.18. A 57%Mn-43%Cu alloy, solution treated for 2 hours at 850°C, water quenched and heat treated for 1½ hours at 450°C. Shows the propagation of fine microtwins along the directions of the tweed striations. x 57,000.

Fig. 19. A 57%Mn-43%Cu alloy, solution treated for 2 hours at 850°C, water quenched and heat treated for 6 hours at 400°C. Shows microtwins and tweed pattern prior to the heating of the sample within the electron microscope. x 29,000.

Fig. 20. Same area as in Fig. 19 showing the microstructure at a temperature above the fcc/fct transformation temperature. x 29,000.

Fig. 21. A 50%Mn-50%Cu alloy, solution treated for 84 hours at 800°C, quenched to 450°C and held at this temperature for 16 hours before water quenching. Shows evidence for the pre-precipitation of a second phase at A, B and C. x 128,000

Fig. 22. Same area as in Fig. 21, using a {200} dark-field reflection. Shows asymmetrical images at D, E and F. x 128,000.

Fig. 23. A 40%Mn-60%Cu alloy, solution treated for 84 hours at 800°C, quenched to 450°C and held at this temperature for 16 hours before water quenching. Shows evidence for the pre-precipitation of a second phase at G, H and I. x 173,000.

Fig. 24. A 30%Mn-70%Cu alloy, solution treated for 84 hours at 800°C, quenched to 450°C and held at this temperature for 16 hours before water quenching. Shows evidence for the pre-precipitation of a second phase in the Bragg contrast fringes. x 69,000.

Fig. 25. Unit cell parameters for Mn-Cu alloys, measured at room temperature.

Fig. 26. Change in axial ratio, measured at room temperature, with the heat treatment time at 400°C given to various Mn-Cu alloys.

Fig. 27. The effect of temperature on the axial ratios of a number of heat treated samples of a solution treated 57%Mn-43%Cu alloy.

Fig. 28. Neutron diffraction traces taken at room temperature and 4.3°K from two samples of a 57%Mn-43%Cu alloy. Both samples have been solution treated for 4 weeks at 850°C and water quenched. One sample has been given a further heat treatment of 7 hours at 400°C.

Fig. 29. A 70%Mn-30%Cu alloy, solution treated for 4 weeks at 850°C, water quenched and heat treated for 2 hours at 400°C. Neutron diffraction traces taken at 23°C and 153°C.

Fig. 30. The temperature and stress-dependence of the damping capacity of a 60%Mn-40%Cu alloy. Samples have been either rolled or solution treated for 28 days at 850°C and water quenched and then heat treated for various times at 400°C.

Fig. 31. The effect of temperature on the damping capacity of a 60%Mn-40%Cu alloy. Samples have been either rolled or solution treated for 28 days at 850°C, water quenched and then heat treated for various times at 400°C. Damping capacities have been measured at two surface shear stress levels.

Fig. 32. The temperature and stress-dependence of the damping capacity of a 70%Mn-30%Cu alloy. Samples have been rolled, solution treated for 2 hours at 800°C, water quenched and heat treated for various times at 400°C.

Fig. 33. The effect of plastic strain on the damping properties of a 60%Mn-40%Cu alloy, which has been solution treated for 2 hours at 800°C, water quenched and heat treated for 6 hours at 400°C.

Fig. 34. An analysis of the fringe pattern in bright and dark-field images of a microtwin boundary.

Fig. 35. A 57%Mn-43%Cu alloy, solution treated for 2 hours at 850°C, water quenched and heat treated for 6 hours at 400°C. Shows the fringe patterns associated with widely separated microtwin boundaries. x 39,000.

Fig. 36. Same area as in Fig. 35 using a $\{200\}$ dark-field reflection. x 39,000.

Fig. 37. Schematic diagram showing the lattice orientation relationships and the sense of slope of the boundaries in Fig. 35.

Fig. 38. Schematic diagram showing the lattice orientation relationships and the sense of slope of the boundaries shown in Fig. 36.

Fig. 39. Schematic representation of regions bounding a microtwin or an antiferromagnetic domain boundary.

Fig. 40. The Mn-Fe thermal equilibrium diagram with selected alloy compositions superimposed.

Fig. 41. The Mn-Ni thermal equilibrium diagram with selected alloy compositions, Néel temperatures and fcc/fct transformation temperature superimposed.

Fig. 42. A 75%Mn-25%Fe alloy, water quenched from 1200°C and heat treated for 140 minutes at 600°C. Shows striations associated with the use of many etching reagents. x 230.

Fig. 43. Replica taken from the structure in Fig. 42 showing the rectangular profile of the channels and their association with particles embedded in the surface. x 6,000.

Fig. 44. A 75%Mn-25%Fe alloy, water quenched from 1200°C; shows the initiation of microtwins at dislocations. x 27,000.

Fig. 45. Same area as in Fig. 44 showing further microtwin propagation. x 27,000.

Fig. 46. A 80%Mn-20%Ni alloy, water quenched from 1000°C. Shows angular-shaped artefacts due to the etching reagent as well as surface tilting resulting from the fcc/fct transformation temperature. x 90.

Fig. 47. A 50%Mn-50%Ni alloy, water quenched from 1000°C, showing dense dislocation tangles. x 28,000.

Fig. 48. A 50%Mn-50%Ni alloy, furnace cooled from 1000°C, heated to 800°C inside the electron microscope and slowly cooled. Shows microtwins which formed at about 700°C and which were photographed at room temperature. x 31,000.

Fig. 49. A 60%Mn-40%Ni alloy, as-cast and heat treated for 3 days at 500°C. Shows a severely striated structure and probable precipitate particles within grain boundaries. x 210.

Fig. 50. A 65%Mn-35%Ni alloy, water quenched from 1000°C and heat treated for 1 week at 500°C. Shows the discontinuous nucleation of MnNi particles on dislocations. x 28,000.

Fig. 51. A 85%Mn-15%Ni alloy in the as-cast state. Shows surface tilting resulting from the fcc/fct transformation in the dendrite structure; βMn particles are present in the grain boundaries. x 240.

Fig. 52. A 85%Mn-15%Ni alloy, solution treated for 2 hours at 1000°C and water quenched. Shows clearly defined surface tilting associated with the fcc/fct transformation. x 200.

Fig. 53. A 85%Mn-15%Ni alloy, solution treated for 48 hours at 1000°C, water quenched and heat treated for 1 week at 500°C. Shows tweed pattern and intersecting microtwins. x 26,000.

Fig. 54. Same area as in Fig. 53 showing the further propagation of intersecting microtwins. x 26,000.

Fig. 55. A 85%Mn-15%Ni alloy, solution treated for 48 hours at 1000°C, water quenched and heat treated for 4 weeks at 500°C. Shows clearly defined tweed pattern and microtwins propagating in the same directions as the striations in the tweed pattern. x 39,000.

Fig. 56. Unit cell parameters for water quenched Mn-Ni alloys.

Fig. 57. The effect of temperature on the axial ratios of a number of heat treated samples of a 85%Mn-15%Ni and a 80%Mn-20%Ni alloy.

Fig. 58. The stress-dependence of the damping capacity of alloys 85%Mn-15%Ni and 80%Mn-20%Ni which have been given a variety of heat treatments.

Fig. 59. The effect of temperature on the damping capacity of two samples of a 85%Mn-15%Ni alloy. Both samples have been solution treated for 1 week at 1000°C and water quenched. One sample has been given a further heat treatment of 4 weeks at 500°C.

Fig.60. Binary equilibrium diagrams Mn-Fe, Mn-Ni and Fe-Ni incorporating the nominal compositions of selected ternary alloys.

Fig.61. The phases present in various cast Mn-Ni-Fe alloys.

Fig.62. The phases present in various water quenched Mn-Ni-Fe alloys.

Fig.63. The binary equilibrium diagrams of Cu-Fe, Mn-Fe and Mn-Cu including the selected ternary compositions.

Fig.64. Alloy T26(70%Mn-5%Fe-25%Cu), rolled, water quenched from 900°C and heat treated for 3 hours at 500°C. Shows the presence of αMn in the grain boundaries. x 530.

Fig.65. Alloy T26(70%Mn-5%Fe-25%Cu) rolled, water quenched from 900°C and heat treated for 3 hours at 700°C. Shows stringers of βMn particles. x 530

Fig.66. Change in axial ratio and hardness (H_V), measured at room temperature, with the heat treatment time at 400°C given to alloy T26(70%Mn-5%Fe-25%Cu).

Fig.67. The stress-dependence of the damping capacity of alloy T26 (70%Mn-5%Fe-25%Cu) which has been solution treated for 5 days at 850°C and given a variety of heat treatments.

Fig.68. The Ni-Cu, Mn-Cu and Mn-Ni binary equilibrium diagrams and the essential features of the ternary Mn-Ni-Cu section at 0°C. The selected ternary alloy compositions have been superimposed.

Fig.69. Change in axial ratio and hardness (H_V), measured at room temperature, with the heat treatment time at 400°C given to various Mn-Ni-Cu alloys.

Fig.70. Comparison of the change in axial ratio with heat treatment time at 400°C given to various Mn-Ni-Cu alloys.

Fig.71. The effect of temperature on the axial ratio of a number of heat treated samples of alloy T16(80%Mn-5%Ni-15%Cu).

Fig.72. The stress-dependence of the damping capacity of alloy T16(80%Mn-5%Ni-15%Cu) which has been given a variety of heat treatments.

Fig. 73. The effect of temperature on the damping capacity of two samples of alloy T16(80%Mn-5%Ni-15%Cu). Both samples have been solution treated for 1 week at 1000°C and water quenched. One sample has been given a further heat treatment of 24 hours at 400°C.

Fig. 74. The effect of temperature on the axial ratio of alloys 85%Mn-15%Ni, 85%Mn-15%Cu, T24(85%Mn-10%Ni-5%Cu) and T23(85%Mn-5%Ni-10%Cu). All alloys have been solution treated and water quenched.

Fig. 75. The stress-dependence of the damping capacity of alloy T24(85%Mn-10%Ni-5%Cu) which has been given a variety of heat treatments.

Fig. 76. The effect of temperature on the damping capacity of two samples of alloy T24(85%Mn-10%Ni-5%Cu). Both samples have been solution treated for 1 week at 950°C and water quenched. One sample has been given a further heat treatment of 24 hours at 400°C.

Fig. 77. The stress-dependence of the damping capacity of alloy T23(85%Mn-5%Ni-10%Cu) which has been given a variety of heat treatments.

Fig. 78. The stress and temperature-dependence of the damping capacity of alloy T23(85%Mn-5%Ni-10%Cu) which has been given a variety of heat treatments.

Fig. 79. A 593°C isothermal section of the Mn-Cu-Zn ternary equilibrium diagram including the selected alloy compositions.

Fig. 80. Change in axial ratio and hardness (H_v), measured at room temperature, with the heat treatment time at 400°C given to various Mn-Cu-Zn alloys.

Fig. 81. Comparison of the change in axial ratio with heat treatment time at 400°C given to various Mn-Cu-Zn alloys.

Fig. 82. The effect of temperature on the axial ratio of alloys T27(70%Mn-25%Cu-5%Zn) and T29(85%Mn-10%Cu-5%Zn) which have been given a variety of heat treatments.

Fig.83. The stress-dependence of the damping capacity of alloys T27(70%Mn-25%Cu-5%Zn), T28(80%Mn-15%Cu-5%Zn) and T30(70%Mn-20%Cu-10%Zn) which have been given a variety of heat treatments at 400°C.

Fig.84. The stress and temperature-dependence of the damping capacity of alloy T29(87%Mn-3%Zn-10%Cu) which has been given a variety of heat treatments.

Fig.85. Alloy T32(60%Mn-38.4%Cu-1.6%Be), rolled and water quenched. Shows particles of Be_2Mn lying in the Mn-rich dendritic regions. x 1,100.

Fig.86. Alloy T32(60%Mn-38.4%Cu-1.6%Be), solution treated for 5 days at 850°C, water quenched and heat treated for 4 hours at 450°C. Shows precipitate particles of Be_2Mn and αMn. x 1,100.

Fig.87. Change in axial ratio and hardness (H_V), measured at room temperature, with the heat treatment time at 400°C and 450°C, given to alloys T32(60%Mn-38.4%Cu-1.6%Be) and Q41(80%Mn-14.8%Cu-0.2%Be-5%Ni).

Fig.88. The stress-dependence of the damping capacity of a number of alloys based on 80%Mn which have been given a variety of heat treatments.

Fig.89. Alloy Q33(80%Mn-14%Cu-5%Ni-1%Si), solution treated for 5 days at 950°C, water quenched and heat treated for 8 hours at 450°C. Polarised light micrograph showing βMn particles in the grain boundaries. x 600.

Fig.90. Alloy Q33(80%Mn-14%Cu-5%Ni-1%Si), solution treated for 5 days at 950°C, water quenched and aged for 4 hours at 500°C. Shows βMn precipitate particles. x 600.

Fig.91. Change in axial ratio and hardness (H_V), measured at room temperature, with heat treatment times at 400°C and 450°C given to alloy Q33(80%Mn-14%Cu-5%Ni-1%Si).

Fig.92. Change in axial ratio and hardness (H_V), measured at room temperature, with heat treatment time at 400°C given to various alloys containing Al.

Fig.93. Comparison of the change in axial ratio with heat treatment time at 400°C given to various alloys containing Al.

Fig.94. Change in axial ratio and hardness (H_V), measured at room temperature, with the heat treatment time at 400°C given to alloys Q39(80%Mn-10%Cu-5%Ni-5%Fe) and R40(80%Mn-10%Cu-5%Fe-5%Ni-0.1%C).

Fig.95. The change in axial ratio, measured at room temperature, with heat treatment time at 400°C given to various alloys based on 70%Mn.

Fig.96. The change in axial ratio, measured at room temperature, with heat treatment time at 400°C given to various alloys based on 80%Mn.

Fig.97. The change in axial ratio, measured at room temperature, with heat treatment time at 400°C given to various alloys based on 85%Mn.

Fig.98. The effect of temperature on the axial ratio of alloys based on 85%Mn. All alloys have been solution treated and water quenched.

CHAPTER 1

INTRODUCTION

1.1 INTRODUCTION, INCLUDING A SUMMARY OF THE THESIS.

Following the introduction of electrolytic manganese in 1944, Dean and his co-workers at the Bureau of Mines in the U.S.A. embarked on a survey of the properties of Mn and its alloys which have since been summarised in the book 'Manganese'[1]. The exceptional damping properties of certain Mn-Cu alloys came to light and since that time a considerable amount of data has been accumulated by a number of workers on damping and ancillary properties.

A failure by some to realise the marked heterogeneity of the alloys and on occasion a misinterpretation of artifact structures led to conflicting and confusing evidence. A satisfactory explanation of the basic mechanism conferring the high damping property did not emerge. Furthermore a major drawback to the commercial exploitation of the alloys concerned the drastic fall in damping capacity which occurred on heating the alloys just above room temperature.

The programme of research described in this thesis was therefore initiated with the aim of developing an alloy which did not suffer from the drawbacks of Mn-Cu alloys. As a first step in this programme it was necessary to identify those structural features which were responsible for the high damping properties, in the anticipation that it would then be possible to duplicate these features within the framework of an improved alloy system. Although the identification of the basic damping mechanism was considered a desirable subsidiary goal, it was not the prime motivation behind the programme of work.

For this reason, a direct structural examination has been chosen in contrast to an experimental approach involving those techniques associated with the study of internal friction and which have proved successful in obtaining a basic understanding of atom arrangements and defects in metal structures.

As it seemed likely from the evidence available at the time,

that the physical features responsible for the high damping capacity were of very small dimensions, it was decided to use electron microscope and X-ray crystallographic methods to attempt to identify the more important of them. The conclusions derived from the results of these two techniques indicated the necessity for further experimental work using neutron diffraction. It was these results, which were at variance with other published work using magnetic techniques[2], which provided the necessary conclusive evidence for the importance of antiferromagnetism in high damping Mn-Cu alloys. It was then possible to suggest a mechanism in which it is the antiferromagnetic interaction between Mn atoms which induces the martensitic transformation from the cubic (fcc) to the tetragonal (fct) structure and it is the mobility of microtwins under the application of an applied stress which leads to the high damping properties.

It was then possible to draw up a list of pre-requisites which would need to be satisfied before alternative alloys could be selected. At the same time, standard experimental procedures were developed in which the change in axial ratio with heat treatment and temperature could be used as an aid in the selection of suitable alloy compositions and heat treatments, thus removing the necessity for excessive numbers of time-consuming damping capacity determinations. The first alternative alloys were selected from the Mn-Ni and Mn-Fe systems.

Completely independently of the work described in this thesis, other workers at the Admiralty Materials Laboratory and at Leeds University were approaching the problem in a very similar manner and as a result three separate publications on the damping mechanism appeared in 1968[3,4,5]. A substantial agreement was found in all three publications concerning the salient features leading to the high damping properties. It was at this time that the Ministry of Defence (Navy) placed a research contract with Delta Metal Research to proceed with an examination of alternative alloy systems to Mn-Cu. The aims of this research project were to develop

alloys with improved damping properties at elevated temperatures, improved mechanical properties, especially moduli,and improved corrosion resistance. Greatest emphasis was to be placed on the first requirement.

A concurrent programme of work was also undertaken by other personnel at Delta Metal Research to convert the damping capacity data into a form suitable for its incorporation into engineering design formulae. Later on in this programme, high damping material was incorporated into a number of engineering components to reduce noise or vibration.

It soon became apparent that the binary alloys selected from the Mn-Ni and Mn-Fe system, although conforming to the essential features of the damping mechanism, as predicted, suffered from other drawbacks. A number of ternary alloys were therefore selected leading to the development of alloys with greatly improved damping properties at elevated temperatures.

Attention was then turned to certain other additions in the hope of improving mechanical properties and corrosion resistance. The additions were made with these property improvements in mind and would not have been made from a consideration of damping properties alone. However, some of these minor additions unexpectedly exerted a considerable indirect influence over the damping properties by enabling a degree of control over the ageing process which had hitherto been lacking.

Mechanical and corrosion properties are important to the commercial success of an alloy but as they do not shed any further light on the damping properties they have been omitted from the text.

In an area of work as active as Mn-based alloys, more detailed information, especially concerning antiferromagnetic properties frequently appears in the scientific press. Although the thesis has been written chronologically, it was thought necessary to bring all aspects of the damping mechanism in Mn-Cu alloys up to date in the first part of the thesis, as this then provides a more complete picture against which to judge the latter part of the programme.

Fortunately,this more recent information did not invalidate any of the previous work.

In chapter 1 the Mn-Cu system is introduced and an assessment is made of the published work on Mn-Cu alloys up to the initiation of this research work. Three important properties of Mn alloys recur repeatedly throughout the work and these are antiferromagnetism, the fcc/fct transformation and,of course, damping properties. A brief description is therefore given of each property.

The main experimental programme starts in chapter 2 and the preparation of alloys and the various techniques used to examine their structure and measure their properties are described.

Chapter 3 is then devoted to a description of the results obtained from structural studies using electron microscope, X-ray crystallographic and neutron diffraction techniques. This is then followed by the damping results after corresponding heat treatments.

The results are analysed and their significance discussed in chapter 4 and a mechanism is proposed to explain the high damping properties of Mn-Cu alloys. The salient features necessary for the high damping properties are thereby enumerated and the selection of alternative systems made on this basis.

Chapter 5 includes the examination of selected alloys from the Mn-Ni and Mn-Fe systems; based on the further knowledge gained, a number of ternary alloys were selected and these are examined and discussed in chapters 6 to 8.

With the establishment of alloys exhibiting good damping properties at elevated temperatures, attention was then turned to mechanical and corrosion properties and several further elemental additions were made. Chapter 9 covers the unexpected additional benefits relating to the shorter heat treatments required to develop high damping properties.

Finally in chapter 10 the necessary conditions leading to high damping properties are reviewed in the light of the results from all the alloys described in the thesis and an assessment is made of the success achieved in satisfying the original aims of the project.

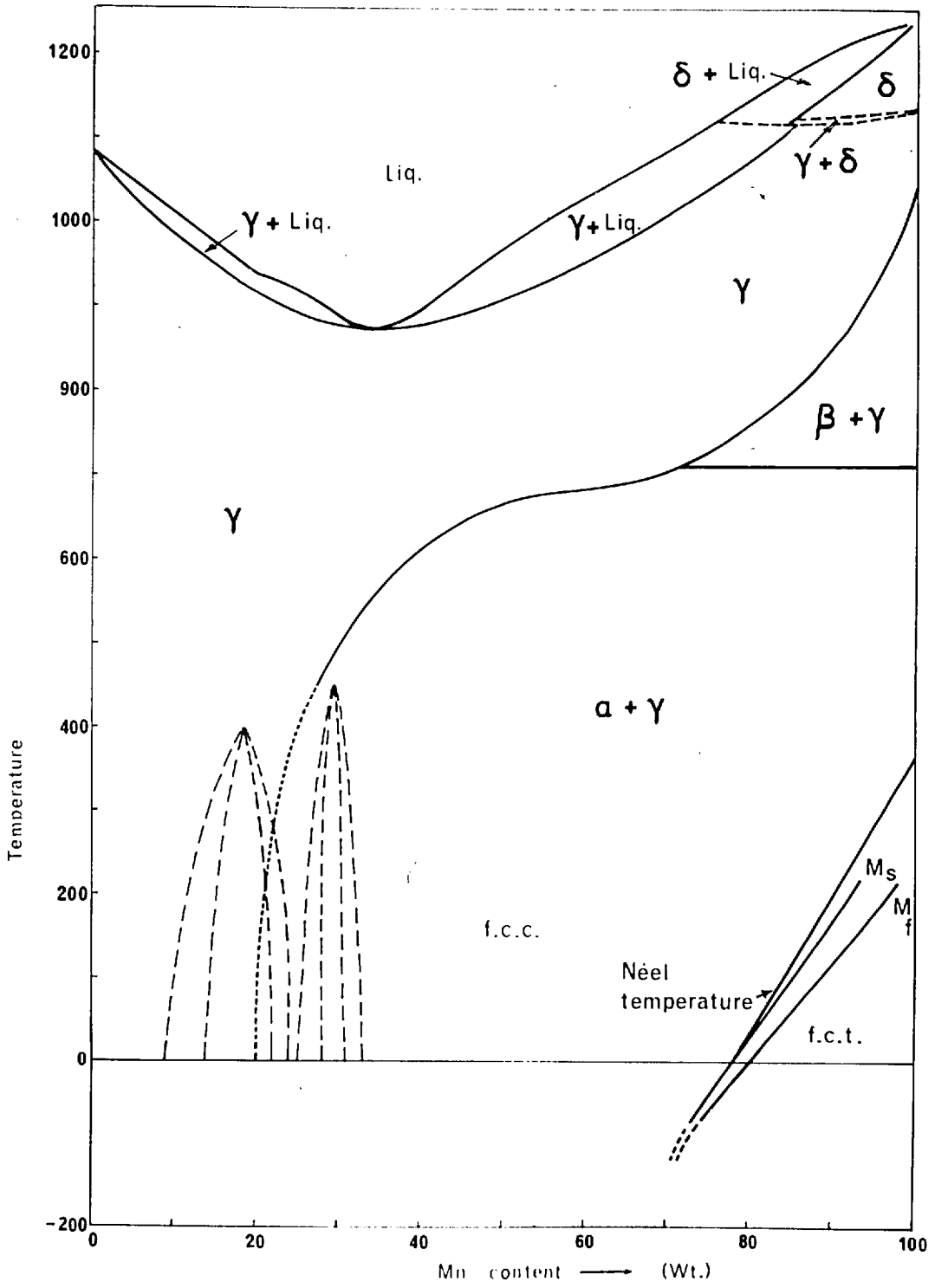


Fig. 1 The Mn - Cu thermal equilibrium diagram with superimposed Néel temperatures and f.c.c./f.c.t. transformation temperatures. Refs. 1, 9, 7 and 12.

1.2 THE Mn-Cu SYSTEM - CHEMICAL AND MAGNETIC STRUCTURES.

The generally accepted thermal equilibrium diagram proposed by R.S.Dean et al[6] has subsequently been modified[7] at the copper-rich end to include two ordered phases based on Cu_5Mn and Cu_3Mn. The equilibrium diagram, incorporating the suggested modifications is shown in Fig. 1.

Because of the wide freezing range of Mn-Cu alloys containing more than 50%Mn, the cast structures are severely cored and it has been shown by optical microscopy and quantitative microprobe analysis, that solution treatment times approaching 4 weeks are necessary to homogenise the structure[8]. A failure to realise this by some workers must cast some doubt on quoted property values, especially lattice parameters.

Mn exists in four allotropic modifications, namely α, β, δ and γ. Cu has negligible solubility in either αMn or βMn but forms a continuous series of solid solutions with γMn.

The crystal structure of αMn is cubic containing 58 atoms in the unit cell[1]. The basis of the structure is a body-centred cubic lattice of side 8.89 kX units, each point being associated with a cluster of 29 atoms. The βMn structure is also cubic with a lattice parameter of 6.29 kX units[1]. In this case there are 20 atoms in the unit cell. The δMn phase is body-centred cubic (b.c.c) with a lattice parameter of 3.075 kX at 1140°C[9]. Both δ and β phases in the Mn-Cu system cannot be retained by quenching.

The γMn structure is fcc at elevated temperatures but on quenching those alloys containing more than 70%Mn, a diffusionless martensitic transformation occurs, leading to a fct structure with axial ratio varying from 1 to about 0.94[1], depending on the Mn content and the temperature of measurement. Frequent reference is made throughout the thesis to the results of Basinski and Christian[9] and these have been superimposed on to Fig. 1 to show the temperatures at which the martensitic transformation starts (M_s) and finishes (M_f). The temperature at which the change occurs increases with the Mn content from about -183°C

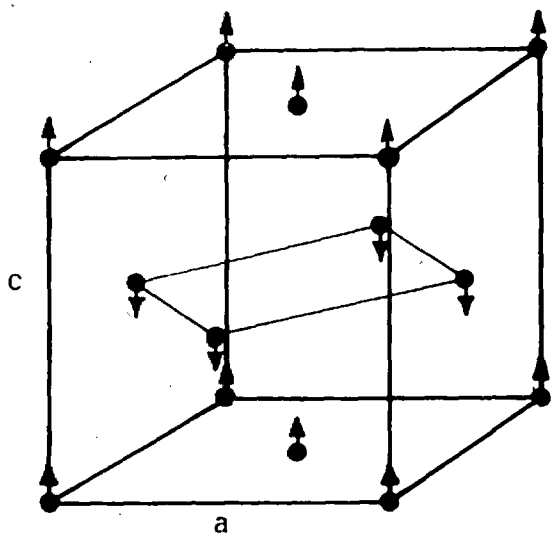


Fig. 2 Antiferromagnetic structure approached by the γ Mn f.c.t. phase of the Mn-Cu system at large Mn compositions. The magnetic moments alternatively point up and down at distances of $C/2$ along the C axis.

Ref. 11

at about 70%Mn to between 160°C and 200°C for an alloy containing 93.5%Mn.

The γMn phase can be retained by quenching over all those compositions which, under equilibrium conditions, would be $\gamma + \alpha$ at room temperature. The equilibrium $\gamma + \alpha$ structure only develops in quenched material after a suitable heat treatment at some temperature between 375°C and 650°C, depending on the Mn content. According to Dean et al[6] the time taken to achieve equilibrium varies in an unsystematic manner with Mn content. The αMn precipitates out of solid solution primarily in grain boundaries and subsequently inside the grains.

Following the isothermal heat treatment of alloys containing between 50% and 70% Mn at temperatures between 375°C and 650°C or alternatively by furnace cooling from the solution treatment temperature to room temperature, the γMn structure, which is fcc in the quenched state over this composition range, develops the fct structure[10].

Those alloys containing more than 70%Mn which are fct in the quenched state, exhibit moderate damping properties at temperatures below the fcc/fct transformation temperature. Those alloys containing between 50% and 70%Mn which transform to the fct structure only after an ageing heat treatment, develop very high damping properties in the aged condition. It therefore seemed very likely that the damping properties were associated with the fct structure and that they would disappear when the alloy reverted to the fcc structure by heating above the fcc/fct transformation temperature. Greatest commercial interest has been shown in Mn-Cu alloys containing between 50% to 70%Mn.

Alloys containing more than about 70%Mn which transform to the fct structure on quenching, also possess antiferromagnetic properties. Neutron diffraction studies by Meneghetti and Sidhu[11] first revealed the antiferromagnetic coupling approached by the quenched γMn solid solution at large Mn concentrations, Fig.2. This magnetic structure involves the antiparallel alignment of

magnetic moments associated with ions on adjacent (002) planes of the fct structure. The fct/fcc transformation in Mn-rich alloys has been correlated approximately with the disappearance of long range antiferromagnetic ordering, otherwise known as the Néel temperature[12]. In view of the importance of these results in later discussions, the change in Néel temperature with Mn content, has also been superimposed on the thermal equilibrium diagram, Fig.1.

Quenched alloys containing less than about 70%Mn are not antiferromagnetic[13] and the absence of antiferromagnetic ordering has also been reported[2] in those alloys containing between 50% and 70%Mn which have been heat treated to yield the fct structure and the associated high damping properties. Before the work described in this thesis was commenced, the presence of antiferromagnetism could not therefore be linked with the martensitic transformation from the fcc to the fct structure. It was only after neutron diffraction experiments which are described later, that conclusive proof was obtained that these alloys are also antiferromagnetic in the aged condition and the relationship between the antiferromagnetic properties, the martensitic transformation and the damping properties in Mn-Cu alloys was established.

1.3 THE fcc/fct TRANSFORMATION.

The martensitic transformation from the fcc to the fct structure, which is a feature of certain compositions in the Mn-Cu system, has also been reported in a number of other alloy systems. The crystallography of the transformation was first deduced from experimental results on polycrystalline samples of In-Tl alloys[14,15] and later elaborated in considerable detail after further work on single crystals[16,17,18]. The fcc/fct transformation in Mn-Cu alloys is essentially the same[9], although in contrast to In-Tl, Mn-Cu alloys exhibit an axial ratio less than 1.

The fcc/fct transformation in polycrystalline samples results in microstructures which exhibit parallel lamellae and these can either be seen as relief effects produced on a smooth surface

after transformation, or after polishing and etching. Sub-bands also form within the main bands and these subtend an angle of 60° with the main band boundaries[14].

On cooling a sample from above the transformation temperature, the transformation takes place over a temperature range and is propagated by the movement of one or more interfaces. When the transformation proceeds by the movement of one interface, the main bands form behind and parallel to the interface between the fcc and fct regions[14].

The first bands propagate suddenly, extending from one grain boundary to the opposite boundary. The grain further transforms by a rapid broadening of existing bands or by the propagation of new bands parallel and adjacent to those already existing. The surfaces of two adjacent bands contrast not only with each other but also with the untransformed surface. The reverse events take place on heating and the contrast between adjacent bands diminishes[14]. However, when the fcc/fct transformation takes place on cooling, the lamallae first form at a temperature which is several degrees lower than that at which they last disappear when the fcc/fct transformation takes place on heating. The first bands to form have a small but discrete axial ratio and as the specimen is allowed to cool, the axial ratio increases[14].

The transformation takes place by a double shear mechanism on $\{110\}$ planes[15]. The main bands represent regions where the first homogenous shear has occurred and adjacent bands show up in different contrast because this first shear occurs in opposite senses, at successive boundaries, as the interface proceeds across the grain. The atom movements can be mathematically described by means of a first shear occurring, for instance, on the (101) plane in the $[\bar{1}01]$ direction which would lead, in the absence of further shear, to a monoclinic structure. A second shear (011) $[0\bar{1}1]$ is required to form a triclinic structure which, because of the very small shears involved, can be considered to be fct. The physical manifestation of the second shear is the formation of sub-bands within the main bands[15]. In practice

the two shears should not be considered as occurring separately; the atom movements occur together at the visible interface and the fct structure is produced immediately behind the interface[17].

There are a number of shear combinations in the fcc structure because of the multiplicity of $\{110\}$ and as a result each fcc crystal can give rise to a total of 36 different fct orientations with axial ratio either greater or less than one[17]. The second shear occurs at 60° to the first, thus accounting for the observed angle between sub-band and main band boundaries[15].

The double shear mechanism is flexible enough to explain the observed change in axial ratio with temperature by the accommodation of further shear on the same systems[15].

When propagation of the transformation occurs from separate points in the same grain, interpenetration of the main bands is possible. Two different situations can be distinguished; when the main bands lie at 60° to each other, interpenetration is common and when they lie at 90° to each other, the bands meet at a common interface without penetration[14].

The bands and sub-bands can also be considered as fct twins and two types can be considered, those involving a-a diagonals and those involving a-c diagonals. It has been calculated[16,18] that the increase in length along a $[1\bar{1}0]$ diagonal in going from a cube to a tetragonal twin with a c-a diagonal, is one half the decrease in length involved in going to an a-a diagonal. The average strain along the $[1\bar{1}0]$ direction can then be made equal to zero if there are twice as many c-a diagonals parallel to it, as there are a-a diagonals, or in microstructural terms, the thickness ratios of the two types of twin should be in the ratio 2 : 1 to relieve the transformation strains in the shear direction.

The theory has been confirmed by measurements on single crystals and detailed observations have been made on the effect of stress on the transformation[16] and on the movement of twin boundaries[18]. The application of stress to a single crystal is found to increase the transformation temperature and by increasing the load

sufficiently it is possible to arrive at a situation where the transformation temperature on cooling the stressed specimen is above that of the transformation temperature on heating the unstressed specimen. Accordingly, it is then possible to transform the specimen isothermally from fcc to the fct phase and back again by the application and removal of a sufficient load[16].

A single crystal specimen consisting of a series of fine parallel twin crystals may be deformed by movements of the twin boundaries. The simplest deformation results from the application of a uniaxial compressive or tensile stress. If the twin boundaries are sufficiently mobile they will move perpendicular to themselves, increasing or decreasing the proportion of the orientation which is appropriate to the sign of the stress. With a compressive stress, the twins having a smaller repeat distance along the stress axis, will grow at the expense of others. The process can be continued until the specimen becomes a single crystal and the maximum strain will depend on the orientation of the stress axis and the relative amounts of the two twins initially present.

The case of bending is more complex and involves the rotation of the twin boundaries through small angles from their original positions, tapering in opposite directions so that in the case of a thin bent beam, the top surface can be composed of lattices from one of the original twins, whereas the bottom surface can be composed of the other original twin orientation[17]. The movement of twins under stress in polycrystalline samples has not been reported. A number of authors have remarked on the "rubber-like" behaviour of certain In-Tl alloys. Two types of relaxation phenomenon have been identified at high and low temperatures. It has been suggested that the "rubber-like" behaviour at high temperatures is due to the stress induced transformation from fcc to fct above the M_s temperature. The peculiar mechanical properties at lower temperatures are caused by a temperature controlled relaxation process[18].

The crystallography of the transformation and the

microstructural features in certain Mn-Cu alloys are the same as those already described for In-Tl alloys, although in the case of Mn-Cu alloys the axial ratio is less than one[9]. Much of the particular "rubber-like" behaviour in In-Tl alloys is not duplicated in the Mn-Cu alloys and so it would be unwise to make comparisons in this direction.

1.4 ANTIFERROMAGNETIC BEHAVIOUR.

The magnetic properties of an atom are due to the orbital motions of the electrons and their spins. Explanations have been developed for the origin of the various types of magnetic behaviour, namely, diamagnetism, paramagnetism, ferromagnetism, antiferromagnetism and ferrimagnetism. The theories are less advanced when consideration is given to solids and there have been two main approaches, the atomistic and the collective electron approach. Both theories attempt to interpret the fundamental magnetic parameters, the magnitude of the atomic moments and the strength and sign of the coupling between these magnetic moments. According to convention, a positive coupling tends to align magnetic moments parallel to each other resulting in ferromagnetic behaviour and a negative coupling tends to align magnetic moments in an antiparallel manner leading to antiferromagnetic behaviour.

The magnetic behaviour of Mn is a consequence of the incomplete 3d electron shell. In crystalline solids such as γMn metal, the orbital motion of the electrons is quenched and it is the spinning electron which is the magnetic carrier. In the atomistic approach, the five electrons in the 3d electron shell of Mn are assumed to be tightly bound to the Mn ion and the consequence of this approach is a net magnetic moment per ion which is equal to an integral number of individual electron magnetic moments.

The collective electron approach assumes that the energy levels associated with the 3d and 4s energy levels are broadened into energy bands which overlap to a certain extent, resulting in a non-integral number of electrons per energy band. On the other hand, it is still possible to classify and describe the intrinsic magnetic

parameters using the molecular field theory, which was historically developed from the atomistic model, as long as due allowance is made for non-integral atomic moments. In this theory, the net exchange coupling between a given atom and all its neighbours is approximated by the interaction of its magnetic moments with an arbitrary molecular field. When all interactions in the system are positive a spontanious magnetisation at $0^{o}K$ corresponds to a parallel alignment of all the atomic moments, which at higher temperatures progressively become misaligned because of thermal agitation.

In the simplest type of antiferromagnetic system, all the magnetic atoms are chemically and crystallographically equivalent and, as a consequence of the negative interactions between them, they divide into two interpenetrating sub-lattices having oppositely oriented moments and there is no magnetisation of the system as a whole. However, each individual sub-lattice has a saturation intensity of magnetisation induced by the molecular field of the other. In the presence of an applied magnetic field there is an increase in magnetisation in one lattice and a fall in the other. As a result, in a randomly-oriented polycrystalline antiferromagnetic material, the susceptibility increases as the temperature rises from $0^{o}K$ reaching a peak value at the magnetic disordering temperature known as the Néel temperature. The susceptibility then decreases above the Néel temperature. For a long time this was the only method available for detecting antiferromagnetic behaviour. In more recent years, there has been a considerable growth in the study of antiferromagnetism and this can be traced to the development of the civil nuclear power programme and the subsequent growth in the number of experimental neutron diffraction facilities.

Coherent nuclear scattering occurs at the regularly spaced nuclei within a crystal giving rise to characteristic diffraction reflections according to the Bragg equation. There will also be an interaction between the neutron beam and the magnetic structure. In a simple antiferromagnetic crystal, for instance Mn-Cu, where there is an ordered array of parallel and antiparallel magnetic moments

on adjacent (002) planes, then the scattered neutron waves from parallel spin sites will be 180^{o} out of phase with the antiparallel spins. The scattering power then varies from one site to another in the ordered fashion that is characteristic of a superlattice, resulting in extra reflections which do not occur either in nuclear or ferromagnetic scattering. The reflections resulting from nuclear scattering, then give information about the crystal structure of the material and the antiferromagnetic reflections give information about the orientation of the magnetic moments with respect to the crystal axes. Using this approach it has been shown that the magnetic moments in Mn-Cu alloys lie in [001] in the manner shown in Fig. 2[11]. A domain structure also develops in antiferromagnetic materials in an analagous manner to the domain structure of ferromagnetic materials. An antiferromagnetic domain is a region in which there is only one direction of antiferromagnetic alignment. The domain geometry is most probably determined by strain and defects in the lattice.

The coherent scattering amplitude for neutrons, termed 'b', shows no variation with scattering angle and unlike X-ray diffraction, depends on the atomic number in an irregular way. This property proves to be invaluable when examining Mn-Cu for long and short range order. Corresponding X-ray scattering factors for Mn and Cu are so similar that such ordering, if present, would be difficult to detect. Furthermore, certain elements exhibit negative neutron scattering amplitudes, for instance Mn, and it is possible by the appropriate selection of compositions to identify a solid solution which, although crystalline, yields no crystalline diffraction pattern; such a composition is 68%Mn-32%Cu and this is known as a "null matrix" alloy.

Prior to the commencement of this research work there had been relatively few publications on the antiferromagnetic behaviour of Mn-Cu alloys and these papers agreed on all the essential magnetic features of the Mn-Cu system. Since that time, there has been considerable controversy over the possible presence of short

range magnetic or atomic ordering. As the experimental results described later on in the thesis have a marked bearing on the controversy, a literature survey on this particular aspect of the antiferromagnetic behaviour has been incorporated in Section 4.5.

The intensities of magnetic neutron reflections have their maximum values at $0^{\circ}K$ and from the absolute intensity of the $\{110\}$ antiferromagnetic superlattice reflections, it is possible to determine the average magnetic moment per atom[12]. The Mn ionic moment varies from 0 at about 78%Mn to an extrapolated value of 2.4 Bohr magnetons at 100%Mn[12]. The variation of susceptibility with temperature exhibits a cusp at the Néel temperature for alloys containing 85%Mn and 90%Mn[12], as would be expected from alloys exhibiting antiferromagnetic behaviour.

The proposed reorientation of crystallites having particular 'c' axis directions by the application of a compressive stress[18], was confirmed experimentally by observing the change in intensity of the $\{110\}$ neutron reflection with increasing compressive stress[12]. In an alloy containing 90%Mn which was subjected to a compressive stress, there was little change in neutron intensity with stresses up to $15Kg/mm^2$* and the intensity recovered after the stress was removed. Most of the change in $\{110\}$ reflection intensity occurred for stresses lying between 15 and $30Kg/mm^2$* and stresses greater than $30Kg/mm^2$* produced little further increase in intensity. When a stress greater than $25Kg/mm^2$* was removed, practically all of the stress-induced orientation remained[12]. In a later publication[13] the pronounced minimum in Young's modulus at the fct/fcc transformation temperature was explained by proposing two strain components, one of these being the normal elastic strain and the other being a strain relaxation due to the preferential growth of domains which are more favourably oriented with respect to the direction of the applied stress. There was no attempt made to relate the antiferromagnetic domain boundaries with crystallographic interfaces, although twinning was suggested if the deformation was sufficiently large[12].

* $15 Kg/mm^2 = 21,334$ p.s.i
$25 Kg/mm^2 = 35,558$ p.s.i
$30 Kg/mm^2 = 42,668$ p.s.i

Most of the scientific papers attempting to relate crystallographic and antiferromagnetic properties in Mn-Cu alloys, have been restricted to alloys containing more than 80%Mn. The work which has been proceeding for a number of years at the Bureau of Mines has been concerned with alloys containing between 60% to 80%Mn which exhibit very high damping properties. They found that following an ageing heat treatment at 450°C an alloy containing 70%Mn yielded partial precipitation of αMn with an accompanying change from the fcc to the fct structure[10]. Furthermore, the change in magnetic susceptibility with temperature did not exhibit the cusp which is normally associated with antiferromagnetic materials[2]. They assumed, from these results, that the 70%Mn-30%Cu alloy developed paramagnetic and not antiferromagnetic behaviour after heat treatment. Based on these findings, it was implied that the fct structure was not necessarily associated with antiferromagnetism and an alternative suggestion was postulated. They claimed that because of the simultaneous development of the fct structure and the partial precipitation of αMn in the heat treated 70%Mn alloy, then alloys containing more than 80%Mn which develop the fct structure on quenching, must also have undergone a partial transformation from $\gamma \rightarrow \gamma + \alpha$ during the quenching. Their hypothesis therefore involved a fcc/fct transformation which resulted from αMn precipitation.

1.5 DAMPING CAPACITY.

In his review of internal friction in metals, Nowick[19] classifies the various mechanisms that produce damping into two categories of non-elastic behaviour.

I Viscoelasticity (dynamic hysteresis)
- a) Anelasticity
  - 1 Single time of relaxation.
  - 2 Superposition of relaxation.
  - 3 Coupled relaxation.
- b) Processes involving viscous flow.

II Static hysteresis.

Internal friction results when stress and strain are not unique functions of one another in vibration and the dynamic stress-strain relationship is a hysteresis loop. Viscoelasticity arises as a result of time derivatives in the stress-strain equation and the dynamic nature of the experimental test. The damping properties of the material are particularly dependent on the frequency of the oscillatory stress and are amplitude-independent.

On the other hand, static hysteresis is strongly amplitude dependent and frequency independent. In this form of internal friction there is a definite value of strain for each stress and the strain is achieved simultaneously with the application of stress. During a cycle of stress, the level of strain associated with increasing stress is different to the level of strain associated with a decreasing stress and a static hysteresis loop results which is unaltered by the rate of traversal of the loop.

This latter form of amplitude-dependent internal friction has been observed in single crystals of a number of materials and has been developed into a theory based on the break away and subsequent movement of anchored dislocations [20]. The shape of the hysteresis loop associated with this dislocation behaviour is known as "wasp-waisted" and is unusual in that there is no remanent strain associated with the zero stress. The dislocation line returns to its original position after half of the complete stress cycle has been completed.

Magneto-elastic damping is also stress-dependent and occurs with the movement of magnetic domain boundaries, either through the application of a magnetic field or by an externally applied stress. Depending upon the sign of the magnetostrictive dilation and the sign of stress of the internal stress peaks, then the domain boundary can run forward in an unstable Barkhausen jump. The damping properties exhibit a maximum with increasing stress, because at stresses above those that cause near magnetic saturation, no further domain wall motion arises and the magneto-elastic strains can increase no further [21]. The published damping results on

Mn-Cu alloys[10] and all the damping results described in this thesis are amplitude dependent and it has been reported that the damping properties are frequency independent[10]. The internal friction in Mn-Cu alloys is therefore of the static hysteresis type.

There are a number of ways in which internal friction can be quantified[23] and it appears to be generally accepted engineering parlance to use the term "specific damping capacity" which is the ratio of the energy absorbed in one cycle of vibration to the potential energy at maximum displacement in that cycle, expressed as a percent. This term is usually used when the stresses used in the appropriate test rig simulate those of actual service conditions; the term is often reduced to "damping capacity".

There are also a number of methods by which the damping capacity can be determined and a multitude of test rigs have been designed to accomplish this[22]. Most of the published results on Mn-Cu alloys have been based on the free decay of a torsional pendulum[10]. When the work described in this thesis was initiated, there had been a previous history of damping capacity determinations using this sort of equipment at the Delta Metal Research Laboratories. As the damping capacity determinations were only to be used for comparitive purposes and not as a means of elucidating the damping mechanism, it was decided to continue the use of the method.

Siefert and Worrel[23] first measured the damping properties of an 88%Mn-12%Cu alloy. They found that the damping properties decreased following an ageing heat treatment at 625°C. Optical examinations undertaken at the same time showed the presence of many fct twins which they claimed decreased in area as the ageing process continued. In view of their admitted difficulties with the etching technique, the way in which they infer an association between the damping properties and the presence of tetragonal twins is dubious, although the conclusions, if incorrectly arrived at, have subsequently been justified. McCrary and Rogers[24] plotted the change in damping properties with temperature for quenched alloys containing 72, 76, 80, 84 and 92%Mn and observed

a maximum in the damping properties at temperatures between about -40^0 to -60^oC and a fall in damping properties which occurred at lower temperatures with lower Mn content. Because damping properties were retained at temperatures above the fcc/fct transformation temperature as quoted by Basinsky and Christian[9] and above the Néel temperature as quoted by Bacon et al[12], they concluded that the damping properties in Mn-Cu alloys could not be associated with either the movement of fct twins or the antiferromagnetic behaviour. For many years the results of McCrary and Rogers[24] were the only experimental data available and their conclusions inhibited an acceptance of a damping mechanism based on twin movement in high Mn alloys. Although their results have not been satisfactorily explained, two factors which they did not consider have subsequently come to light. Considerable solution treatment times are necessary to homogenise samples of Mn-Cu and stress is now known to increase the fcc/fct transformation temperature in Mn-Cu alloys.

In a comprehensive publication summarising considerable work at the Bureau of Mines, Jensen and Walsh[10] showed that very high damping capacities of about 30% or more, could be developed in alloys containing 50, 60 and 70%Mn after an ageing heat treatment at various temperatures. Probably because of the considerable number of variables that they examined, they decided to limit these heat treatments to a duration of 2 hours at various temperatures. A limitation of the experimental programme to one heat treatment temperature and a variety of heat treatment times, would have revealed the important trends which were not to appear until much later. In direct contrast with McCraryand Rogers[24], Jensen and Walsh[10]found that the damping properties of an 81.2%Mn alloy in the quenched condition, decreased to a very low level at the fcc/fct transformation temperature quoted by Basinsky and Christian for that composition[9]. They[10]also found a correlation between the fcc/fct transformation temperature and a rapid deterioration in damping properties in a 75%Mn alloy which had first been given

an ageing heat treatment to develop the high damping condition. The workers at the Bureau of Mines were the first to identify the development of high damping properties in Mn-Cu alloys containing 60 and 70%Mn after an appropriate ageing heat treatment and realised the possible commercial significance of their discovery[10]. They, like McCrary and Rogers[24] concluded from experimental magnetic measurements that antiferromagnetic behaviour was not important. A most confusing situation therefore existed at the commencement of the work described in this thesis because the major publications on the subject in the previous ten years had firmly claimed that neither the presence of fct twins nor the antiferromagnetic behaviour exhibited by certain of the Mn-Cu alloys, were important factors in developing the high damping properties.

CHAPTER 2.

EXPERIMENTAL PROCEDURE FOR Mn-Cu ALLOYS.

2.1 PREPARATION OF Mn-Cu ALLOYS.

Eight alloys were cast ranging in composition from 30% to 90%Mn. Samples from the top and bottom of the ingots with nominal composition ranging from 50% to 90%Mn were taken for chemical analysis and the results are given in Table 1. After machining, hot rolling to 9/16" bar and cutting to suitable lengths, each alloy was solution treated for four weeks at 850°C in an atmosphere of argon. Samples for subsequent electron microscopy were then hot rolled to about .010" thick, annealed for two hours at 850°C and quenched into water. The 57%Mn alloy was examined in detail by electron microscopy, X-ray crystallography and neutron diffraction; the other alloys were examined in less detail.

The 57%Mn alloy was aged at 400°C for a variety of times. The ageing temperature of 400°C was chosen because at this temperature observable changes were found to occur in a reasonable time and also because a direct correlation could then be obtained with damping capacity measurements which had been proceeding for some time previously, under the direction of R.J. Goodwin[8]. Some samples however, were examined at 450°C and 500°C for short ageing times. Unless specifically stated to the contrary, it should be assumed throughout the thesis that all compositions have been quoted in weight percentages and all samples have been given a homogenising treatment followed by a water quench. Where a further heat treatment has been involved, this also will have been followed by a water quench.

2.2 METALLOGRAPHY OF Mn-Cu ALLOYS.

Many etching reagents have been used by different workers to show up structural details in Mn-Cu alloys. In this work either a 0.5%Nital solution or a 5% Citric acid solution has been used to detect heterogeneity and to show up the distribution of αMn precipitate particles. It is much more difficult to detect

the fine twinned structure which is present in alloys which have the fct structure and in this case etching in ammonia solution, or the method of electropolishing used by Basinski and Christian[9] was employed. More vigorous etching reagents lead to artefact structures in Mn-Cu alloys.

2.3 ELECTRON MICROSCOPY.

Preparation of electron microscope samples from .01" thick sheet involved a two stage thinning process. Chemical thinning using a 50/50 mixture of nitric acid and glacial acetic acid was followed by a final electrolytic polish in a solution of 15 gms. chromic acid in 4cc. water and 100 cc. glacial acetic acid. The polishing voltage used was 20V at a current density of about 0.15 A/cm^2. Samples containing appreciable quantities of αMn precipitate, did not provide satisfactory thin films because of preferential attack at the αMn particles.

A Siemens Elmiskop Ia electron microscope operated at 100 KV and fitted with a Valdré goniometer stage, allowing a 22° tilt was employed for thin film examination. When applicable, high-resolution tilted dark-field microscopy and electron diffraction were utilised to aid in the interpretation of the image. On a few occasions controlled heating of the sample was required during the examination and use was made of a commercially available heating stage.

2.4 X-RAY CRYSTALLOGRAPHY.

2.4.1 Selection of a suitable X-radiation.

Three main requirements were considered in the selection of a suitable X-radiation and these are discussed below.

2.4.1.1 Axial ratio measurement.

The axial ratio has been determined from the Bragg angle of certain reflections from which both 'a' and 'c' values can be derived, namely the (200,020) and (002) or (220) and (022,202) reflections. A more detailed account of this axial ratio determination is given in section 2.4.2. Because of the close similarity in 'a' and 'c' values in all the alloys examined, it

was common to find overlapping of reflections. The separation between X-ray reflections increases if the wavelength of the incident X-radiation is increased . On the other hand there is a decrease in the number of reflections within the angular range of the Philips diffractometer.

A compromise was therefore necessary between the requirements for the separation of fcc and fct reflections and the need for a reasonable number of reflections when phase identification was a more important factor. The effect of using different X-radiations on the angular separation of the (200,020) and (002) reflections for a fct unit cell with a typical axial ratio of 0.98 is shown in Table 2.

2.4.1.2 Atomic ordering.

Certain alloys which undergo a fcc/fct transformation, also exhibit long range ordering, for instance CuAu[25], CuPd[26], MnNi[27], Cu_3Pd[28] and Ni_3V[29] and various attempts have been made to relate the long range order parameter with the axial ratio.

There was still a great deal of uncertainty at the outset of the programme concerning the driving force behind the fcc/fct transformation in Mn alloys and the possibility of an ordering reaction could not be dismissed. Furthermore, an ordering reaction leading to the formation of intermetallic compounds Cu_5Mn and Cu_3Mn had been reported[7]. The latter compound corresponds to the terminal composition of the $\gamma + \alpha$ phase boundary at about $400^{\circ}C$. Under equilibrium conditions this composition could then correspond to one of the decomposition products resulting from the heat treatment of quenched alloys within the $\gamma + \alpha$ phase field. It was therefore clearly necessary in the early stages of the work to establish the presence or absence of any atomic ordering, especially in those alloys which only developed the fct structure after heat treatment. It should be mentioned that the reported formation of the intermetallic compounds Cu_5Mn and Cu_3Mn were inferred from thermal analysis data and superlattice reflections

could not be identified by X-ray means. The particular X-radiation used was not quoted[7]. The atomic scattering factors for Mn and Cu are 25 and 29 respectively and it can be calculated that the ratio of the intensity of a superlattice reflection, if it were present, to the intensity of the fundamental reflection at small angles is about .005; it is therefore unlikely that a superlattice reflection could be positively identified.

It is possible however, to increase the relative intensity of the superlattice reflections by the careful selection of the incident X-ray wavelength. When the incident X-ray wavelength is nearly equal to the wavelength of the K absorption edge of the scattering element, there is an anomalous change in scattering factor. The corrected scattering factors have been calculated from published graphs[30] for those elements which have X-ray Kα wavelength values near the K absorption edge for Cu and Mn. The corrected relative intensities for superlattice and fundamental peaks for each of these wavelengths are shown in Table 2, and if long range ordering were present, it should be possible to detect its presence using FeKα radiation.

2.4.1.3 Peak to background ratio.

The use of X-radiation of wavelengths close to the K absorption edge of the elements being examined has its drawbacks, because secondary fluorescence can occur which results in a uniformly increased background over the entire angular range. The effect is most severe when the atomic number of the target material is 2 or 3 more than that of the elements present in the sample. All of the information presented above is summarised in Table 2. After considering all the factors described in this chapter, Fekα radiation was clearly the best compromise; a tube was therefore purchased and used throughout the investigation. The tube was rated at 24 kW, 12 mA and a Mn filter was always used between the tube and the specimen, to eliminate Kβ radiation. In all cases except one, the sample was mounted in the diffractometer and the results recorded on chart paper. The one exception

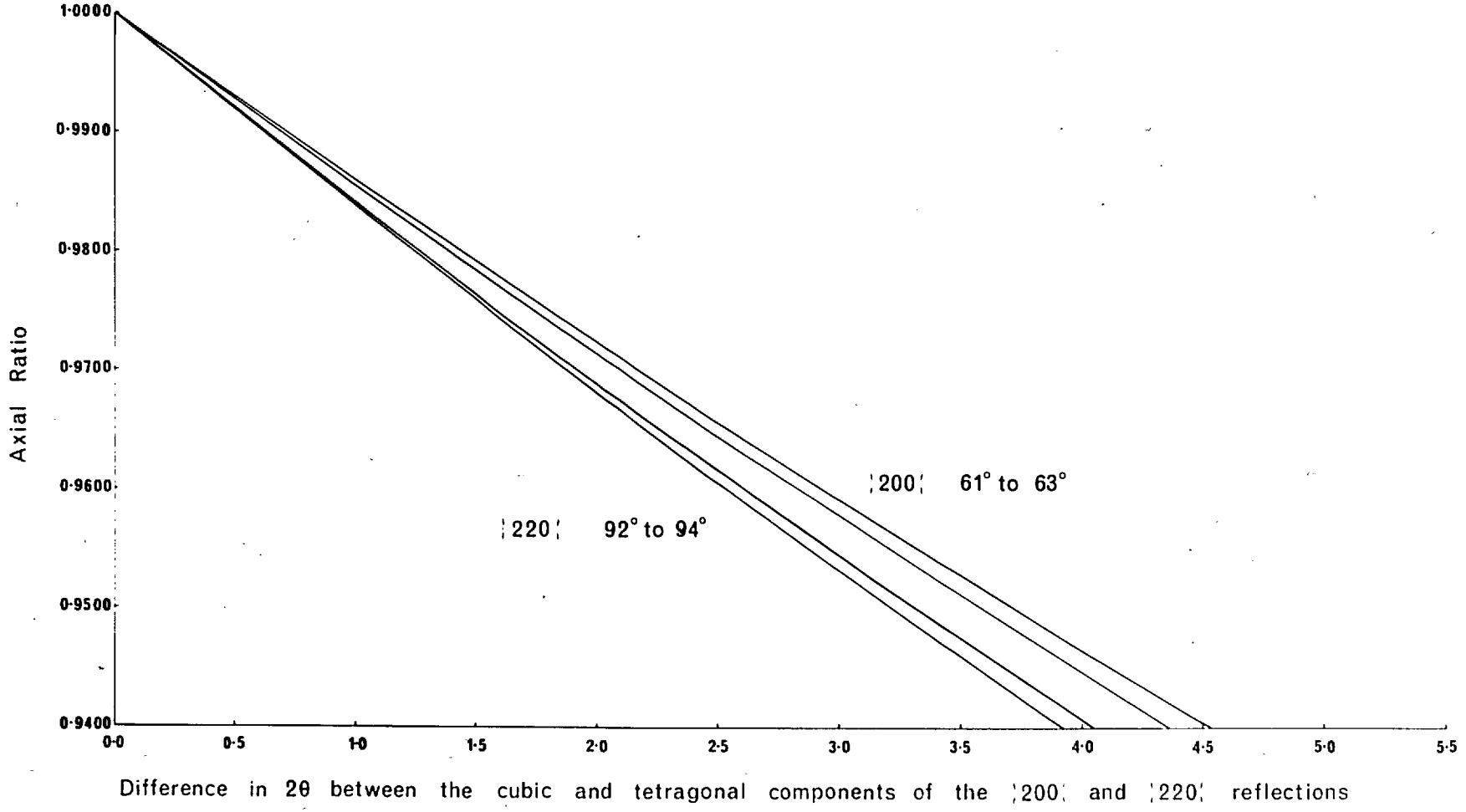


Fig. 3 Relationships between the axial ratio and the angular difference between the cubic and tetragonal components of the {200} and {220} reflections.

involved the use of a Debye-Scherrer powder camera which utilises photographic film and enables long exposures to be used.

2.4.2 Determination of the axial ratio.

Throughout the research programme extensive use has been made of the degree of tetragonality or axial ratio. Having decided upon the particular X-radiation, the Bragg equation $n\lambda = 2d \sin\theta$ in conjunction with the equation for interplanar lattice spacings in a fct unit cell $\frac{1}{d^2} = \frac{h^2 + k^2}{a^2} + \frac{l^2}{c^2}$ can be used to determine 'a' and 'c' separately and hence determine the c/a ratio.

Although greater separation of the cubic (h.k.0) and tetragonal (h,k,l) components of a particular reflection occurs at higher Bragg angles, a parallel improvement in definition of the $\alpha_1\alpha_2$ doublet also appears. In many cases the axial ratio is very close to 1, implying appreciable overlap of the cubic (h,k,0) and tetragonal (h,k,l) reflections. The additional appearance of the α_2 component in these cases was therefore a hindrance rather than an aid to greater accuracy of measurement. All axial ratio measurements have therefore been derived from the (200,020) and (002) or the (220) and (202,022) reflections.

The derivation of the c/a ratio from the (200,020) and (002) reflections was straight forward because the 'a' and 'c' values are simply twice the corresponding 'd' spacings. However, in the case of the (220) and (202,022) reflections, the calculation though simple, proved tedious and time consuming.

Measurement of the angular difference between the two reflections was found to be much simpler and graphs were accordingly constructed covering the 2θ range in which the $\{200\}$ and $\{220\}$ reflections occurred, so that the angular difference between the tetragonal (h,k,l) and cubic (h,k,0) components of the reflection could be directly correlated with the c/a ratio. For axial ratios close to 1 the relationship between the separation of the tetragonal (h,k,l) and cubic (h,k,0) components and the c/a ratio is relatively insensitive to the absolute 2θ value of the combined reflection, Fig. 3. Accordingly the graphs were drawn

so that the absolute 2θ value of the {200} reflection lay within the range 61° - 63° and the absolute 2θ value for {220} lay within the range 92° - 94°.

By interpolation for angles between 61° to 63° and 92° to 94°, the axial ratio could be determined to an accuracy better than $\pm$ .001.

When due allowance is made for the multiplicity factor, the ratio of the intensity of the cubic component to the tetragonal component of the {200} and {220} reflections is 2: 1 and 1 : 2 respectively. This intensity relationship and the various factors which influence it, proved to be important during the development of possible mechanisms to explain the high damping properties of Mn alloys and is dealt with in greater detail in Section 4.3

2.4.3 Heating, cooling and straining the sample during X-ray examination.

A study of the effect of heating, cooling and tensile stress on the axial ratio proved desirable and in all cases very simple equipment was constructed.

By firmly attaching a thin sheet of the sample to an electrically heated copper block, controlled heating to 300°C was easily achieved. Similarly by attaching the specimen to a small copper box through which a flow of liquid nitrogen was passed, a degree of temperature control could be exerted for sub-zero temperatures. Both heating and cooling stages were attached to a "Sindanyo" block which allowed accurate positioning of the specimen height with respect to the X-ray beam and also enabled the stages to be mounted into the diffractometer holder. Adequate heating control was obtained through the use of a variable D.C. supply. Steady temperatures were developed quickly and could be maintained during the measurement of the axial ratio. Temperature control of the cooling stage was poor by comparison and a temperature variation of less than 10°C during axial ratio measurements was considered acceptable for the purposes of the experiment.

In one particular experiment it proved necessary to ascertain the effect of stress on the axial ratio. This was accomplished by firmly attaching a thin sheet sample to two brackets which could then be separated to a variable degree by turning a screw thread; in this way an unknown tensile stress could be generated within the sample.

2.5 NEUTRON DIFFRACTION EXAMINATION.

The neutron diffraction experimental work was undertaken by Professor G.E. Bacon at Harwell who used a monochromatic neutron beam of wavelength 1.04A which was generated by the DIDO reactor. Two samples of the 57%Mn alloy were provided, both solution treated for 4 weeks at 850°C and quenched into water; one was then given a further heat treatment for 7 hours at 400°C. The samples were mounted in a vanadium cryostat and neutron diffraction traces were obtained at room temperature and at 4°K. At a later date one further sample was supplied containing 70%Mn, which had been solution treated and quenched and given a further heat treatment of 2 hours at 400°C. In this case the neutron diffraction traces were obtained at 23°C, 147°C and 153°C. The intention in this case was to plot the change in intensity of the $\{110\}$ magnetic peak with temperature and hence determine the Néel temperature.

2.6 DAMPING CAPACITY DETERMINATION.

Prior to the start of the research work described in this thesis[8], and subsequently[31], Mr. R.J. Goodwin of Delta Metal Research had been recording damping capacities of Mn-Cu alloys using a torsional pendulum technique. It is worthwhile incorporating details of the technique at this point because the method, with small modifications, was later adopted by the author.

The square-ended test pieces were 7" long with a solid cylindrical gauge length of diameter .357" and length of 3". One end of the test piece was rigidly clamped into a massive steel base. The upper end was rigidly clamped into a central hole in a 30" long inertia bar. A small mirror was clamped to the centre of the

inertia bar and a pencil of light from a fixed source was reflected by the mirror onto photographic paper and in this way the torsional deflection of the test piece could be found. The deflections corresponding to surface shear stresses of 1,000, 2,000, 3,000, 4,000 and 5,000 p.s.i. were determined using standard weights whose load was transmitted by means of fine wire over pulleys to the ends of the inertia bar. The test piece was then released from a position corresponding to about 6,000 p.s.i. surface shear stress and the decay of the free torsional oscillations were recorded on the photographic paper which moved at a fixed speed normal to the light beam. The frequency of the oscillations was about 5 cycles per second. The specimen could be immersed either in heated oil or in a cooling medium.

The specific damping capacity ψ was determined for the nth cycle vibration using the following equation:-

$$\psi_n = \frac{A_n^2 - (A_{n+1})^2}{A_n^2} \times 100\%$$

where A_n and A_{n+1} are the stress amplitudes at the start of the nth and $(n + 1)$ the cycles. When $A_n > 1.05A_{(n+1)}$ successive amplitudes could be measured with sufficient precision, i.e. when $\psi_n > 9\%$. When $A_n < 1.05A_{(n+1)}$ the change in amplitude was measured over 10 cycles and an approximation due to Norton[32] was used to calculate the average damping capacity ψ_a.

$$\psi_a = \frac{40(A_n - A_{(n+10)})}{(A_n + A_{(n+10)})}\%$$

The energy loss in the apparatus itself, including the air damping of the inertia bar, corresponded to a specific damping capacity of less than 1% over the temperature range -210°C to 250°C and about 0.1% damping capacity when operated at room temperature. Samples were cut from the ends of many of the damping test pieces for optical, X-ray and electron microscope examination by the author.

When the damping capacity determinations on Mn-Cu alloys were

completed it was decided to alter the recording part of the damping rig so that damping capacity determination could be completed in a shorter time. Instead of the photographic recording technique, the movements of the inertia bar attached to the test sample were recorded by means of displacement transducers and the generated electrical impulse was recorded on a chart by means of a UV recorder. Responsibility for damping capacity determinations on all alternative alloys to Mn-Cu were then taken over by the author using the modified rig.

Fig. 4.

Fig. 5.

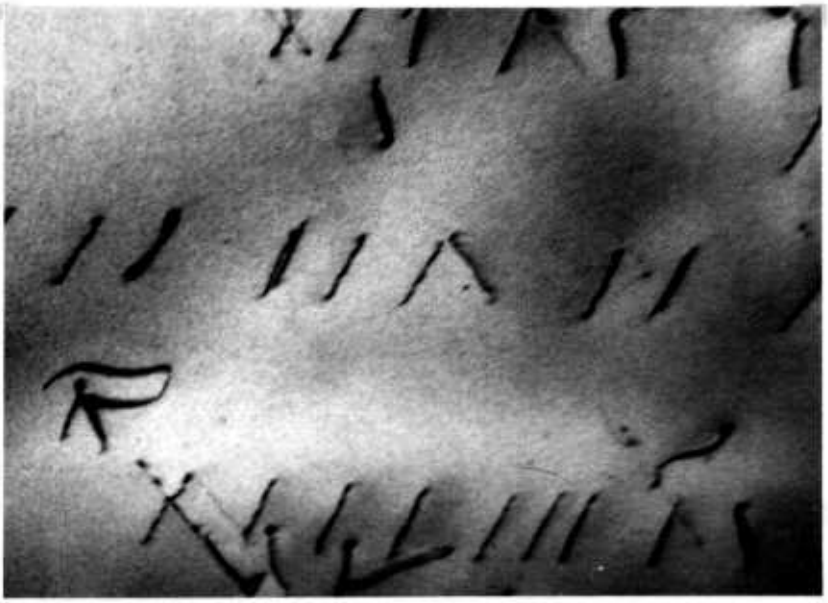


Fig. 4. A 57%Mn-43%Cu alloy, solution treated for 2 hours at 850°C and water quenched. Shows dislocation features typical of any quenched metal. x 55,000.

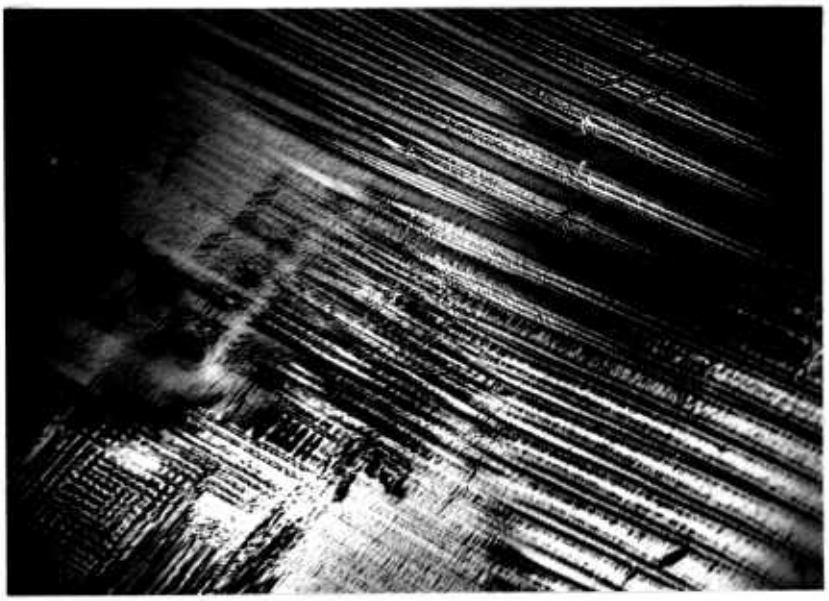


Fig. 5. A 57%Mn-43%Cu alloy, solution treated for 2 hours at 850°C, water quenched and heat treated for 7 hours at 400°C. Shows a high density of boundaries. x 30,000.

Fig. 6.



Fig. 6. A 57%Mn-43%Cu alloy, solution treated for 2 hours at 850°C, water quenched and heat treated for 6 hours at 400°C. Shows boundaries lying edge-on in a [100] oriented foil. x 37,000.

CHAPTER 3.

RESULTS ON Mn-Cu ALLOYS.

3.1 ELECTRON MICROSCOPY.

The following relevant features were observed during the examination of the alloys in the electron microscope.

3.1.1 Structure formed on quenching samples into water.

The 57%Mn alloy quenched into water from 850°C was included for comparison purposes and exhibited dislocation structures, Fig. 4 typical of any metal examined by electron microscopy. Samples of the 57%Mn alloy quenched from 850°C and heat treated for 30 mins. or 1 hour at 400°C were very similar in appearance.

3.1.2 Microtwin boundaries.

A few occasional boundaries having a marked diffraction contrast were observed in the 57%Mn samples which had been heat treated for 3 and 4 hours at 400°C. Their number increased considerably with ageing heat treatment times until after 6 to 8 hours, their density was so high that considerable overlaps occurred, Fig. 5. At longer ageing heat treatment times, thin foils were difficult to prepare but in those areas that were transparent to electrons, fewer boundaries were seen. The boundaries were always seen in parallel pairs, lying on or near $\{110\}$ planes, traversing across grains or terminating within grains, in which case they produced a wedge-shaped region, as can be seen in Fig. 6 where all the boundaries are viewed edge-on.

No detectable difference in the position of the diffraction spots occurred when traversing the electron beam across any particular boundary, apart from a slight movement in Kikuchi pattern when this was observable. The orientation difference across the boundary was therefore very small. These boundaries, which will subsequently be referred to as microtwins, have been observed to show characteristic diffraction contrast in several materials exhibiting a slight tetragonal or rhombohedral distortion of the unit cell, for example MnNi[27] and Ni_3V[29], including Mn-Cu[33] and have been the subject of a detailed theoretical

Fig. 7.

Fig. 8.



Fig. 7. A 57%Mn-43%Cu alloy, solution treated for 2 hours at 850°C, water quenched and heat treated for 6 hours at 400°C. Shows the initiation of microtwins at dislocations. x 21,000.

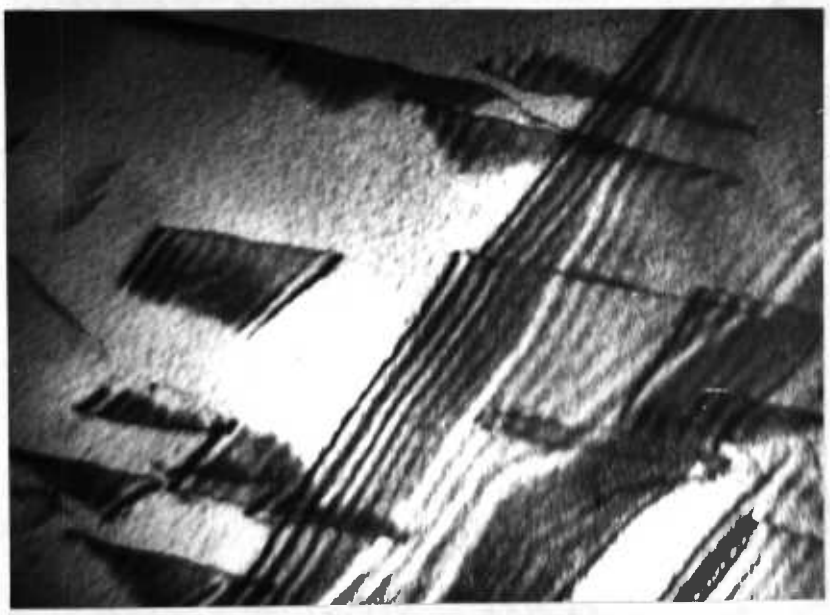


Fig. 8. Same area as in Fig. 7, showing further microtwin propagation. x 21,000.

Fig. 9.

Fig. 10.

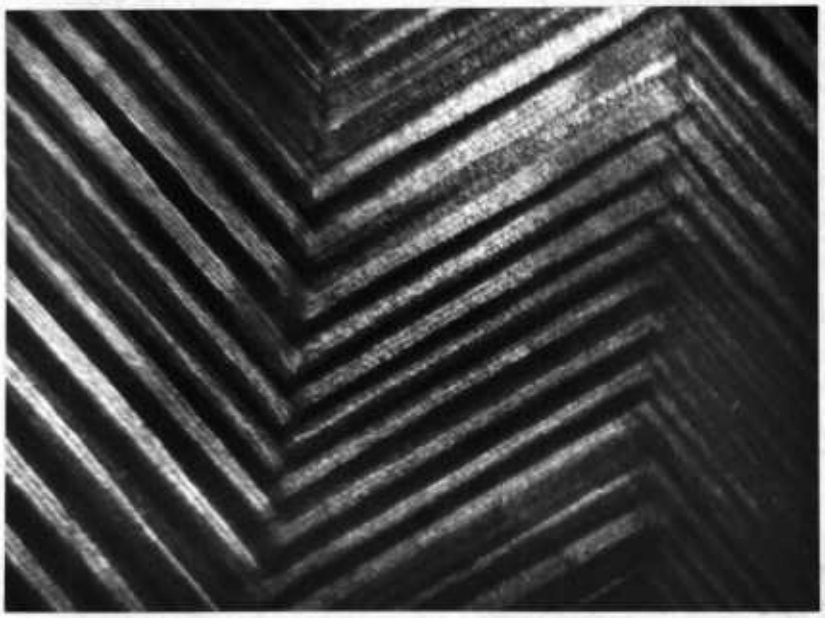


Fig. 9. A 57%Mn-43%Cu alloy, solution treated for 2 hours at 850°C, water quenched and heat treated for 6 hours at 400°C. Shows a substructure of microtwins with larger stable microtwins. x 37,000.

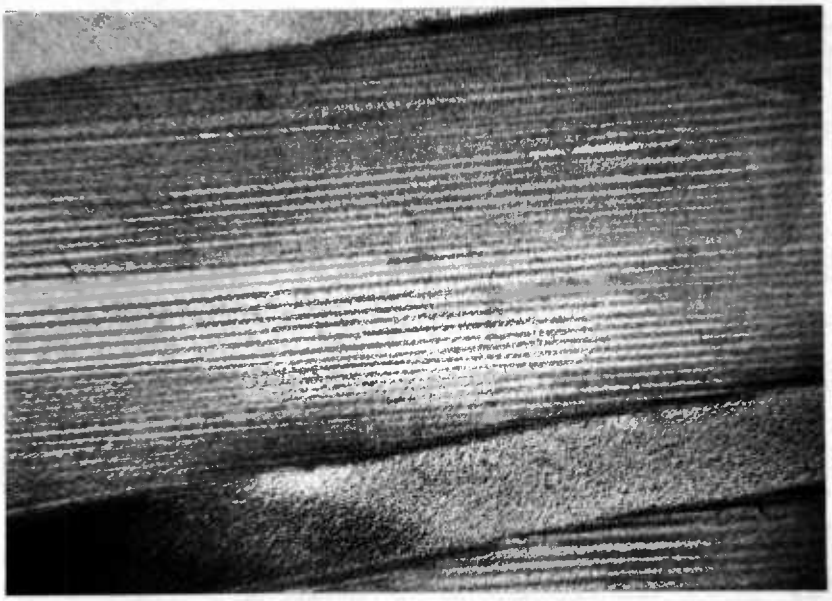


Fig.10. A 57%Mn-43%Cu alloy, solution treated for 2 hours at 850°C, water quenched and h eat treated for 6 hours at 400°C. Shows the lengthwise growth of microtwins within a large stable microtwin. x 18,000.

Fig. 11.

Fig. 12.



Fig.11. A 57%Mn-43%Cu alloy, solution treated for 2 hours at 850°C, water quenched and heat treated for 6 hours at 400°C. Shows the growth of microtwins in one orientation at the expense of microtwins in another orientation. x 28,000.



Fig.12. A 57%Mn-43%Cu alloy, solution treated for 2 hours at 850°C, water quenched, heat treated for 6 hours at 400°C and reduced 6% in thickness by cold rolling. Microtwin movement has been reduced or prevented by the dislocation tangles. x 29,000.

Fig.13.

Fig.14.

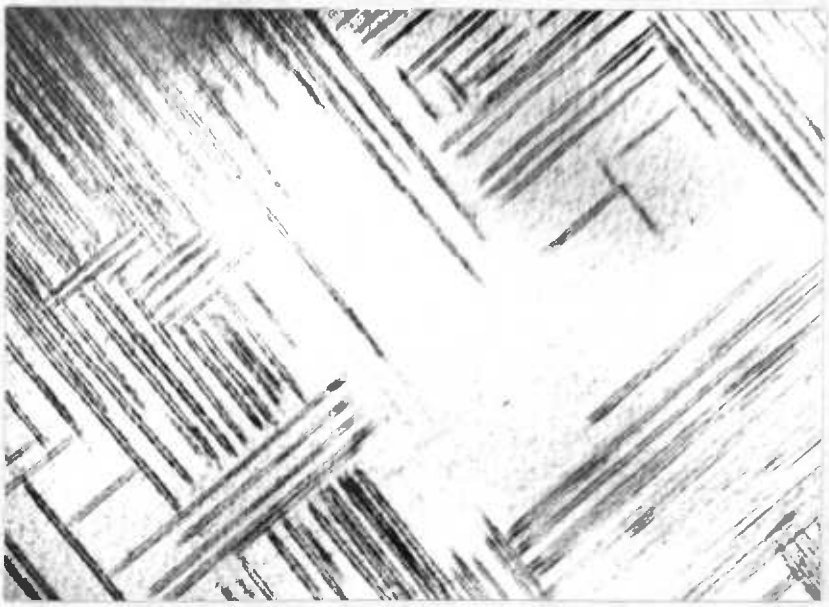


Fig.13. A 57%Mn-43%Cu alloy, solution treated for 2 hours at 850°C and furnace cooled. Shows the fine nature of the microtwin distribution formed on slow cooling x 38,000.



Fig.14. A 57%Mn-43%Cu alloy, solution treated for 2 hours at 850°C, water quenched and heat treated for 24 hours at 400°C. Shows microtwins terminating at an αMn particle. x 41,000.

in another orientation. In these circumstances the microtwins, which were favoured by the operating stress, increased in numbers.

Dislocations were also found to be points of hindrance to the movement of existing microtwins. A sample of the 57%Mn alloy was heat treated for 6 hours at 400°C to establish the high damping condition and then reduced in thickness by about 6% by rolling. The resulting dislocation tangles made microtwin observation difficult because of the competing diffraction effects and few were seen, Fig. 12. However, all movement as previously seen inside the electron microscope, was prevented.

If the sample was heated inside the microscope, either by electron beam heating or using a heating stage, to a temperature where the microtwins disappeared, a re-distribution of microtwins took place on a much finer scale on cooling to room temperature again. The same sort of microtwin distribution was often observed in samples which had been furnace cooled from the solution treatment temperature, Fig. 13.

The presence of microtwins was also observed in the 70%Mn alloy after more than 2 hours heat treatment and in the 90%Mn alloy in the quenched condition. Diffraction patterns obtained from the 90%Mn alloy exhibited a detectable splitting of the diffraction spots indicating a greater orientation change across the microtwin boundary than that found in the 57%Mn alloy.

3.1.3 The precipitation of αMn.

Preferential precipitation of αMn occurred at grain boundaries in the 57%Mn alloy after ageing for about 6 hours at 400°C and within grains at longer ageing heat treatment times. The initial stage of αMn precipitate growth was never seen in any Mn alloy examined by electron microscopy, although many samples were examined which would have been expected to show the early stages of precipitate formation and growth. Over-ageing produced large quantities of αMn precipitate particles within grains which have been shown[33] to adopt a Kurjumov-Sachs orientation relationship[39] with the matrix. In those cases where αMn

Fig. 15.

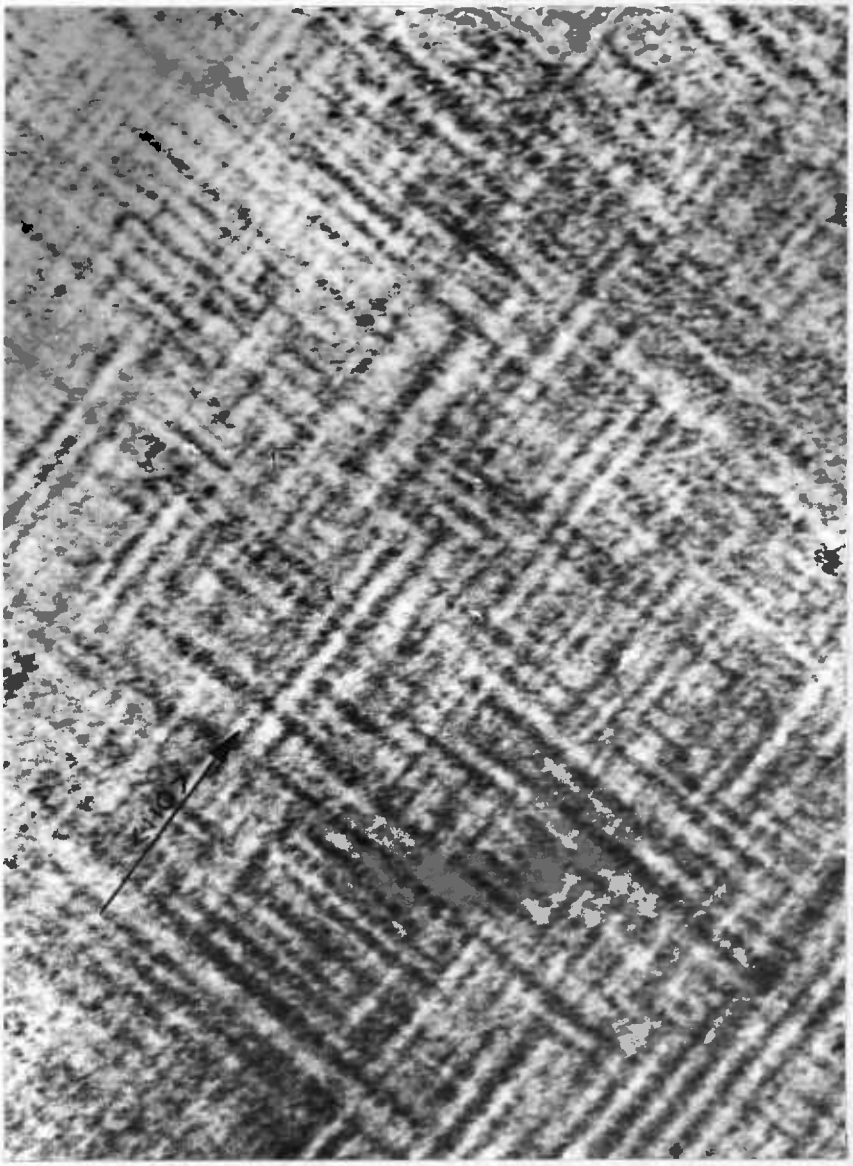


Fig.15. A 57%Mn-43%Cu alloy, solution treated for 2 hours at 850°C and furnace cooled. Shows the striated structure known as "basket-weave" or "tweed". A fine substructure consisting of closely-spaced streaks lies within the striations. Approx. x 180,000.

Fig. 16.

Fig. 17.

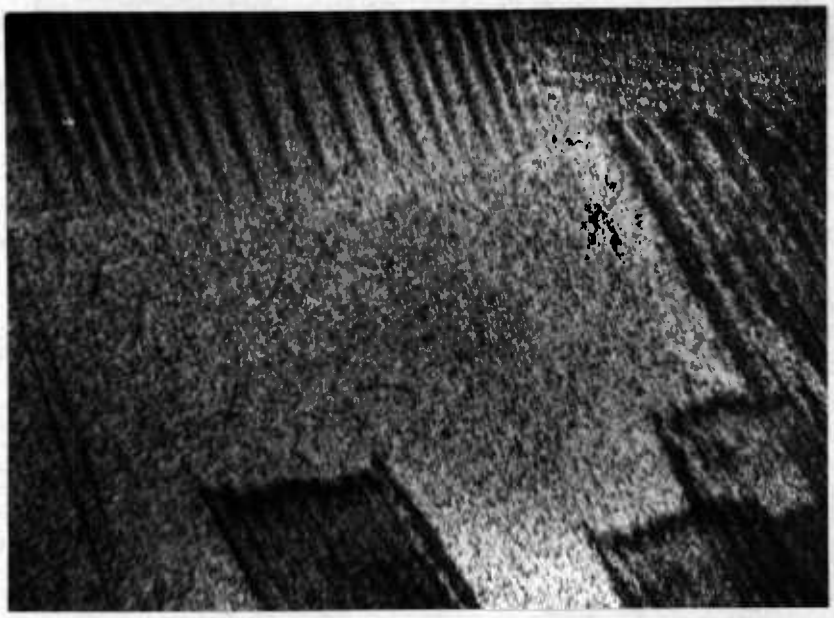


Fig.16. A 57%Mn-43%Cu alloy, solution treated for 2 hours at 850°C, water quenched and heat treated for 6 hours at 400°C. Shows the unidirectional component of the tweed pattern with a $\{111\}$ type reflection operating. x 42,000.

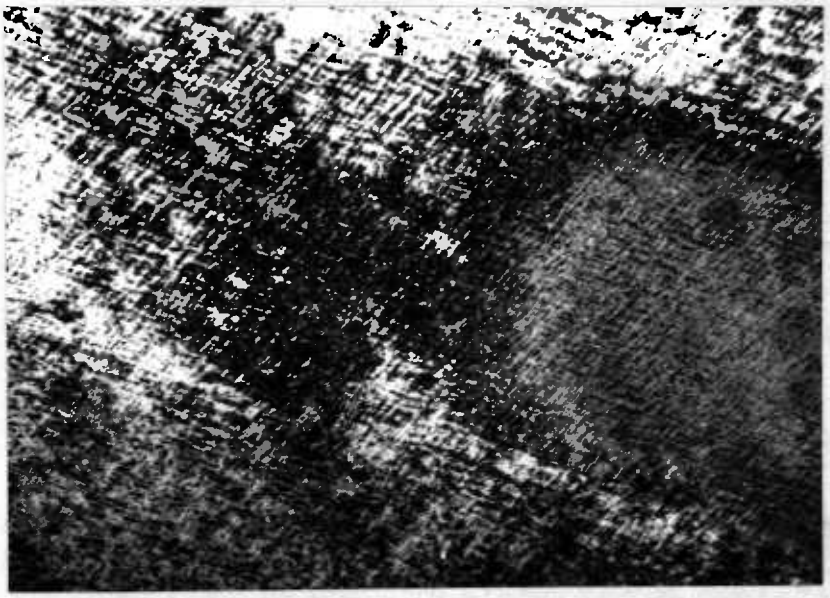


Fig.17. A 57%Mn-43%Cu alloy, solution treated for 2 hours at 850°C, water quenched and heat treated for 6 hours at 400°C. Shows tweed striations lying in two directions with a $\{220\}$ reflection operating. x 59,000.

particles were not removed during the preparation of the foil, existing microtwin movement was prevented at the particles, Fig.14, although initiation of new microtwins at αMn particles could also occur.

3.1.4 Tweed and related structures.

3.1.4.1 Diffraction contrast associated with alloys containing 57% or more Mn.

A rather indistinct structure became evident in samples aged for longer than 2 hours at 400°C which was difficult to distinguish from polishing irregularities. On occasion, a similar diffuse mottling was observed in quenched alloys, but in this case little reliability could be placed on the evidence for its existence. In those samples of the 57%Mn alloy which were given an ageing heat treatment at 450°C, others which were quenched to 450°C and then heat treated and some that were furnace cooled from the solution treatment temperature, the definition of the mottling in diffraction contrast improved considerably exhibiting a striated structure, Fig. 15. This particular form of diffraction contrast has been observed during pre-precipitation in certain alloy systems, especially Cu-Be[40] and has been referred to as a basket-weave or tweed structure. The effect appeared with greatest clarity near Bragg contrast fringes, which is an effect common to small coherent precipitate particles.

Analysis of a number of micrographs and associated diffraction patterns indicated that the striations lay in <110> directions. At high magnifications an internal structure could be discerned consisting of alternately dark and light streaks lying parallel to <100> directions. Attempts at analysis using tilted dark field techniques did not prove very successful, although it was established that when a {111} reflection was operating in bright field then tweed pattern striations were observed in only one direction, Fig. 16; when using a {220} reflection, striations in two directions at 60° to each other were common, Fig. 17 and when using a {200} reflection, striations in two directions at 90°

Fig. 18.



Fig.18. A 57%Mn-43%Cu alloy, solution treated for 2 hours at 850°C, water quenched and heat treated for 1½ hours at 450°C. Shows the propagation of fine microtwins along the directions of the tweed striations. x 57,000.

Fig. 19.

Fig. 20.



Fig.19. A 57%Mn-43%Cu alloy, solution treated for 2 hours at 850°C, water quenched and heat treated for 6 hours at 400°C. Shows microtwins and tweed pattern prior to the heating of the sample within the electron microscope. x 29,000.

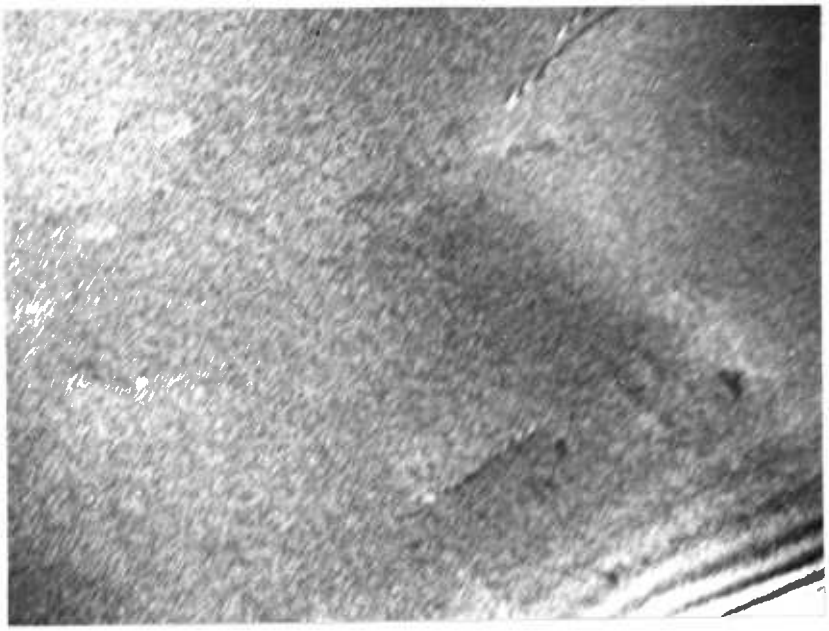


Fig.20. Same area as in Fig.19 showing the microstructure at a temperature above the fcc/fct transformation temperature. x 29,000.

to each other were found, Fig. 15.

When examining areas exhibiting tweed pattern in clear contrast, there was invariably considerable movement caused by the heating effect of the electron beam. This movement took the form of microtwin propagation along the striations in the tweed pattern, sometimes on an extremely fine scale. In many instances the microtwins were so small and uniform in distribution, that it was difficult to distinguish them from areas of tweed in which no propagation of microtwins had taken place, Fig. 18. During the propagation of these small microtwins the substructure continuously flashed in and out of contrast.

It was not clear at this stage if the tweed pattern was associated with matrix coherency strains due to the aggregation of atoms or if it was symptomatic of the internal strains created by the fcc/fct martensitic transformation. Samples of the 57%Mn alloy were therefore heated above the fcc/fct transformation temperature in a Siemens heating stage. The microtwins and tweed pattern which were present at room temperature, Fig. 19 disappeared leaving a mottled structure, Fig. 20 which did not possess the striated structure of the tweed pattern but may have arisen from the fine internal substructure within the tweed striations, which is often masked by the superimposed diffraction contrast of the striations.

At a later stage in the research programme an explanation of the tweed structure proved desirable; in particular there was a need to establish if Cu atoms or Mn atoms were aggregating together. Alloys richer in Cu were therefore examined, especially in the heat treated condition, when it was known from previously published work[10] that the fct structure would not develop.

3.1.4.2 Diffraction contrast associated with alloys containing 50% or less Mn.

Alloys containing 50, 40 and 30%Mn were solution treated for 3 days at 800°C, quenched to 450°C and maintained at that temperature for 16 hours before water quenching; these were conditions

Fig. 21.

Fig. 22.

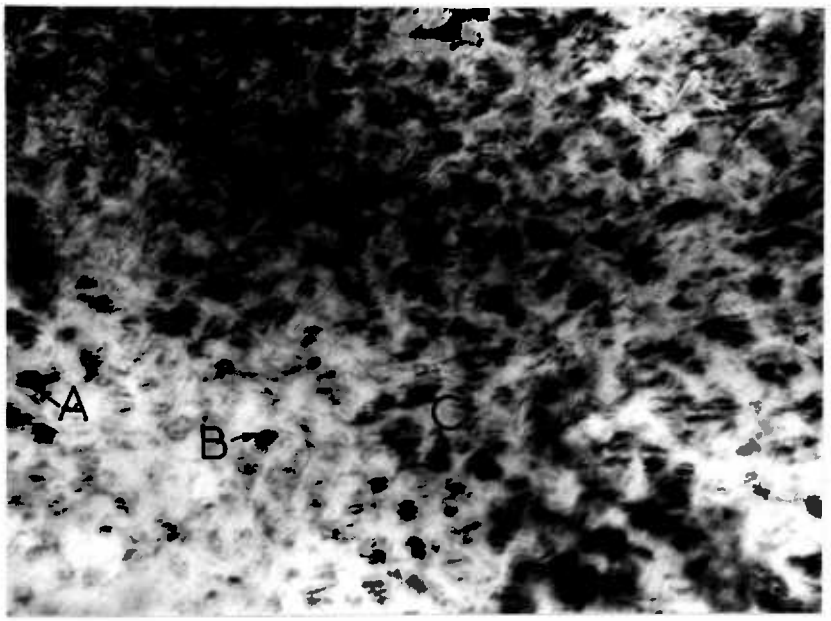


Fig.21. A 50%Mn-50%Cu alloy, solution treated for 84 hours at 800°C, quenched to 450°C and held at this temperature for 16 hours before water quenching. Shows evidence for the pre-precipitation of a second phase at A,B and C. x 128,000.



Fig.22. Same area as in Fig. 21, using a {200} dark-field reflection. Shows asymmetrical images at D, E and F. x 128,000.

Fig. 23.

Fig. 24.

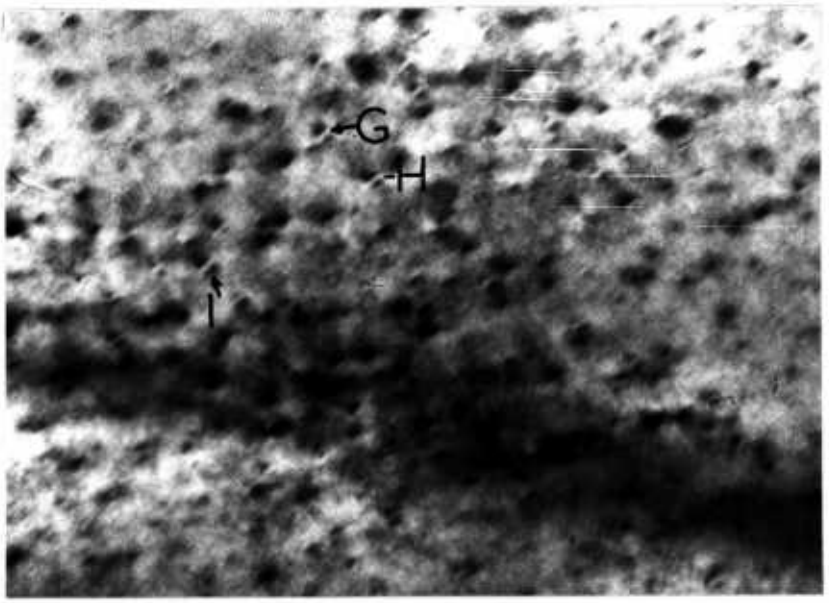


Fig.23. A 40%Mn-60%Cu alloy, solution treated for 84 hours at 800°C, quenched to 450°C and held at this temperature for 16 hours before water quenching. Shows evidence for the pre-precipitation of a second phase at G,H and I. x 173,000.



Fig.24. A 30%Mn-70%Cu alloy, solution treated for 84 hours at 800°C, quenched to 450°C and held at this temperature for 16 hours before water quenching. Shows evidence for the pre-precipitation of a second phase in the Bragg contrast fringes. x 69,000.

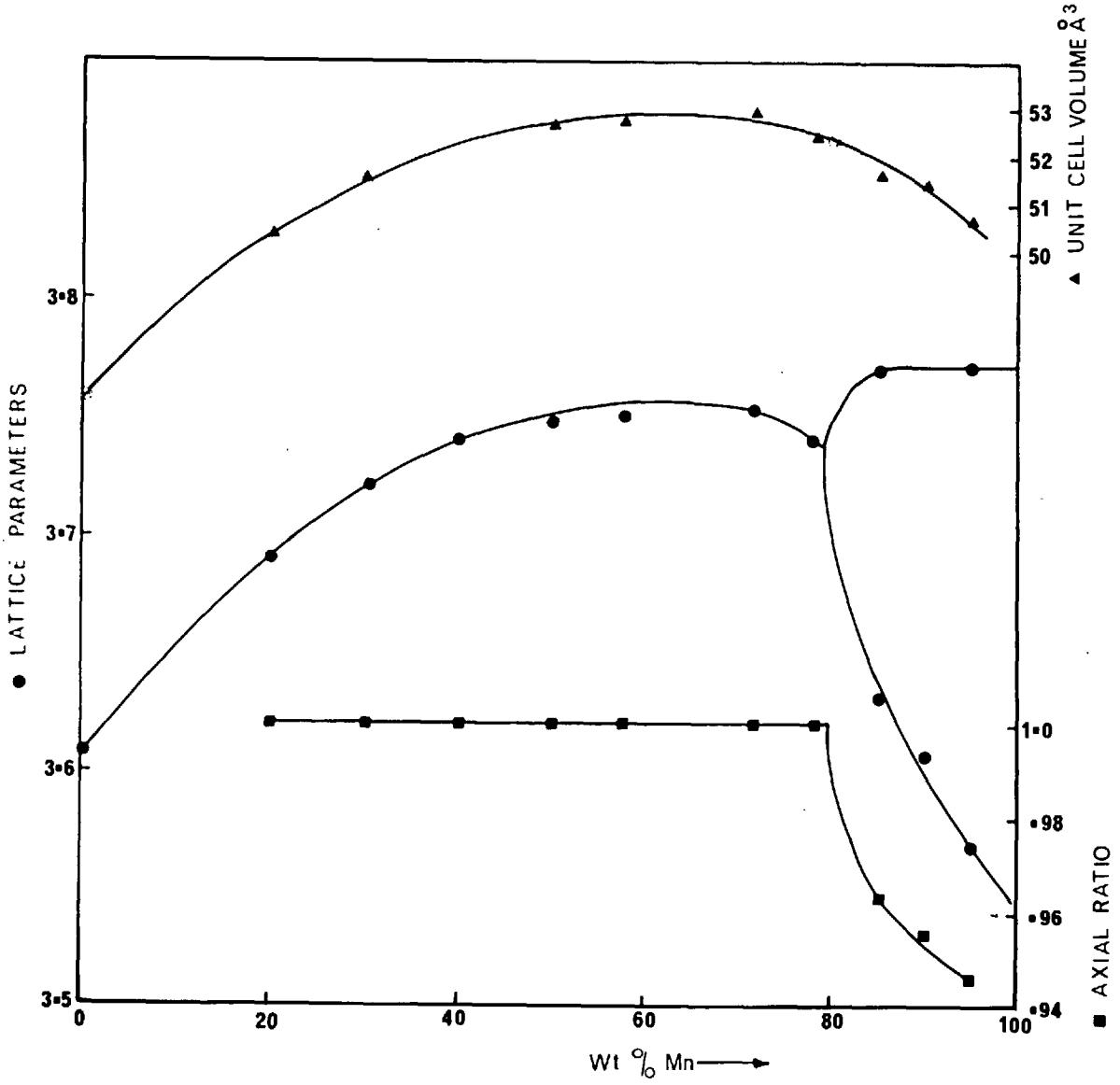


Fig. 25 Unit cell parameters for Mn–Cu alloys measured at room temperature.

that were known to produce the tweed structure in clear contrast in higher Mn concentration alloys. Interpretation of the diffraction contrast involved the use of tilted dark field microscopy at very high magnifications. The total angle of tilt is very limited in the Seimens Elmiscop 1A and the tilting operation, which is mechanically operated, usually results in large shifts in the illumination across the sample. In Mn-rich alloys the technique is therefore restricted to the use of {111} and {200} reflections and because of the time taken to realign the beam, the sample becomes contaminated with C. The results obtained have been lacking in quality and not completely unambiguous in interpretation.

A bright field micrograph taken from the 50%Mn alloy exhibited diffraction contrast typical of small aggregations of a second phase, see for instance A, B and C, Fig. 21. Large asymmetrical images which result from the relaxation of strain fields associated with particles near to the surface of the foil are shown at D, E and F in Fig. 22, which is a dark field image of the same area. These images are important in determining the species of atom aggregating and are discussed further in Section 4.5. The diffraction contrast associated with the 50%Mn alloy was in general mottled and confused and in parts reminiscent of the tweed pattern, although X-ray results, even at liquid nitrogen temperatures, confirmed that the structure remained fcc.

The second phase particles were more clearly defined but fewer in number in the 40%Mn alloy, for instance G, H and I, Fig. 23 and this trend continued in the 30%Mn alloy, Fig. 24. In neither case were satisfactory high resolution dark field micrographs obtained.

3.2 X-RAY DIFFRACTION RESULTS.

In view of the doubt about the heterogeneity of the samples used by previous workers, it was thought worthwhile to plot the change in lattice parameter with Mn concentration for all the alloys used in the programme. In Fig. 25 the unit cell parameters,

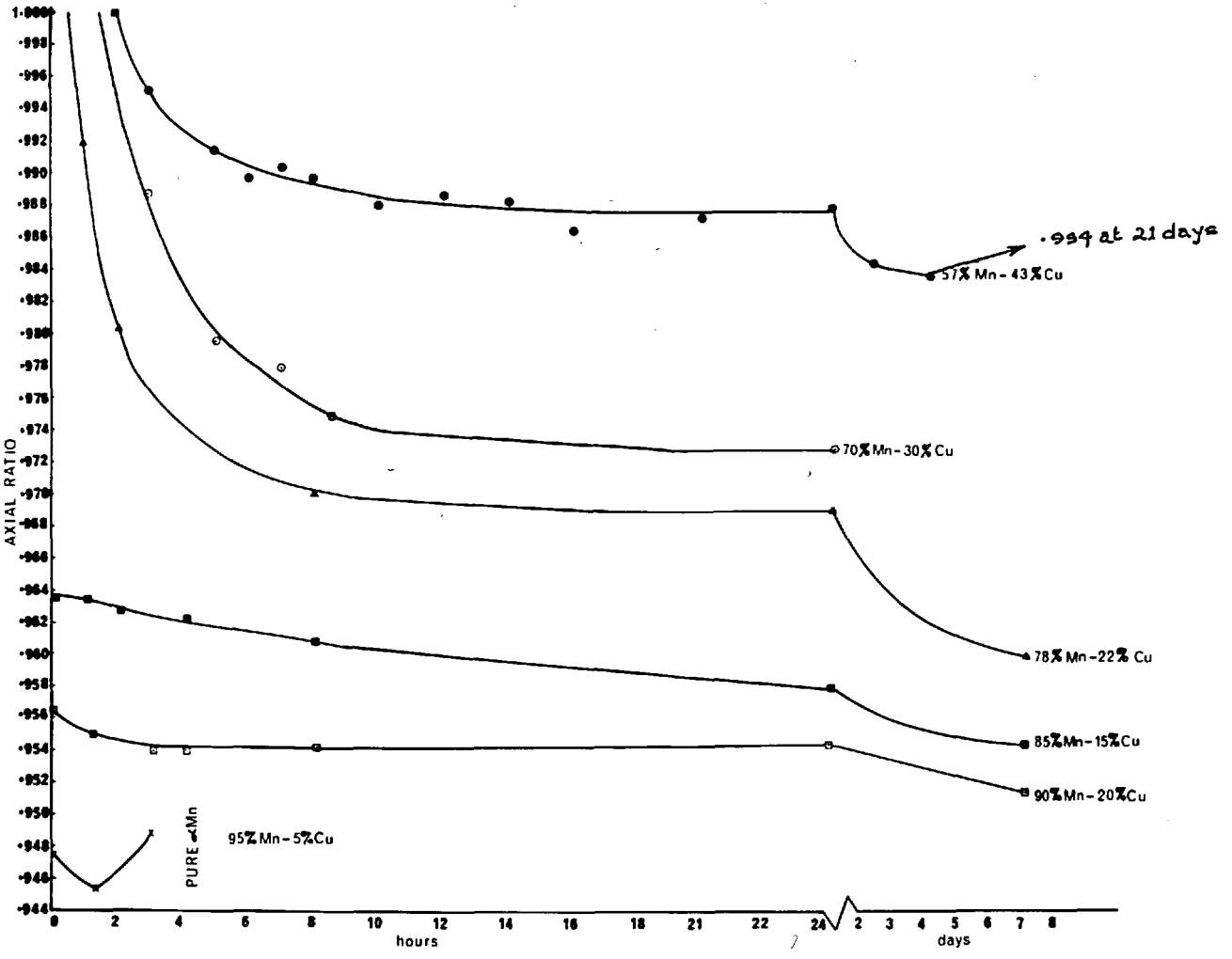


Fig. 26 Change in axial ratio, measured at room temperature, with the heat treatment time at 400 °C given to various Mn—Cu alloys.

the unit cell volume and the axial ratio are all plotted against Mn concentration. Good agreement was obtained with previously published work[41] for alloys containing less than 50%Mn but there was no agreement at Mn concentrations higher than this because of the use of furnace cooled samples by other workers[1,41] resulting in an indeterminate heat treatment. The change in the room temperature axial ratio with ageing heat treatment time at 400°C has been recorded for various Mn alloys in Fig. 26. It can be seen that the change in axial ratio with heat treatment time becomes progressively less with increasing Mn content, although the axial ratio value is lower with increasing Mn contents. The 95%Mn alloy very quickly transformed into αMn at 400°C and in view of the absence of γMn reflections in the transformed state, there would appear to be some doubt concerning the published limit of solid solubility of Cu in αMn[1] which was shown in Fig. 1.

There were departures from the expected X-ray reflection intensities even on different areas of the same sample and different surface finishes affected the reflection intensities in an irregular manner; this problem was only partially resolved later in the programme. In those cases where a good peak to background ratio was established, the correct intensity ratio of the (200,020) : (002) and the (220) : (022,202) reflections was found as described in Section 2.4.2.

Prior to the precipitation of αMn within the grains, the X-ray reflections correspond to a single phase structure. At longer times accurate lattice parameter measurements proved impossible because of the considerable overlapping of reflections. For instance, over an angular range of 3° in which the {200} fcc peak splits into the (200,020) and (002), in the over-aged condition, five reflections appear corresponding to {332} αMn, {422} αMn, {200} γMn (Cu-rich), (200,020) γMn (Mn-rich), and (002) γMn (Mn-rich).

Basinski and Christian[9] have already indicated the manner in which the axial ratio of quenched alloys, containing more than 80%Mn, changes with the temperature of measurement. In view of the

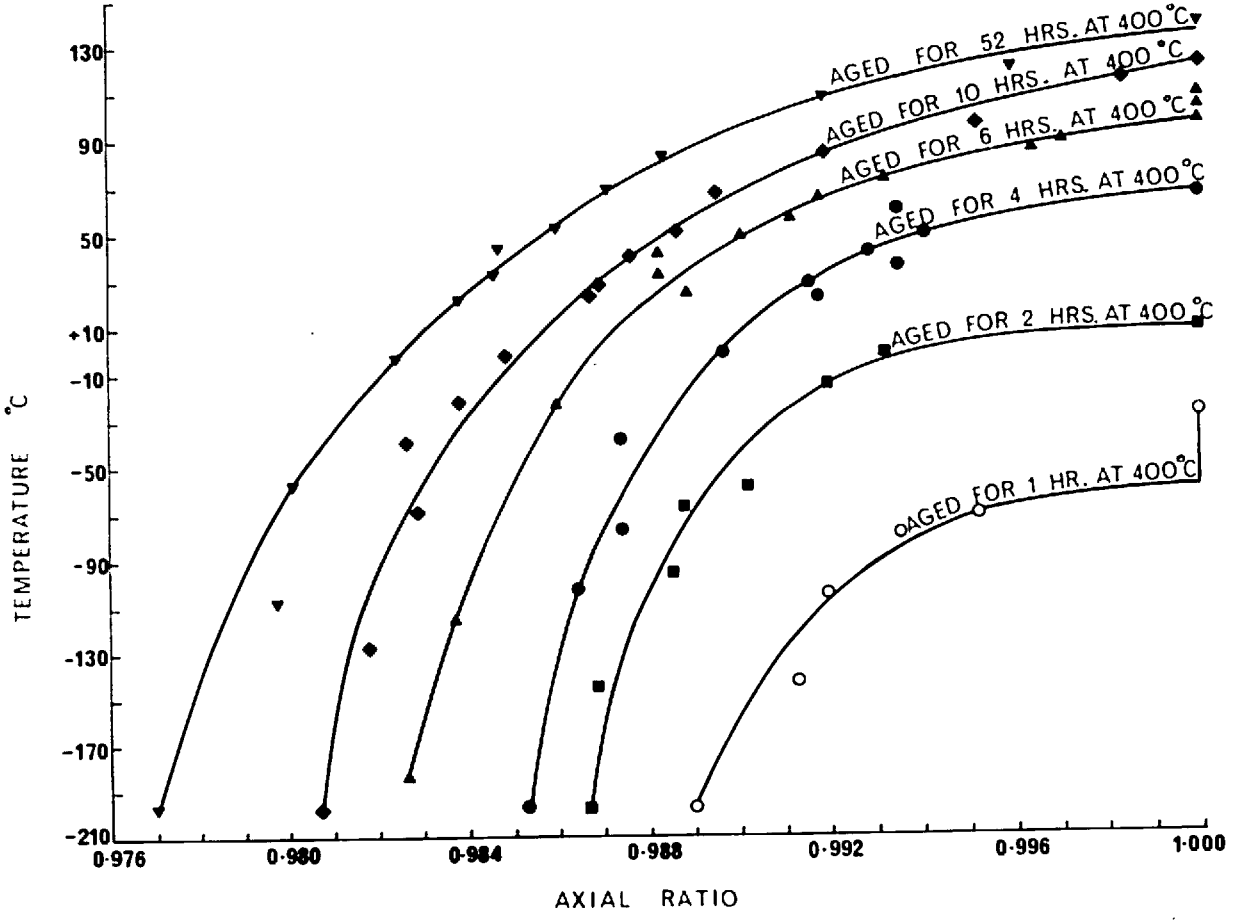


Fig. 27 The effect of temperature on the axial ratio of a number of heat treated samples of a solution treated 57% Mn — 43% Cu alloy.

development of the fct structure in aged alloys containing less than 80%Mn, it was of obvious interest to compare the change in axial ratio with temperature exhibited by a 57%Mn alloy given progressively longer heat treatments at 400°C, Fig. 27. The fcc/fct transformation temperature can be seen to increase with increasing ageing heat treatment time up to about 52 hours; it then progressively decreases.

The development of damping properties in samples which had been given an insufficient heat treatment at 400°C to develop the fct structure at room temperature, required an explanation later in the programme. Samples of the 57%Mn alloy which had been heat treated for ½, 1 and 2 hours and which were known to be fcc at room temperature, were therefore stressed using the jig described in Section 2.4.3. The samples aged for 1 and 2 hours exhibited reflections arising from the fct structure on the application of stress and maintained, within experimental error, a constant axial ratio to fracture. Stress was found to exert no discernible effect on samples aged for longer times when the experiment was conducted at room temperature.

In order to check the possibility that the tweed pattern observed by electron microscopy was indicative of an atomic ordering process, Debye-Scherrer photographs were obtained from a 57%Mn alloy, quenched and aged for 2 hours at 450°C, and also another quenched to 450°C and aged for 2 hours; conditions which were known to give a clearly defined tweed pattern. An exposure of 72 hours using FeKα radiation failed to reveal any superlattice reflections. It is likely that the superlattice reflections, if present, would have been of sufficient intensity to allow detection as outlined in Section 2.4.1.2 and Table 2.

3.3 NEUTRON DIFFRACTION RESULTS.

Antiferromagnetic ordering of the type associated with Mn alloys containing more than 80%Mn is associated with the appearance of {110} and {210} superlattice reflections. These reflections were found in neutron diffraction traces from the 57%Mn alloy

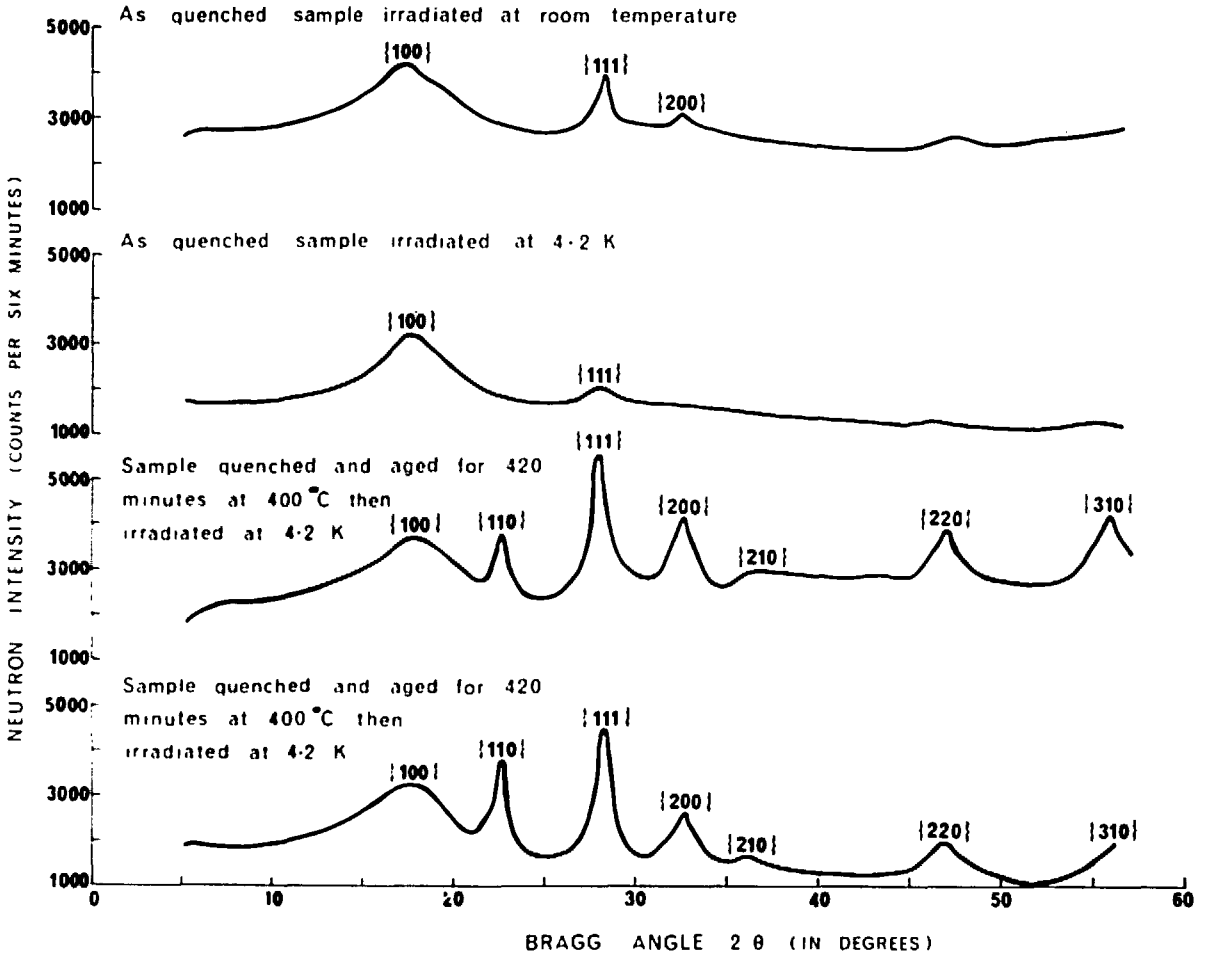


Fig. 28 Neutron diffraction traces taken at room temperature and 4·2 K from two samples of a 57 % Mn – 43 % Cu alloy. Both samples have been solution treated for 4 weeks at 850 °C and water quenched. One sample has been given a further heat treatment of 7 hours at 400 °C.

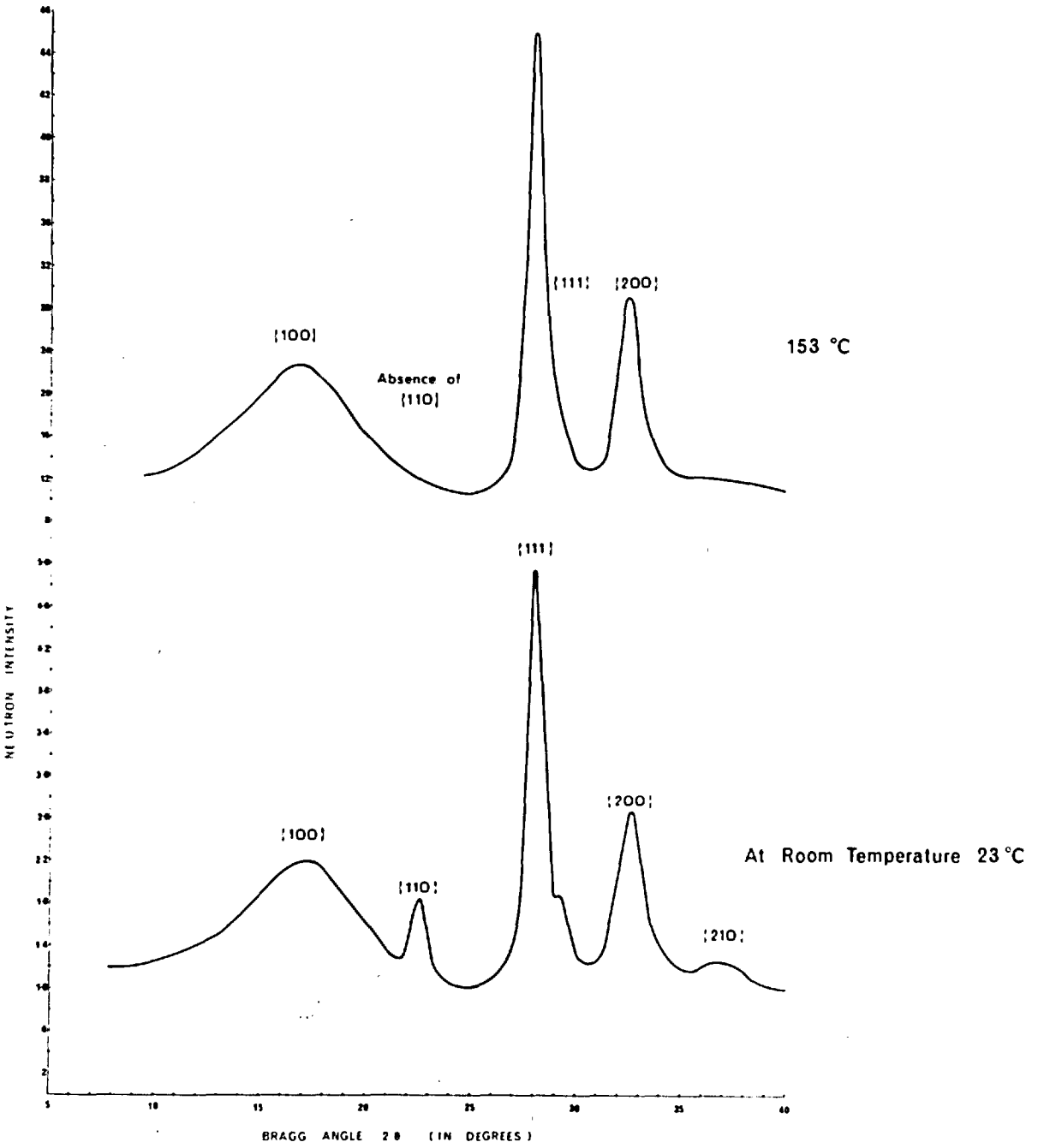


Fig. 29 A 70 % Mn – 30 % Cu alloy, solution treated for 4 weeks at 850 °C, water quenched and heat treated for 2 hours at 400 °C. Neutron diffraction traces taken at 23 °C and 153 °C

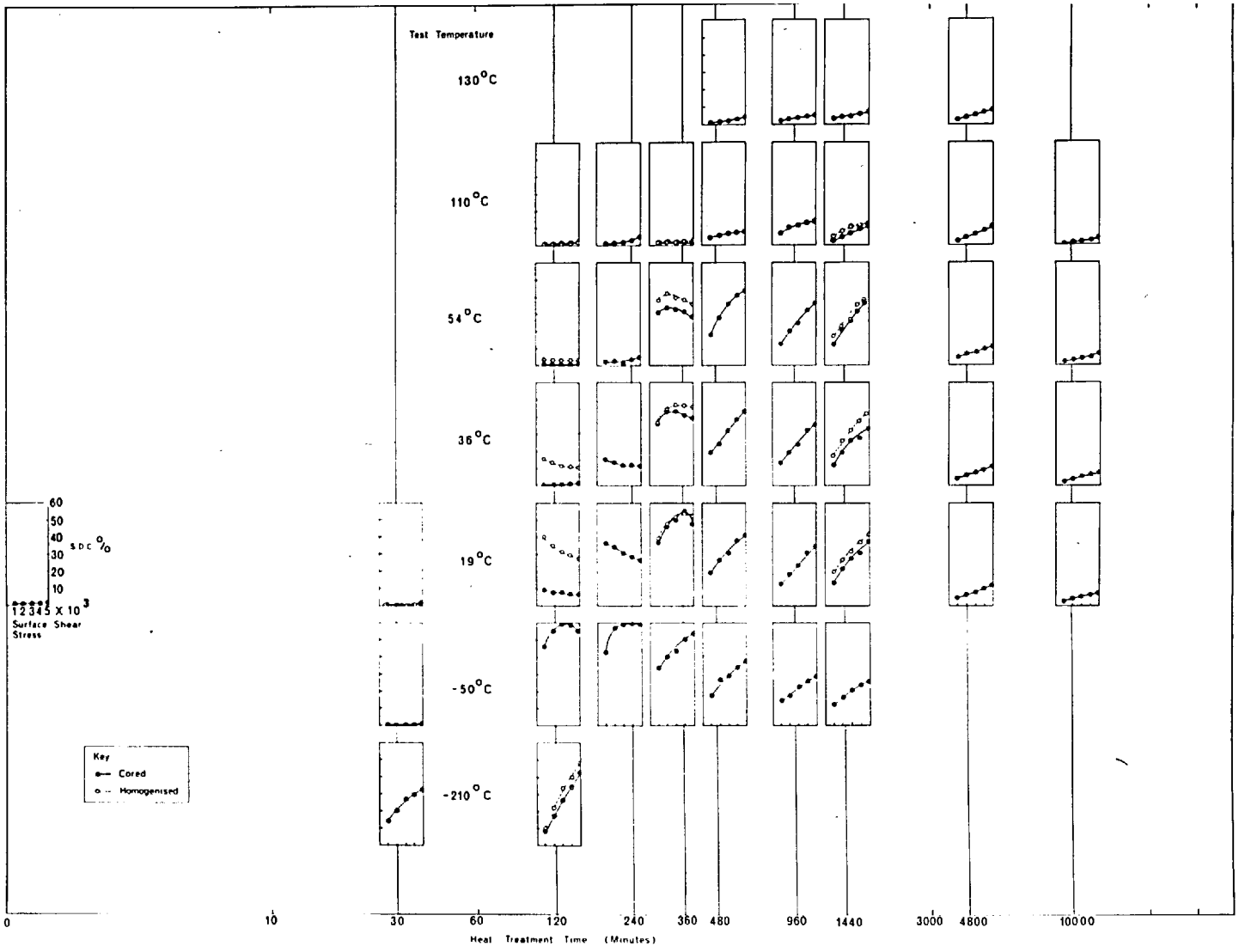


Fig. 30 The temperature and stress - dependence of the damping capacity of a 60 % Mn — 40 % Cu alloy. Samples have been either rolled or solution treated for 28 days at 850°C, water quenched and then heat treated for various times at 400°C

which had been given an ageing heat treatment of 7 hours at 400°C, Fig. 28 proving conclusively that antiferromagnetism is associated with the fct structure. The significance of the broad {100} reflection, present both in quenched and aged samples and the similarity between the half-peak widths of fundamental and superlattice reflections will be discussed later.

In Section 1,4 a null-matrix alloy containing 68%Mn was mentioned and its behaviour described. A 70%Mn alloy was already available and it was anticipated that this alloy would be sufficiently close in composition to the null matrix alloy to attenuate the fundamental reflections and leave the magnetic superlattice reflections. It was the intention then to follow the change in intensity of the {110} magnetic peak with temperature, determine the Néel temperature and compare this with the fcc/fct transformation temperature which was determined by X-ray means. Unfortunately, the fundamental reflections did appear, Fig. 29, and the neutron intensity of the {110} reflection obtained from the 70%Mn aged for 2 hours at 400°C, although clearly identifiable, rapidly decreased in intensity as the temperature increased. The experiment did however provide confirmation of the earlier results on the 57%Mn alloy and indicated a Néel temperature of less than 153°C for the 70%Mn alloy.

3.4 DAMPING CAPACITY MEASUREMENTS.

The damping results which are summarised in Figs. 30 to 33 are all due to Mr. R.J. Goodwin[31] and are included at this point for comparison purposes and because they logically follow on from the structural studies on the same material given the same heat treatments. Fig. 30 shows the variation in specific damping capacity with surface shear stress at different temperatures and after a variety of heat treatments. This composite form of graph is convenient for illustrating that

a) there is a change from decreasing to increasing damping capacity with stress as the isothermal

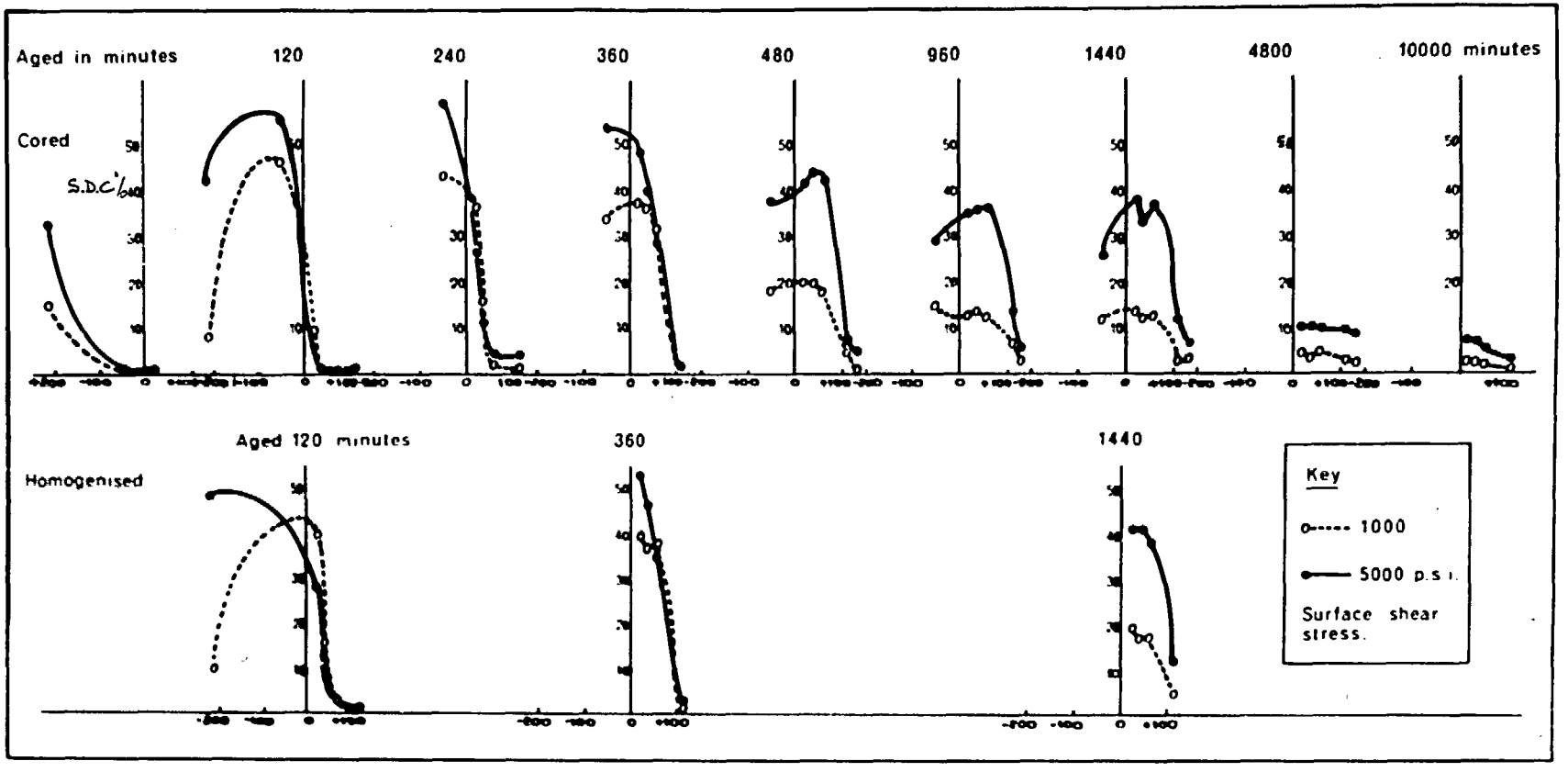


Fig. 31. The effect of temperature on the damping capacity of a 60 % Mn — 40 % Cu alloy. Samples have been either rolled or solution treated for 28 days at 850 °C, water quenched and then heat treated for various times at 400 °C. Damping capacities have been measured at two surface shear stress levels.

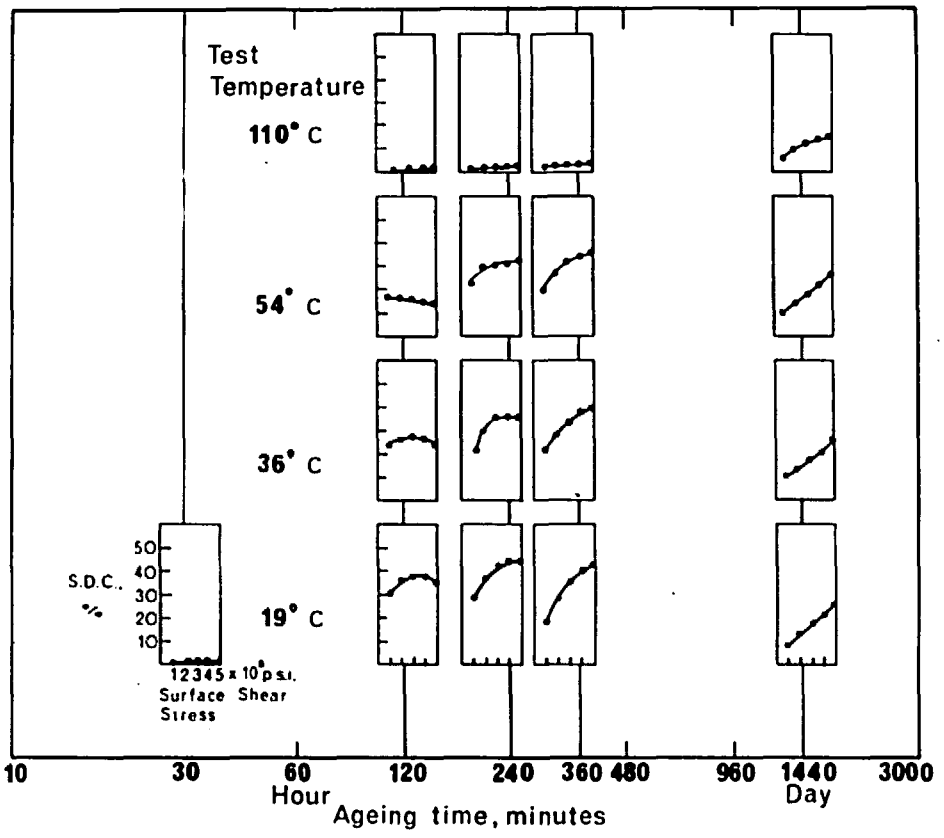


Fig. 32 The temperature and stress dependence of the damping capacity of a 70 % Mn – 30 % Cu alloy. Samples have been rolled, solution treated for 2 hours at 800 °C, water quenched and heat treated for various times at 400 °C.

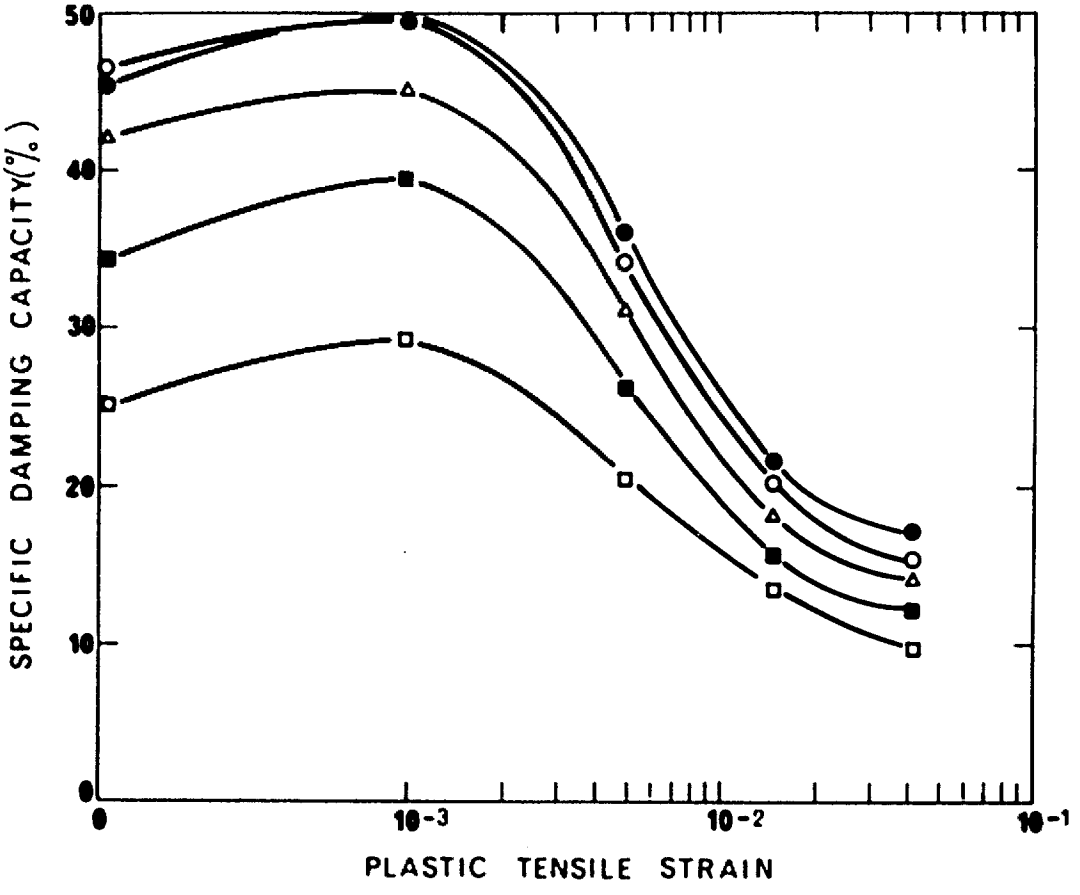


Fig. 33 The effect of plastic strain on the damping properties of a 60 % Mn — 40 % Cu alloy which has been solution treated for 2 hours at 800 °C, water quenched and heat treated for 6 hours at 400 °C.

ageing time is increased.

b) longer ageing times are required to reach the peak damping level at higher ambient temperaturesand,

c) the change occurs after shorter times at higher ageing temperatures or higher Mn contents.

Fig. 31 shows the fall in specific damping capacity at surface shear stress levels of 1,000 and 5,000 p.s.i. as the test temperature is increased, Fig. 32 relates to the 70%Mn alloy and is an equivalent construction to that shown in Fig. 30 for the 60%Mn alloy. Fig. 32 shows that the high damping properties are established at shorter ageing times and the levels of damping capacity are in general less than that found for the 60%Mn alloy. Fig. 33 shows the effect of increasing plastic strain on the damping properties of a 60%Mn alloy which has been given an ageing heat treatment of 6 hours at 400^{o}C to develop the maximum damping properties.

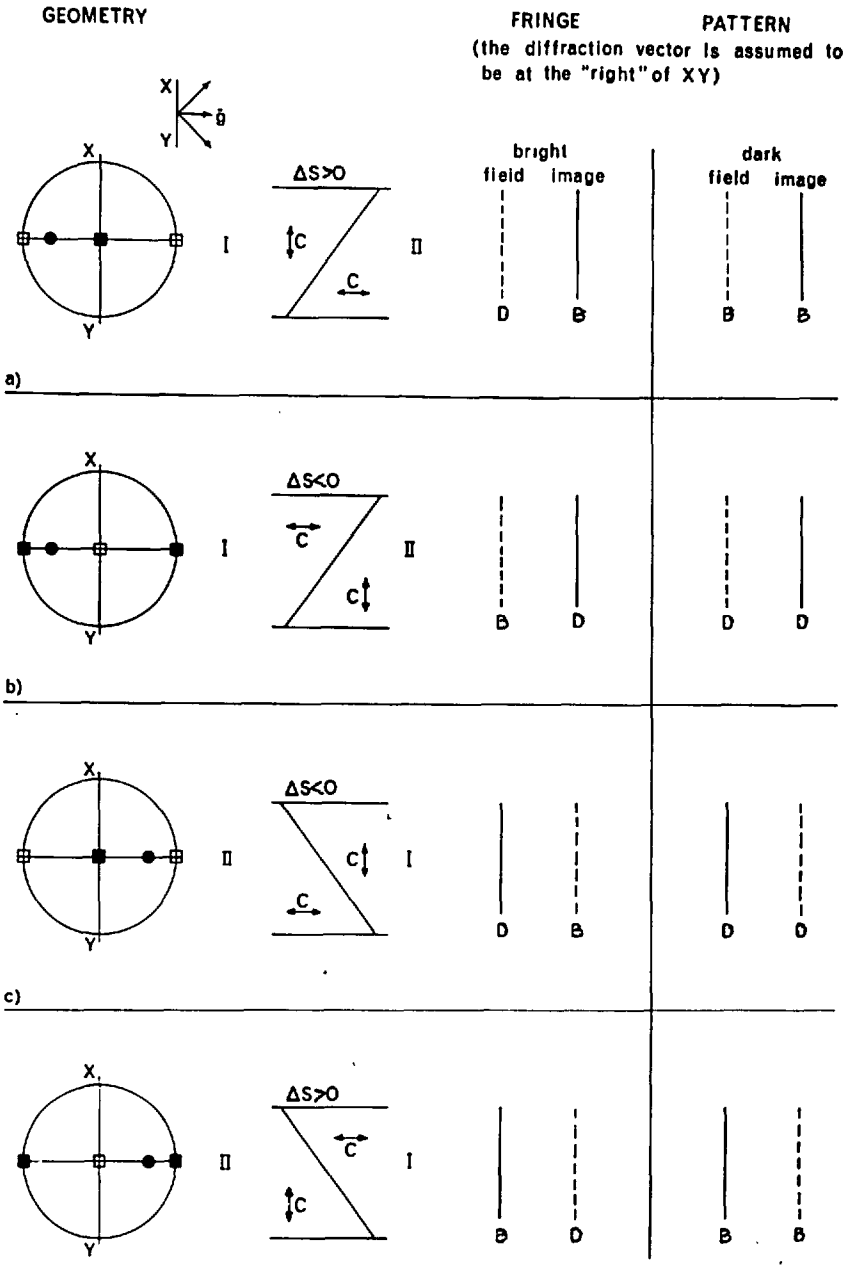


Fig. 34 An analysis of the fringe pattern in bright and dark field images of a microtwin boundary due to Gevers etal.[35]
All possible configurations for [110] boundaries are considered. The top fringe is indicated as a full line and the bottom fringe by means of a dotted line. The nature of these fringes is indicated by means of the letters B (bright) and D (dark) In all cases the diffraction vector is at the right of the line XY

- Boundary normal plotted on upper hemisphere;
- Direction of fourfold axis for part I
- Direction of fourfold axis for part II

Fig. 35.

Fig. 36.

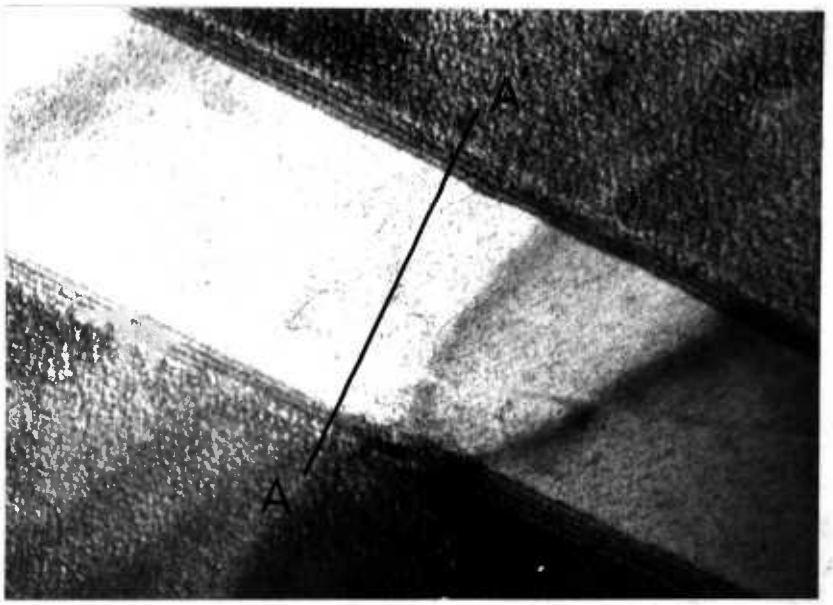


Fig.35. A 57%Mn-43%Cu alloy, solution treated for 2 hours at 850°C, water quenched and heat treated for 6 hours at 400°C. Shows the fringe patterns associated with widely separated microtwin boundaries. x 39.000.

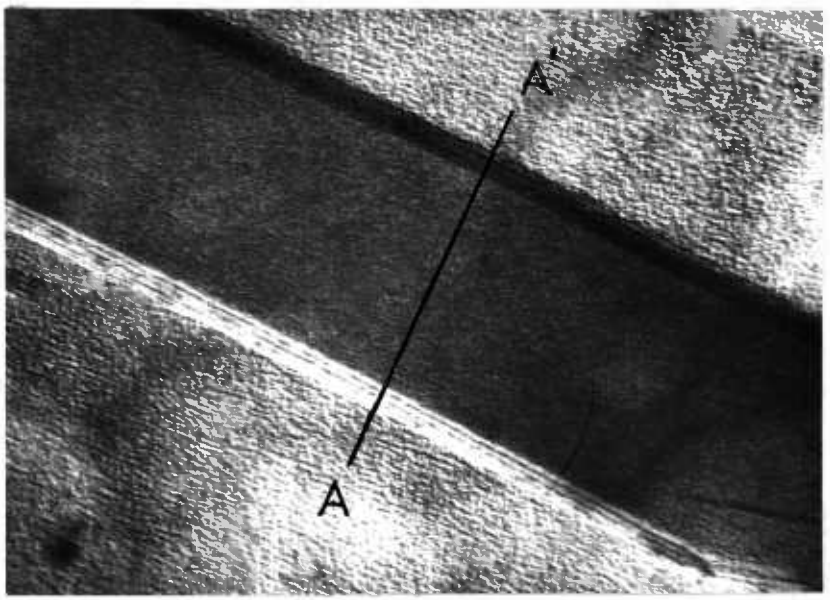
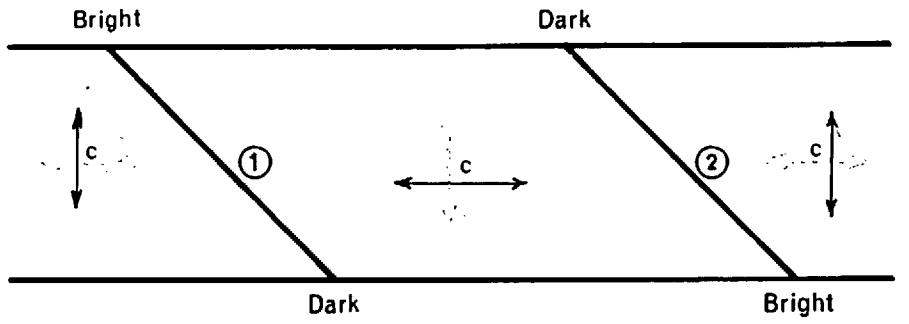


Fig.36. Same area as in Fig. 35 using a {200} dark-field reflection. x 39,000.

Fig. 37 Schematic diagram showing the lattice orientation relationships and the sense of slope of the boundaries shown in Fig. 35 .

Section AA′ from Fig. (35)

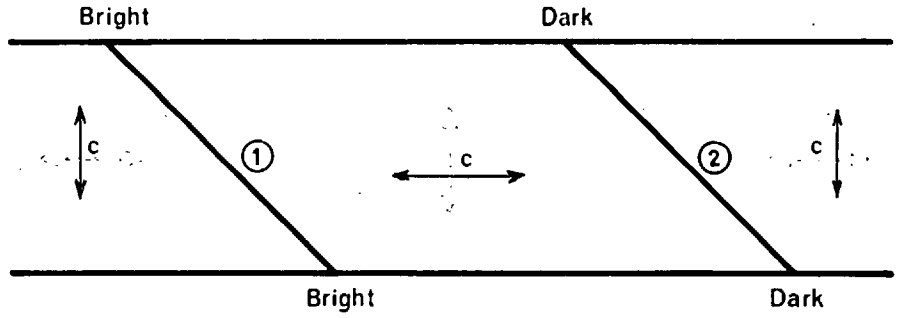


Boundary ① corresponds to the bright field image of case (d) in Fig. 34

Boundary ② corresponds to the bright field image of case (c) in Fig. 34

Fig. 38 Schematic diagram showing the lattice orientation relationships and the sense of slope of the boudaries shown in Fig. 36

Section AA′ from Fig. (36)



Boundary ① corresponds to the dark field image of case (d) in Fig. 34

Boundary ② corresponds to the dark field image of case (c) in Fig. 34

By examination of the nature of the first and last fringes of the boundary in bright and dark field with known diffraction vector "g" it is possible to determine the top and bottom of the foil and the "c" directions or directions of the magnetic spin vectors.

CHAPTER 4.

DISCUSSION ON Mn-Cu ALLOYS.

4.1 ELECTRON MICROSCOPY.

The internal boundaries which are observed by electron microscopy have so far been referred to as microtwins, although this nomenclature has not yet been justified. The lack of movement in the electron diffraction spots when traversing across a microtwin boundary simply indicates a very small orientation change across the boundary.

The axes of the tetragonal cells lie almost at 90° to each other and both lie at an angle of nearly 45° to the $\{110\}$ boundary wall. The relatively small angle, which is about 1° between the 'a' axis on one side of the boundary and the 'c' axis on the other, gives rise to the microtwin nomenclature.

The theoretical analysis of the diffraction contrast exhibited by microtwin boundaries has been calculated in considerable detail based on an examination of a number of materials exhibiting this type of structure[34-38]. The analysis indicates that, if no overlapping of the microtwin boundaries occurs when viewed from the direction of the electron beam, then from a knowledge of the nature of the first and last fringe in light and dark field, it is possible to determine the top and bottom of the foil, the sense of slope of the boundary and the directions of the 'c' axis on either side of the boundary. The analysis, summarised in Fig. 34, is due to Gevers et al[34] and when applied to the boundaries shown in Fig. 35 which is a light field micrograph and Fig. 36 which is a micrograph of the same area taken under dark field conditons, then the only possible sense of slope of the boundaries as well as the orientation of the fct unit cell is shown in schematic form in Figs. 37 and 38. If overlapping occurs as it does in many cases, the detailed analysis of the fringes is more difficult, a simple test however, can be utilised[36]. When traversing across any microtwin the fringes should be symmetrical in light field and asymmetrical

in dark field. In this way the fringes initiated at dislocations in Figs. 7 and 8 can each be shown to arise from two overlapping boundaries of the associated microtwin.

When single boundaries alone are considered, the only possible doubt about the nature of the boundary lies in the possible confusion between microtwins and stacking faults which exhibit the same type of periodic diffraction contrast. Single microtwin boundaries show asymmetrical fringes in light field diffraction conditions whereas stacking faults show symmetrical fringes. In view of the agreement between the experimental results and the theoretical treatments[34-38], it is justifiable to continue the use of the term microtwin throughout the thesis.

Microtwins have so far been identified with different classes of materials all involving a slight distortion of the cubic unit cell, although it is not always known why the distortion occurs. Some of the reasons behind the lattice distortion can be found in ferroelectric interactions, e.g. $BaTiO_3$(42) antiferromagnetic interactions e.g. CoO[43], NiO[44] impurity atoms lying in interstitial sites, e.g. C in Va[45], ordering of certain solid solutions, e.g. CuAu[25], CoPt[26] and superconducting alloys, e.g. V_3Si[46], Nb_3Sn[47].

4.2 NEUTRON DIFFRACTION.

The neutron diffraction work was undertaken as a consequence of the electron microscope and X-ray results, because of the very strong indications that antiferromagnetism was responsible for the martensitic transformation in alloys containing between 50 and 80%Mn which had been given an ageing heat treatment at 400°C. A previous publication[2] based on magnetic susceptibility measurements clearly propounds that these particular alloys and heat treatments, result in paramagnetic and not antiferromagnetic behaviour. The interpretation placed upon these magnetic susceptibility results must be in error because the neutron diffraction traces of the aged 57% and 70%Mn alloys are the same as those observed by Bacon[12] for the quenched 82%Mn

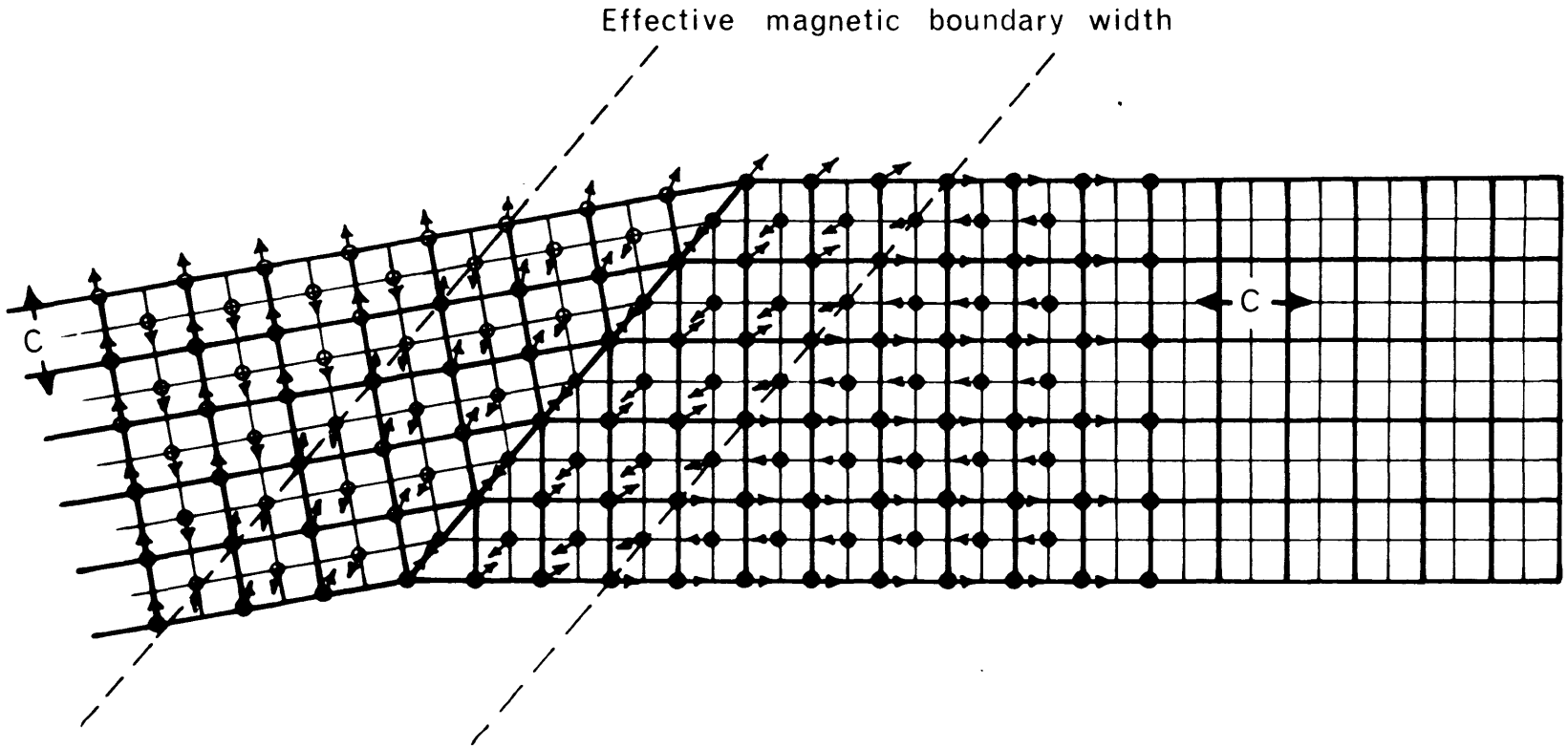


Fig. 39 Schematic representation of regions bounding a microtwin or an antiferromagnetic domain boundary.

alloy and can only be explained[11] by the antiferromagnetic structure shown in Fig. 2.

The traces shown in Figs 28 and 29 show that there is little difference in half-peak widths between fundamental and superlattice reflections and there is little difference between the half-peak widths of fundamental reflections above and below the Néel temperature, although there is a considerable increase in intensity, including an increase in peak widths after the ageing heat treatment, Fig. 28. Scherrer broadening[48] of the superlattice reflections alone would indicate very small volumes of magnetically coherent material.

As no appreciable broadening of the {110} peak occurs, it is likely that the magnetically coherent regions can be correlated with the volumes of material having specific 'c' axis orientations; these regions are the microtwins and are bounded by microtwin boundaries. The microtwin boundaries can therefore also be considered as antiferromagnetic domain boundaries and by analogy with ferromagnetic materials probably have a magnetic structure of the kind shown in Fig. 39.

The presence of the very broad peak at the {100} angular position will be discussed in Section 4.5 as this has been the subject of much controversy in the scientific press and probably relates to the tweed pattern observed by electron microscopy.

It seems certain that there is a close relationship between the development of antiferromagnetic properties and the fcc/fct martensitic transformation structure. There were strong indications of such a link from the work of Basinski and Christian[9] and Bacon et al[12] who showed that the Néel temperature was very similar to the fcc/fct transformation temperature for alloys containing more than 70%Mn, Fig. 1. The experimental work described in this thesis now links antiferromagnetic behaviour with the fcc/fct martensitic transformation for those alloys containing between 50 and 70%Mn in the quenched and heat treated condition, even though the

nominal Mn concentration is insufficient to develop antiferromagnetic properties. Apart from a rather ill-defined temperature range between the Néel temperature and the fcc/fct transformation temperature, those Mn-Cu alloys which are antiferromagnetic are fct and vice-versa, those alloys which are fct exhibit antiferromagnetic behaviour.

It now remains to establish which of these phenomena develops first. It has already been mentioned that very similar martensitic transformations have already been observed in other alloy systems which are not antiferromagnetic and it could be argued that the martensitic transformation alters the interatomic distances to those in which antiferromagnetic interactions occur. It seems on the evidence available that the reverse is much more likely to be the case.

In the fcc lattice, the atomic sites are all equivalent crystallographically. If reference is made to Fig. 2, it can be seen that each Mn atom can only have 8 of its 12 nearest neighbours with antiparallel spins and the other 4 nearest neighbours with parallel spins. As the antiferromagnetic interaction is favoured, the fcc lattice therefore shears to the fct structure by a martensitic transformation in order that the total magnetic energy may be lowered at the expense of lattice distortion energy.

4.3 X-RAY CRYSTALLOGRAPHY.

If it is accepted that antiferromagnetism is the driving force behind the fcc/fct transformation and during heat treatment the alloy gradually becomes enriched in Mn prior to Mn precipitation, then the main features of the X-ray results shown in Figs, 25, 26 and 27 can be explained. The way in which the Mn atoms aggregate is a matter of controversy and will be examined in greater detail in Section 4.5. Consideration will first be given to those alloys containing between about 50 to 75%Mn which only develop the fct structure after an ageing heat treatment.

The reaction $\gamma \rightarrow \gamma + \alpha$ proceeds at 400°C and Mn atoms aggregate together. On subsequent quenching to room temperature those regions which have a Mn concentration greater than 80% become antiferromagnetically ordered. The martensitic transformation is initiated at the Néel temperature, or more probably at a temperature just below this. The degree of antiferromagnetic alignment of electron spins becomes greater as the temperature decreases and it is therefore not surprising that the axial ratio decreases, Fig. 27. Quenched alloys containing from about 75 to 80%Mn only exhibit tetragonality at sub-zero temperatures probably because it is only at these temperatures that the antiferromagnetic interaction is sufficient to induce the martensitic transformation. Then, for the same reason, the quenched 57%Mn alloy, which is fcc, will first develop a fct structure at temperatures below room temperature after a short heat treatment, because the Mn concentration is only then sufficient to develop long range antiferromagnetic order at these lower temperatures, Fig. 27. At slightly longer heat treatment times the Mn concentration has increased sufficiently to raise the Néel temperature above room temperature and hence X-ray reflections due to the fct structure are recorded at room temperature. As the ageing process proceeds the fcc/fct transformation temperature increases as shown in Fig. 27, and the axial ratio, measured at room temperature, continuously decreases.

After the 57%Mn alloy has received an ageing heat treatment of 5 to 6 hours at 400°C, the rate of change of axial ratio with ageing time, decreases, Fig. 26 and this coincides with the appearance of αMn particles. The αMn particles effectively remove a region of antiferromagnetic γMn which was subscribing to the low axial ratio and for this reason the increasing appearance of αMn with longer ageing times corresponds to a levelling in the slope of axial ratio against heat treatment time and at some stage reflections appear corresponding

to a Cu-rich unit cell. At very long ageing heat treatment times the axial ratio reverts to 1 again, Fig. 26 and this corresponds to the point where the reaction $\gamma \rightarrow \gamma + \alpha$ is almost complete; the transformed γ is then Mn depleted and as a result it is no longer antiferromagnetic and the structure reverts to fcc.

In alloys containing more than 80%Mn which when quenched, are fct at room temperature, there is a much more gradual change in axial ratio after increasing ageing heat treatment times. This corresponds to a surprising lack of αMn precipitation. It would be reasonable to expect that the reaction $\gamma \rightarrow \gamma + \alpha$ would proceed more rapidly at higher Mn concentrations; but this is not the case. Only when the Mn content is as high as 95%Mn does the transformation occur rapidly and in view of the rather pronounced change in the behaviour between alloys containing 90 and 95%Mn, there is a possibility that the 95%Mn alloy at room temperature lies within the α phase field, in contrast to the published equilibrium diagram[1] which indicates a $\gamma + \alpha$ phase field. An examination of Fig. 26 will show that the axial ratios of the lower Mn content alloys, even at long ageing heat treatment times, do not overlap the axial ratio values of quenched alloys containing more than 80%Mn. The explanation of the development of a fct structure has however been based on the assumption that the Mn content must exceed 80%Mn before antiferromagnetic properties and hence the fct structure can be developed. It will be shown in Section 4.5 that this apparent anomaly can be explained if it is assumed that the Mn-rich areas are coherent with the Cu-rich areas. There is therefore a competing effect between the Cu-rich regions which would normally revert to fcc and the Mn-rich regions which, through the antiferromagnetic interaction, would otherwise develop even lower axial ratios. These opposing influences result in an intermediate axial ratio value which can differ markedly from the axial ratios associated with the

high Mn containing alloys.

The correct intensity ratios of the (220): (202,022) and (200,020) : (002)reflections were obtained in many cases, especially those in which the $K\alpha_1$ and $K\alpha_2$ doublet could be clearly resolved, confirming that in the early stages of the ageing process the Cu-rich and Mn-rich regions were in fact single phase. In those cases where an incorrect ratio was found, it was assumed to be due to variations in surface finish or the coverage of an insufficient number of grains to provide a statistical average. The intensity ratio also depends on the detailed microtwin structure in the sample surface which, in turn, is dependent on the presence of localised stresses. Using neutron diffraction techniques, Bacon et al[12] have shown that it is possible to completely alter the intensity ratios by application of stress alone.

4.4 THE DAMPING MECHANISM.

4.4.1 Structural considerations.

There is little doubt that the movement of microtwin boundaries provides the high damping properties of Mn-Cu alloys, although the mechanism by which the moving boundary converts the vibrational energy to heat has yet to be considered. It is also clear that the presence of these microtwins is a direct consequence of a martensitic transformation induced by antiferromagnetic ordering. Any more detailed interpretation of the damping properties based on observations made on thin foils inside the electron microscope must be treated with caution, because of the stress relaxation effects in thin foils and the heating effect of the electron beam. It is therefore only possible to speculate on the likely rearrangement of microtwin boundaries in bulk material during the application of an externally applied stress in, for instance, the test for determining the damping capacity.

On cooling through the Néel temperature, each grain in the material develops a number of microtwins which extend from one

grain boundary to the next and within these main bands there are many smaller microtwins which arise simultaneously from the double-shear mechanism outlined in Section 1.3. When observed in the electron microscope these smaller microtwins are particularly mobile and the main microtwins are static, although the main bands have been observed to move when examined by optical microscopy at stress levels utilised in the damping capacity test[49].

As the temperature is lowered further, the axial ratio decreases and the number of microtwins also increases. Similarly, when the alloy is given an ageing heat treatment, the Mn concentration increases, the antiferromagnetic interaction becomes stronger, the axial ratio decreases and the number of microtwins increases. Energy absorption takes place because the level of strain associated with an increase in stress is different to the level of strain associated with a decreasing level of stress and a static hysteresis loop results as described in Section 1.5. As the stress is applied, the microtwin boundary moves forward in unstable jumps as it passes through the local internal stress peaks and when the stress is removed, the microtwin boundary returns to its original starting point. The jerky motion of microtwin boundaries observed in the electron microscope is then probably very analogous to the Barkhausen jumps associated with ferromagnetic domains[21]. The level of energy absorption will depend on a large number of factors, although these can be broadly divided into two classes, those factors associated with the microtwins and those associated with the matrix through which the microtwins move. For instance, the total area of moving microtwin boundary, the distance moved by the microtwin boundaries and the orientation difference across the microtwin boundary, are all likely to influence the damping properties. On the other hand, the ease of microtwin movement through the matrix will be affected by the distribution of internal stress peaks and the ability of the material to withstand

shear along {110} planes, which, in turn, will depend on the temperature and the form in which the decomposition products of the $\gamma \rightarrow \gamma + \alpha$ reaction appear. It is quite conceivable that those conditions which lead to the optimum microtwin structure for high damping properties, could discourage the development of the ideal matrix structure for high damping properties and vice-versa.

It has been possible by using electron microscope techniques and by the critical examination of more recent neutron diffraction results by other workers, to arrive at some conclusions about the nature of the fine substructure through which the microtwin boundaries move. This substructure which is discussed in Section 4.5 will give rise to numerous internal stress peaks.

The application of a simple compressive stress to a single crystal would favour a 'c' axis orientation in the [100] direction closest to the direction of the applied stress, whereas a simple tensile stress favours a 'c' axis orientation in the [100] direction closest to the normal to the applied stress. In a polycrystalline material, a more complicated process of grain reorientation will take place, although the restraints imposed by neighbouring grains will prevent a complete reorientation within individual grains.

4.4.2 The application of the damping mechanism to the damping capacity results.

There are drawbacks associated with the non-equilibrium method of measuring the specific damping capacity, especially relating to the observations of Birchon et al[39] that many cycles of stress are required before consecutive hysteresis loops are identical. It is therefore possible to comment only on the general trends observed in the damping capacity results, Figs. 30, 31, 32 and 33.

Consideration will first be given to the changes in microstructure occurring during the first quarter cycle of stress at room temperature in a sample which exhibits a maximum in damping capacity as the surface shear stress level is increased,

for example a 60% alloy aged for 6 hours at 400°C, Fig. 30. When the shear stress is first applied during the damping capacity test, some grains will already lie in an orientation favoured by the shear stress. These grains will not then be re-oriented to any appeciable extent, although microtwins lying within the grain would be expected to retract. In other grains with a slightly different orientation, microtwins having an orientation favoured by the shear stress would be nucleated and start to grow while others retract. In this way a grain of a particular orientation would gradually re-orient with increasing stress. The terminal stage is not clear and there appears to be two possibilities. Microtwin density may become so high that the distance between adjacent microtwin boundaries starts to approach unit-cell dimensions and further growth would stop. Growth of microtwins to form high densities has been observed inside the electron microscope, for instance Figs. 5 and 9. On the other hand, annihilation of microtwin boundaries has also been observed inside the electron microscope and it may be possible that when the density of the 'c' - 'c' type of microtwin becomes high and the stress continues to increase, they will coalesce. Whichever mechanism operates, in any particular grain microtwin production and growth will occur with increasing shear stress and finally slow down or even stop as the grain is re-oriented to a degree determined by the external stress and by the constraining influence of the surrounding grains. During the process just described, as the stress is gradually increased, the resolved shear stress will have become high enough in less favourably oriented grains to intitiate microtwin production and growth. In any one grain therefore, there will initially be a rapid increase in the number and movement of microtwin boundaries, until a saturation point is reached as described above. The results of Bacon et al[12] on the increase in neutron reflection intensity of the $\{110\}$ peak reflection on the application of a compressive test would seem to indicate that stress levels

about seven times higher than the highest surface shear stress level used in the damping capacity determination test are necessary before saturation occurs in the sample as a whole. As a correlation has been implied between the volume of material swept out by the operating microtwin boundaries and the damping capacity, then the damping capacity would be expected to pass through a maximum with increasing surface shear stress if saturation re-orientation occurred in many of the most favourably oriented grains. The second quarter of the stressing cycle would then be similar to the first quarter, only in reverse order.

Ignoring for the purposes of this general discussion the effect of the matrix on the damping properties, an increase in axial ratio would be expected to involve an easier 'c' axis re-orientation within any grain, by the production and growth of microtwins and this would then result in a movement of the maximum damping capacity to lower stress levels. Referring again to Figs. 26 and 30, the axial ratio measured at room temperature decreases with increasing ageing heat treatment time and the maximum damping capacity moves to higher surface shear stress levels. The maximum in the damping capacity versus surface shear stress graph, which occurs at the shorter ageing heat treatment times, has not been incorporated in the diagram because it occurs at some stress level between zero and the minimum stress level used in the damping capacity test. The same trend can be observed for other ageing times and testing temperatures, Figs. 27 and 30. For instance, if the results from the sample which has been heat treated for 6 hours at 400^{o}C are examined, it will be seen that as the temperature is increased, the axial ratio approaches 1 and the maximum damping capacity moves to lower surface shear stress levels. Probably the most successful application of the damping mechanism has been in providing an explanation for the rapid fall in damping capacity as the temperature is increased in those commercially viable alloys

based on 60 and 70%Mn which require a heat treatment to develop the high damping condition. As the axial ratio decreases, the reverse situation occurs and the maximum damping capacity moves to higher surface shear stress levels. This occurs on ageing for longer times, for example, samples aged for 6 hours, 8 hours and 16 hours tested at 19 ^{o}C, Fig. 30. In this particular case the maximum damping capacity has not been achieved at the highest stress levels operating in the damping capacity test. At these longer ageing times the rate of change of the axial ratio diminishes considerably and it is thought that the major influence on microtwin movement is the presence of αMn precipitate particles. The same trend is observed when the temperature is lowered, the axial ratio decreases and the maximum damping capacity moves to higher surface shear stress levels; for instance a sample aged for 4 hours at 19^{o}C and -50^{o}C, Fig. 30.

The sample aged for 120 minutes exhibited appreciable damping properties at room temperature although X-ray and electron microscope results failed to reveal the fct structure. However, it has been shown in Section 3.2 that stress alone is sufficient to cause the fcc/fct transformation. This is only thought to be of importance at the shorter ageing times and at higher temperatures, where again the axial ratio is close to 1 and is on the point of transforming back to the fcc structure.

The change in damping properties following upon successively higher levels of plastic strain, Fig. 33, is also capable of explanation using the proposed damping mechanism. Small amounts of plastic strain result in an increase in damping properties. Electron microscope observations have shown that microtwins are often initiated at dislocations and an increase in their number could provide higher damping properties, or alternatively, dislocations could be considered as internal stress peaks and a small increase in their number could also improve damping properties. On the other hand, electron microscope observations have shown that appreciable plastic strain results in a high

density of tangled dislocations which effectively prevent any microtwin movement and it is therefore not surprising that the damping capacity is drastically reduced at higher levels of plastic strain.

4.5 THE $\gamma \rightarrow \gamma + \alpha$ REACTION.

4.5.1 Introduction.

Apart from Section 3.1.4 concerning electron microscope observations of the fine substructure in Mn-Cu alloys, the results which have been described and discussed in Sections 2 to 4 have been published by the author[4]. Other research workers who approached the same problem independently, published their results at about the same time[3,5]. A unanimous agreement was evident in all the essential features of the proposed damping mechanism. In one of the papers, an explanation was provided for the so-called "room temperature ageing effect" which results in a deterioration of damping properties on storage[10]. This explanation takes into account the restriction on the movement of the large microtwins through the continuing propagation of the fine microtwins within them.

Due to the absence of experimental observations at that time, there was a degree of speculation in all three publications concerning the details of the ageing reaction $\gamma \rightarrow \gamma + \alpha$, before the appearance of αMn precipitate particles. Since then, there have been a number of neutron diffraction studies related to the same problem and these results appear to have further complicated the problem, rather than provided an answer. It is worthwhile therefore, at this stage, to state the problem and list the various interpretations which have been proposed.

In view of the lack of solubility of Cu in αMn there needs to be a considerable degree of Mn enrichment within the matrix during the heat treatment of the 60%Mn alloy before αMn starts precipitating out from solid solution. There must also be a corresponding enrichment of Cu in other parts of the sample. The experimental evidence for Mn enrichment can be summarised

briefly as follows.

a) Both X-ray diffraction and electron diffraction have identified the presence of αMn at longer ageing times.

b) The fct structure develops on quenching after short ageing heat treatment times. Only when the Mn concentration has exceeded about 75%Mn will the antiferromagnetic interaction induce the fcc/fct transformation at or above room temperature.

c) The presence of the $\{110\}$ and $\{210\}$ neutron diffraction reflections in samples aged for 6 hours at 400°C confirmed the presence of antiferromagnetic behaviour and hence the enrichment of the matrix in Mn.

The following observations must therefore be explained if there is Mn depletion in some parts of the sample and a corresponding enrichment in Cu in other parts.

d) X-ray results indicate that the alloy remains as a single phase during the ageing process until such a time that αMn particles appear and a considerable further heat treatment is necessary before X-ray reflections associated with a Cu-rich phase can be identified.

e) The intensity ratio of the cubic (h.k.0) and tetragonal (h,k,1) components of the various X-ray reflections in the early stages of ageing correspond to the intensity ratio which would be expected from a fct phase alone. Co-existence of a fct and a fcc phase would alter the intensity ratio.

f) The existence of certain neutron diffraction reflections and the width of the reflection profiles can only be explained in terms of long range antiferromagnetic order. There are no magnetic effects associated with Cu atoms and it is unlikely that antiferromagnetic coherence would be transmitted from one Mn-rich area through Cu-rich regions to another Mn-rich area.

An explanation for these apparent contradictions has been

sought in the tweed pattern and its substructure, which was first noticed by the author in electron micrographs, for instance Fig. 15 and in the presence of the broad neutron diffraction reflection which appears at a Bragg angle corresponding to a $\{100\}$ reflection, for instance Figs. 28 and 29 and which has been analysed primarily by other workers. The suggested explanations which have appeared in the scientific press are summarised below.

g) Dean et al[1] suggested that a preliminary tetragonal intermediate phase Σ forms during the $\gamma \rightarrow \gamma + \alpha$ reaction.

The more recent evidence described above is clearly not in agreement with this suggestion and it will not be considered further.

h) Birchon et al[3] suggested a possible ordering of atoms which then interacted with microtwin boundaries leading to the high damping properties.

i) The author[4] suggested that many small Mn-rich zones are formed during the ageing process and these zones give rise to the substructure within the tweed pattern, Fig. 15. When each zone transforms to the fct structure. it remains fully coherent with the Cu-rich material lying in between, which also then adopts a fct structure. The drawback inherent in this suggestion concerns the degree of regularity and uniformity on a very fine scale, which must be exhibited by the Mn-rich zones, as it is unlikely that the tetragonal coherency strains associated with the Mn-rich zones would be transmitted through many Cu-rich atom planes.

j) Butler and Kelly[5] suggested that very small Cu-rich zones are first formed which remain fully coherent with the Mn-rich matrix; these Cu-rich zones also then adopt the fct structure. This explanation successfully

explained the tetragonality of both Cu and Mn-rich regions as well as the retention of long range magnetic coherency because of the consequent continuity of the Mn-rich areas. Direct experimental evidence was not offered in support of the suggestion.

k) More recently, Bacon and Cowlam[50] have examined the {100} neutron diffraction peak in some detail. They concluded that in the solution treated condition, as well as in the early stages of the ageing process, there is a preference for unlike atoms to aggregate to form zones of short range order, which, on further heat treatment give way to Mn aggregation. Short range ordering in alloys encourages the formation of compound structures and the tentative identification[7] of Cu_5Mn and Cu_3Mn structures which have compositions close to the terminal composition of the $\gamma + \alpha$ phase field, gives this interpretation some attraction.

l) Vance et al in a number of publications[51-53], based on neutron diffraction evidence, also claim that a degree of heterogeneity exists on a very fine scale in the solution treated condition. They, however, interpret the {100} neutron diffraction peak in terms of magnetic short range order and support their claim by the behaviour of the {100} neutron diffraction reflection when the sample is heated through the Néel temperature. Their conclusions are in direct disagreement with those of Bacon and Cowlam[50] although they agree that chemical short range ordering predominates in those alloys which have compositions close to Cu_3Mn and Cu_5Mn.

In view of all the conflicting interpretations, the author conducted further experimental electron microscopy on alloys exhibiting the tweed pattern and extended the work to alloys of lower Mn content. These results were described in Section 3.1.4. A more detailed examination of the neutron diffraction results

described in Section 3.3 was also undertaken in an attempt to reconcile the conflicting conclusions between the neutron diffraction, electron microscope and X-ray results.

4.5.2 The electron microscope evidence.

An examination of Fig. 25 will show that the lattice parameter 'a' of solution treated and water quenched materials, increases with increasing Mn content up to about 65%Mn. In order to identify the atom species of the separating phases by their effect on the electron diffraction contrast, it is desirable to select a composition in which the difference between the lattice parameters of the separating phases is as large as possible to counteract the similarity in electron scattering factors of the Mn and Cu atoms. It is necessary to avoid those compositions and heat treatments which give rise to the fct structure, because it is then impossible to be certain about the lattice parameters of the separating phases. Furthermore, such treatments yield the tweed pattern which effectively prevents analysis of the substructural details by dark-field microscopy. For these reasons, the 50%Mn alloy was selected for examination and the results obtained were described in Section 3.1.4.2. By comparing the phase diagram, Figs 1 and 25, it can be seen that during an ageing heat treatment, the 50%Mn alloy will eventually separate into αMn and a Cu-rich phase of composition about 27.5%Mn having a lattice parameter at room temperature of about 3.71A. During the particular heat treatment of this alloy, the fct structure did not develop even at liquid nitrogen temperatures, and enrichment of the matrix in Mn could not therefore have exceeded 75%Mn. The lattice parameter of the separating Mn-rich fraction, when measured at room temperature, must be about 3.75A. If it is the Cu-rich phase that separates out in the form of small coherent particles within a Mn-rich matrix, then these particles will be in a state of tension. When zones of one atom species are very close to the surface of the foil, large asymmetrical images can be seen in the electron microscope because of the

surface relaxation of the strain field[54]. In bright field electron microscopy, the sense of the asymmetry depends on whether the particle is near the top or the bottom surface of the foil, but in the dark-field case, it depends only on the sign of 'g' the reciprocal lattice vector[54]. When the images are white in the direction of positive 'g', as they are in Fig. 22 at D, E and F, then the particles are in tension and are therefore Cu-rich. It should be pointed out that because of the experimental difficulties associated with the preparation of thin foils in the Mn-Cu alloy system and because of the difficulties associated with the operation of the dark-field technique at very high magnifications, that Fig. 22 is the only micrograph in which anomalous images in the dark-field were observed and the contrast quality of this micrograph is rather poor. It would therefore be desirable to obtain further confirmatory evidence before the positive identification of Cu-rich particles can be claimed.

If these observations are conditionally accepted and if the reaction proceeds in the same manner in the more Mn-rich alloys which exhibit the tweed pattern, then it would seem very likely that the fine detail within the tweed pattern can be identified as arising from Cu-rich zones. The state of stress between the zones and the matrix can, however, alter in the more Mn-rich alloys which develop the fct structure on ageing, as outlined below.

The Cu-rich zones shown in Fig. 15 lie on $\{100\}$ planes and it seems reasonable that at the ageing temperature, the Cu-rich zones remain coherent with the matrix in a $\langle 100 \rangle$ Cu-rich : $\langle 100 \rangle$ matrix orientation. The Cu-rich zones can then lie in any one of the three $\langle 100 \rangle$ directions. At room temperature, if the matrix is sufficiently rich in Mn, it will have transformed to the fct structure. About two-thirds of the particles will then be lying in an 'a' orientation and will be subjected to a tensile stress, as already explained and about

one-third will be lying in a 'c' orientation with respect to the matrix and will either be under a state of compression or tension, depending on the particular 'c' value, Figs. 25 and 26.

Although the tweed pattern prevents a detailed analysis of the underlying structure, certain pertainent information can be inferred from its orientation and its diffraction contrast in light and dark-fields. Tanner[40] has shown by electron microscopy that the precipitation of <100> disc shaped GP zones in a Cu-2%Be alloy is accompanied by the appearance of striations parallel to the traces of {110} planes in the microstructure and <110> relrods normal to these planes are observed in the diffraction patterns. He has shown that the striations or tweed pattern arise from the elastic shear strains induced by the conditions of tetragonal coherency and the high elastic anisotropy of Cu is given as the reason for this type of strain distribution adjacent to the disc shaped zones. If the zones nucleate parallel to {100} planes, then the maximum resolved shear stress will lie at 45^{o} to these planes or along <110> which is the observed direction of the tweed striations.

The tweed pattern reported for heat treated Cu-Be alloys[40], is identical in appearance to that observed in the heat treated Cu-Mn alloys. Tanner[40] has calculated which orientations of the tweed pattern will be present or absent when using various dark-field reflections. He has also calculated the corresponding angles of intersection between the striations when these reflections are operating. All these features are duplicated in an identical fashion in the Mn-Cu alloys as described in Section 3.1.4.1. Although Tanner postulated[40] the presence of a fine substructure within the tweed striations corresponding to the <100> GP zones, he was unable to resolve these. In Mn-Cu alloys it is possible to distinguish this substructure at high magnifications as has already been described, Fig. 15. On the other hand Tanner[40] was able to observe <110> relrods

associated with the diffaction spots and arising from the elastic shear strain within the matrix. This effect has never been observed in the diffraction patterns obtained from Mn-Cu alloys. Relrods arise from the interaction between the electron beam and very thin second phase particles. The relrod length is inversely proportional to the particle thickness and the relrod intensity depends on the difference in electron scattering factors between Mn and Cu atoms. It is not surprising then, that under these circumstances the relrods are not visible in Mn-Cu alloys, because, if present, they would be long and very weak in intensity. Relrods can also arise in diffraction patterns due to strain effects in the matrix adjacent to the precipitating particle. In the case of the 57%Mn-Cu alloy, the mismatch between the Cu-rich zone and the matrix is about 1%, whereas in the case of Be-rich zones within a Cu matrix, the misfit is about 13%; the absence of relrods in Mn-Cu diffraction patterns is therefore reasonable.

Tanner has pointed out[55], that a tweed structure has also been observed in Ni_3V which undergoes an ordering reaction from fcc to fct and the transformation strains are relieved by the formation of microtwins. He further implies in his communication[55] that the shear strains induced by precipitation could therefore be responsible for the fcc/fct transformation in Mn-Cu alloys, instead of an explanation based on antiferromagnetism. This explanation is not thought likely for a number of reasons. The misfit between Cu-rich zones and the matrix is too small to generate appreciable shear strains and there is good agreement between the fcc/fct transformation temperature and the Néel temperature in alloys containing more than 75%Mn. It would also be difficult to reconcile the low axial ratios recorded for quenched high Mn alloys with a mechanism based on pre-precipitate coherency strains, especially when these pre-precipitate zones will have had little, if any time, to develop.

Although there is little doubt that the main driving force behind the fcc/fct transformation is the antiferromagnetic interaction and the microtwins form as a consequence of this transformation, it is also likely that the shear strains created by the coherent Cu-rich zones exert an influence on the ease of microtwin movement and the damping capacity which results from the motion of the microtwins.

4.5.3 The neutron diffraction evidence.

Bacon et al[50] explained the broad {100} reflection appearing in the neutron diffraction trace from a 80%Mn-20%Au alloy in terms of the short range ordering of atoms. Alloys within the Mn-Au system behave in the same manner as Mn-Cu alloys. A convenient way of describing short range order was introduced originally by Cowley[56-58]. In this treatment, an atom is considered as being surrounded by a series of concentric shells of nearest, second nearest, third nearest neighbouring atoms and so on. In an alloy consisting of A and B atoms where x_A and x_B are the fractions of elements A and B respectively, then $\alpha(n)$ the short range order coefficient for the nth shell of atoms is given by

$$\alpha(n) = \frac{1 - P_A(n)}{x_A} = \frac{1 - P_B(n)}{x_B}$$

When there is a preference for unlike neighbours $P_A(n) > x_A$ and $\alpha(n)$ is negative and short range order results; when the preference is for like neighbours, $\alpha(n)$ is positive and clustering of like atoms results; when $\alpha(n) = 0$ there is complete randomness.

Bacon and Cowlam[50] calculated the variation in neutron intensity with Bragg angle assuming ordering in the first two shells of nearest neighbours and compared this against the experimentally determined variation in neutron intensity with Bragg angle. It was assumed that the first shell around an Au atom includes 10 Mn and 2 Au atoms, giving $\alpha_1 = 0.043$ and the second shell includes 4.4 Mn and 1.6 Au atoms, giving

$\alpha_2 = 0.084$. By contrast, a random distribution with no short range order would require 9.6Mn atoms in the first shell and 4.8Mn atoms in the second shell. They therefore postulated a first shell slightly enriched in Mn and a second shell slightly deficient; a case of short range order.

In view of this apparent contradiction with previous electron microscope and X-ray results, which had shown the need for Mn clustering prior to Mn precipitation, the author decided to repeat the analysis using the Delta computer to allow the inclusion of a wide range of $\alpha(n)$ parameters ranging from negative to positive. The results confirmed Bacon and Cowlam's work,[50] that the position and intensity of the $\{100\}$ peak could be explained using their figures. By changing α_1 from negative to positive which corresponds to a change from short range order to clustering, then, theoretically, the peak appearing in the $\{100\}$ position would become less intense and move to higher Bragg angles.

The position was partly resolved by Vance et al[51-53] in a number of papers, who measured the change in intensity of the $\{100\}$ peak with increasing temperature and found that the intensity increased to a maximum at the Néel temperature and then progressively decreased. Based on this observation, they proposed that the $\{100\}$ reflection was primarily magnetic in origin and using an analogous approach to Bacon and Cowlam[50], proved that a more likely explanation for the reflection involved magnetic short range ordering. It is a well known observation that chemical short range ordering can exist above the critical long range ordering temperature in certain alloys and, in an analogous manner, Vance et al[53] proposed that short range magnetic alignment between Mn ions could also occur above the Néel temperature. They did not, however, go on to consider the implications of their proposals on the separation of the Mn and Cu-rich regions during the ageing process. Magnetic short range order arises from regions where there are alternate

antiparallel and parallel alignment of spins. As only the Mn ion is magnetic, then magnetic short range order must imply clustering of Mn atoms. At first sight this would seem to be a contradiction of the earlier experimental results by Bacon and Cowlam[50] and their confirmation by the author. The difficulty in an approach which involves finding a best fit for experimental results, lies in allowing for the additive effect on the neutron diffraction pattern of the contributions from a number of possible atomic or magnetic configurations. The various possibilities are listed below -

1	Chemical short range order	Mn-Cu-Mn-Cu	can fit the experimentally observed {100} reflection.
2	Magnetic short range order	↑ Mn ↑ Mn Mn ↓ Mn ↓	can fit the experimentally observed {100} reflection.
3	Chemical clustering of Mn atoms	Mn-Mn-Mn-Mn	cannot fit the experimentally observed {100} reflection.
4	Chemical clustering of Cu atoms	Cu-Cu-Cu-Cu	cannot fit the experimentally observed {100} reflection.

Vance et al[53] have shown that the {100} reflection is best explained by magnetic short range ordering and this implies clustering of Mn atoms but does not preclude the clustering of Cu atoms. The absence of a contribution from the clustering of Cu atoms to the formation of the {100} reflection, cannot be taken to imply either the existence or absence of Cu atom clustering.

It is unfortunate that the fundamental reflections at higher Bragg angles swamp any influence on the scattered neutron intensity which would be derived from either chemical clustering of Mn or Cu atoms. The neutron diffraction work therefore confirms the tendency for Mn aggregation but cannot unambiguously confirm the tendency for Cu aggregation.

It is worthwhile summarising the neutron diffraction, electron microscope and X-ray evidence surveyed in this chapter, by examining the detailed breakdown of the $\gamma \rightarrow \gamma + \alpha$ reaction in a 57%Mn alloy. In the solution treated condition, there is

a tendency towards Mn clustering, resulting in the alignment of spins over small regions. The effect will be emphasised when solution treatment has not been continued long enough to equalise the macroscopic Mn fluctuations. During ageing at 400°C, Cu atoms probably aggregate to form zones, a few atom layers thick, lying in a <100> matrix orientation; the spacing between the zones is about 100A. There is a corresponding enrichment of the matrix in Mn and after an ageing heat treatment of 2 hours the Mn content of the matrix exceeds about 80%Mn and on quenching to room temperature, long range antiferromagnetism develops at the Néel temperature and subsequently induces the fcc/fct transformation. The Cu-rich zones deform along with the matrix and thereby retain their coherency. Depending on the orientation of the Cu-rich zones, some will adopt a lattice parameter equivalent to the 'a' parameter of the tetragonal cell and some will adopt a parameter commensurate with the 'c' parameter of the tetragonal cell. It is possible that those Cu-rich zones which are coherent with the 'c' parameter of the tetragonal cell, may be under tension after short ageing times, yet be under a state of compression at longer ageing times because the 'c' parameter decreases with increasing Mn content as a result of the longer ageing heat treatment. The tweed pattern is then a manifestation of the elastic stresses resulting from the two opposing tendencies of the Cu-rich zones to revert to their equilibrium fcc structure and a tendency for the matrix to become increasingly tetragonal. The axial ratio developed would not be expected to be as low as the axial ratio developed by a matrix of the same Mn concentration in which the Cu-rich particles were absent, for example in an alloy containing more than 75%Mn which is in the quenched condition. The maximum resolved shear stress within the matrix will lie at 45° to the Cu zone habit plane or along <110> directions in the matrix; microtwin growth could therefore be encouraged.

The microtwins pass through a matrix which consists of alternating regions under compression and tension on an extremely fine scale and such a situation could be expected to yield very high damping properties. At longer ageing heat treatment times the matrix becomes further enriched in Mn and αMn nucleates, denuding the matrix of Mn and leaving areas of more Cu-rich material which then yield an X-ray diffraction pattern characteristic of fcc material.

A structure consisting of numerous fine coherent zones of Cu within a fct matrix rich in Mn would then explain the apparently contradictory statements listed at the beginning of this chapter. It allows the separation of the material into Cu-rich and Mn-rich phases whilst yielding an X-ray diffraction pattern equivalent to a single phase and it allows long range magnetic coherency in a structure which contains an appreciable proportion of a non-magnetic constituent, Cu.

4.6 CRITERIA NECESSARY FOR THE DEVELOPMENT OF HIGH DAMPING PROPERTIES.

All of the experimental work described and discussed in the first four chapters has been aimed at identifying those physical features which are necessary to develop the high damping properties in Mn-Cu alloys. It was hoped that by the application of the information so gained, it would be possible to identify alternative alloys which did not suffer from the drawbacks of the Mn-Cu system, especially the poor retention of damping properties at elevated temperatures. It is therefore worthwhile summarising these criteria which have been deduced as necessary for the development of high damping Mn alloys, as these are used as a basis for the selection of alternative systems which have been examined in the second part of the programme.

a) Alloys based on Mn should be antiferromagnetic. In Mn-Cu alloys containing more than 75%Mn, this property develops on quenching and can be further influenced by subsequent ageing. For those alloys containing between 50 to 75%Mn, an ageing

heat treatment is essential to produce the Mn enrichment necessary for the development of antiferromagnetism.

b) The development of antiferromagnetic behaviour in metals is markedly dependent on the interatomic spacing and hence on the crystal system. In Mn alloys antiferromagnetism develops in the γ phase, when this is sufficiently rich in Mn, although the α phase is also antiferromagnetic at very low temperatures. The antiferromagnetic interaction must be such that a martensitic transformation is induced, resulting in the formation of the fct structure from the original fcc structure. The transformation temperature must be appreciably higher than the envisaged temperature of application of the damping alloy. This implies a high Néel temperature which in turn is more likely to be developed in an alloy containing a high percentage of the antiferromagnetic element. Dilution of that element reduces the Néel temperature.

c) Microtwins are formed within the martensitic structure and the nature of the matrix should be such that the microtwins can move easily, but in doing so can interact with the microstructure resulting in a high absorption of vibrational energy.

d) The γMn structure in Mn alloys is normally a high temperature phase, it must cover a reasonably wide composition range for practical purposes and be sufficiently stable to be retained on quenching to room temperature. The equilibrium phases at room temperature in Mn alloys should be a mixture of $\gamma + \alpha$.

e) For commercial reasons, it would clearly be desirable for the alloy to possess a combination of good mechanical and corrosion resistant properties and it should be easy to cast and fabricate. In the second part of the programme it has been the prime aim to develop good damping properties at elevated temperatures whilst retaining or improving damping properties at room temperature. It will be seen in

subsequent sections that some of these requirements are mutually incompatible.

CHAPTER 5.

THE SELECTION OF ALTERNATIVE ALLOYS.

5.1 SUMMARY OF PUBLISHED WORK.

Few metals exhibit antiferromagnetism and apart from the Pt series[56] and the rare earth group[59] which have both been dismissed on the grounds of cost, only Cr[60-64] and Mn[60,11,12] in the elemental form have been shown to exhibit antiferromagnetic behaviour. Cr with a Néel temperature of 37°C[63] would not be of practical interest and the antiferromagnetic ordering which is developed induces a lattice distortion which is barely measureable by the most sophisticated techniques[65-67]; γMn has an extrapolated Néel temperature at 100%Mn of 387°C[13].

Much work has been undertaken on the relationship between antiferromagnetism and internal friction in Cr and its alloys[70-74] with the aim of understanding the effect of interstitial elements, C and N on the antiferromagnetic properties. Apart from the work on Mn-Cu[3,4,5], there has been no attempt to use antiferromagnetic behaviour as a basis for the selection of other high damping alloys.

A number of elements form intermetallic compounds with Mn and many of these have also been shown to be antiferromagnetic, namely Mn_2As[75], MnAu[76,77], $MnAu_2$[78], $MnAu_3$[79], Mn_3Ge[80], MnNi[81,82], $MnPd_3$[83], MnRh[84], MnSe[85], $MnSe_2$[86], Mn_3Sn[87], $MnSn_2$[88], MnTe[89] and $MnTe_2$[90]. Although all these intermetallic compounds satisfy the requirement of antiferromagnetism and a number exhibit associated martensitic transformations, it is unlikely that any would possess suitable mechanical properties. However, the ordered equiatomic compound MnNi is of special interest because of the exceptionally high Néel temperature of about 800°C that it exhibits[82]. This compound is also fct and an electron microscope examination has revealed the presence of microtwins[27]. There was every incentive to examine ways of circumventing the problem of poor mechanical properties in this compound. It was decided therefore, to

incorporate MnNi in the experimental programme.

Relatively little work on the antiferromagnetic properties of the Mn-rich γ phase alloys has been undertaken, with the exception of Mn-Cu.

In the MnFe system, γ phase alloys with Fe contents varying from 70 at.%Fe to 47 at.%Fe are antiferromagnetic but do not undergo a structural transformation[91,92]. The structural transformation is also absent in ternary Fe-Ni-Mn γ phase alloys with compositionsapproximating to $(NiFe)_3Mn$[93].

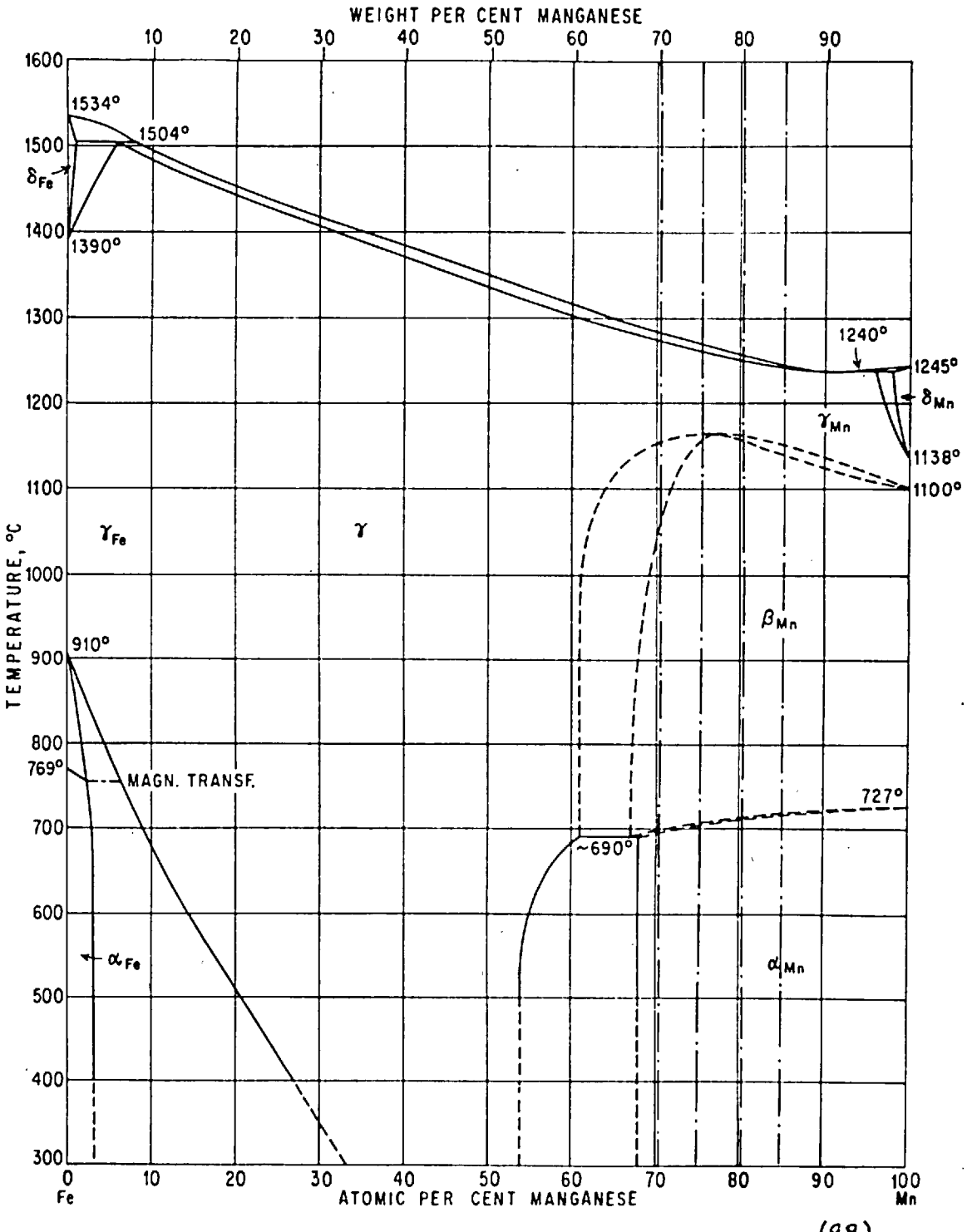
The important point to emerge from this brief review of the literature on antiferromagnetism in Mn alloys is that, unlike Mn-Cu, the presence of long range antiferromagnetic behaviour does not automatically imply a crystallographic transformation.

In the absence of more comprehensive data on antiferromagnetic behaviour, it is fortunate that structural studies on some Mn-rich γ phase alloys have been reported. The martensitic transformation from fcc to fct has been recorded in Mn-Ge, Mn-Ga, Mn-Zn and Mn-Ag alloys[94]. The critical Mn composition below which the fct structure does not develop on quenching is, for the Mn-Ge system, 84%Mn, for Mn-Ga it is 74%Mn, for Mn-Zn it is 78.5%Mn and for Mn-Ni it is 80%Mn. In ternary Mn-Cu-Ni alloys, the critical Mn composition was found to be 85%Mn[95].

During a metallographic study, many different structures were reported relating to the γMn phase in Mn-Ni alloys. Some of these surface relief effects were identified as being typical of the tetragonal γMn phase[96,97].

From the preceeding review of literature and from an examination of the thermal equilibrium diagrams of all Mn alloys[98,99] in order to identify those systems in which large γ phase fields form, an initial choice was made of the Mn-Fe and Mn-Ni systems. It was thought that these systems would be most likely to provide a superior alternative to Mn-Cu.

Subsequent to the experimental work on Mn-Ni alloys described later, further confirmatory evidence for the choice of this



(98)

Fig. 40 Manganese - Iron thermal equilibrium diagram. with selected alloy compositions superimposed.

Selected alloy compositions —·—·—

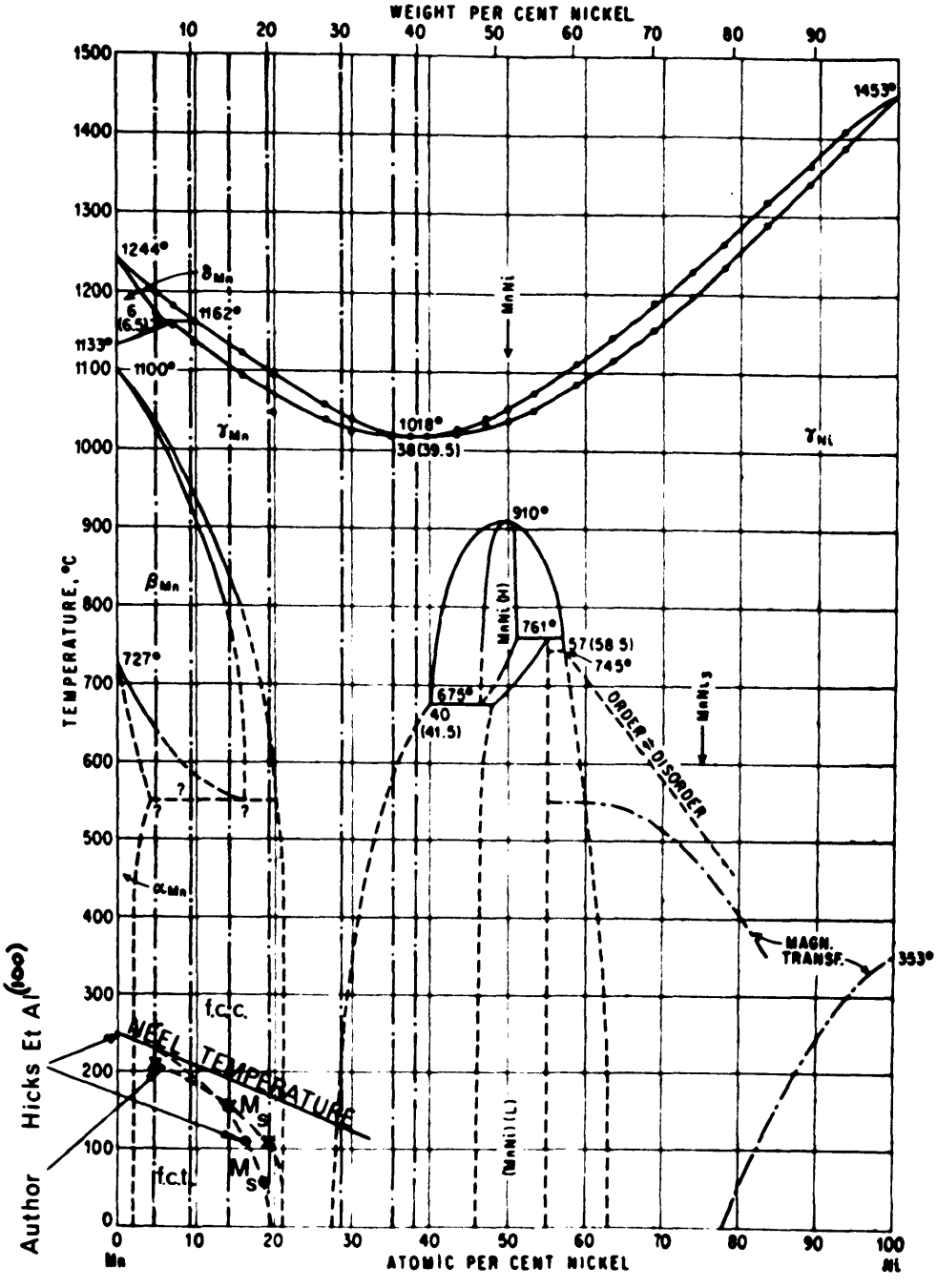


Fig. 41 Manganese - Nickel thermal equilibrium diagram with selected alloy compositions, Néel temperatures and f.c.c./ f.c.t. transformation temperatures superimposed. (98)

system appeared in a publication[100] relating antiferromagnetic properties with the development of the fct structure. In this publication[100] high Mn alloys were shown to transform from fcc to fct at the Néel temperature. Alloys containing more than 15 at.% Ni were fcc below the Néel temperature and did not distort until much lower temperatures. In the more solute rich alloys, the structural transformation was suppressed entirely.

5.2 THE THERMAL EQUILIBRIUM DIAGRAMS OF Mn-Fe AND Mn-Ni.

5.2.1 The Mn-Fe system.

The selection of compositions in the Mn-Fe system has been based on the equilibrium diagram shown in Fig. 40[98,99]. There are several pertinent differences between the behaviour of high Mn, Mn-Fe and Mn-Cu alloys. In the Mn-Fe system, the γ phase field extends over a much larger composition range at intermediate temperatures. The α phase field extends over a composition range from about 68 wt.% Mn to pure Mn in the Mn-Fe system, whereas in the Mn-Cu system Cu is claimed to be insoluble in αMn. The $\gamma + \alpha$ phase field extends from about 54 wt.% Mn to 68 wt.% Mn in the Mn-Fe system, whereas it extends from about 20 wt.% to 100 wt.% Mn in the Mn-Cu system. It was therefore essential to retain the γ phase in the Mn-Fe system without any transformation to the β or α structures.

An alloy composition within the $\gamma + \alpha$ phase at room temperature would not be expected to develop the fct structure after an ageing heat treatment because of the low concentration of Mn in the α phase.

Four alloy compositions were selected containing 70, 75, 80 and 85 wt.% Mn and these have been included on the thermal equilibrium diagram, Fig. 40[98,99].

5.2.2 The thermal equilibrium diagram for Mn-Ni.

The equilibrium diagram used for the selection of compositions in the Mn-Ni system is shown in Fig. 41[98]. The addition of Ni to Mn stabilises the γ phase to such an extent, that in the composition range from about 70% to 78%Mn, the γ phase is stable

at room temperature. The solubility of Ni in α Mn is very restricted as it is in the Mn-Cu system. The $\gamma \rightarrow \gamma + \alpha$ phase field is somewhat limited, extending from about 78% to about 98%Mn. The β Mn phase field in the Mn-Ni system is a little larger than that occurring in the Mn-Cu system. The Néel temperature at different compositions[100] has also been superimposed on the equilibrium diagram, so that a direct comparison can be made with the Mn-Cu equilibrium diagram, Fig.1.

Of additional interest in the Mn-Ni system is the intermetallic compound MnNi which, as mentioned previously, is antiferromagnetic with a Néel temperature of about 800°C[82]. Application of the data derived from Mn-Cu would suggest that the intermetallic compound MnNi could possibly provide high damping capacity at high temperatures. As it was realised that the intermetallic compound would probably be very brittle, attempts have been made to incorporate it in a finely divided state in a matrix of the γMn phase. It was anticipated that this might result in a ductile metal with a high damping capacity at temperatures up to 800°C.

Seven alloy compositions were selected containing 60. 63, 70, 80, 85, 90 and 95 wt.% Mn and these have been included on the thermal equilibrium diagram, Fig. 41[98].

5.3 EXPERIMENTAL PROCEDURE.

5.3.1 Alloy preparation.

It is worthwhile at this stage to outline the standard general experimental approach to these Mn-Fe and Mn-Ni alloys and all subsequent alloys. All alloys have been cast into 10 lb. ingots under a reduced pressure of argon as previously described. In all the cast high Mn alloys coring was a dominant feature and ideally all heat treatments should have been conducted on material which had been completely homogenised to avoid ambiguous results. It was decided, in the case of the ternary alloys, to conduct heat treatments on materials which were either in the as-rolled condition or after they had been given a brief solution

treatment of about 2 hours at an elevated temperature. Most of the severe coring was removed by this treatment. The decision to use these heat treatments was taken in view of the considerable time it would have taken to completely homogenise all samples. It was also obvious that many of the cast alloys would not provide suitable high damping material, although it was considered advantageous to determine the stability of the various phases present in order to identify and select more promising alternative compositions at a later date. Accordingly many of the alloys have been isothermally heat treated at a variety of temperatures to obtain some idea of the temperature range over which the various phases are stable. When damping properties proved to be promising, homogenisation was taken to completion to ensure representative results. It was possible by this procedure to quickly identify appropriate solution treatment temperatures, as well as the temperature range over which the material could be mechanically reduced.

In this part of the programme four main experimental techniques have been used to aid in the identification of alloy compositions possessing the desired properties as well as the most likely heat treatment required to optimise these properties.

5.3.2 Metallography.

After casting, rolling down and appropriate solution treatment, most of the alloys have been examined by optical microscopy in order to identify, where possible, those phases present and also to aid in the detection of the fct structure through the presence of shear traces left on the surface during the transformation.

The identification of suitable etching reagents to show up the structural features presented a major problem throughout the work. With few exceptions, different etching reagents or combinations of etching reagents were required for each alloy system and quite often for each different alloy composition within the same system. Furthermore, no one reagent would show up all the features of interest and it was necessary to resort to three or four

different reagents to show up the presence of grain boundaries in the γ phase, αMn precipitate, the β phase or the surface striations resulting from the fcc/fct transformation. It was also necessary to develop a number of polishing solutions to prepare thin films for electron microscopy. Although this part of the programme represents an appreciable effort, it would become tedious to provide a detailed description of the procedures adopted for each alloy composition. A few of the more widely used reagents will therefore be mentioned and some of the problems associated with an incorrect choice of reagents, which result in artefact structures, will be described along with the rest of the results obtained for Mn-Fe and Mn-Ni alloys.

During the etching of Mn-rich alloys, a surface film builds up and in some alloys it is possible to distinguish the structure before it is obscured by the surface film. In these cases a very weak acid reagent proved successful, such as ½% Nital or 5% citric Acid. In the majority of cases the film build-up using weak acids occurred before the structural features had time to develop. In this case a relatively strong acid combination usually based on nitric and acetic acid was employed. The reaction was vigorous, often resulting in an over-etched structure, but the build-up of the surface film was usually avoided. A final polish in a chromic-acetic mixture was used to remove any remaining surface film and also as a means of levelling the over-etched surface.

5.3.3. X-ray crystallography.

The crystallographic structures of the phases present were determined by X-ray diffractometry using a Mn filtered FeKα X-ray beam, see Table 2. The axial ratios recorded in this latter part of the research programme were often appreciably lower than those encountered in the study of Mn-Cu alloys. The method of calculating the axial ratios described in Section 2.4.2 and Fig. 3 was therefore abandoned in favour of a comprehensive set of tables constructed with the aid of the

Delta computer, relating the separation of (200,020) and (002) or (220) and (022,202) and the axial ratio for 2θ values of 60 to 64° and 90 to 95° in steps of 0.5°. To help in the identification of the most suitable ageing heat treatments, the change in room temperature axial ratio has been recorded after various ageing heat treatment times. Vickers hardness measurements were also recorded to provide additional information on the progress of the $\gamma \rightarrow \gamma + \alpha$ reaction. Extensive use of X-ray measurements has been used throughout the work where this would limit the number of time-consuming damping capacity determinations and this is especially true of the axial ratio determinations which provide an indication of the temperature at which damping properties are most likely to be lost. When an interesting alloy composition or heat treatment had been established in this manner, damping capacity determinations were undertaken at various temperatures.

5.3.4 Electron microscopy.

During the study of Mn-Ni and Mn-Fe alloys, evidence was still lacking to prove the general applicability of the mechanism of damping in Mn-Cu alloys to other antiferromagnetic Mn alloys. It was therefore thought advisable to examine some of the alloy compositions in the electron microscope in an attempt to identify the possible presence of those features which were known to be important from the previous examination of Mn-Cu alloys.

5.3.5 Heat treatment procedure.

When it was necessary to homogenise samples to remove the cored cast structure, this was accomplished by heating in the γ phase field at temperatures varying from $950^{\circ}C$ to $1200^{\circ}C$ depending on the alloy composition. Except for a few samples of Mn-Fe and Mn-Ni in the early stages of this work, which were heat treated in air and which formed nitride surface layers, ageing heat treatments have been conducted in an atmosphere of argon.

Some of the figures incorporate a lot of detail and, for the

Fig. 42.

Fig. 43.

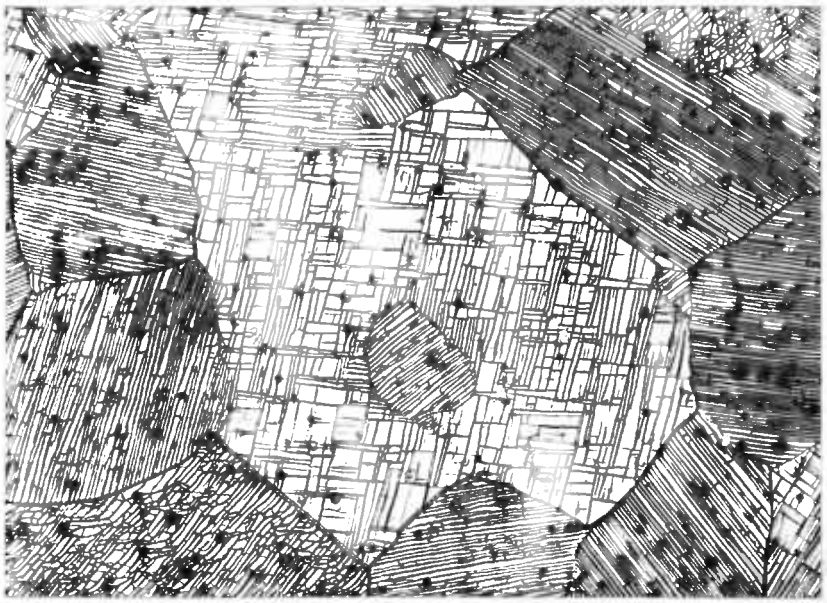


Fig.42. A 75%Mn-25%Fe alloy, water quenched from 1200°C and heat treated for 140 minutes at 600°C. Shows striations associated with the use of many etching reagents. x 230.

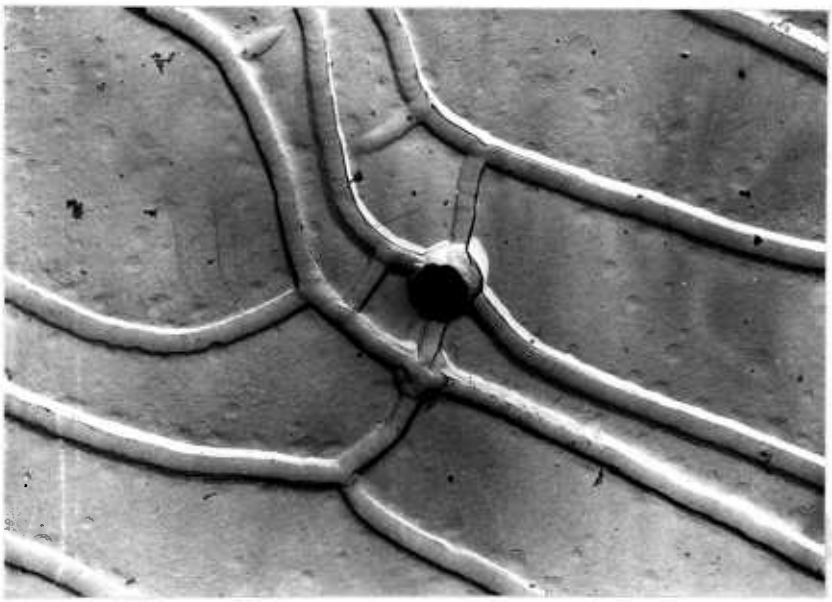


Fig.43. Replica taken from the structure in Fig. 42 showing the rectangular profile of the channels and their association with particles embedded in the surface x 6,000.

sake of clarity, acronyms have been employed on occasion. Thus S.T. stands for solution treated, H.T. stands for heat treated, W.Q. stands for water quenched, S.D.C. stands for specific damping capacity and S.S.S. stands for surface shear stress.

5.3.6 Damping capacity.

Damping capacity determinations were conducted at room and elevated temperatures using the procedure already described in Section 2.6. A very simple test for ascertaining the presence or absence of an appreciable damping capacity involved striking the sample. If the sample exhibited more than a few percent damping capacity, then a dull note was emitted. If the damping properties were less than this, then a ringing note resulted. This test was never used in isolation to reject or accept a particular alloy composition.

5.4 THE Mn-Fe SYSTEM.

5.4.1 Results.

5.4.1.1 Artefact structures.

During early work on both the Mn-Fe and Mn-Ni systems, γMn phase structures were found similar to those previously recorded for other Mn alloys and which have been interpreted as being representative of the alloy structure[96,97]. In Mn-Fe alloys, these structures took the form of striations, often oriented in specific directions, Fig. 42. Replicas taken from areas showing the striated effect indicated that they were in fact channels with an approximately rectangular-shaped profile, Fig. 43. There was also an obvious association between the channels and impurity particles adhering to the surface. From the evidence obtained, it was assumed that during the initial chemical etching a brittle film built up on the surface of the metal. After reaching a certain thickness, this film split at points of stress such as grain boundaries and impurities standing proud of the surface. Within grains the film split along certain directions, presumably related in some way to the orientation of the underlying grain. At this point, the thin film provided a protective coating

Fig. 44.

Fig. 45.



Fig.44. A 75%Mn-25%Fe alloy, water quenched from 1200°C, shows the initiation of microtwins at dislocations. x 27,000.



Fig.45. Same area as in Fig. 44 showing further microtwin propagation. x 27,000.

against further reagent attack, except at those regions where the film had cracked. It was possible to remove the coating by electrolytic polishing and a surface was then left attacked at those points where the original cracks in the film had been. Prolonged polishing using this second solution did eventually yield a smooth topography and a structure more representative of the alloy. It was not always possible to completely remove the spurious effect which was present, as can be seen in some of the accompanying figures illustrating other structures.

5.4.1.2 Structural studies.

The four Mn-Fe alloys that were cast contained nominally, 70, 75, 80 and 85%Mn; chemical analyses of these and all subsequent alloys are incorporated in Table 3. All the cast alloys were extremely brittle and fell into small pieces when removed from the casting mould. X-ray and optical examination and hardness measurements indicated that in the cast state the alloys were composed entirely of the βMn structure. Samples from all the cast alloys were heated in air at 1200°C for 1 hour and water quenched and in all cases a thin shell of γMn had formed on the outside of the sample. As the γ phase was not sufficiently stable in these Mn-Fe alloys, work on all compositions apart from the 75%Mn alloy was terminated. Work continued on the 75%Mn-25%Fe alloy because it was thought that further data might provide a more sensible choice of possible ternary additions and compositions.

A small portion of the γMn shell, with a hardness of $H_V = 134$, was removed from a sample which had been water quenched from 1200°C and this was thinned and examined in the electron microscope revealing the presence of mobile microtwins, Figs. 44 and 45. The appearance of the fct structure in the water quenched 75%Mn alloy was somewhat unexpected as the work on Mn-Cu and the published information on other Mn systems, apart from Mn-Ga[94], had indicated that a minimum of about 78%Mn was required before the fcc/fct transformation temperature increased

Fig.46.

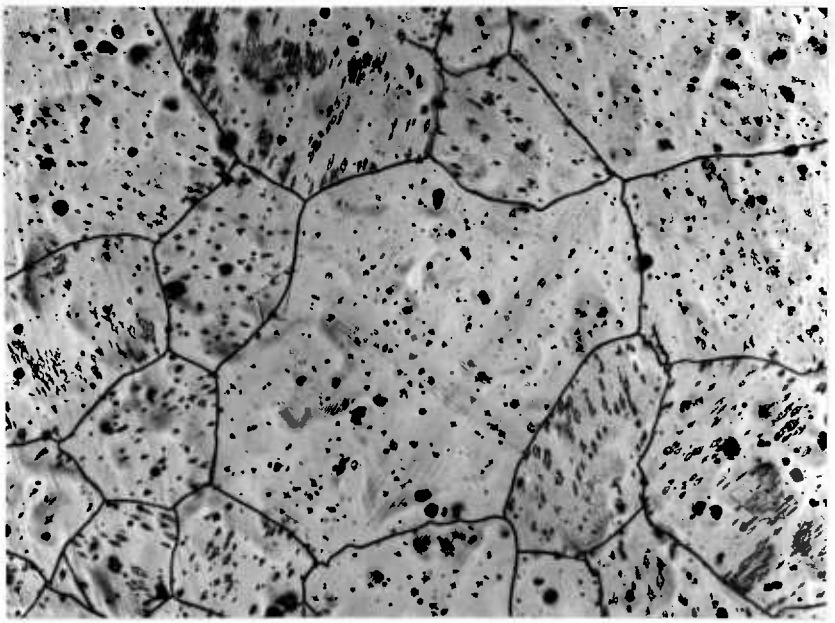


Fig.46. A 80%Mn-20%Ni alloy, water quenched from 1000°C. Shows angular-shaped artefacts due to the etching reagent as well as surface tilting resulting from the fcc/fct transformation temperature. x 90.

Fig. 47.

Fig. 48.

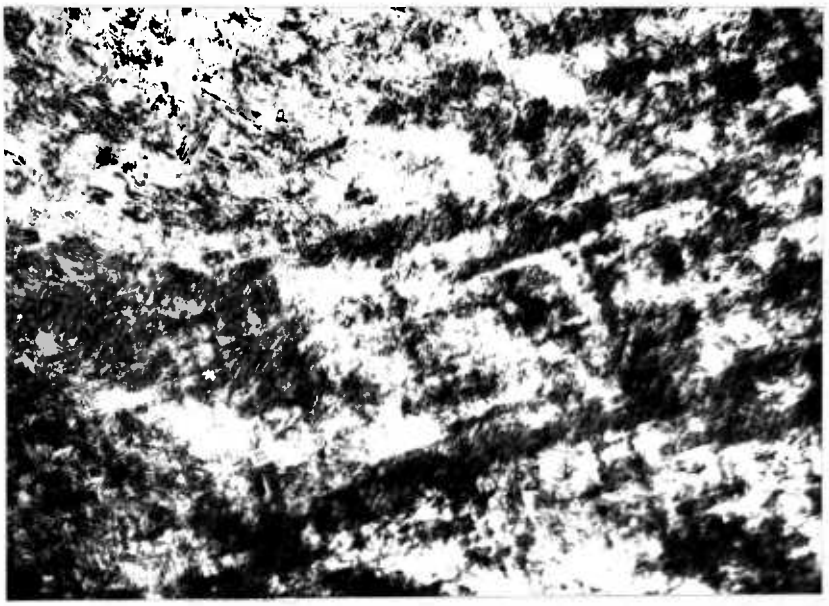


Fig.47. A 50%Mn-50%Ni alloy, water quenched from 1000°C, showing dense dislocation tangles. x 28,000.

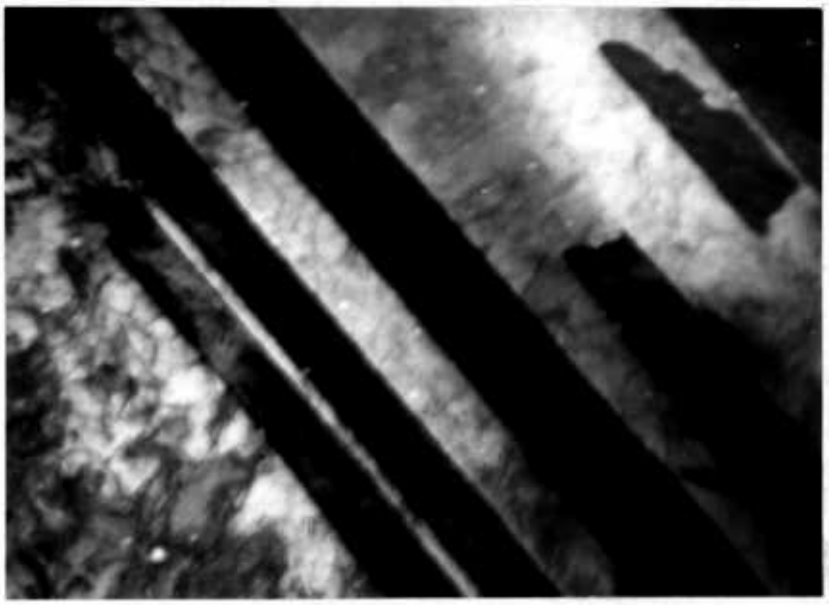


Fig.48. A 50%Mn-50%Ni alloy, furnace cooled from 1000°C, heated to 800°C inside the electron microscope and slowly cooled. Shows microtwins which formed at about 700°C and which were photographed at room temperature. x 31,000.

above room temperature.

On heating the quenched β structure at 600°C for 140 minutes in the α phase field, no change from the cast structure was seen.

5.4.2 Discussion.

Although the γMn phase in the Mn-Fe system extends across the equilibrium diagram at high temperatures to include all compositions, the rate of cooling during casting is sufficiently slow to allow the complete transformation of Mn-rich alloys to the βMn structure at lower temperatures. However, quenched alloys with more than 75%Fe exhibit all those features in the γMn phase which are necessary to promote high damping capacity. The thermal equilibrium diagrams of Mn-Cu, Fig. 1 and Mn-Ni, Fig. 41 both exhibit large γMn phase fields and relatively small βMn phase fields. It was therefore decided to cast ternary alloys based on the Mn-Fe-Cu and Mn-Fe-Ni systems, in the hope of producing alloys in which the γMn phase was sufficiently stable to be retained during casting.

5.5 Mn-Ni ALLOYS.

5.5.1 Results.

5.5.1.1 Artefact structures.

In Mn-Ni alloys the artefact structures tended to be different to those observed in Mn-Fe alloys and angular-shaped features were formed with most etching reagents, Fig. 46. Such structures had previously been reported to be representative of the γ structure in the Mn-Ni system[96,97].

5.5.1.2 Alloys based on the precipitation of the intermetallic compound Mn-Ni.

In the cast state the intermetallic compound MnNi was extremely hard and brittle. Electron microscopy on a sample quenched from 1000°C gave an ordered diffraction pattern, as expected, and a complex microstructure consisting of many tangled dislocations lying in bands, Fig. 47. A heating experiment conducted inside the electron microscope resulted in the removal

Fig. 49.

Fig. 50.



Fig.49. A 60%Mn-40%Ni alloy, as-cast and heat treated for 3 days at 500°C. Shows a severely striated structure and probable precipitate particles within grain boundaries. x 210.



Fig.50. A 65%Mn-35%Ni alloy, water quenched from 1000°C and heat treated for 1 week at 500°C. Shows the discontinuous mucleation of MnNi particles on dislocations. x 28,000.

of the complex dislocation structures at high temperatures and on cooling from 800°C, microtwins rapidly came into contrast at a temperature of approximately 700°C. No further movement of the microtwins could be observed as the temperature cooled further, Fig. 48.

Water quenched samples of the 70%Mn-30%Ni alloy were single phase with a γMn structure, confirming the equilibrium diagram, Fig. 41.

In the as-cast state the microstructure of the 60%Mn-40%Ni alloy was relatively featureless, although a second phase was present in grain boundaries in sufficient quantities to ensure it was not an impurity; there was not sufficient present to detect by X-ray diffraction. On the first pass through the rolls, the material broke up transversely across the bar. Work continued with the aim of assessing the feasibility of a damping system based on an intimate mixture of a fct phase within a fcc matrix and a sample of the as-cast material was heat treated at 500°C for 3 days. An optical micrograph, Fig. 49 showed heavy precipitation at grain boundaries and a striated structure similar to that observed in the 50%Mn-50%Ni alloy. An axial ratio of 0.971 was recorded by X-ray measurement, but as the structure of the γMn and MnNi phases was very similar, it was not possible to discern if the tetragonality referred only to the MnNi precipitate or if the tetragonality had also been induced, by coherency strains, into the γMn phase.

Optical examination of the 65%Mn-35%Ni alloy revealed an as-cast structure which was heavily cored and long faint lines of closely spaced precipitate particles within the grains. This was confirmed by electron microscopy on samples which had been water quenched from 1000°C and aged at 500°C for 1 week. Precipitation occurred in long straight lines and on dislocations, Fig. 50. At grain boundaries a very fine mixture of γMn and MnNi had formed. As nucleation of the intermetallic precipitate within this alloy was heterogeneous, no further work

Fig. 51.

Fig. 52.

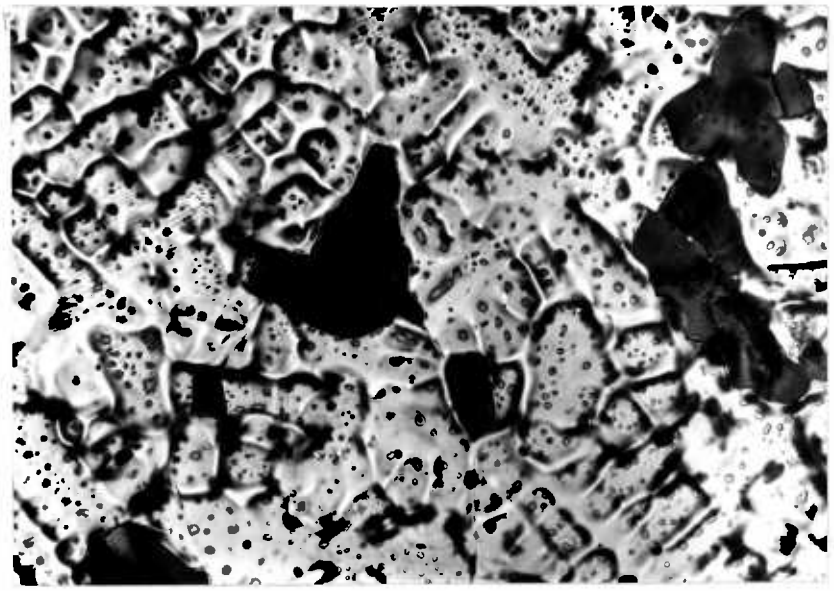


Fig.51. A 85%Mn-15%Ni alloy in the as-cast state. Shows surface tilting resulting from the fcc/fct transformation in the dendrite structure; βMn particles are present in the grain boundaries. x 240.

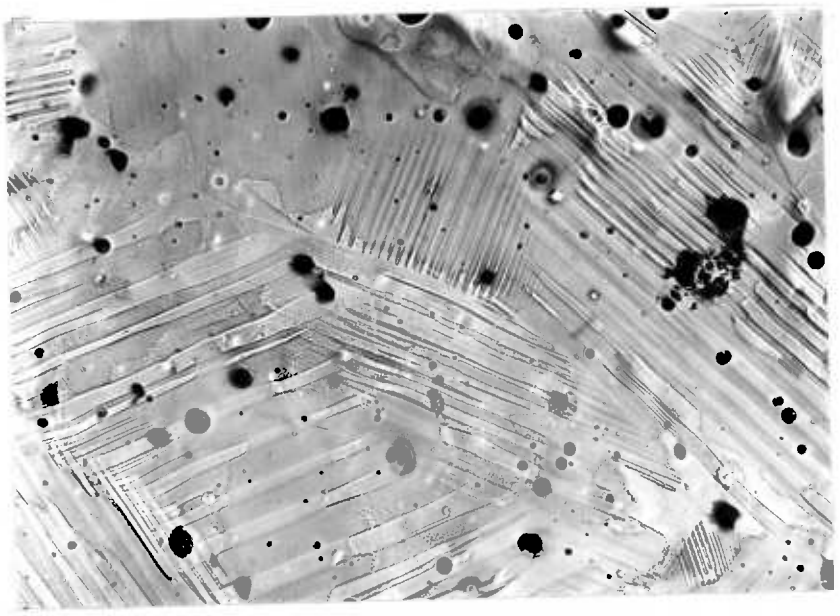


Fig.52. A 85%Mn-15%Ni alloy, solution treated for 2 hours at 1000°C and water quenched. Shows clearly defined surface tilting associated with the fcc/fct transformation. x 200.

Fig. 53.

Fig. 54.



Fig.53. A 85%Mn-15%Ni alloy, solution treated for 48 hours at 1000°C, water quenched and heat treated for 1 week at 500°C. Shows tweed pattern and intersecting microtwins. x 26,000.



Fig.54. Same area as in Fig. 53 showing the further propagation of intersecting microtwins. x 26,000.

was undertaken.

5.5.1.3 85%Mn-15%Ni alloy.

The cast alloy proved difficult to roll and it was necessary to maintain the temperature between about 800°C to 1000°C to prevent cracking. In the cast state the alloy was found to consist predominantly of the heavily cored γMn phase which exhibited surface tilts, indicating an fct structure, Fig. 51. Small regions of the βMn phase were also present, providing a probable explanation for the difficulty in rolling the material. However, after a solution treatment of 2 hours at 1000°C, followed by water quenching, all the βMn phase and much of the coring had been removed and the surface tilting could be seen in marked contrast, Fig. 52. The black spots on this micrograph are thought to be very small impurity particles which have been greatly exaggerated in size by the action of the etching reagent. After solution treatment, heat treatments at temperatures up to 500°C and for times up to 4 weeks, produced little alteration in the microstructure although fine particles could be seen in the grain boundaries after very long ageing times at 500°C. Ageing at 600°C resulted in a complete structural transformation to the βMn phase.

Hardness measurements confirmed that there was little, if any, precipitation occurring during ageing. In the water quenched condition the hardness was found to be $H_V = 85$. After ageing for 1 day at 500°C the hardness was $H_V = 86$ and after ageing for 4 weeks at 500°C the hardness was $H_V = 88$.

Examination of a water quenched sample in the electron microscope revealed an ill-defined tweed structure and typical long separated microtwin boundaries terminating at grain boundaries. After an ageing heat treatment of 1 week at 500°C the tweed pattern was more clearly defined and the generation of intersecting microtwins proceeded during examination in the electron microscope, Figs. 53 and 54. After a heat treatment of 4 weeks at 500°C, the tweed pattern was pronounced and it

Fig. 55.

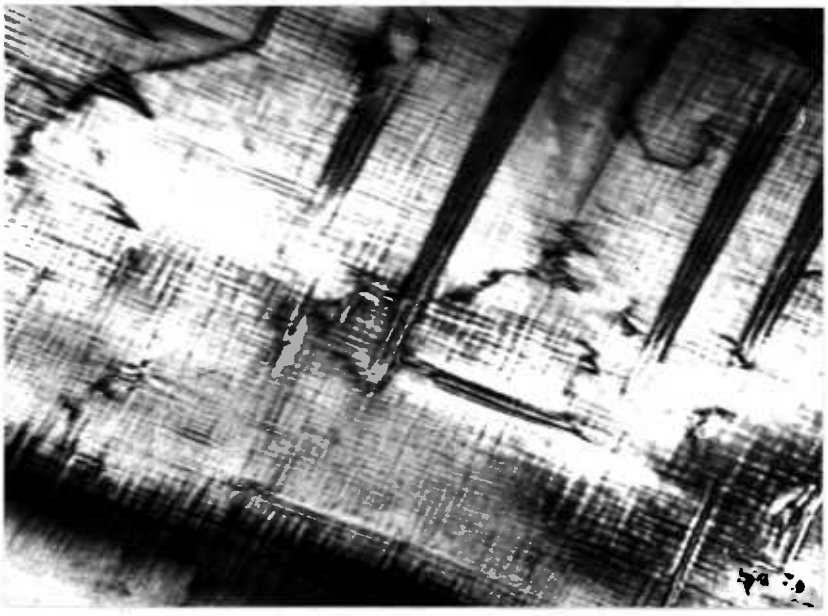


Fig.55. A 85%Mn-15%Ni alloy, solution treated for 48 hours at 1000°C, water quenched and heat treated for 4 weeks at 500°C. Shows clearly defined tweed pattern and microtwins propagating in the same directions as the striations in the tweed pattern. x 39,000.

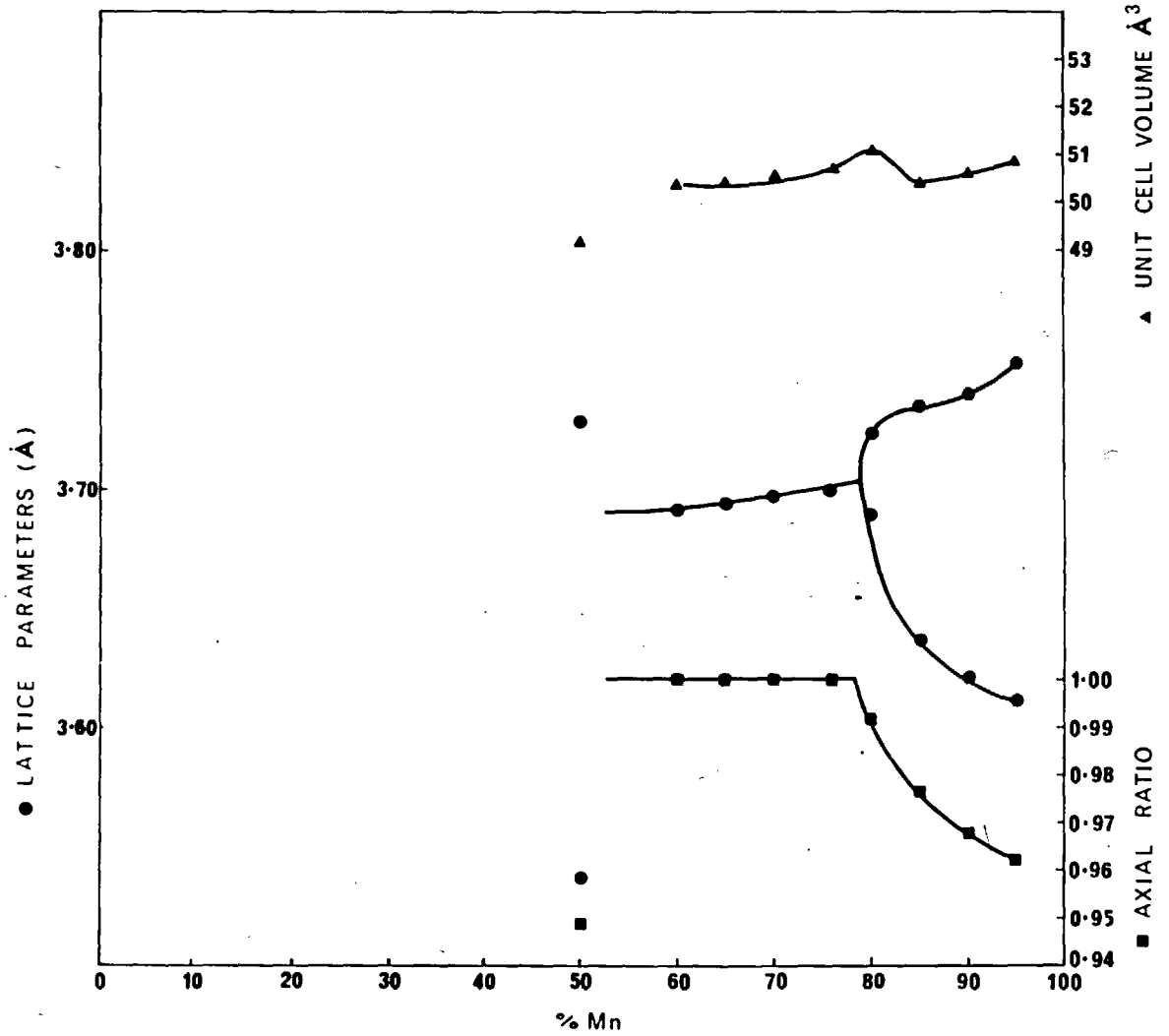


Fig. 56 UNIT CELL PARAMETERS FOR WATER QUENCHED Mn-Ni ALLOYS.

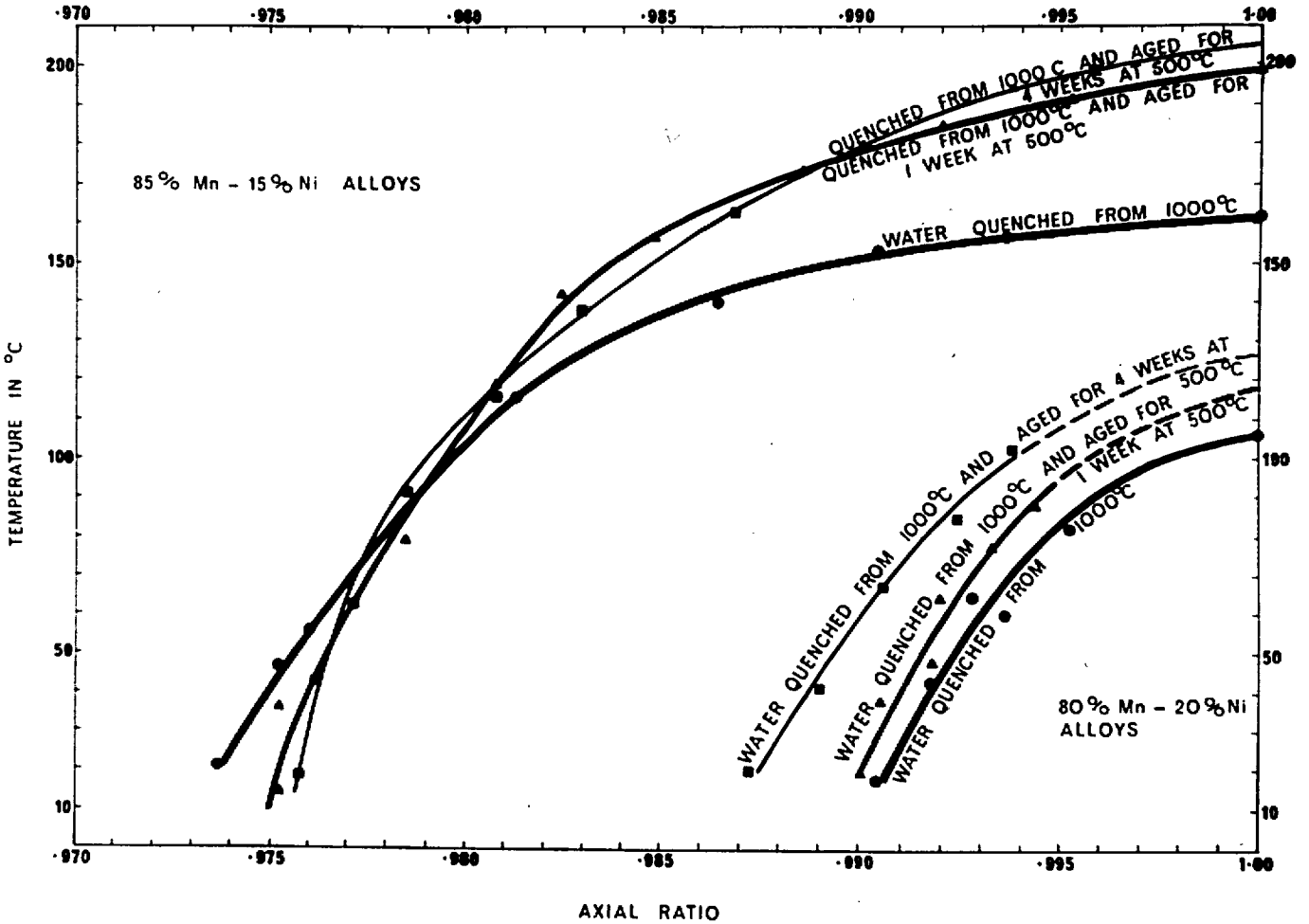


FIG. 57

THE EFFECT OF TEMPERATURE ON THE AXIAL RATIOS OF A NUMBER OF HEAT TREATED SAMPLES OF 85 % Mn – 15 % Ni AND 80 % Mn – 20 % Ni ALLOYS.

proved difficult to differentiate between fine microtwins and tweed pattern, Fig. 55.

X-ray measurements of the axial ratio were found to show a wide degree of scatter, even from the same sample. Furthermore, the peak profiles of the {200} and {220} reflections were broad and uneven at short solution treatment times. This would be expected from a variation in Mn content associated with the heavy coring. Quite often three peaks were found associated with the {200} and {220} reflections instead of the expected two. With long solution treatment times the average grain size had enlarged appreciably and it was difficult to find grains lying in a suitable orientation to diffract the X-rays. The reflections obtained from these homogenised samples were more clearly defined. However, the scatter in axial ratio measurements from different grains within the same sample was still appreciable. After measuring the room temperature axial ratios of a considerable number of samples, it was concluded that neither solution treatment time nor subsequent ageing time at 500°C had any appreciable effect on the axial ratio. Fig. 56 shows the variation in lattice parameters with Mn content for the Mn-Ni alloys examined and it can be seen that at the high Mn end of the diagram the lattice parameters are very sensitive to small changes in composition. In this series of alloys it was anticipated that the high Mn content would provide a high Néel temperature and hence a high fcc/fct transformation temperature. For this reason, and bearing in mind the scatter in results, it was thought worthwhile to conduct some heating tests to determine the fcc/fct transformation temperature. Grains were selected which gave clearly defined separation of the cubic and tetragonal components of the {200} or {220} reflections. The transformation temperature was found to vary from about 150°C to just above 200°C, Fig. 57. In view of the apparent lack of response to the ageing heat treatment, the trend towards a higher transformation temperature with longer ageing times

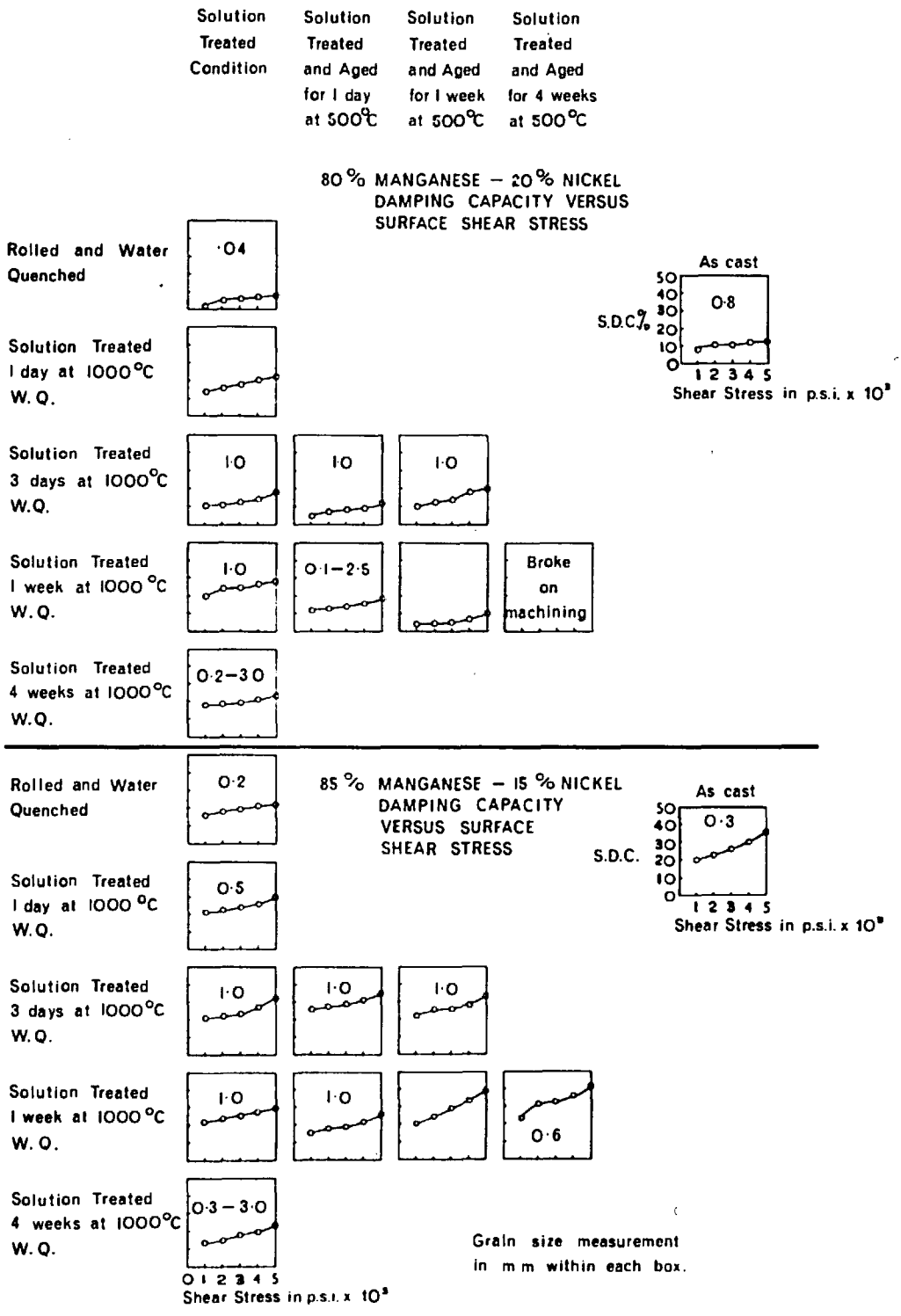


Fig. 58 The stress-dependence of the damping capacity of alloys 85 % Mn – 15 % Ni and 80 % Mn – 20 % Ni which have been given a variety of heat treatments.

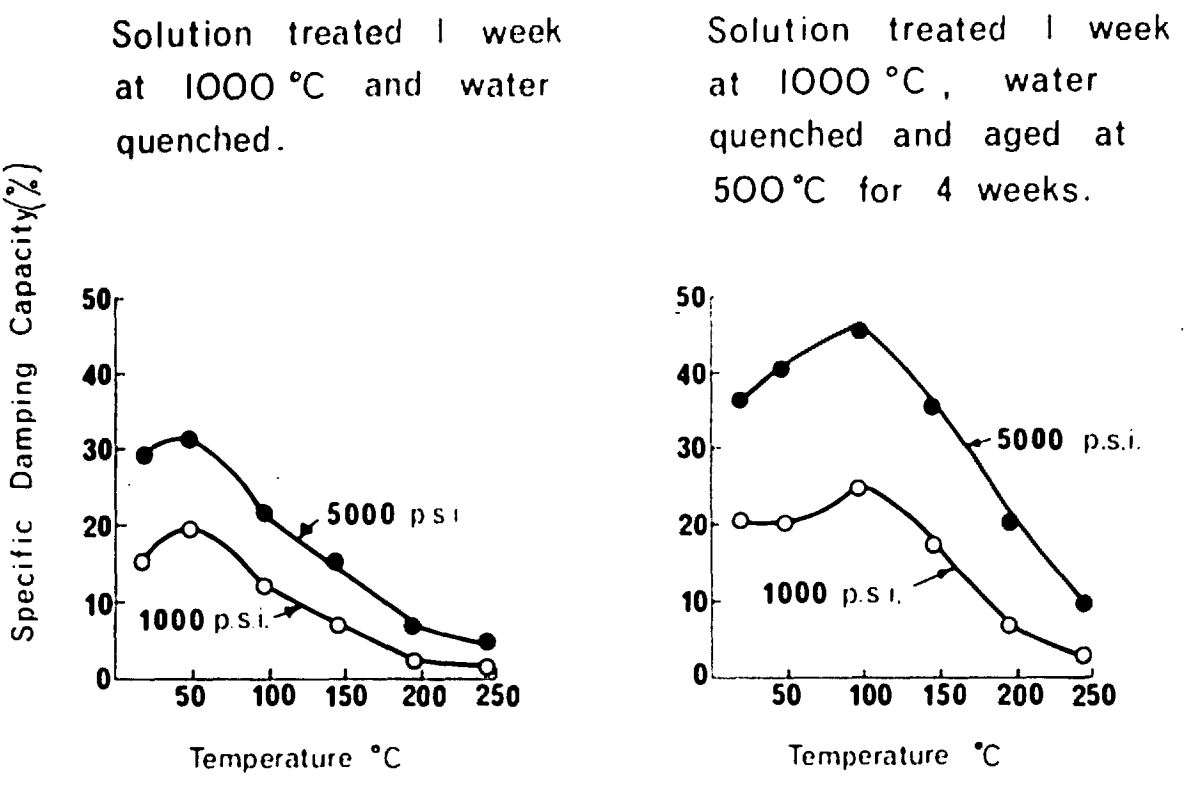


Fig. 59 The effect of temperature on the damping capacity of two samples of a 85 % Mn – 15 % Ni alloy. Both samples have been solution treated for 1 week at 1000 °C and water quenched. One sample has been given a further heat treatment of 4 weeks at 500 °C.

was somewhat surprising.

The damping capacity was determined after a variety of solution treatment and ageing heat treatment times, Fig. 58. There was a slight trend towards increasing damping capacity at all stress levels with increasing solution treatment times of up to 1 week. After 4 weeks solution treatment the damping capacity had fallen slightly again. The variation in grain size with solution treatment time may be affecting these results to a certain extent. There was also a small tendency for increased damping capacity with increasing ageing times at 500°C. The damping results which were measured at a variety of temperatures, Fig. 59, confirmed the tentative X-ray results and produced outstandingly higher damping capacities at elevated temperatures than previously reported for any other Mn-Cu alloy, Fig. 31. In view of the excellent high temperature damping properties of the 85%Mn-15%Ni alloy, a repeat damping capacity measurement at room temperature was made on a sample which had previously been tested 6 months before. The results on average were about 3% lower, indicating that the reported room temperature ageing effect in Mn-Cu alloys[5] does not present a problem in the 85%Mn-15%Ni alloy.

5.5.1.4 80%Mn-20%Ni alloy.

The trends observed in the 80%Mn-20%Ni alloy were very similar to those in the 85%Mn-15%Ni alloy. However, the cast structure was entirely γMn and the βMn phase was absent; probably because of this the 80%Mn alloy was found easier to roll.

After a two hour solution treatment at 1000°C followed by a water quench, all the coarse coring had been removed and surface tilting associated with the fct structure could just be seen. Because of the sluggishness of the transformation from $\gamma \rightarrow \gamma + \alpha$ in the 85%Mn-15%Ni alloy, all ageing treatments on the 80%Mn alloy were also conducted at 500°C.

Electron microscopy revealed the presence of both tweed pattern and microtwins, which were seen to move easily in all

samples of the 80%Mn-20%Ni alloy which had been given a variety of solution treatments at 1000°C and ageing treatments at 500°C.

After a solution treatment of 3 days at 1000°C the hardness of the alloy was $H_v = 90$. A further ageing heat treatment of 1 day at 500°C gave $H_v = 94$ and after ageing for 1 week at 500°C, $H_v = 95$.

The same difficulties in obtaining reproducible X-ray results, which were encountered in the 85%Mn alloy, were also experienced with the 80%Mn-20%Ni alloy. The axial ratios were, in all cases, closer to 1 than those found in the 85%Mn alloy and because of the close proximity of the (220) and (022 + 202) reflections, accurate measurements were difficult. In the solution treated and water quenched condition the fcc/fct transformation temperature was about 110°C and this temperature increased only slightly when further samples were given progressively longer ageing heat treatments, Fig. 57.

The damping results for the 80%Mn-20%Ni alloy indicated that considerable improvement in damping capacity could be achieved by a solution treatment of 1 week at 1000°C, Fig. 58. Subsequent ageing resulted in a decrease in damping capacity.

5.5.1.5 90%Mn-10%Ni alloy

In the cast state the 90%Mn alloy was found to be very hard and brittle. Optical microscopy and X-ray diffraction examination confirmed that the alloy had a βMn structure. The transformation to βMn was largely prevented in a sample of the alloy which had been solution treated for 2 hours at 1050°C and then water quenched. The surface tilting associated with the fct transformation was clearly defined. in the retained γMn structure.

5.5.1.6 95%Mn-5%Ni alloy

The 95%Mn alloy behaved in a similar manner to the 90%Mn alloy and the βMn structure with a hardness of $H_v = 850$ was formed on casting. The fct γMn structure could be retained by water quenching from 1050°C.

5.5.2 Discussion

5.5.2.1 Alloys based on the intermetallic compound MnNi.

Observations on microtwin formation and movement during the heating of the intermetallic compound MnNi inside the electron microscope indicated that damping properties would probably only be developed in a narrow temperature range close to the ordering temperature of about 700°C.

The selection of alloys 60%Mn-40%Ni and 65%Mn-35%Ni was based on the premise that an intimate mixture of a fcc phase with a fct phase, if coherent, would lead to a fct structure of intermediate axial ratio in an analogous manner to the structures developed in aged Mn-Cu alloys. Unfortunately, precipitation occurred in a heterogeneous form in the 65%Mn-35%Ni alloy. There were indications that the required structure may have formed in the 65%Mn-35%Ni alloy. However, the lack of workability of the material and the severely distorted appearance of the microstructure militated against a more detailed approach.

5.5.2.2 High Mn alloys in the Mn-Ni system

Some of the reasons for the poor reproducibility in the X-ray results for high Mn alloys can be suggested, although a completely satisfactory explanation was not found. By analogy with the Mn-Cu system, Fig. 1, it is quite possible for the 80%Mn-20%Ni alloy to have only partially transformed from the fcc to the fct structure at room temperature and intensity relationships between the cubic and tetragonal components of the X-ray reflections would alter accordingly. Short solution treatment times would leave Mn concentration gradients largely unaltered and a corresponding lack of resolution in X-ray reflections at room temperature would result. On the other hand prolonged solution treatments resulted in a Mn loss of the order of 0.5%Mn after 42 hours at 1000°C. Thus Mn loss would probably be much greater at the sample surface. The results of Hicks et al[100] on axial ratio measurements in the Mn-Ni system, which were published after this experimental work had been completed, were in reasonable agreement and both sets of results have been superimposed on the thermal equilibrium diagram, Fig. 41.

However, in a subsequent publication by Japanese workers[101], similar variations in the relative intensities of the X-ray reflections were recorded. The interpretation given involved a change from a fct structure with axial ratios less than 1 to an axial ratio greater than 1 as the Mn concentration increased from about 85 to 87 at.% Mn. The results must be treated with scepticism because the samples were solution treated in the form of fine powder and this would almost certainly result in appreciable Mn loss. Furthermore, they solution treated the samples for only 3 hours, which is completely inadequate for accurate lattice parameter determinations in Mn alloys.

Structural work on the high Mn-Ni alloys has indicated that good damping properties would be expected at high temperatures and damping measurements have now confirmed this. The cooling rate during casting is sufficiently slow to cause the transformation from $\gamma \rightarrow \gamma + \beta$ in those alloys containing more than about 85%Mn. Because of this, only alloys in the composition range 80 - 85%Mn are likely to be useful.

Although the high temperature damping properties of the 85%Mn alloy have proved to be outstanding, the heat treatments involved are extremely lengthy and therefore not commercially attractive. Examination by optical microscopy and X-ray diffraction, as well as hardness measurements, did not reveal any obvious structural changes occurring on ageing the 80% and 85%Mn alloys. However, the electron microscope results, the change in the fcc/fct transformation temperature, as well as the much improved damping results at elevated temperatures indicate that there is some Mn aggregation occurring on ageing. The final stages of the transformation leading to the formation of αMn precipitate does not appear to occur.

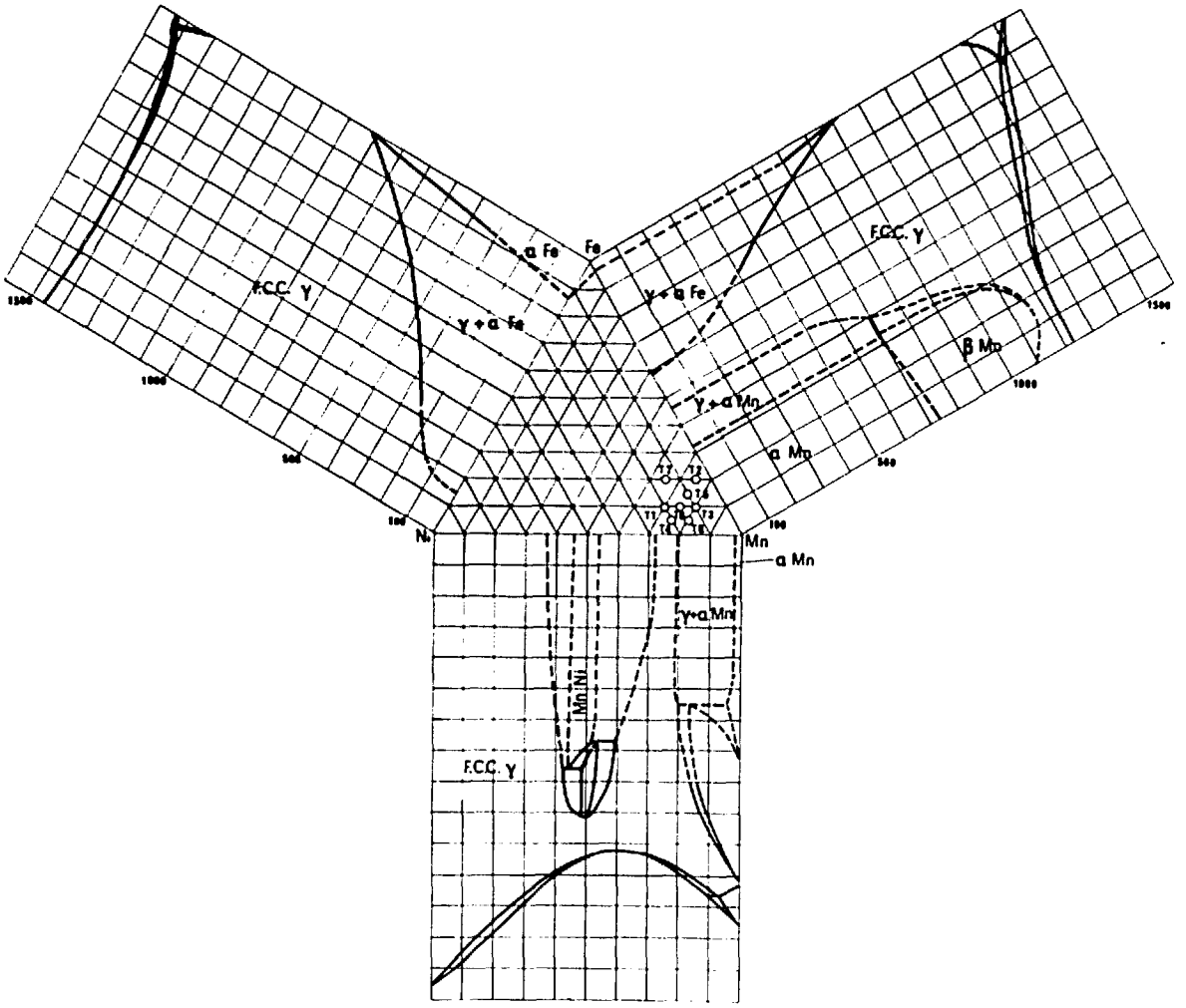
From these results it can be concluded that the addition of Ni to Mn stabilises the γMn phase to such an extent that prolonged ageing, just below the $\gamma \rightarrow \gamma + \beta$ equilibrium temperature, is required before the ageing reaction will proceed and the

transformation from $\gamma \rightarrow \gamma + \beta$ only occurs in slowly cooled alloys containing more than 85%Mn.

In Mn-Cu alloys, the transformation from $\gamma \rightarrow \gamma + \alpha$ occurs at a controllable rate at 400°C and much quicker than this at higher temperatures. It was therefore decided to make additions of Cu to the basic 85%Mn-15%Ni alloy in the hope of exercising a better control over ageing times.

Apart from this approach, the useful composition range of the binary Mn-Ni alloys is very limited and it was thought possible that the useful area of the $\gamma + \alpha$ phase field could be expanded to lower and higher Mn concentrations by the addition of Fe or Cu.

FIG. 60 BINARY EQUILIBRIUM DIAGRAMS OF Mn–Ni , Mn–Fe AND Fe–Ni INCORPORATING THE NOMINAL COMPOSITIONS OF SELECTED TERNARY ALLOYS. Refs. 98 and 99.



CHAPTER 6.

THE Mn-Fe-Ni SYSTEM.

6.1 INTRODUCTION.

In the absence of a ternary equilibrium diagram, the binary systems have been incorporated on one diagram, Fig. 60[98,99] to serve as a guide for the selection of ternary alloy compositions. It was anticipated that useful ternary Mn-Fe-Ni alloys would only be identified if the competing influences of both Ni and Fe on the stability of the various Mn phases was correctly balanced. The important prerequisites are listed below.

a) The large αMn phase field in the Mn-Fe system needs to be counteracted by the lack of solubility of Ni in the αMn phase in the Mn-Ni system, so that the extent of the αMn phase field in the ternary diagram is limited.

b) The area occupied by the $\gamma + \alpha$ phase field in the ternary system should be as large as possible.

c) In the Mn-Ni system the kinetics of the $\gamma \rightarrow \gamma + \alpha$ transformation are very slow and could possibly be increased by the presence of Fe.

d) The stability of the βMn phase in the Mn-Fe system could possibly be reduced by the presence of Ni.

e) The addition of Fe could possibly restrict the ternary composition range of alloys containing the intermetallic MnNi.

The nominal and final compositions of the selected ternary alloys, which have been given identifying numbers T1 to T8, are shown in Table 3 and are superimposed on the ternary section at $0^{o}C$ in Fig. 60.

6.2. RESULTS.

In each case the cast structure was first broken down by rolling; a number of samples were heated to $1100^{o}C$ and water quenched and then given a variety of heat treatments, one treatment for each sample at every $100^{o}C$ from $300^{o}C$ up to $1100^{o}C$. The samples were then quenched to retain, where possible, the

○ γ

ⓣ γ TETRAGONAL

◑ γ + β

◒ γ TETRAGONAL + β

● β

● Mn Ni INTERMETALLIC

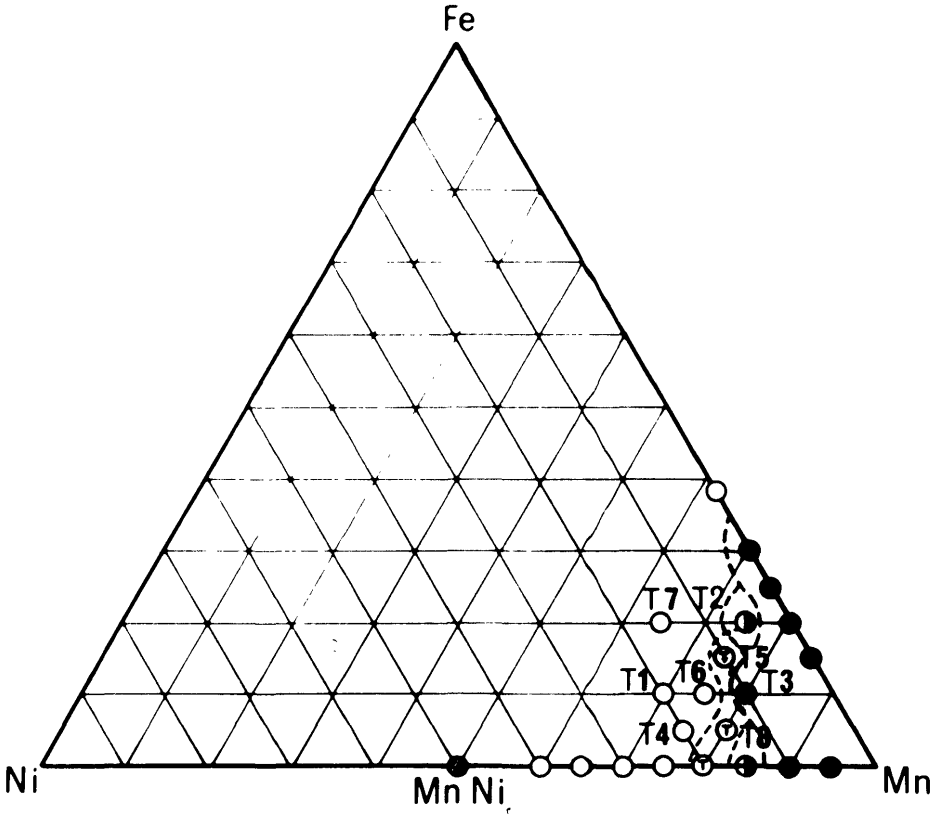


FIG. 61 THE PHASES PRESENT IN VARIOUS CAST Mn – Ni – Fe ALLOYS.

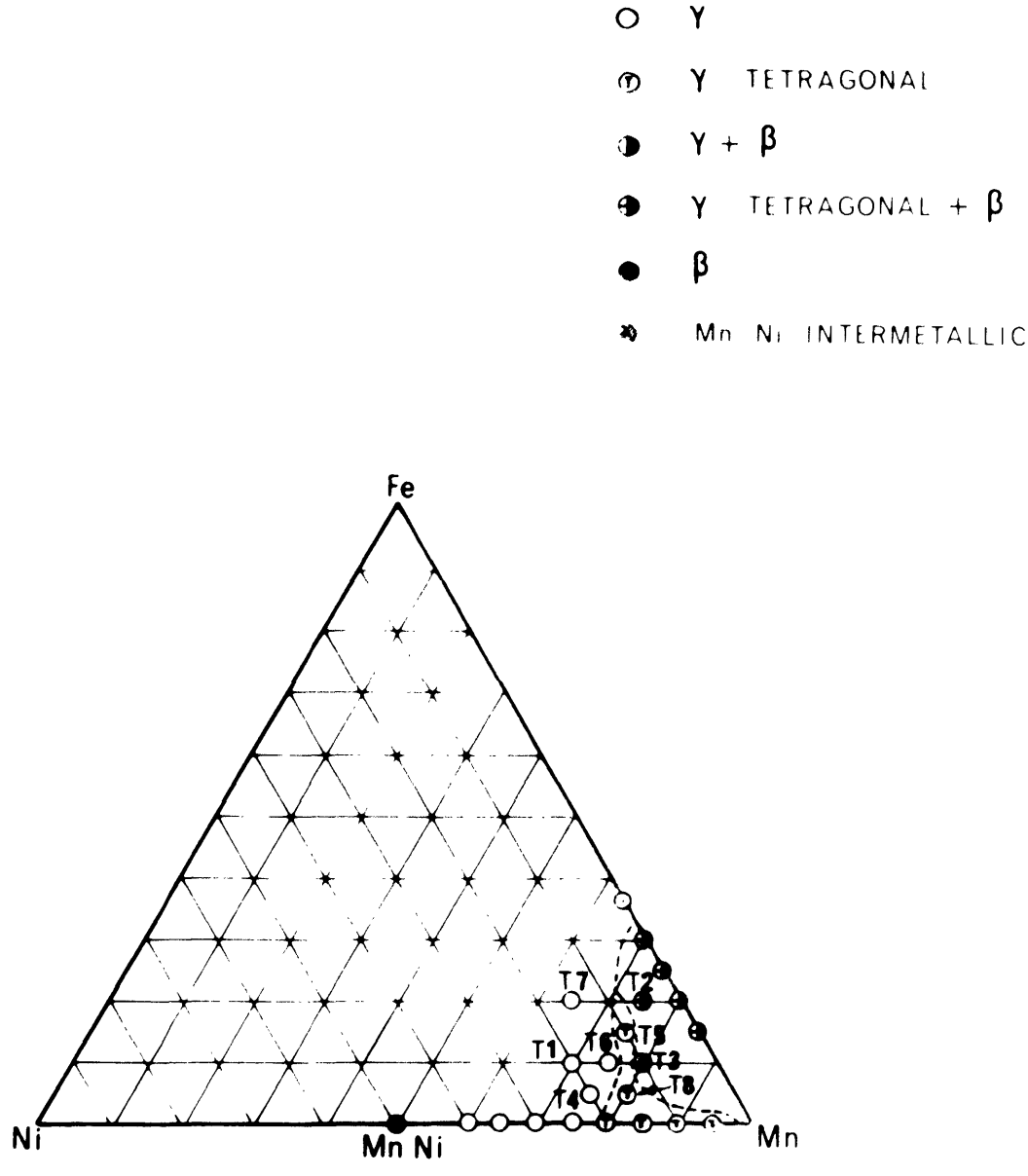


FIG. 62 THE PHASES PRESENT IN VARIOUS WATER QUENCHED Mn—Ni—Fe ALLOYS.

structures which were present at the various temperatures. For the sake of brevity, the essential features of these results have been extracted and recorded in schematic form in Figs.61 and 62.

6.3. DISCUSSION.

It was anticipated that the presence of Ni would decrease the influence of Fe on the stability of the βMn phase and allow the γMn phase to be retained during the casting operation. In this respect the reasoning behind the choice of the alloy compositions has proved correct but, unfortunately, the influence of the Ni was not sufficient and the composition range over which the γMn phase was completely retained in the fct form, was too small to be of much practical value, Fig. 61.

The damping results for alloy T8 (80%Mn-5%Fe-15%Ni) shown in Table 4, indicate that it is possible to develop damping properties in the Mn-Fe-Ni system. Work on this system was terminated because the influence of Fe on the stability of the βMn phase could not be counteracted sufficiently by the presence of Ni.

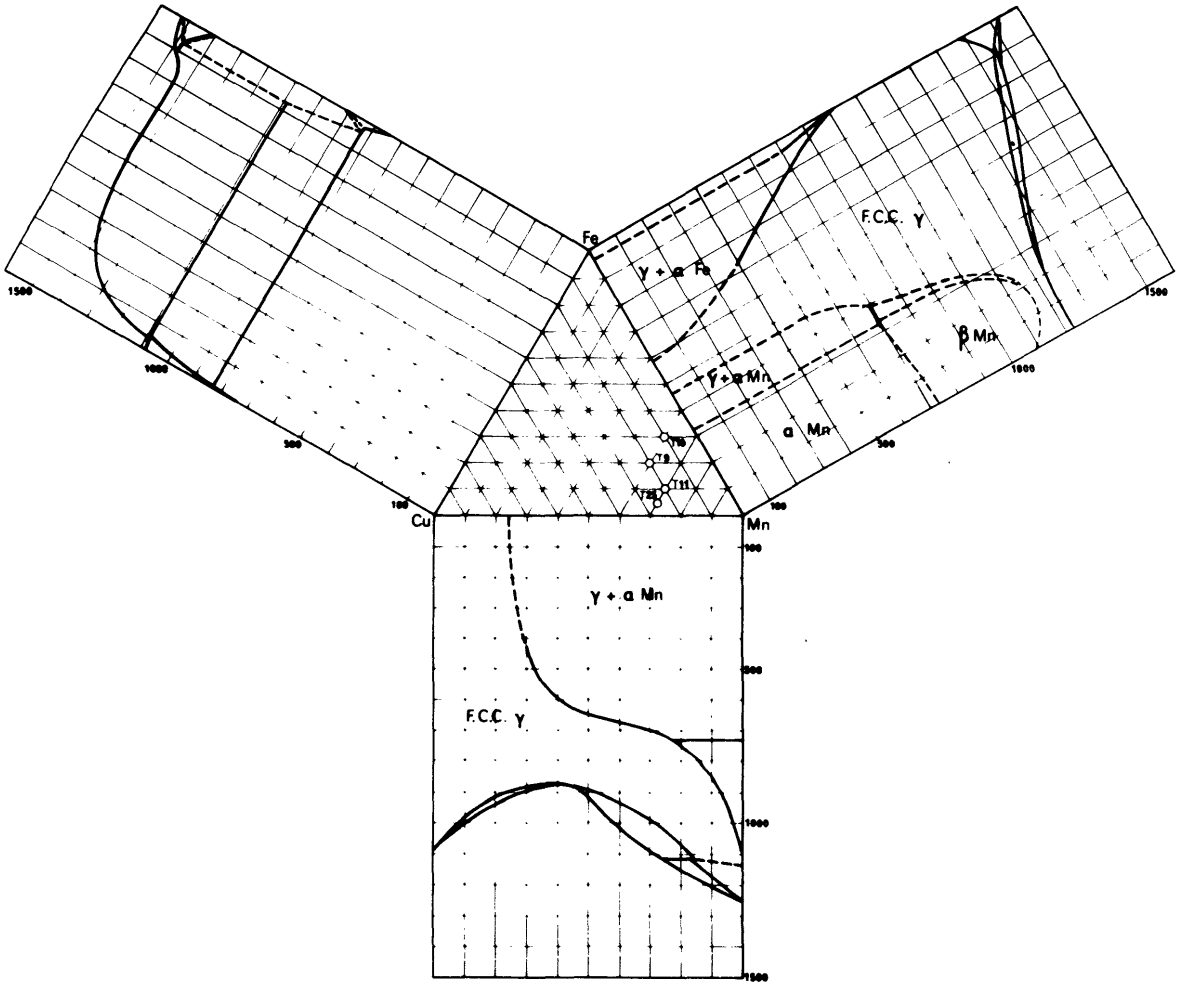


FIG 63 THE BINARY EQUILIBRIUM DIAGRAMS Cu–Fe, Mn–Fe AND Mn–Cu INCLUDING THE SELECTED TERNARY COMPOSITIONS.

Refs. 98 and 99.

Fig. 64.

Fig. 65.

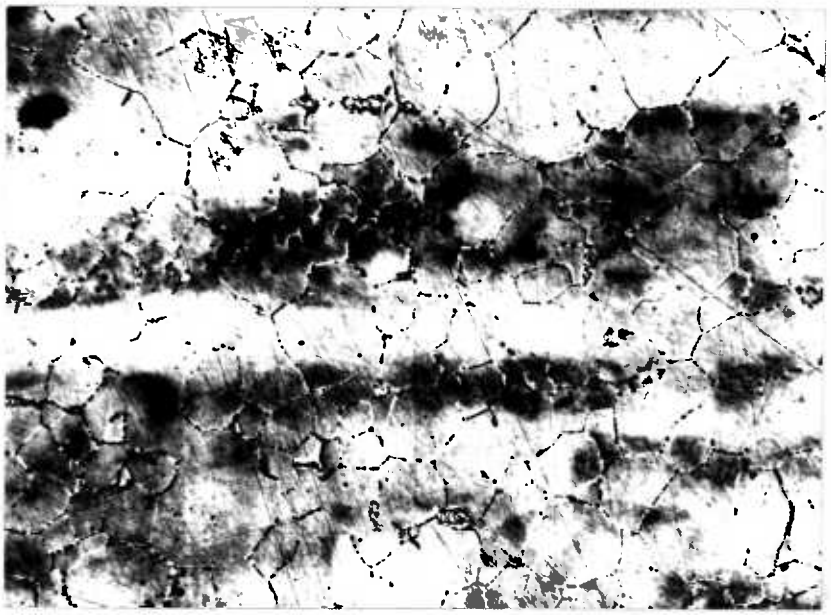


Fig.64. Alloy T26(70%Mn-5%Fe-25%Cu), rolled, water quenched from 900°C and heat treated for 3 hours at 500°C. Shows the presence of αMn in the grain boundaries. x 530.

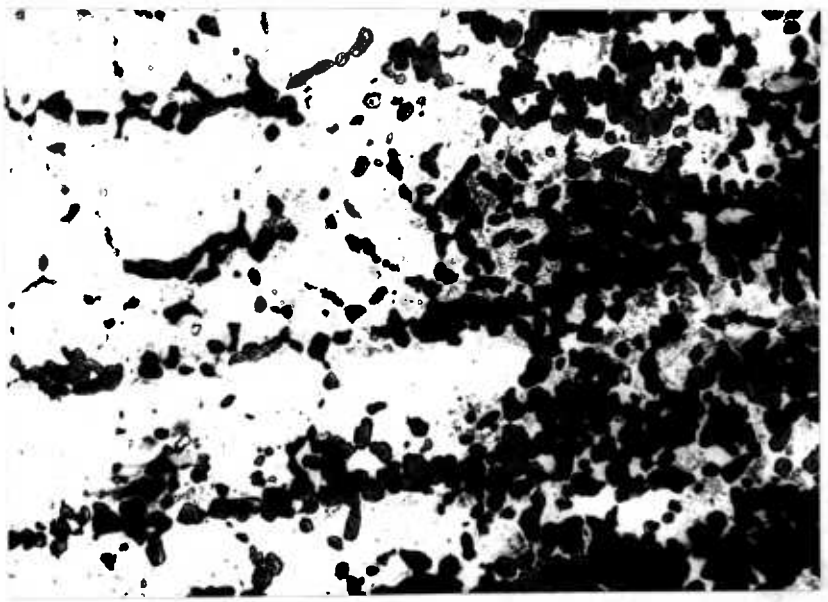


Fig.65. Alloy T26(70%Mn-5%Fe-25%Cu), rolled, water quenched from 900°C and heat treated for 3 hours at 700°C. Shows stringers of βMn particles. x 530.

CHAPTER 7.

THE Mn-Fe-Cu SYSTEM.

7.1 INTRODUCTION.

The three binary equilibrium diagrams Cu-Fe, Mn-Cu and Mn-Fe and the selected ternary compositions are incorporated in Fig. 63[98,99]. Cu is particularly efficient in promoting the stability of the γMn phase and limiting the stability of the βMn phase. It was anticipated therefore, that the presence of Cu might counteract the influence of Fe in stabilising βMn to a greater extent than the addition of Ni reported in chapter 6. The nominal and final compositions of the alloys which have been cast in this system are labelled T9 to T11 and T26 and are recorded in Table 3, and superimposed on the ternary equilibrium diagram, Fig. 63.

7.2. RESULTS.

In the cast state, alloy T9 (60%Mn-20%Fe-20%Cu) and T10 (60%Mn-30%Fe-10%Cu) rang when struck and alloys T11(70%Mn-10%Fe-20%Cu) and T26 (70%Mn-5%Fe-25%Cu) emitted a dull note.

On rolling the first three of these alloys at temperatures from 900°C down to 600°C, they all broke into fragments. If extreme care was taken and the rolling performed at about 600°C, it was possible to reduce the thickness of the material down to 0.1 ins. irrespective of the starting size. Alloy T26 (70%Mn-5%Fe-25%Cu) rolled down to a thin strip without difficulty. In this alloy the structural studies on samples which had been quenched from various temperatures, provided a probable explanation for the brittle behaviour of the other three alloys during the rolling process. At temperatures between 400°C and 600°C, αMn was precipitated, firstly in the grain boundaries and later within the grains, Fig. 64. At temperatures between 700°C and 900°C, large βMn particles formed and these then aggregated into bands, Fig. 65. This effect presumably originated in the Mn-rich dendrites which had been broken down and reoriented during the working schedule. The disintegration

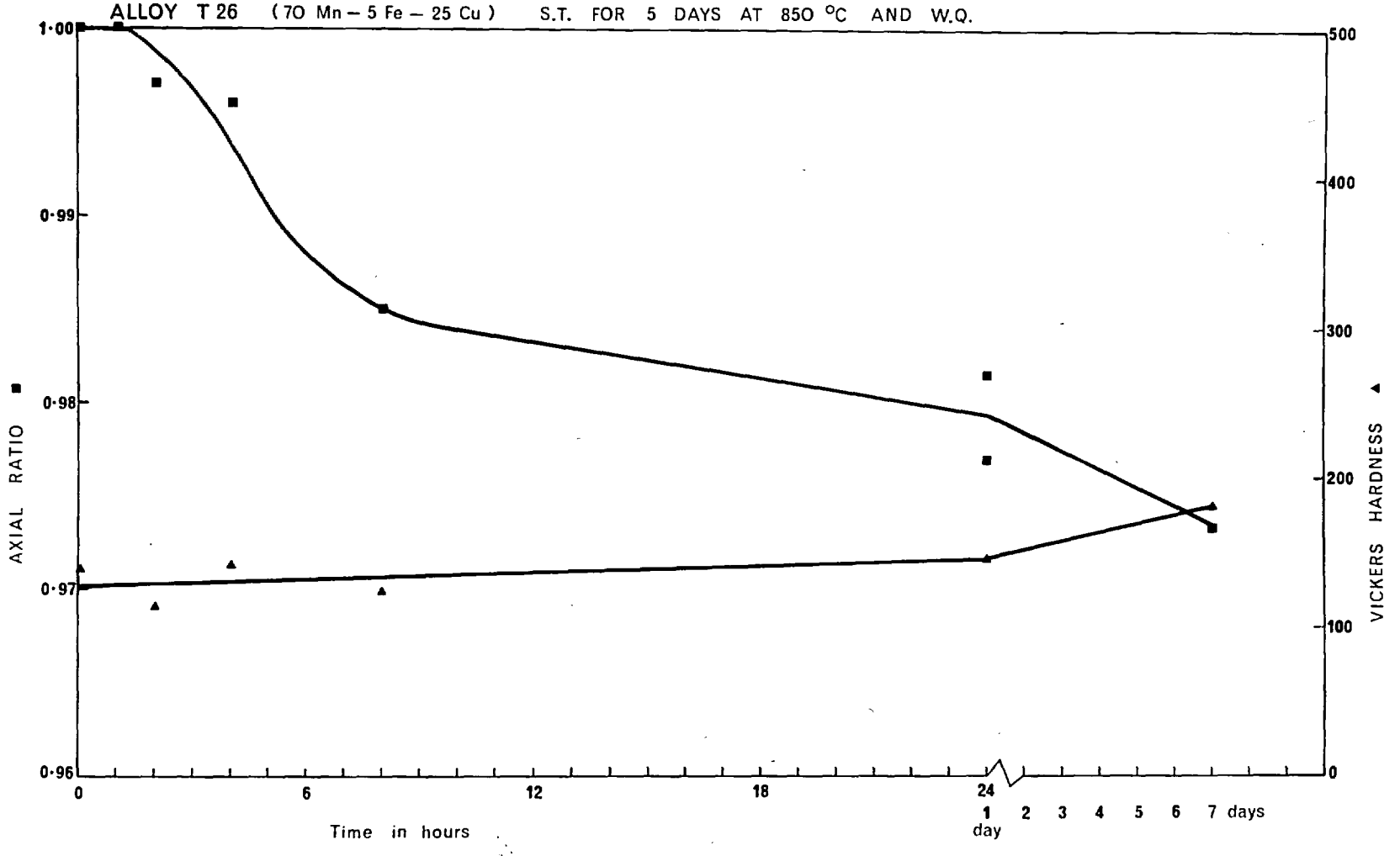


Fig. 66 Change in axial ratio and hardness (H_v), measured at room temperature, with the heat treatment time at 400 °C given to alloy T 26 (70 % Mn – 5 % Fe – 25 % Cu)

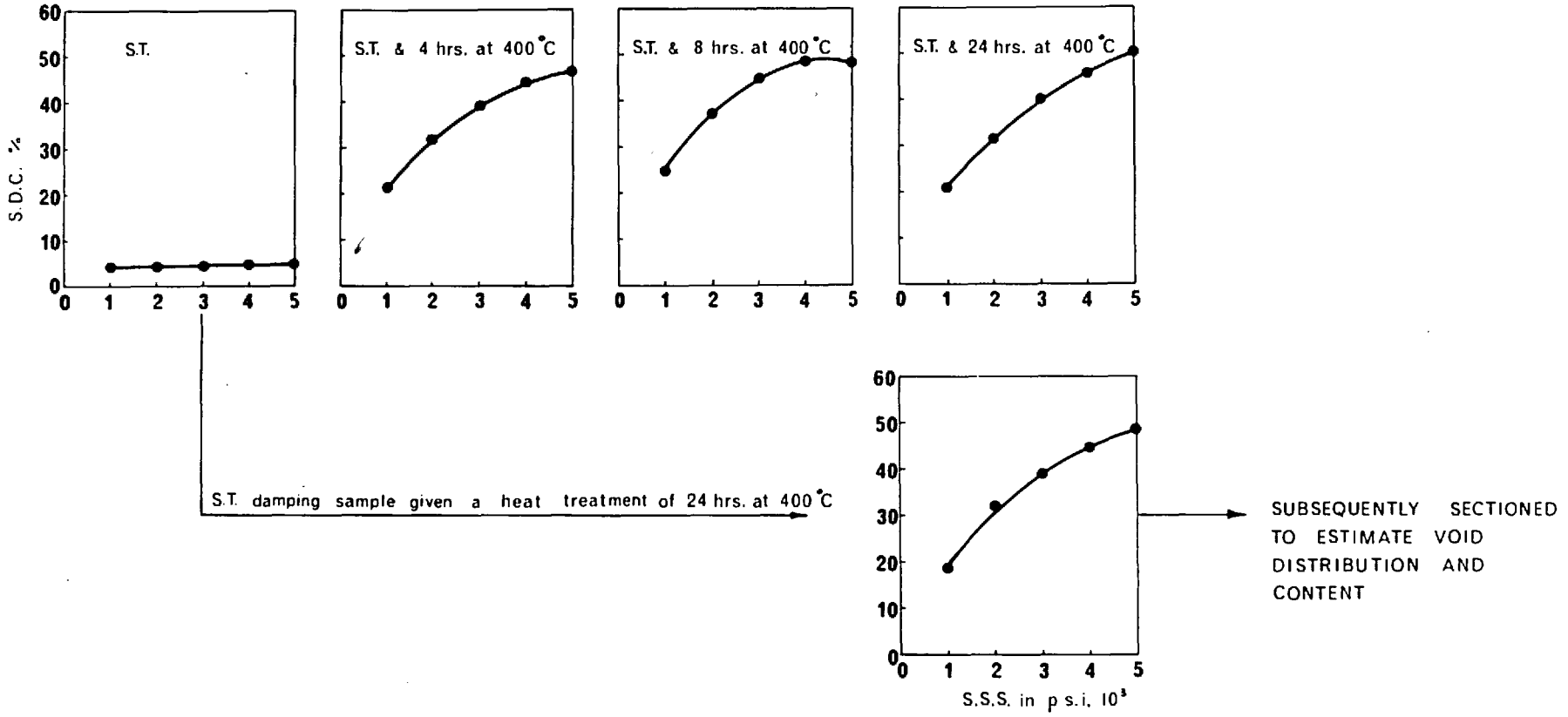


FIG. 67 THE STRESS DEPENDENCE OF THE DAMPING CAPACITY OF ALLOY T 26 (70 % Mn – 5 % Fe – 25 % Cu) WHICH HAS BEEN SOLUTION TREATED FOR 5 DAYS AT 850 °C AND GIVEN A VARIETY OF HEAT TREATMENTS.

during rolling of the other ternary Mn-Fe-Cu alloys with higher Fe contents was therefore due to the formation of βMn at the rolling temperature.

Alloy T26 (70%Mn-5%Fe-25%Cu) was solution treated at 850°C for 5 days, then given ageing heat treatments of 1, 2, 4, 8, 24 hours and 7 days consecutively at 400°C. The change in axial ratio and hardness H_V with ageing heat treatment times is shown in Fig. 66. After an ageing heat treatment of 24 hours at 400°C the fcc/fct transformation temperature was almost 110°C.

The change in damping capacity with ageing heat treatment time, Fig. 67, is similar to that previously described for a 70%Mn-30%Cu alloy, Fig. 32, although in the case of alloy T26 (70%Mn-5%Fe-25%Cu) longer heat treatment times are required to produce a given damping capacity versus surface shear stress relationship. The damping levels in the ternary alloy are appreciable higher than those obtained from the binary 70%Mn-30%Cu alloy.

At about this time the presence of voids was discovered down the central axis of several damping test samples. The effect was traced back to the very long pipe which formed during casting and which could not always be completely removed. It was therefore essential, before work continued on other systems, to ascertain the effect of the presence of voids on the damping capacity determinations and alloy T26 (70%Mn-5%Fe-25%Cu) was selected. In the solution treated and quenched condition this alloy was fcc and would therefore exhibit a very low damping capacity, if internal friction effects were not being introduced by the voids. There was also a clear indication that voids were present in this sample from a visual examination of the sample end. The lack of influence of the voids on the damping capacity is reflected in the low damping results shown in Fig. 67. The sample was subsequently heat treated and developed a high damping capacity almost identical to that found in another sample which had been given the same heat treatment. The presence of voids

down the centre of the sample was confirmed by a longitudinal section. The voids were found to lie within two distinct size groups of about .05 mm. and 1.5 mm; there were appreciable amounts of the former size but only isolated pores of the latter size.

7.3 DISCUSSION.

The inclusion of Fe in high damping alloys is attractive because of its low cost. The work on the binary Mn-Fe system emphasised that Fe has a propensity for promoting the stability of the βMn phase. This tendency was repeated in a less pronounced manner in the ternary Mn-Fe-Cu alloys and although the γMn phase was retained during the casting process, in contrast to many of the Mn-Ni-Fe alloys, subsequent working at elevated temperatures resulted in the transformation to βMn. Only 5%Fe was included in alloy T26 (75%Mn-5%Fe-25%Cu) and the γMn phase was retained during the casting and rolling schedule. The damping capacities recorded for this alloy were appreciably higher than the parent 70%Mn-30%Cu alloy and were very comparable with the damping properties of the 60%Mn-40%Cu alloy, Fig. 30. Alloy T26 (70%Mn -5%Fe-25%Cu) can therefore be considered a competitor to the standard 60%Mn-40%Cu alloy on the grounds of material cost, although the longer ageing heat treatments that are necessary would counteract the savings. The damping properties at elevated temperatures are also likely to be marginally better than 60%Mn-40%Cu, although this has not been determined.

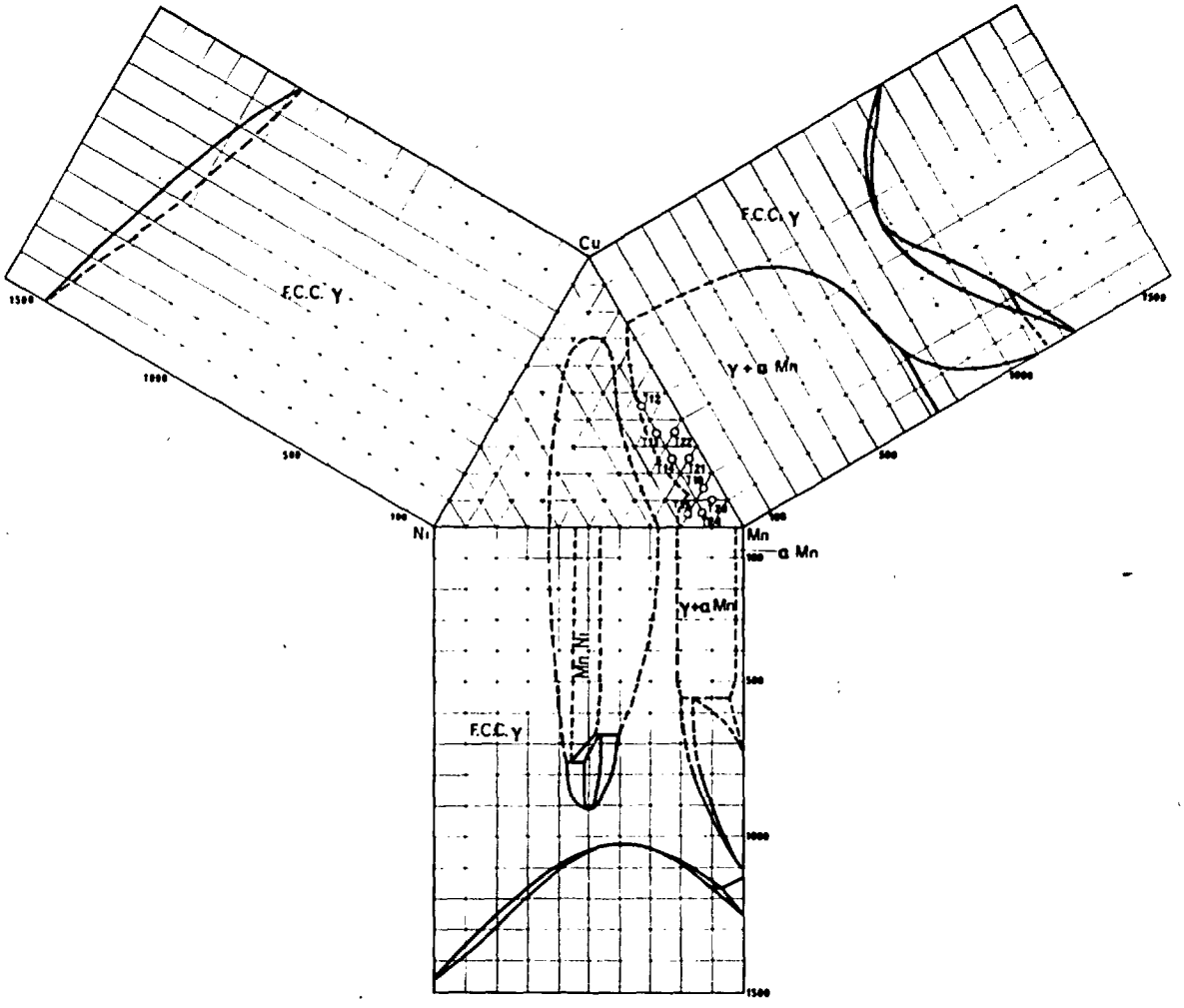


FIG. 68 THE Ni–Cu, Mn–Cu AND Mn–Ni BINARY EQUILIBRIUM DIAGRAMS AND THE ESSENTIAL FEATURES OF THE TERNARY Mn–Ni–Cu SECTION AT 0°C. THE SELECTED TERNARY ALLOY COMPOSITIONS HAVE BEEN SUPERIMPOSED.

Refs. 1, 98 and 99.

CHAPTER 8.

THE Mn-Ni-Cu SYSTEM.

8.1 INTRODUCTION.

The three binary equilibrium diagrams Mn-Ni, Mn-Cu and Cu-Ni have been included in Fig. 68[98,99] as well as the essential features of the ternary equilibrium diagram[1]. The competing influences of Ni and Cu on the stability of the various Mn phases is considered below, as an aid in the selection of appropriate ternary compositions.

a) The rather limited range of the $\gamma + \alpha$ phase field in the Mn-Ni system is expanded considerably in the ternary diagram by the presence of Cu.

b) The very slow kinetics of the $\gamma \rightarrow \gamma + \alpha$ reaction in the Mn-Ni system could possibly be improved by the presence of Cu, because the corresponding reaction in the Mn-Cu system proceeds comparatively quickly, at least at lower Mn concentrations.

c) By the addition of Cu, it was anticipated that it would be possible to take advantage of the exceptional damping properties at elevated temperatures exhibited by the 85%Mn-15%Ni alloy, without the need for heat treatments involving several weeks.

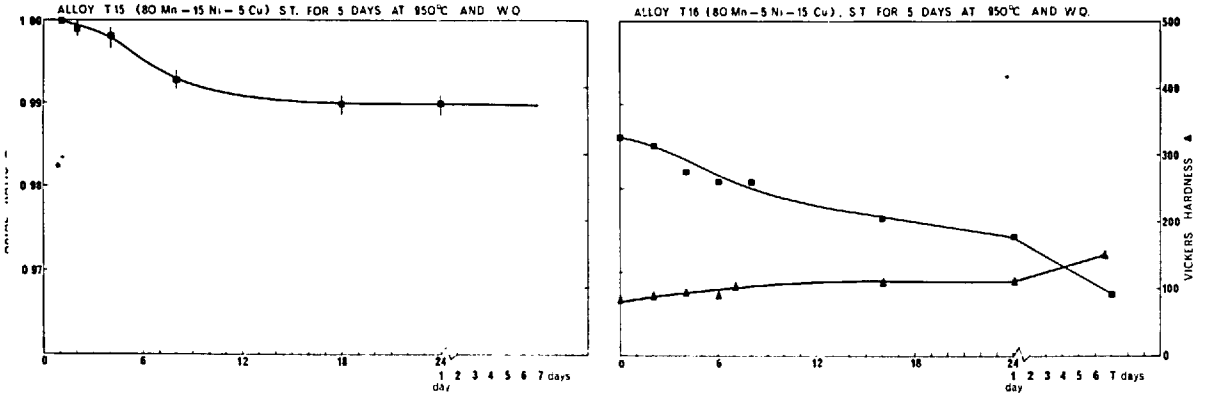
d) The presence of Cu could possibly exert a favourable influence in reducing the tendency towards the βMn formation which created difficulties in the 85%Mn-15%Ni alloy at rolling temperatures.

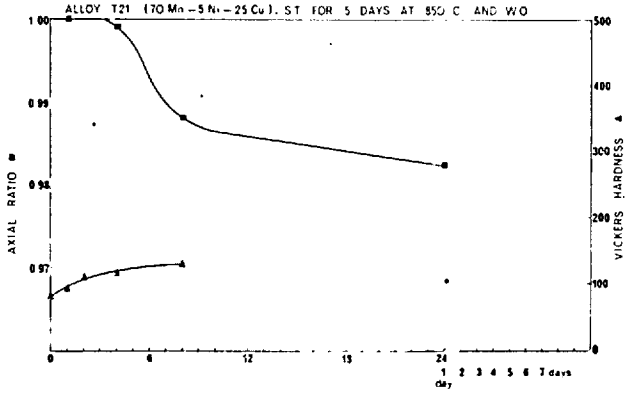
The nominal and final compositions of the alloys have been labelled T12 to T16 and T21 and are shown in Table 3 and are superimposed on Fig. 68.

8.2 RESULTS.

8.2.1 Alloys T12(45%Mn-10%Ni-45%Cu), T13(55%Mn-10%Ni-35%Cu) and T14(65%Mn-10%Ni-25%Cu).

Alloy T12 (45%Mn-10%Ni-45%Cu) quickly broke up on rolling at about 900°C. Optical examination of the etched surface of





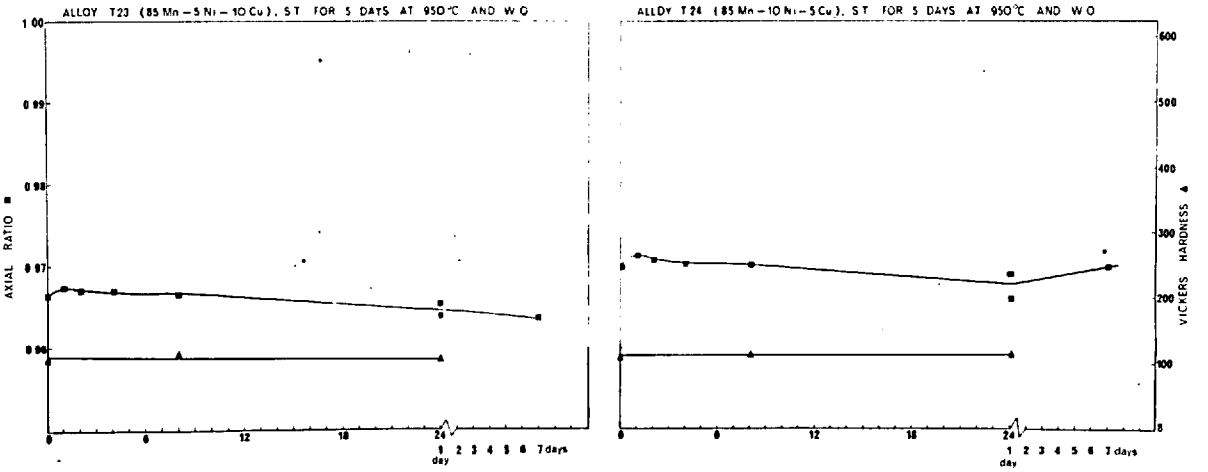


Fig. 49 CHANGE IN AXIAL RATID AND HARDNESS (H_v), MEASURED AT ROOM TEMPERATURE, WITH THE HEAT TREATMENT TIME AT 400°C GIVEN TO VARIOUS Mn-Ni-Cu Alloys.

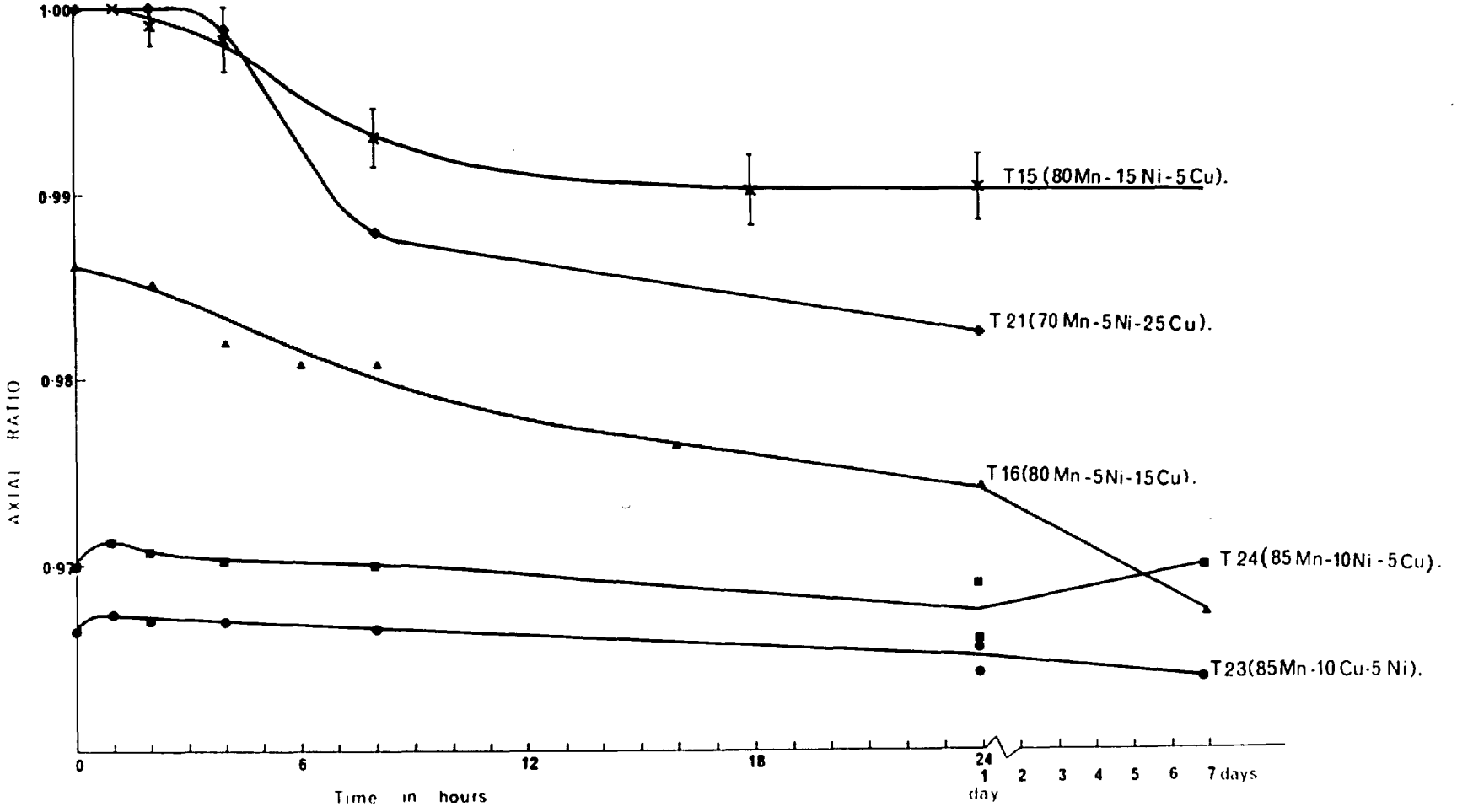


FIG 70 COMPARISON OF THE CHANGE IN AXIAL RATIO WITH HEAT TREATMENT AT 400 °C GIVEN TO VARIOUS Mn - Ni - Cu ALLOYS.

a broken fragment revealed lines of precipitate particles typical of the results obtained from the 60%Mn-40%Ni alloy, described in Section 5.5.1.2. Similar microstructures were observed to a much lesser extent in alloy T13 (55%Mn-10%Ni-35%Cu) and T14 (65%Mn-10%Ni-25%Cu). It was concluded from these results that alloys T12, T13 and T14 lay in the incorrect phase field and that the intermetallic compound MnNi was being precipitated during the heat treatment. The chemical analyses of the alloys is in very close agreement with the nominal compositions, so it must be concluded that the ternary equilibrium diagram, at least around this composition range, is incorrect.

8.2.2 Alloy T22 (60%Mn-5%Ni-35%Cu).

Alloy T22 was solution treated at 850°C for 5 days, water quenched and given a variety of ageing heat treatments at 400°C. The fcc γ structure appeared in all samples following the various heat treatments, apart from possibly the 24 hour heat treatment at 400°C which yielded an fct structure with axial ratio very close to 1. The replacement of 5%Cu by 5%Ni in a 60%Mn-40%Cu alloy had therefore drastically retarded the ageing reaction and because of this further experimental work on the alloy ceased.

8.2.3 Alloy T21 (70%Mn-5%Ni-25%Cu).

Alloy T21 was solution treated at 850°C for 5 days, water quenched and given a variety of ageing heat treatments at 400°C. X-ray results and hardness (H_V) values indicated that the ageing process had proceeded to a limited extent, Figs 69 and 70. The fcc/fct transformation temperature for an ageing heat treatment of 24 hours at 400°C was about 100°C. As no obvious improvements could be achieved over the corresponding 70%Mn-30%Cu alloy, experimental work stopped.

8.2.4 Alloy T15 (80%Mn-15%Ni-5%Cu).

Alloy T15 was solution treated at 950°C, water quenched and given a variety of ageing heat treatments at 400°C. X-ray results are recorded in Figs. 69 and 70.

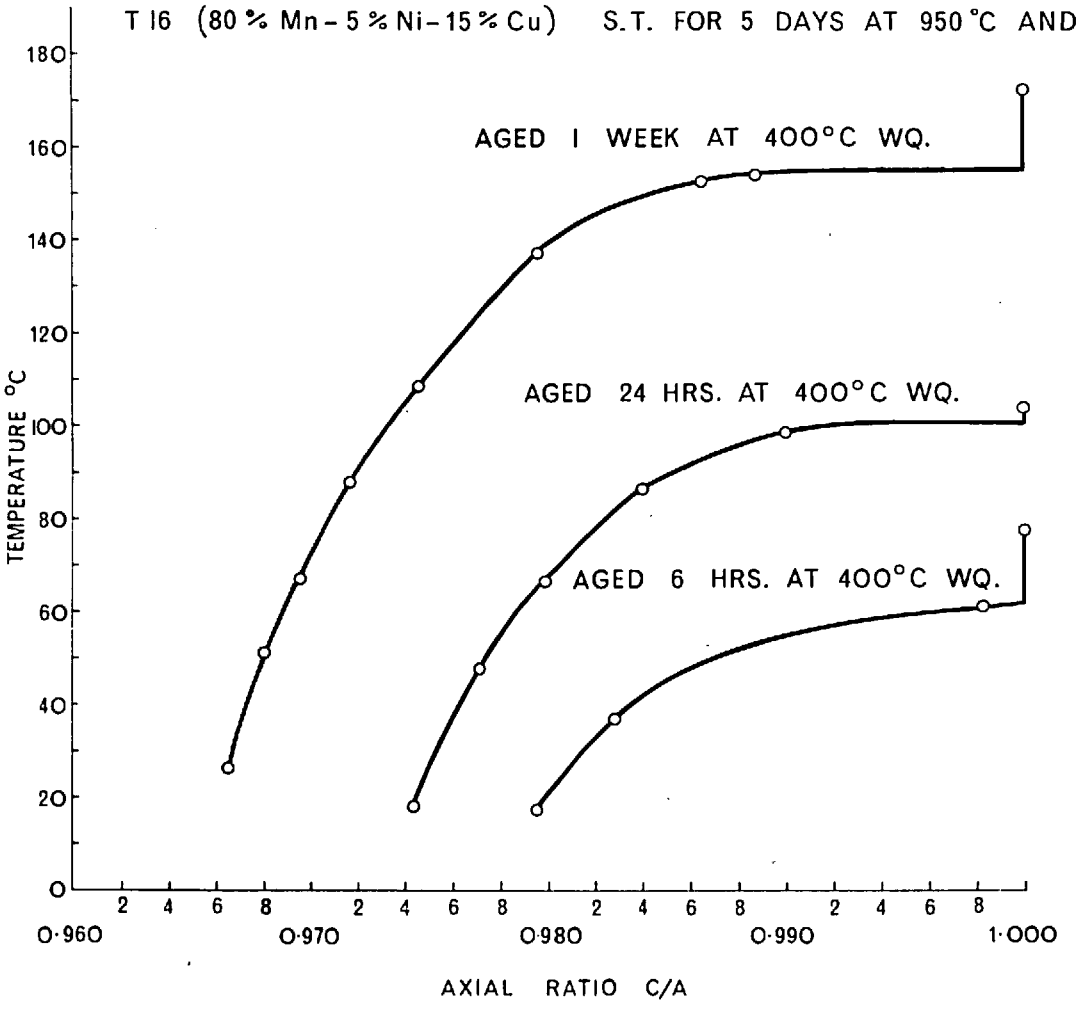


FIG. 71 THE EFFECT OF TEMPERATURE ON THE AXIAL RATIO OF A NUMBER OF HEAT TREATED SAMPLES OF ALLOY T 16. (80 % Mn - 5 % Ni - 15 % Cu)

Suitable samples for the preparation of damping test pieces were respectively rolled and water quenched from 1000°C, solution treated at 1000°C for 1 week then water quenched or solution treated at 1000°C for 4 weeks then water quenched. Unexpectedly, the damping capacity increased considerably with solution treatment time, Table 5, a phenomenon which was subsequently found to be common place in other 80%Mn alloys. Because alloy T15 (80%Mn-15%Ni-5%Cu) showed a lack of response to the ageing heat treatment at 400°C, it was thought unlikely that any radical improvements in the damping properties would result, so work on the alloy was terminated.

8.2.5 Alloy T16 (80%Mn-5%Ni-15%Cu).

Alloy T16 was solution treated at 950°C, water quenched and given a variety of ageing heat treatments at 400°C. X-ray results, Figs 69 and 70, and hardness (H_V) measurements, indicated that the ageing process was proceeding at 400°C. The extent to which the fcc/fct transformation temperature can be increased by heat treatment is shown in Fig. 71.

In many cases where the fcc/fct transformation, as determined by X-ray techniques, has been compared against the temperature at which the damping capacity has fallen to a low level, the former temperature has always been lower than the latter. The accuracy of the X-ray technique is suspect to a certain extent because of the difficulty in measuring axial ratios when the two X-ray reflection peaks overlap. However, this uncertainty is only troublesome at temperatures just below the fcc/fct transformation temperature and it is usually possible to identify a temperature above which peaks corresponding to the X-ray reflections have completely coalesced, even if this does tend to yield a slightly high estimate. It is well known that stress alone can alter the M_S temperature of martensitic reactions and stressing Mn-Cu alloys at room temperature has been shown to affect the onset of the fcc/fct transformation, Section 3.2. Alloy T16 (80%Mn-5%Ni-15%Cu) in the solution treated and quenched condition

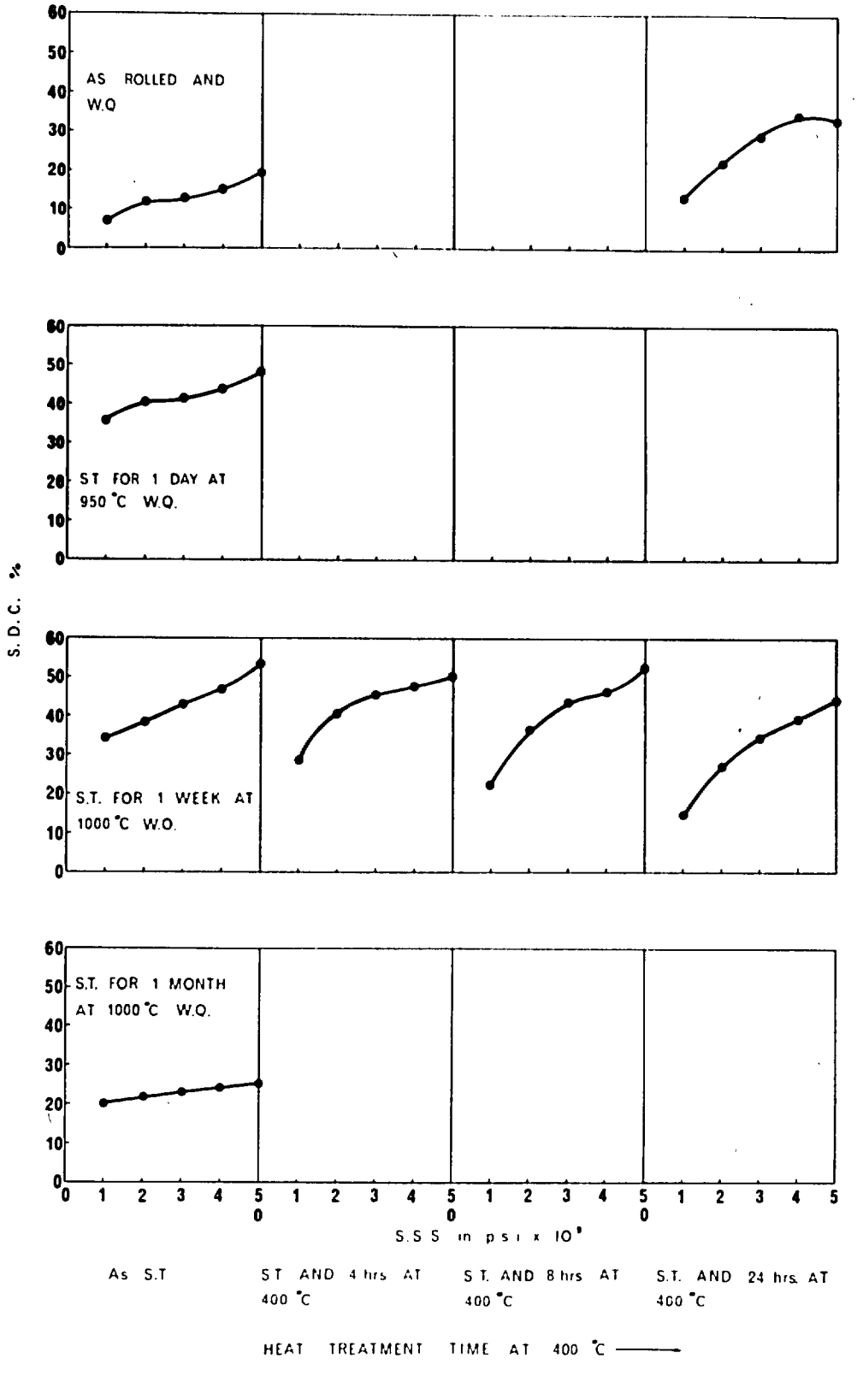


FIG. 72 THE STRESS DEPENDENCE OF THE DAMPING CAPACITY OF ALLOY T 16 (80 % Mn - 5 % Ni - 15 % Cu) WHICH HAS BEEN GIVEN A VARIETY OF HEAT TREATMENTS.

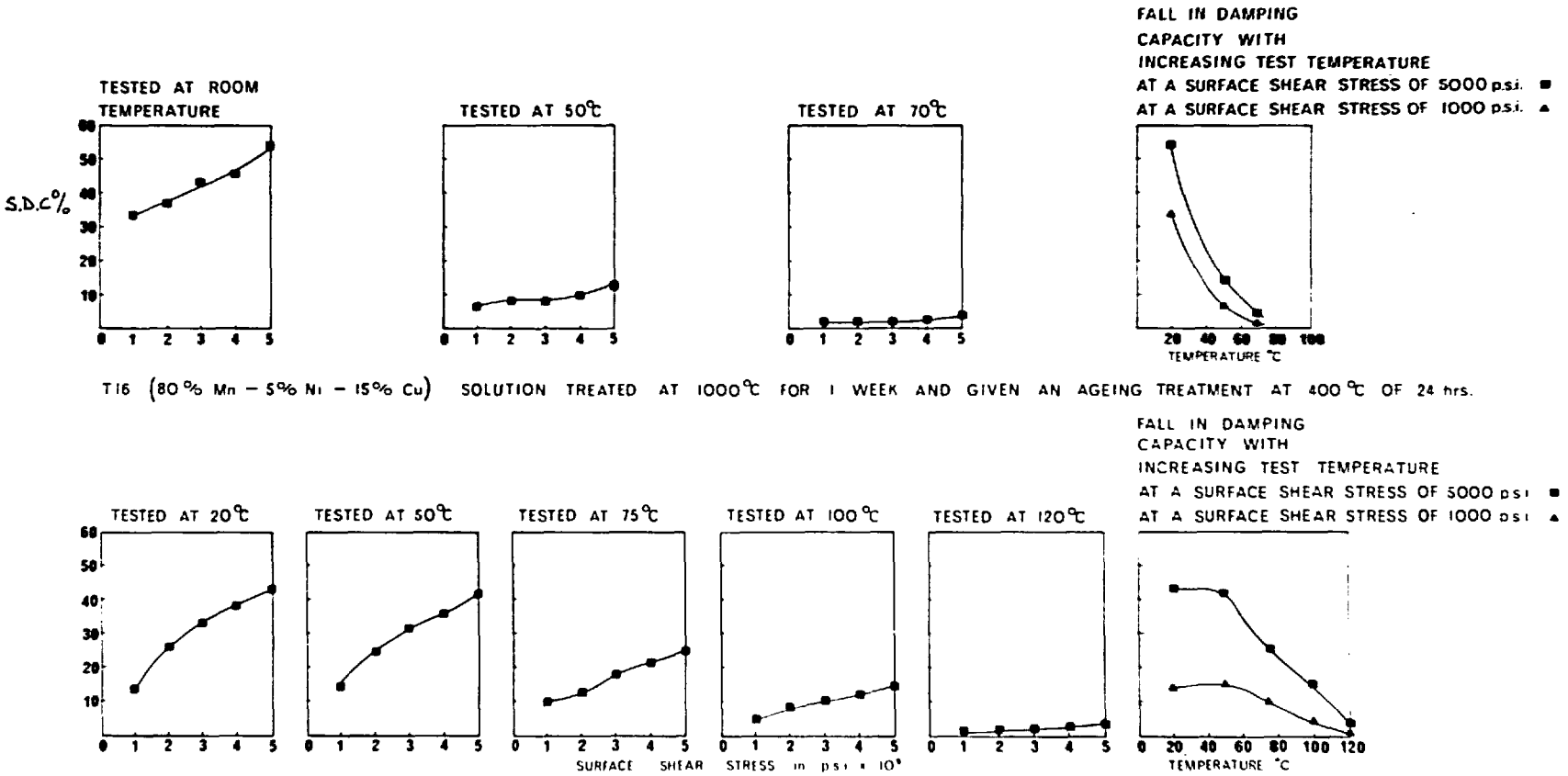


Fig. 73 The effect of temperature on the damping capacity of two samples of alloy T16. Both samples have been solution treated for one week at 1000 °C and water quenched. One sample has been given a further heat treatment of 24 hrs. at 400 °C.

was selected to determine the extent to which the fcc/fct transformation temperature could be raised by stress alone. This alloy was selected because the low fcc/fct transformation temperature of 52°C allowed the combined heating and straining of the sample to be conducted by simple means. The sample was first heated and the axial ratio recorded with increasing temperature until the fcc/fct transformation temperature of 52°C was reached. An unknown tensile stress was then generated in the sample and a noticeable separation of the (200 + 020) and (002) peaks took place. By continuing the heating and maintaining the tensile stress, it was possible to elevate the fcc/fct transformation temperature to 62°C. It therefore seems reasonable to suppose that during damping tests at elevated temperatures the stresses involved in the damping measurements do alter the fcc/fct transformation temperature range.

The damping results on alloy T16 (80%Mn-5%Ni-15%Cu) varied with the solution treatment time given to the alloy and the maximum damping properties developed after a solution treatment of between 1 day and 1 week at 950°C or 1000°C. Samples given a solution treatment of 1 week at 1000°C were given further ageing treatments of 4, 8 and 24 hours respectively at 400°C. The damping capacity in general decreased, with the most noticeable decline occurring at the lower surface shear stress levels, Fig.72. Damping capacities were also determined at elevated temperatures on two test samples, one given a solution treatment of 1 week at 1000°C and the other given a further ageing heat treatment of 24 hours at 400°C, Fig. 73. The sample which had been solution treated and water quenched exhibited a rapid decline in damping properties with increasing temperature in agreement with the conclusions drawn from the X-ray results. Although useful damping properties were maintained up to about 100°C in the sample which had been solution treated and aged for 24 hours at 400°C, the results were not sufficiently better than those

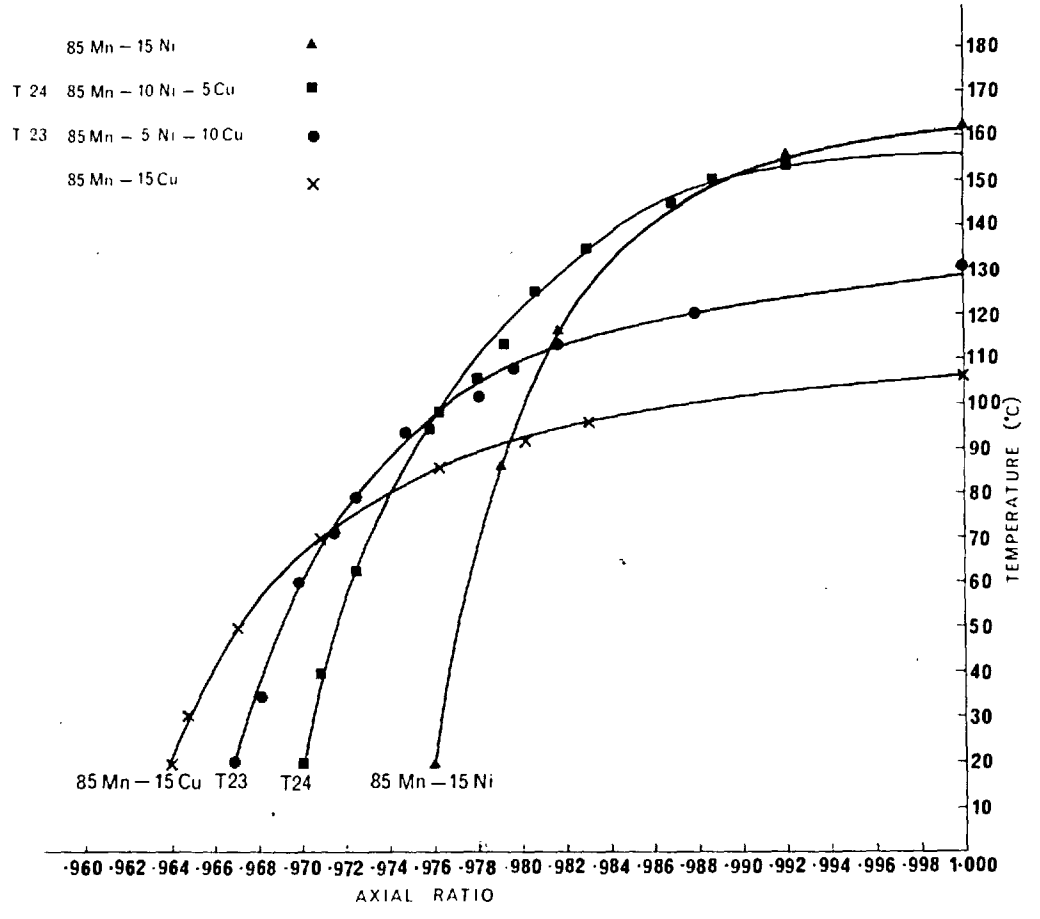


Fig. 74 The effect of temperature on the axial ratio of alloys 85 % Mn – 15 % Ni, 85 % Mn – 15 % Cu, T24 (85 % Mn – 10 % Ni – 5 % Cu) and T 23 (85 % Mn – 5 % Ni – 10 % Cu). All alloys have been solution treated and water quenched.

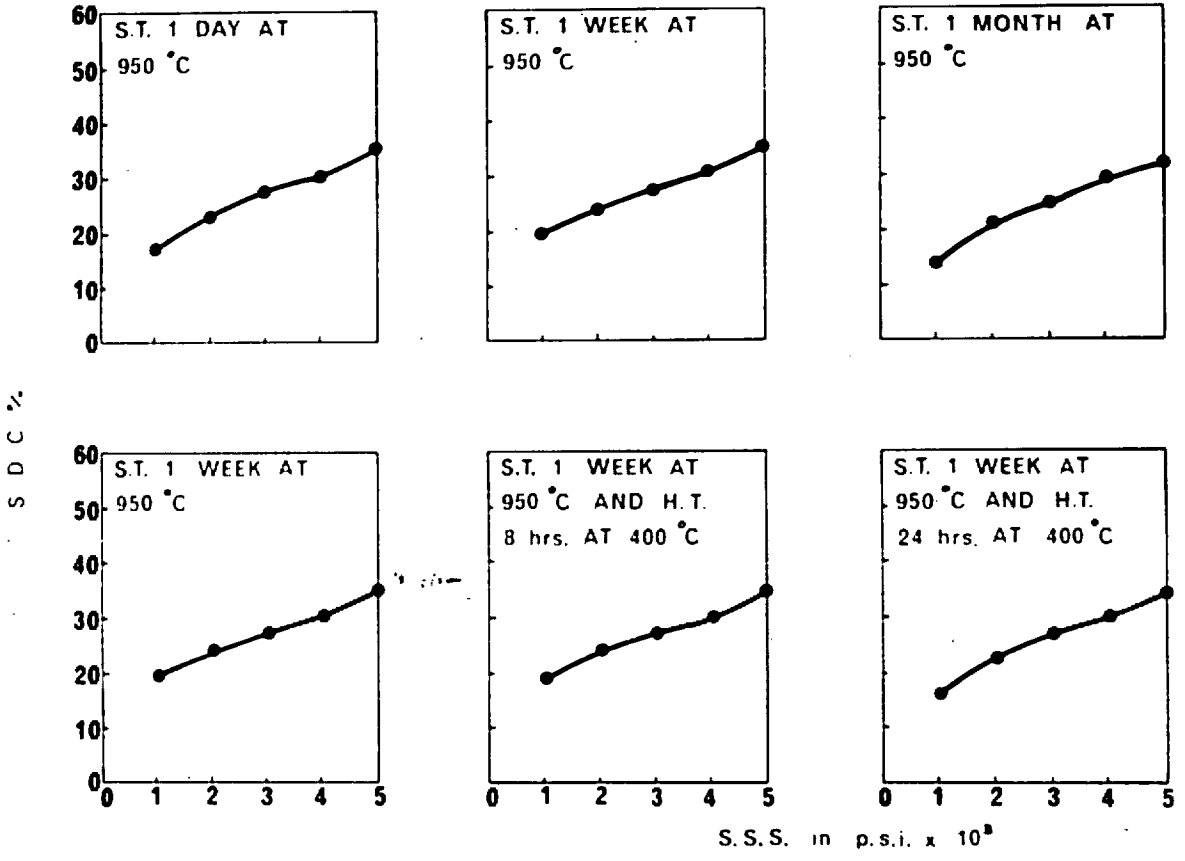


Fig. 75 The stress dependence of the damping capacity of alloy T 24 (85 % Mn - 10 % Ni - 5 % Cu) which has been given a variety of heat treatments.

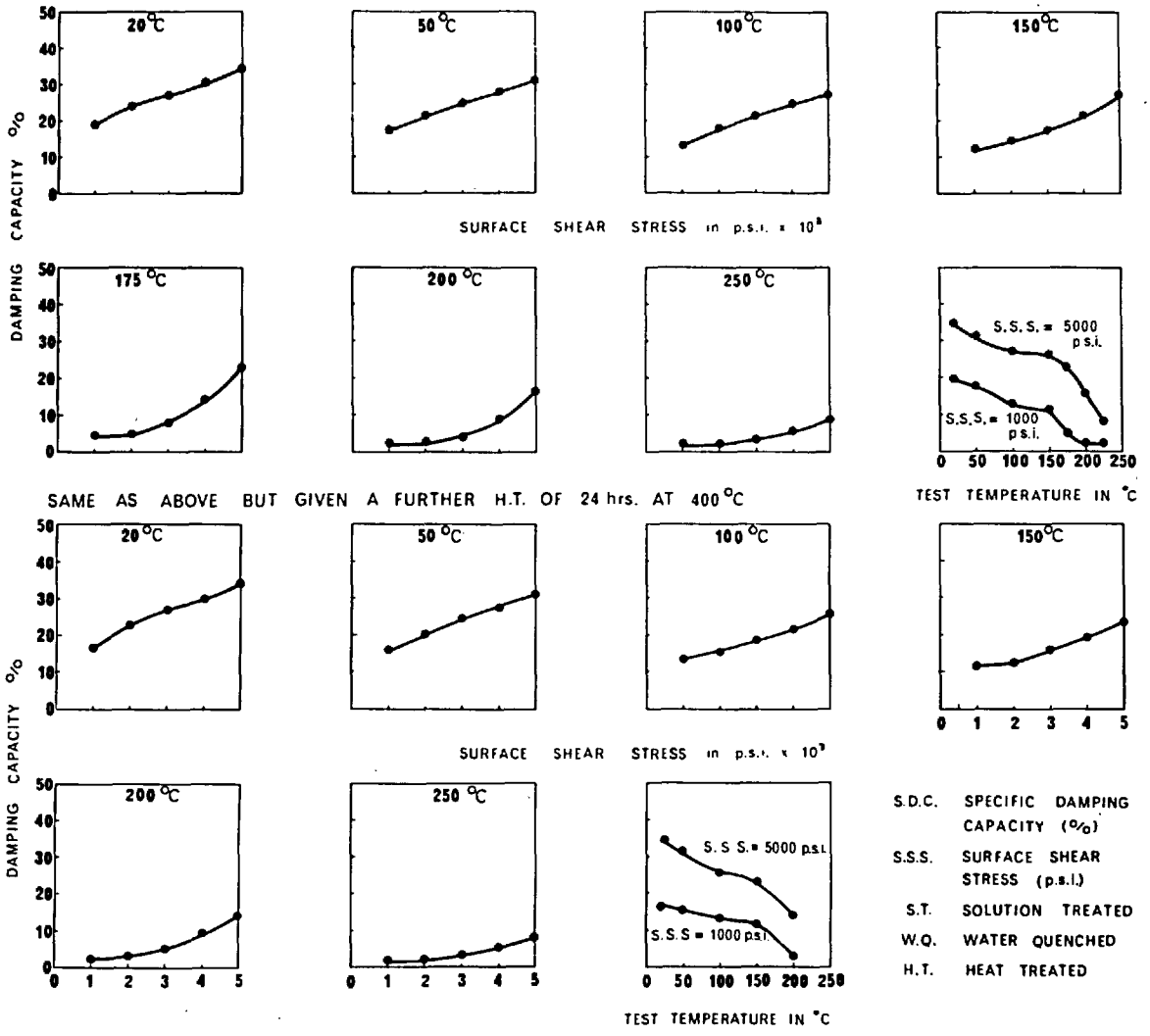


Fig. 76 The effect of temperature on the damping capacity of two samples of alloy T24 (85% Mn–10% Ni–5% Cu) Both samples have been solution treated for one week at 950 °C and water quenched. One sample has been given a further heat treatment of 24 hrs. at 400 °C.

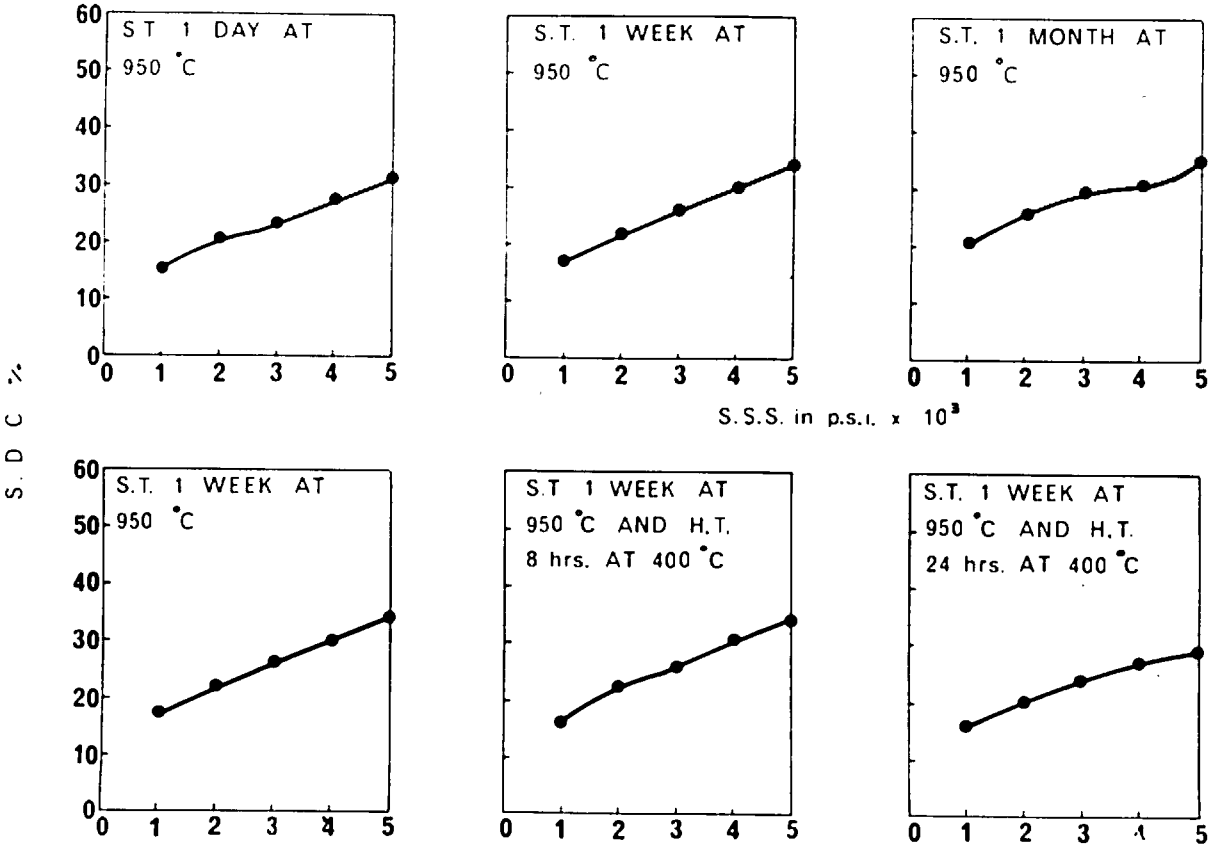
recorded in the Mn-Cu system to warrant further attention.

8.2.6 Alloy T24 (85%Mn-10%Ni-5%Cu).

The 85%Mn-15%Ni alloy exhibited excellent damping properties at elevated temperatures and it was thought that by the replacement of 5% of the Ni by 5%Cu this might avoid the tendency towards βMn formation and decrease the heat treatment times necessary to develop the high damping properties. Alloy T24 (85%Mn-10%Ni-5%Cu) was solution treated at 950°C for 5 days, water quenched and given a variety of ageing heat treatments at 400°C. Very little, if any, change in axial ratio was recorded with increasing ageing time at 400°C, Figs 69 and 70, or at temperatures up to 550°C. The fcc/fct transformation temperature of about 155°C exhibited by the alloy in the solution treated and quenched condition is only slightly lower than that obtained from the 85%Mn-15%Ni alloy, Fig. 74. The damping properties measured at room temperature were apparently uninfluenced by either the solution treatment or the ageing heat treatment, Fig. 75. The damping properties of two samples of alloy T24 (85%Mn-10%Ni-5%Cu) which had been solution treated or solution treated and aged for 24 hours at 400°C respectively, were determined at temperatures up to 250°C, Fig.76. These results show that the damping properties fall continuously with rising temperature above room temperature in contrast to the previous results obtained on the 85%Mn-15%Ni alloy, Fig. 59.

As a commercial proposition, alloy T24 (85%Mn-10%Ni-5%Cu) would need to be insensitive to the reduction of damping properties through "room temperature ageing"[5]. The alloy would therefore need to retain high damping properties at working temperatures even when the component was not being subjected to stress. The damping test pieces used to produce the data shown in Fig. 76 were maintained at 80°C for 1 month to accelerate any "room temperature ageing effect". In both cases the measured damping capacities were reduced by about one fifth, Table 6.

Fig. 77 The stress dependence of the damping capacity of alloy T 23 (85 % Mn - 5 % Ni - 10 % Cu) which has been given a variety of heat treatments.



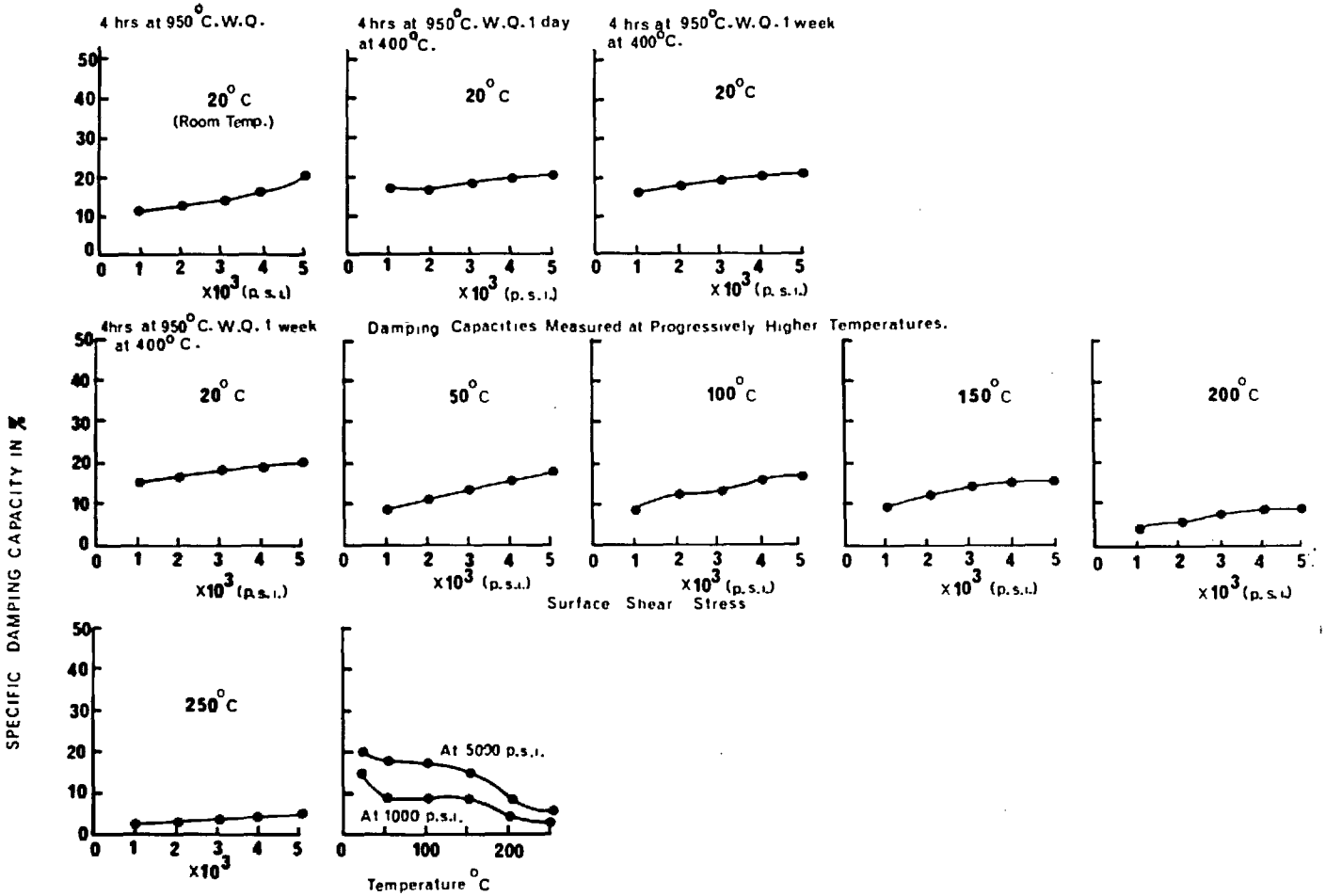


Fig. 78 The stress and temperature dependence of the damping capacity of alloy T 23 (85 % Mn – 5 % Ni – 10 % Cu) which has been given a variety of heat treatments.

8.2.7 Alloy T23 (85%Mn-5%Ni-10%Cu).

The alloy was solution treated at 950°C for 5 days, water quenched and given a variety of ageing heat treatments at 400°C. A small decrease in axial ratio resulted from increasing the ageing heat treatment time, Figs. 69 and 70. By increasing the ageing heat treatment temperature to 500°C or 550°C, similar results were obtained.

Although the addition of Cu was found to encourage the ageing process to a small extent, it was found to have an adverse effect on the fcc/fct transformation temperature, Fig. 74. The damping properties were found to remain reasonably constant with increasing solution treatment times greater than 1 day and further ageing heat treatments did not influence the level of damping properties at room temperature, Fig. 77.

Alloy T23 (85%Mn-5%Ni-10%Cu) was selected as a potential practically useful alloy for use at elevated temperatures and an evaluation was made of mechanical and corrosion properties. In contrast to the experimental approach which was aimed at optimising damping properties through adequate heat treatments, a more commercially-oriented approach was adopted using restricted solution treatments. The damping properties at room temperature, following a solution treatment of 4 hours at 950°C, were lower than those recorded in Fig.77, although useful damping properties were retained up to 250°C, Fig. 78.

8.3 DISCUSSION - THE TERNARY SYSTEM Mn-Ni-Cu.

The presence of Ni in Mn-Ni-Cu alloys has been found to be particularly effective in inhibiting the response of the alloy to the ageing heat treatment at 400°C as indicated by both axial ratio and hardness (H_V) measurements, Figs 69 and 70. For instance, alloy T22 (60%Mn-5%Ni-35%Cu) did not respond to an ageing heat treatment at 400°C, at least up to times of 24 hours, whereas the reaction $\gamma \rightarrow \gamma + \alpha$ in the parent 60%Mn-40%Cu alloy would have been proceeding towards completion after these heat treatment times. On the other hand Ni has been the most effective

addition to make to Mn in order to increase the fcc/fct transformation temperature, Fig. 74.

The damping properties of alloy T15 (80%Mn-15%Ni-5%Cu), Table 5 and T16 (80%Mn-5%Ni-15%Cu), Fig. 72, show a pronounced dependence upon the solution treatment time. It is likely that this effect is related to the inherent heterogeneity exhibited by Mn alloys. There is a critical composition range in quenched Mn alloys of about 78 to 80%Mn in which the fcc/fct transformation temperature is room temperature. In a heterogeneous alloy containing 80%Mn, the Mn concentration within the dendrites will be greater than 80%; they will exhibit a fcc/fct transformation temperature higher than room temperature and therefore they will develop high damping properties at room temperature. The Mn content of the inter-dendritic material will be less than 80%Mn and, at room temperature, that part of the alloy will be fcc and therefore will not develop damping properties. In a water quenched alloy containing 80%Mn the best damping properties can only be achieved when the alloy is homogenous and all parts of the sample have transformed to the fct structure.

The damping capacity results obtained from both alloy T23 (85%Mn-5%Ni-10%Cu) and alloy T24 (85%Mn-10%Ni-5%Cu), Figs. 75 to 78, were remarkably independent of heat treatment, except apparently for solution treatment times of less than 1 day at 950°C, when presumably the heterogeneous nature of the alloys exerts an influence as discussed above. Useful damping properties were retained at temperatures above 200°C in both alloys. Alloy T24 (85%Mn-10%Ni-5%Cu) exhibited no further improvement in damping properties at elevated temperatures following an ageing heat treatment of 24 hours at 400°C and it is assumed that the heat treatment was insufficient to increase the local Mn concentration. Further damping capacity improvements at higher temperatures should be possible if this alloy was given longer heat treatments at 400°C.

An alternative approach involving alloy T23 (85%Mn-5%Ni-10%Cu) was adopted for practical reasons. Although this alloy, in the quenched condition, exhibits a fcc/fct transformation temperature lower than that found in alloy T24 (85%Mn-10%Ni-5%Cu), it should respond to the ageing heat treatment more readily by virtue of its higher Cu content. Although this approach proved effective in retaining damping properties to high temperatures Fig. 78, it became clear that a preliminary solution treatment of at least 1 day was essential to provide high damping properties at room temperature, Fig. 77.

In terms of the proposed damping mechanism, the 85%Mn-15%Ni alloy can be said to have satisfied the aims of the research programme in developing improved damping properties at elevated temperatures. However, in terms of possible commercial application, the damping properties developed in alloys T23 (85%Mn-5%Ni-10%Cu) and T24 (85%Mn-10%Ni-5%Cu) are much more significant, although here too there are inherent drawbacks related to alloy preparation and the duration of the heat treatments. It should be pointed out that these disadvantages are by no means as severe as those encountered in the experimental programme on the 85%Mn-15%Ni alloy.

CHAPTER 9.

OTHER ALLOY ADDITIONS.

9.1 INTRODUCTION.

The programme so far has involved the addition of those elements which were thought likely to favour the development of a stable fct γMn structure and hence exhibit those features which are a prerequisite for high damping properties in Mn alloys. The prime aim of this approach was the development of an alloy exhibiting good damping properties at temperatures which had hitherto resulted in a rapid decline or complete loss in damping properties. This approach proved successful, leading to two suitable alloys, T23 (85%Mn-5%Ni-10%Cu) and T24 (85%Mn-10%Ni-5%Cu). It was also hoped that these elemental additions would beneficially influence ancillary properties or at least maintain them at a level similar to those found in the 60%Mn-40%Cu alloy. All those details of castability, mechanical properties and corrosion resistance have been excluded from this thesis because, apart possibly from Young's modulus, they do not have a direct bearing on phase stability, or the proposed damping mechanism. Unfortunately, it became clear that a satisfactory combination of all the relevent properties was not going to be achieved in any one alloy and attention was turned to find other alloy compositions which could possibly satisfy the ancillary property requirements for particular applications. These alloys have been included in this last chapter dealing with experimental work, not because of their influence on these properties but because of the interesting and surprising way in which they affected the structural features and crystallographic details and hence influenced the damping properties. If only crystallographic considerations and phase stability had been taken into account, most of these additions would not have been considered desirable. In particular, Zn has been added because of its tendency to stabilise the γMn phase in the Mn-Zn binary system at elevated

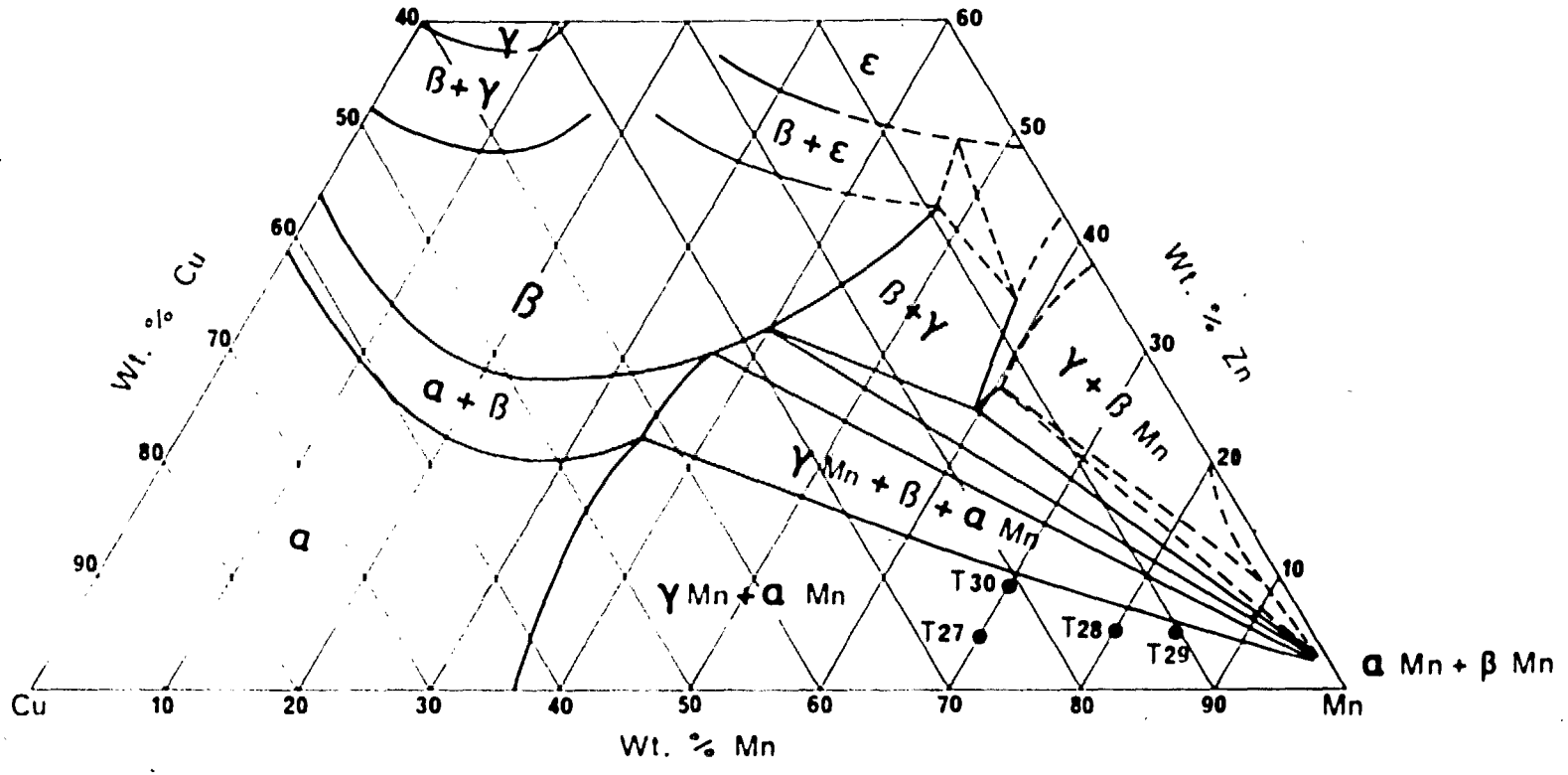


Fig. 79 A 593 °C isotherm section of the Mn-Cu-Zn ternary thermal equilibrium diagram. Selected alloy compositions are superimposed.

Ref. 103

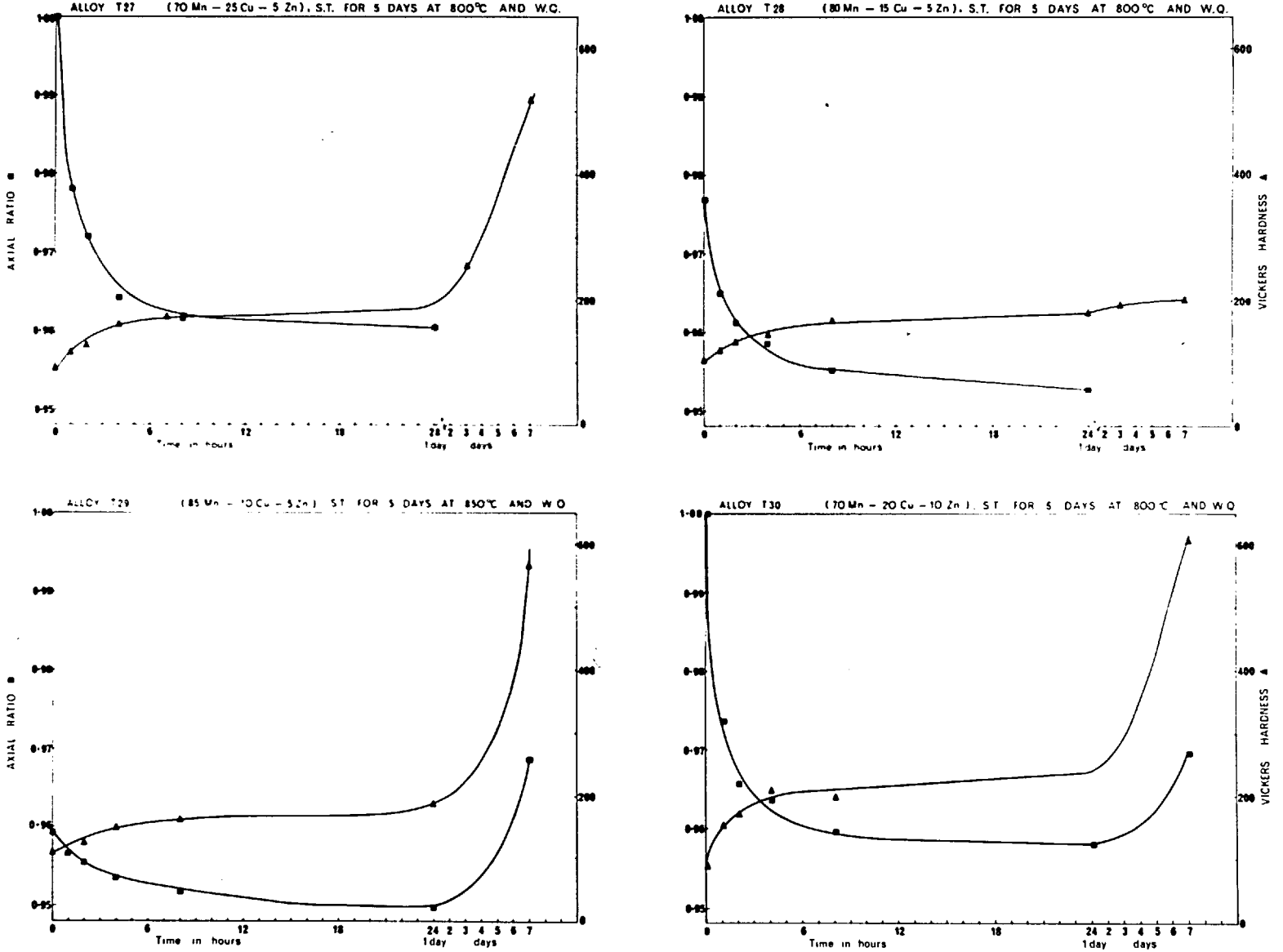


Fig. 80 CHANGE IN AXIAL RATIO AND HARDNESS (H_v) MEASURED AT ROOM TEMPERATURE, WITH THE HEAT TREATMENT TIME AT 400°C GIVEN TO VARIOUS Mn–Cu–Zn ALLOYS

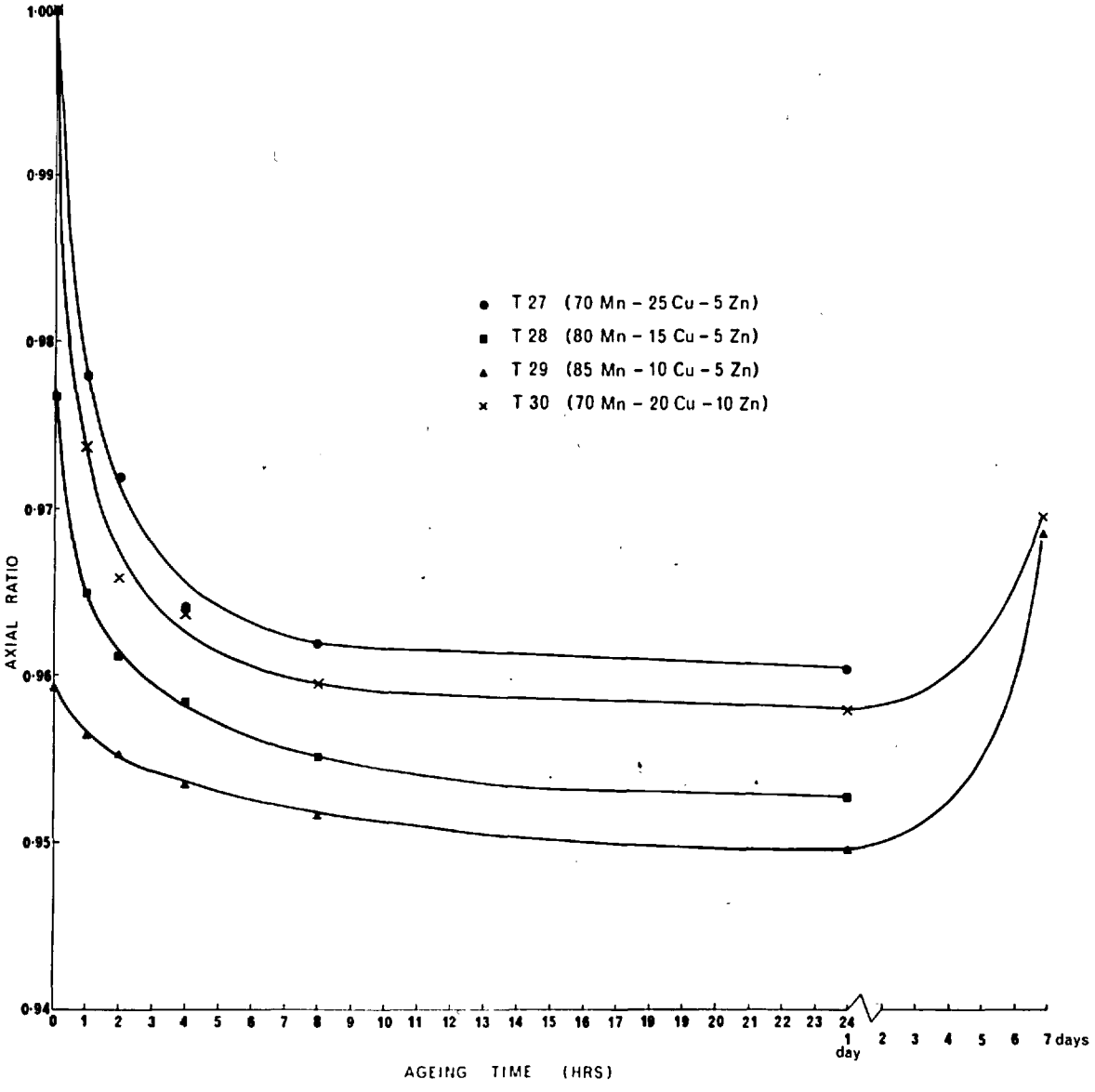


FIG. 81 COMPARISON OF THE CHANGE IN AXIAL RATIO WITH HEAT TREATMENT TIME AT 400 °C GIVEN TO VARIOUS Mn-Cu-Zn ALLOYS.

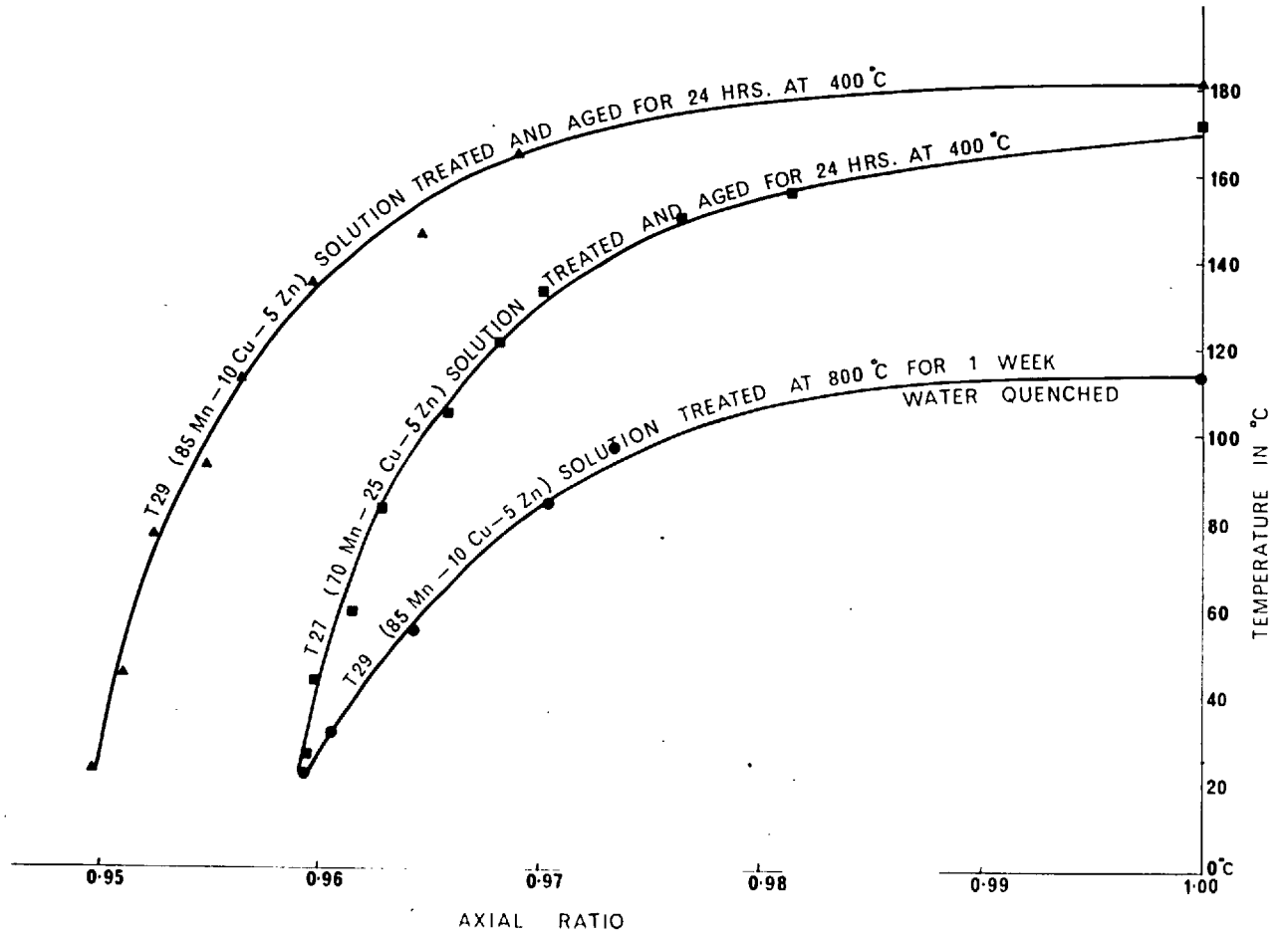


Fig. 82 The effect of temperature on the axial ratio of alloys T 27 and T 29 which have been given a variety of heat treatments.

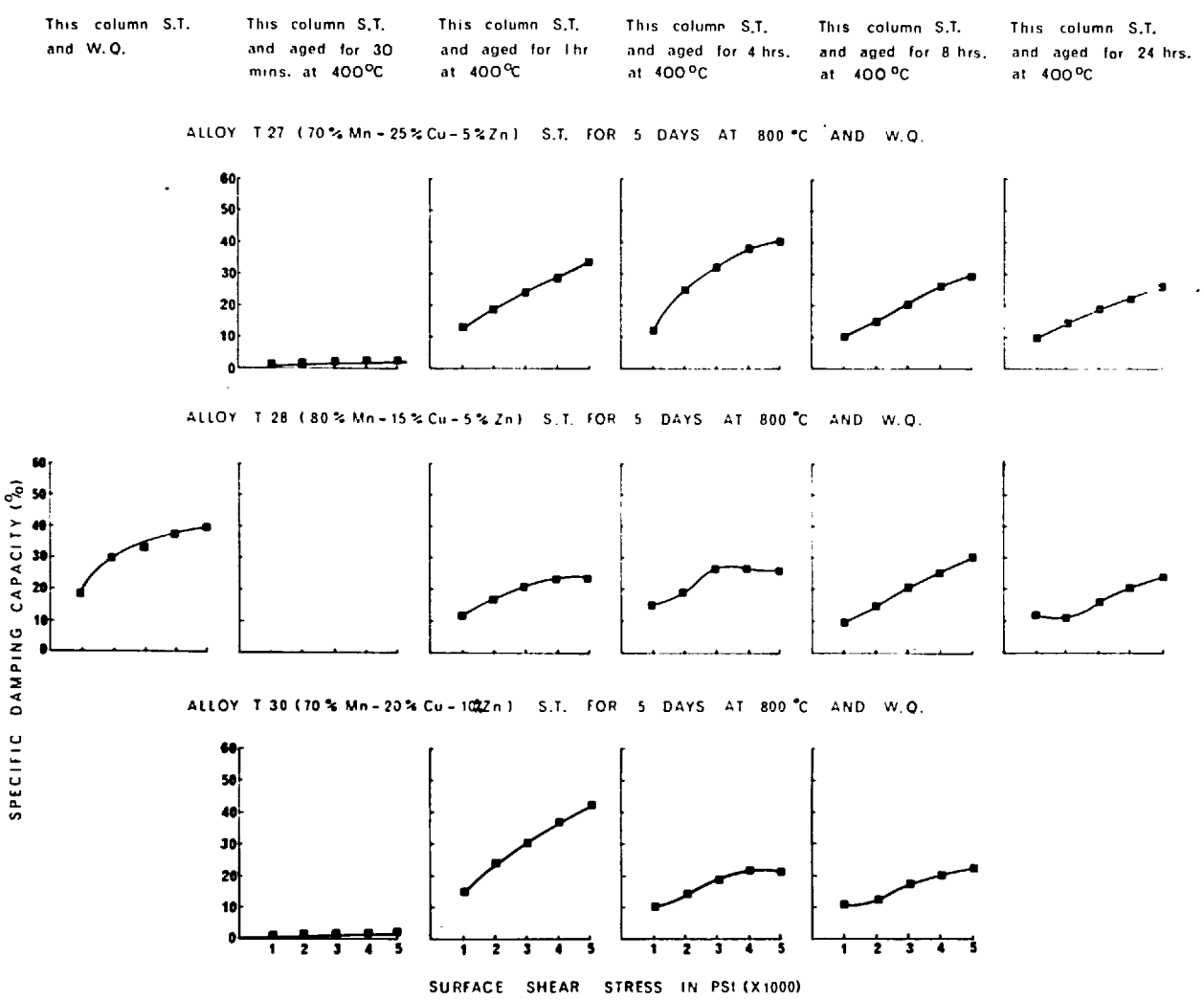


Fig. 83 The stress dependence of the damping capacity of alloys T 27, T28 and T 30 which have been given a variety of heat treatments.

temperatures and because of its low cost. C and Al have been added to certain Mn alloys because of the improvement in corrosion-resistance that they confer on the "Sonoston" range of alloys, which are commercial damping alloys based on the 60%Mn-40%Cu alloy. These alloys are used for the manufacture of ships propellers[102]. Si and Be have also been added at the suggestion of Admiralty Materials Laboratory staff; Si for possible improvement in corrosion resistance and Be for improvement in mechanical properties through a possible precipitation hardening reaction. In the latter case, it appeared that in some applications damping properties could be sacrificed if the Young's modulus could be improved.

9.2 RESULTS AND DISCUSSION.

In this section the results of the various additions are recorded and where necessary are discussed. The significance of all the additions to Mn in the broader context of the damping mechanism is discussed in the final chapter.

9.2.1 The ternary system Mn-Cu-Zn.

A 593°C isothermal section of the Mn-Cu-Zn ternary equilibrium diagram has been incorporated as Fig. 79[103] and the selected alloy compositions are superimposed.

9.2.1.1 Alloy T27 (70%Mn-5%Zn-25%Cu).

The alloy was solution treated at 800°C for 5 days, water quenched and then given a variety of ageing heat treatments at 400°C. The change in axial ratio and hardness (H_V) with ageing heat treatment times is shown in Fig. 80 and a comparison of the ageing characteristics with other alloys containing Zn is shown in Fig. 81. An appreciable change in axial ratio occurred after short ageing heat treatment times at 400°C, indicating a rapid response to the ageing heat treatment. This was also reflected in the high fcc/fct transformation temperature of about 170°C, developed after a heat treatment of 24 hours at 400°C, Fig. 82. The damping properties of alloy T 27 (70%Mn-5%Zn-25%Cu) Fig. 83, were moderate and were comparable with the

damping results from the corresponding 70%Mn-30%Cu alloy, see Fig. 32. The sample which had been given an ageing heat treatment of ½ hour at 400°C yielded negligible damping properties, indicating that even though the ageing response was very rapid, the time of ½ an hour was too short to allow the matrix to attain a composition of more than about 80%Mn.

9.2.1.2 Alloy T30 (70%Mn-20%Cu-10%Zn).

The alloy was solution treated at 800°C for 5 days, water quenched and given a variety of heat treatments at 400°C. The change in axial ratio and Vickers hardness (H_V) values with ageing heat treatment times at 400°C is shown in Figs. 80 and 81. It is interesting to compare this alloy with the previous alloy, T27 (70%Mn-5%Zn-25%Cu). Both are based essentially on a 70%Mn-30%Cu alloy; in the case of alloy T27, 5%Cu has been replaced by 5%Zn, and in the case of T30, 10%Cu has been replaced by 10%Zn. The effect of Zn, in alloy T30, on the change in axial ratio and the change in hardness (H_V) values with ageing time, was even greater than that observed with alloy T27 (70%Mn-5%Zn-25%Cu). The increased response to the ageing process was reflected in the damping results; the optimum damping properties were developed after a heat treatment time of only 1 hour at 400°C, Fig. 83.

9.2.1.3 Alloy T28 (80%Mn-15%Cu-5%Zn).

The alloy was solution treated at 800°C for 5 days, water quenched and given a variety of heat treatments at 400°C. The change in axial ratio and hardness (H_V) values with heat treatment time at 400°C is shown in Fig. 80 and compared with other alloys containing Zn in Fig. 81. The efficacy of Zn in promoting the $\gamma \rightarrow \gamma + \alpha$ reaction and the resulting enrichment of the matrix in Mn is clearly shown by comparing the results of T28 (80%Mn-15%Cu-5%Zn) and T30 (70%Mn-20%Cu-10%Zn). With increasing ageing heat treatment the axial ratios of the two alloys are similar and the hardness values of the (70%Mn-20%Cu-10%Zn) alloy rise above those of the (80%Mn-15%Cu-5%Zn) alloy.

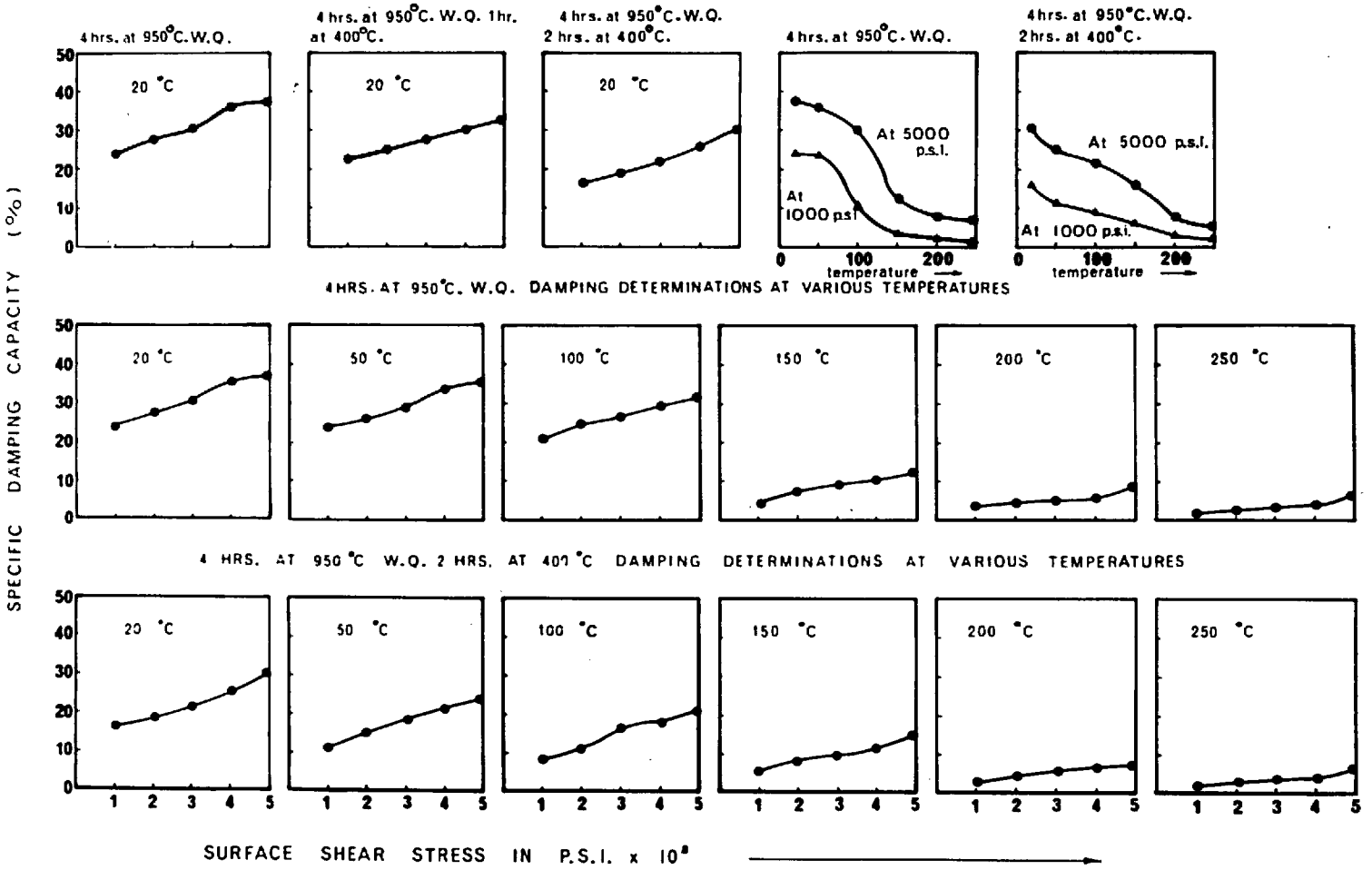


Fig. 84 THE STRESS AND TEMPERATURE DEPENDENCE OF THE DAMPING CAPACITY OF ALLOY T29 (87% Mn-3% Zn-10% Cu) WHICH HAS BEEN GIVEN A VARIETY OF HEAT TREATMENTS.

The damping properties of alloy T28 (80%Mn-15%Cu-5%Zn), Fig. 83 were comparable with other alloys based on 80%Mn and declined with increasing heat treatment time at 400°C.

9.2.1.4 Alloy T29 (85%Mn-10%Cu-5%Zn).

The alloy was solution treated at 850°C for 5 days, water quenched and given a variety of heat treatments at 400°C. The change in axial ratio and hardness (H_V) values with ageing heat treatment time is shown in Fig. 80 and compared with other alloys containing Zn in Fig. 81. The axial ratio values are the lowest to be recorded in this research programme and in contrast to all other alloys containing 85%Mn, the alloy responded readily to the ageing heat treatment at 400°C. In the solution treated and water quenched condition, the fcc/fct transformation temperature of about 150°C was recorded and after a further heat treatment of 24 hours at 400°C, this had increased to about 180°C, Fig. 82. Unfortunately αMn precipitation also proceeded readily and after a heat treatment of 3 hours at 400°C, the alloy had become extremely brittle.

Nevertheless, because of its unique response to the ageing heat treatment, this alloy with slightly less Zn content was selected along with alloy T23 (85%Mn-5%Ni-10%Cu) as the two alloys which would be given a detailed examination to complete the research programme. This particular alloy T29 (87%Mn-3%Zn-10%Cu) yielded excellent damping properties at both room and elevated temperatures, even after short solution treatment and ageing heat treatment times, Fig. 84. The disparity between the fcc/fct transformation temperature and the temperature at which damping properties had fallen to low levels, was most pronounced, Figs. 82 and 84.

9.2.2 Alloys containing Be.

9.2.2.1 Alloy Q31 (80%Mn-14.4%Cu-5%Ni-0.6%Be).

Like many other alloys in this programme, alloy Q31 is based on alloy T16 (80%Mn-15%Cu-5%Ni). The alloy was successfully

Fig. 85.

Fig. 86.

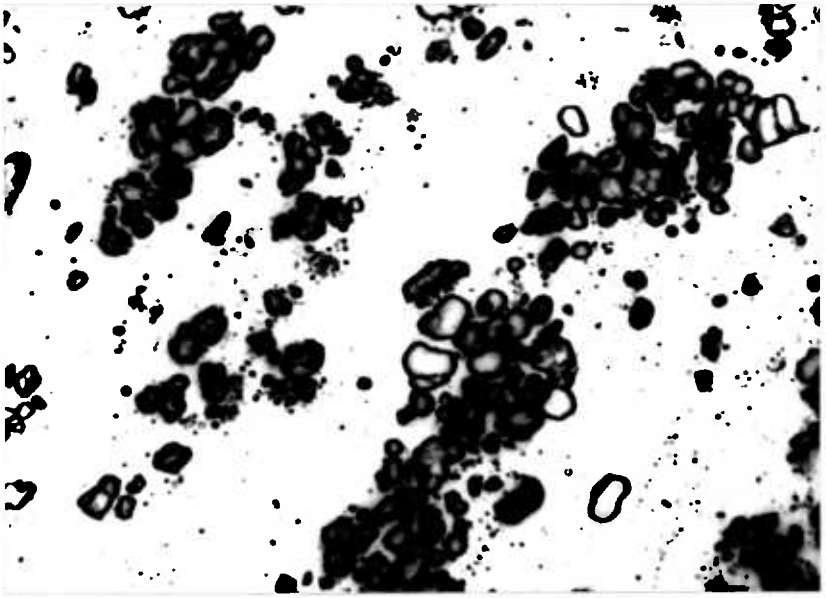
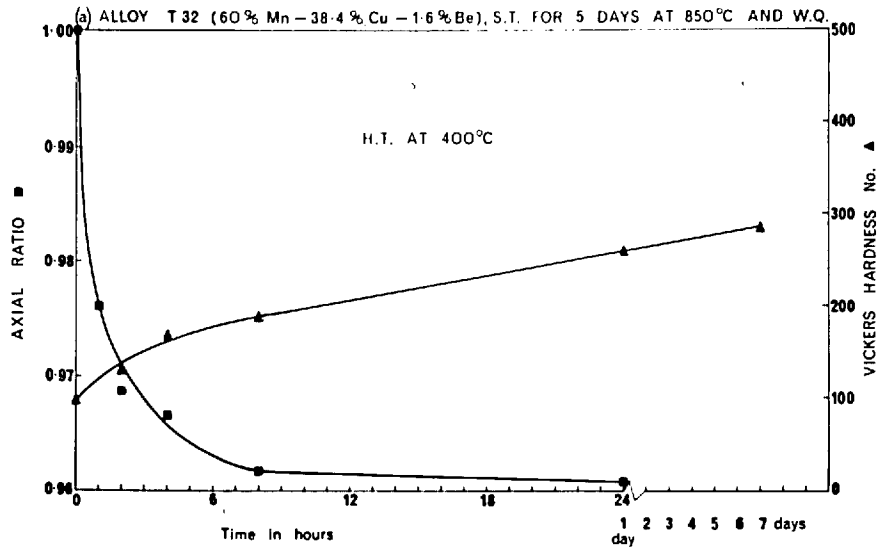
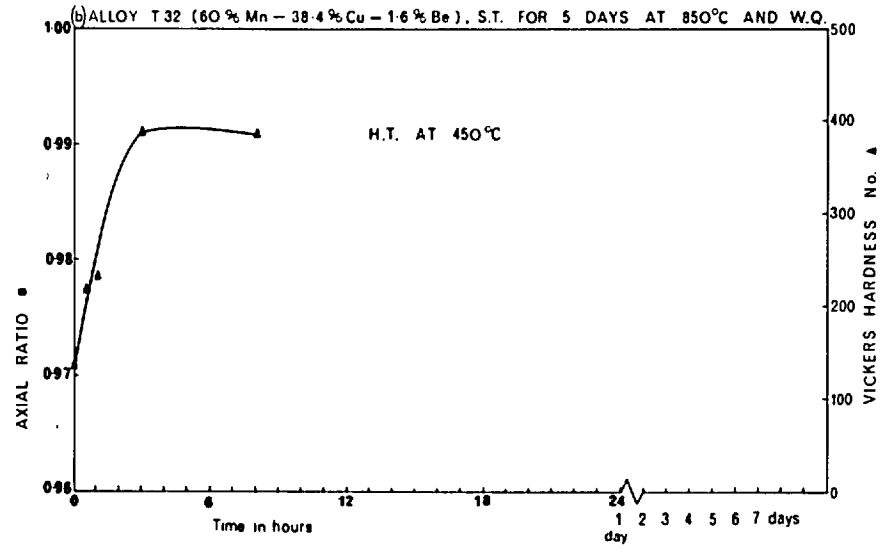


Fig.85. Alloy T32(60%Mn-38.4%Cu-1.6%Be),rolled and water quenched. Shows particles of Be_2Mn lying in the Mn-rich dendritic regions. x 1,100.



Fig.86. Alloy T32(60%Mn-38.4%Cu-1.6%Be),solution treated for 5 days at 850°C, water quenched and heat treated for 4 hours at 450°C. Shows precipitate particles of Be_2Mn and αMn. x 1,100.





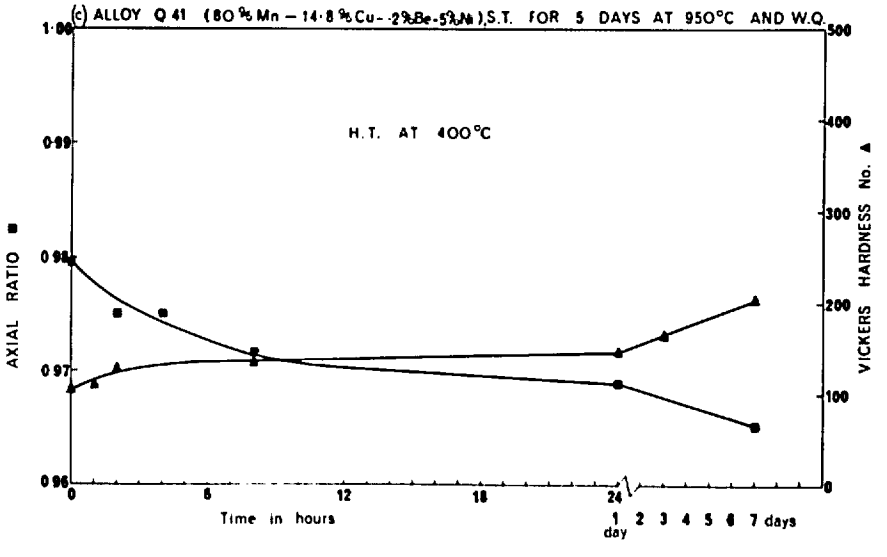


Fig 87 CHANGE IN AXIAL RATIO AND HARDNESS (H_v), MEASURED AT ROOM TEMPERATURE, WITH THE HEAT TREATMENT TIME AT 400 °C AND 450°C GIVEN TO ALLOYS T32 AND Q41.

cast but disintegrated on the third pass through the rolls. Although it had been anticipated that the Be would have combined with the Cu, this did not occur and microprobe analysis inside the electron microscope indicated that the particles were rich in Mn and this was later confirmed by X-ray diffraction, when the intermetallic Be_2Mn was identified. These particles presumably created the brittle condition during the rolling process.

9.2.2.2 Alloy T32 (60%Mn-38.4%Cu-1.6%Be)

In the rolled and water quenched condition, fairly large particles of Be_2Mn were detected Fig. 85 in alloy T32 (60%Mn-38.4%Cu-1.6%Be), and these were taken into solution after a 5 day heat treatment at 850°C. Samples were then given a variety of ageing heat treatments at 400, 450 and 500°C. At 450 and 500°C the intermetallic Be_2Mn was detected both optically, Fig. 86 and by X-ray means. The change in axial ratios and hardness (H_v) values with ageing time at 400°C and at 450°C are recorded in Fig. 87. The effect of the addition of Be on the ageing reaction was even more pronounced than that of Zn and very low axial ratios were recorded in short heat treatment times. X-ray diffraction traces from samples aged at 400°C did not reveal any Be_2Mn, although the change in hardness with ageing time was appreciably different to that which was normally encountered in the $\gamma \rightarrow \gamma + \alpha$ reaction. It is therefore possible that αMn and Be_2Mn are both developing in the pre-precipitation state at 400°C. At 450 and 500°C both αMn and Be_2Mn precipitated out of solid solution, see for instance Fig. 86, resulting in a very rapid hardening response, Fig. 87. Presumably, because of the formation of the Be_2Mn phase during the rolling schedule, the rolled bar cracked and it was not possible to obtain suitable samples for damping determinations.

9.2.2.3 Alloy Q41 (80%Mn-14.8%Cu-5%Ni-0.2%Be).

In view of the rather extreme behaviour resulting from the addition of 0.6%Be a further alloy Q41 (80%Mn-14.8%Cu-5%Ni-0.2%Be) was cast, based on the same parent alloy, but containing only 0.2%Be. Unlike alloy T32 (60%Mn-38.4%Cu-1.6%Be) and Q31

Fig. 88 The stress dependence of the damping capacity of a number of alloys based on 80 % Mn which have been given a variety of heat treatments.

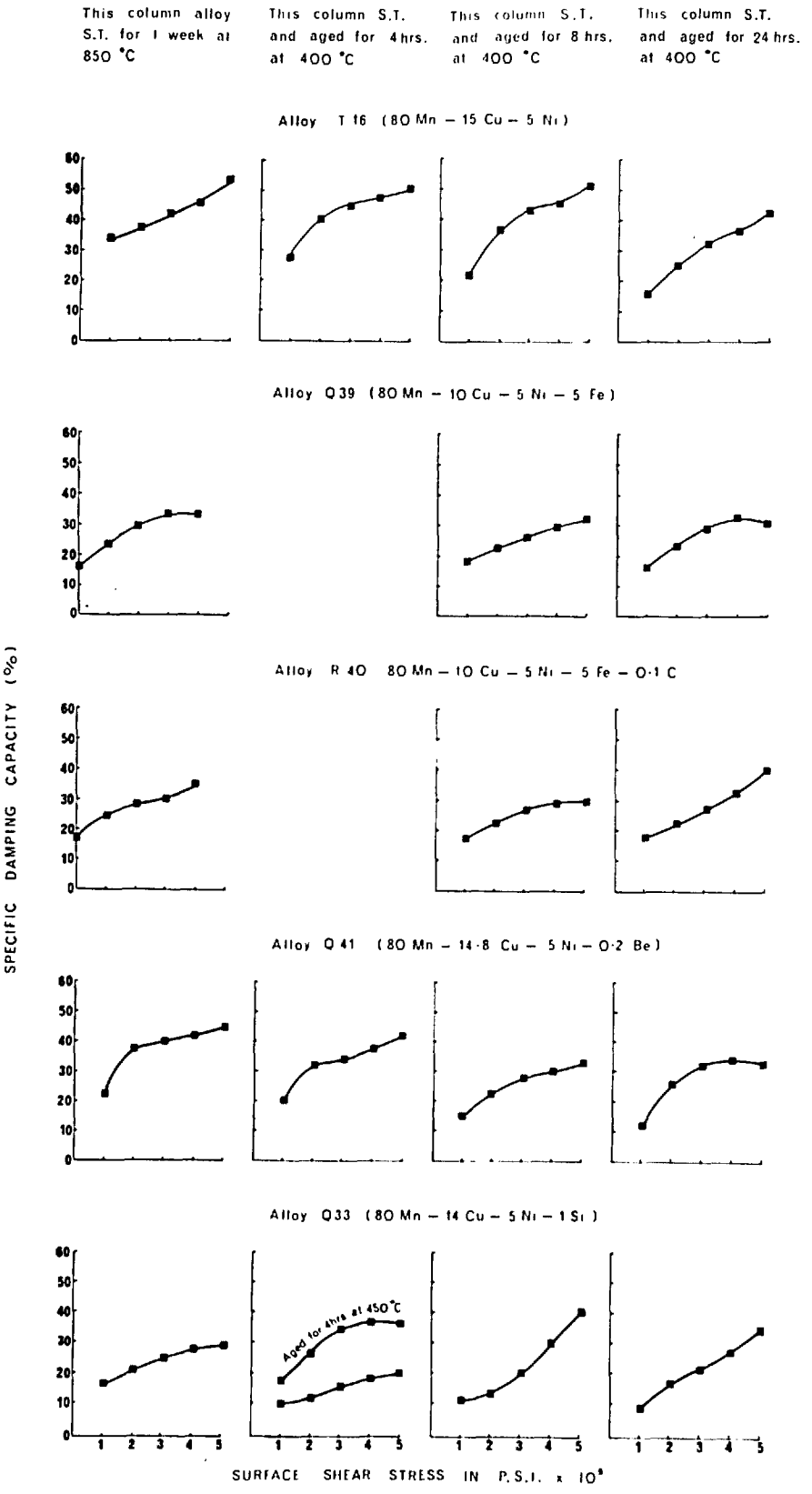


Fig. 89.

Fig. 90.

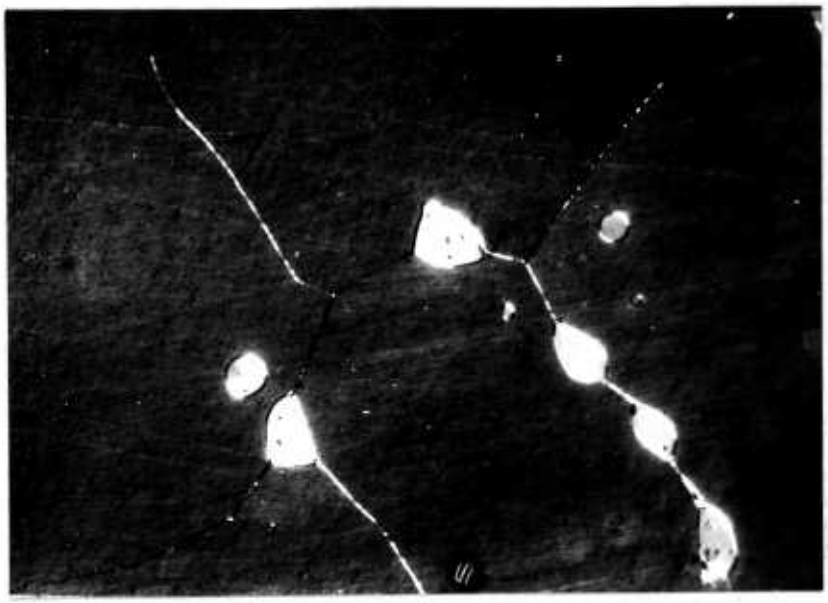


Fig.89. Alloy Q33(80%Mn-14%Cu-5%Ni-1%Si), solution treated for 5 days at 950°C, water quenched and heat treated for 8 hours at 450°C. Polarised light micrograph showing βMn particles in the grain boundaries. x 600.

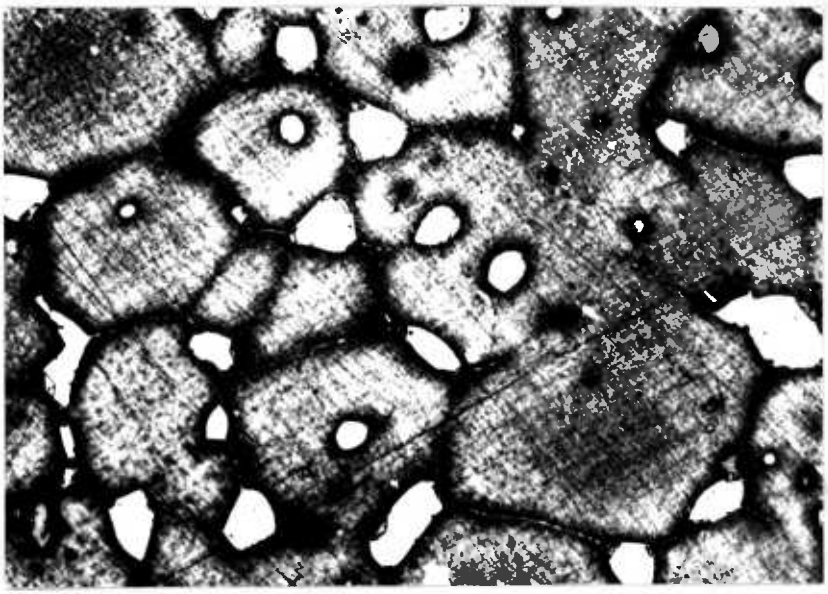
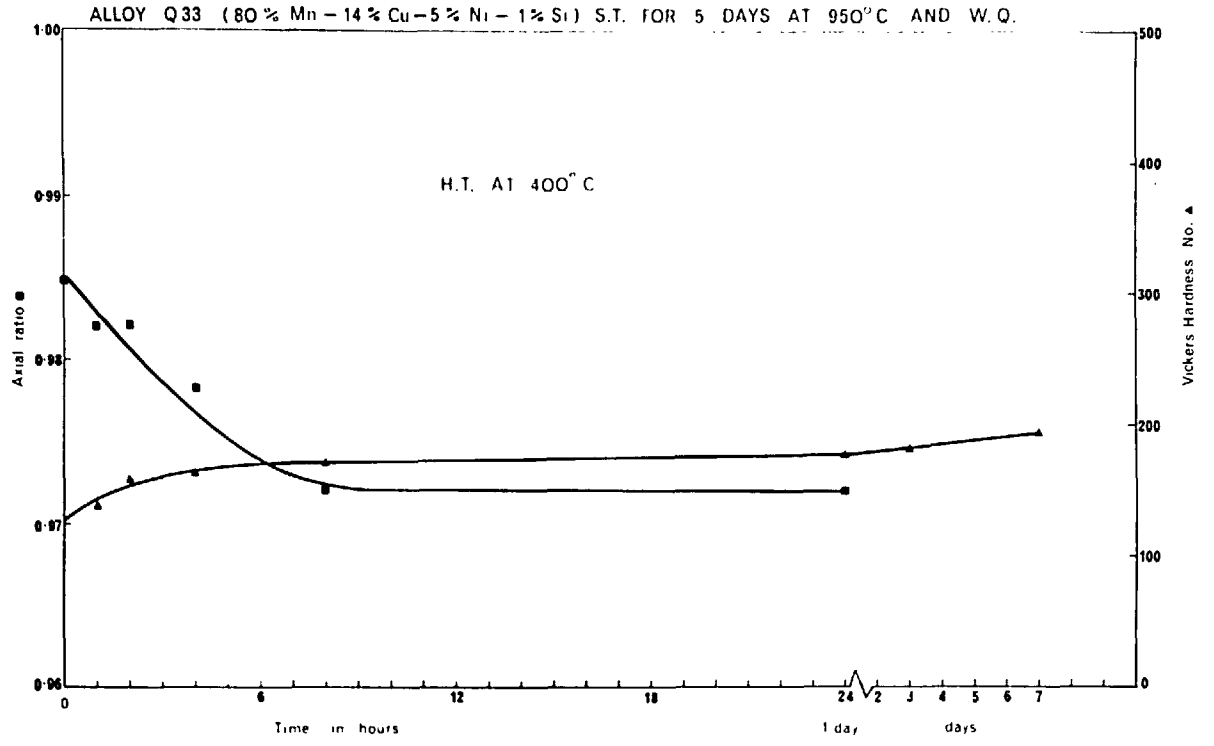


Fig.90. Alloy Q33(80%Mn-14%Cu-5%Ni-1%Si), solution treated for 5 days at 950°C, water quenched and aged for 4 hours at 500°C. Shows βMn precipitate particles. x 600.



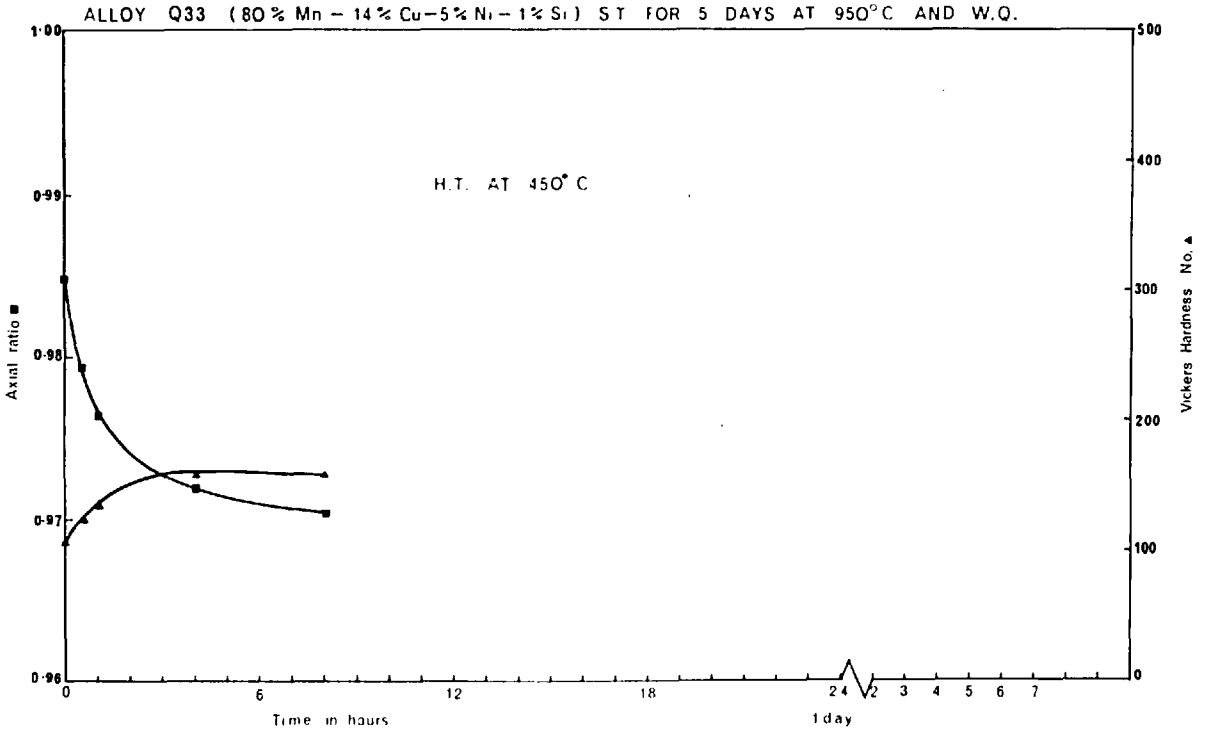


FIG. 91 CHANGE IN AXIAL RATIO AND HARDNESS (H_V), MEASURED AT ROOM TEMPERATURE, WITH HEAT TREATMENT TIME AT 400° C AND 450° C GIVEN TO ALLOY Q 33.

(80%Mn-14.4%Cu-5%Ni-0.6%Be), Be_2Mn could not be detected in the cast state or even after a number of heat treatments at temperatures between 400 and 800°C. The alloy was solution treated for 5 days at 950°C, water quenched and given a variety of ageing heat treatments at 400°C. The change in axial ratio and hardness (H_V) values with ageing heat treatment time are recorded in Fig. 87. The change in hardness (H_V) was appreciably less than that recorded for alloy T32 (60%Mn-38.4%Cu-1.6%Be) confirming the lack of any appreciable hardening reaction due to Be_2Mn precipitation; on the other hand the response to the ageing heat treatment is more pronounced than the parent alloy T16 (80%Mn-15%Cu-5%Ni), Fig. 69, both in respect of the axial ratio and the hardness (H_V). It would appear that the addition of Be at this Mn concentration is rather critical because Be_2Mn precipitated in alloy Q31 (80%Mn-14.4%Cu-5%Ni-0.6%Be) to such an extent that the alloy behaved in a brittle manner during rolling.

The damping properties of alloy Q41 (80%Mn-14.8%Cu-5%Ni-0.2%Be) Fig. 88, were similar to T16 (80%Mn-15%Cu-5%Ni), the parent alloy.

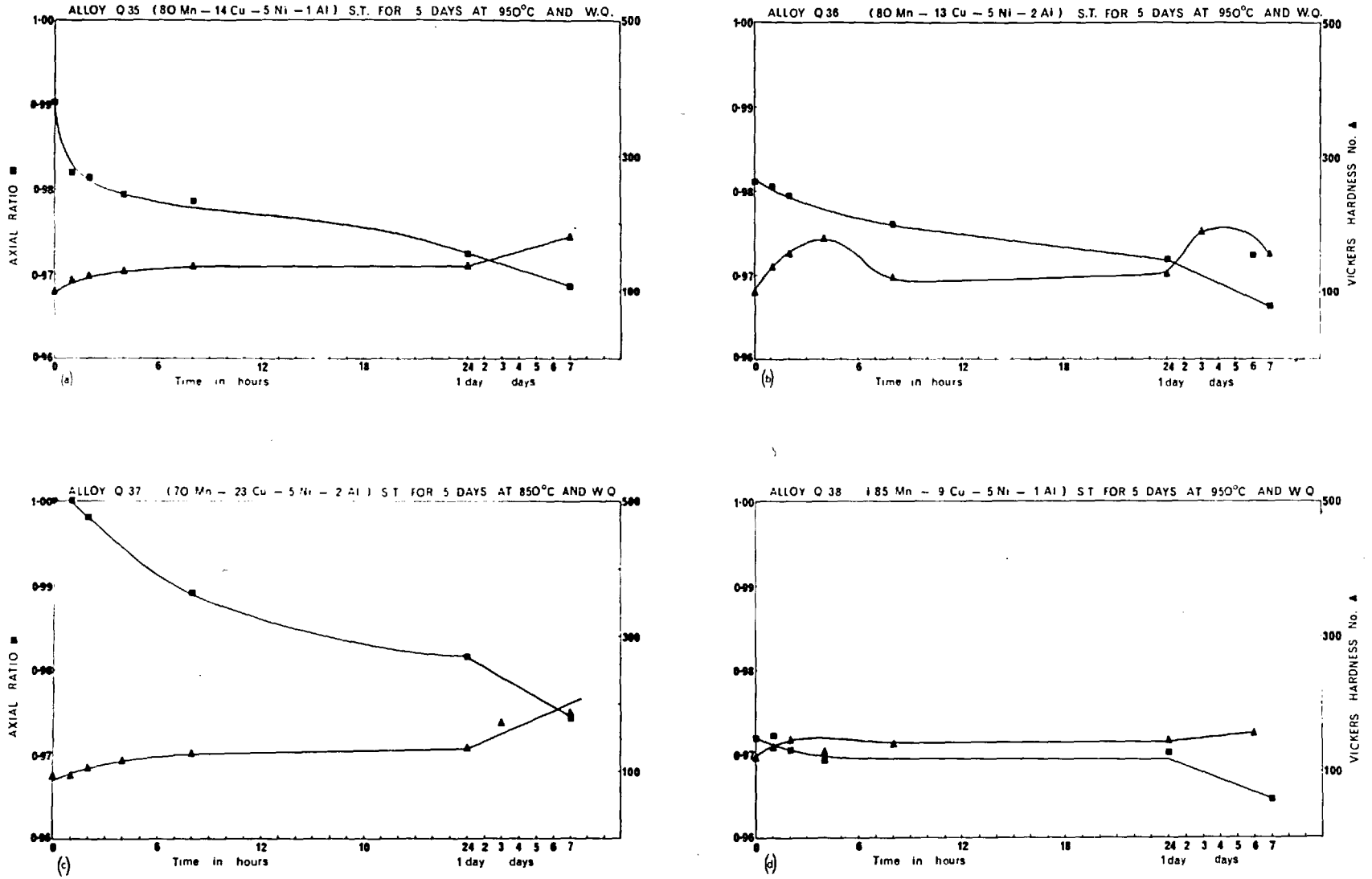
9.2.3 Alloys containing Si.

9.2.3.1 Alloy Q33 (80%Mn-14%Cu-5%Ni-1%Si).

Samples of the alloy were solution treated for 5 days at 950°C, water quenched and given ageing heat treatments at 400°C, 450°C and 500°C for a variety of times. At 450 and 500°C βMn precipitated out of solid solution, Figs. 89 and 90; αMn was not detected, whereas at 400°C αMn was formed, as normal. The change in axial ratio and hardness (H_V) values with ageing heat treatment time at 400°C and 450°C is shown in Fig. 91. It is assumed from these results that the change from $\gamma \rightarrow \gamma + \alpha$ to $\gamma \rightarrow \gamma + \beta$ occurs at some temperature between 400 and 450°C.

The proposed damping mechanism requires a matrix sufficiently rich in Mn to result in the fcc/fct transformation. It should be possible to achieve this by the reaction $\gamma \rightarrow \gamma + \beta$, as well as $\gamma \rightarrow \gamma + \alpha$, although the latter reaction is desirable because

FIG. 92 CHANGE IN AXIAL RATIO AND HARDNESS (H_v), MEASURED AT ROOM TEMPERATURE, WITH HEAT TREATMENT TIME AT 400°C GIVEN TO VARIOUS ALLOYS CONTAINING Al.



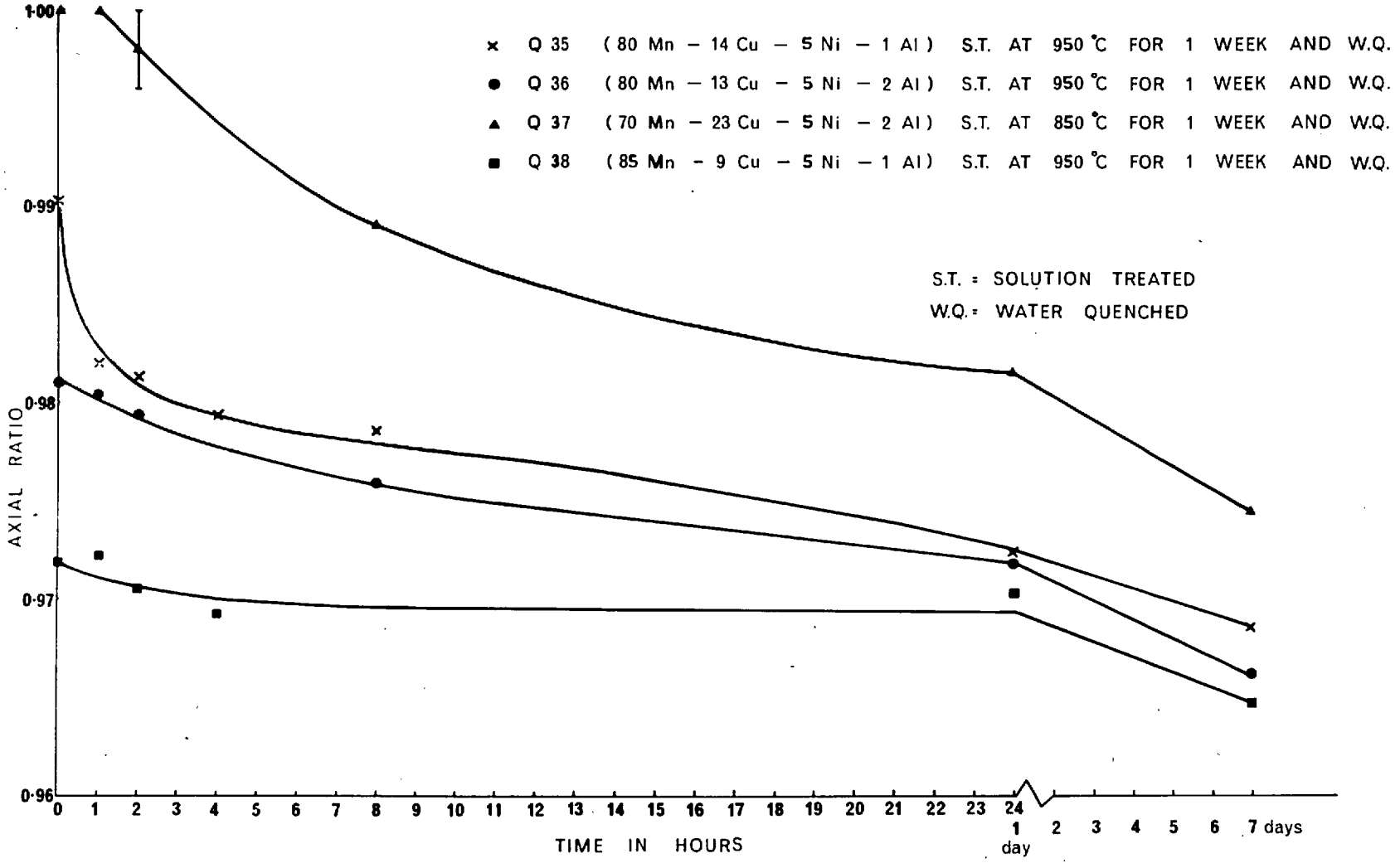


FIG. 93 COMPARISON OF THE CHANGE IN AXIAL RATIO WITH HEAT TREATMENT TIME AT 400° C GIVEN TO VARIOUS ALLOYS CONTAINING Al.

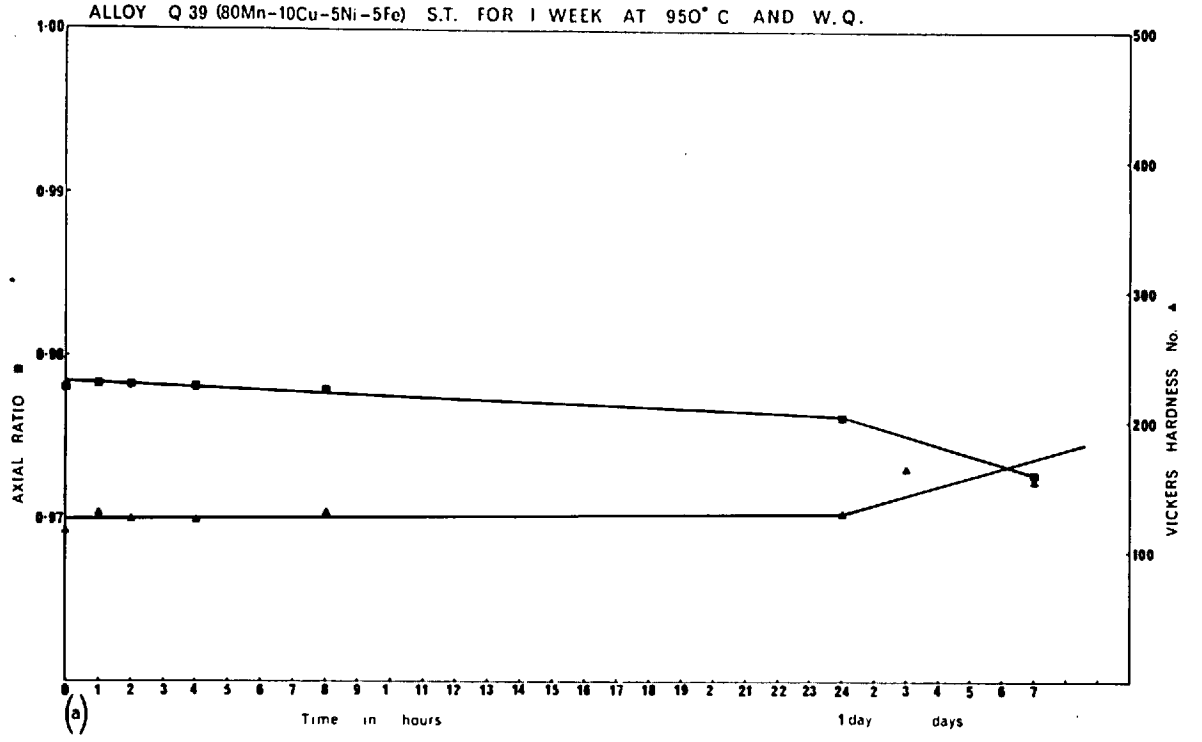
the precipitation is more homogenous in its distribution. The damping results obtained from samples heat treated at 400 and 450°C, confirmed this conclusion, Fig. 88. It is not possible to ascribe any significance to the higher damping levels recorded in the sample aged for 4 hours at 450°C during the reaction $\gamma \rightarrow \gamma + \beta$, compared with the damping levels of the sample aged for 4 hours at 400°C during the reaction $\gamma \rightarrow \gamma + \alpha$, because the kinetics of the ageing reaction at the two temperatures differ. The damping levels in general are a little lower than the parent alloy T16 (80%Mn-15%Cu-5%Ni).

9.2.4 Alloys containing Al.

Al confers corrosion resistance on the "Sonoston" range of alloys [102] and by analogy with Sonoston, Al has been added to a variety of high Mn alloys.

Alloy Q35 (80%Mn-14%Cu-5%Ni-1%Al), Q36 (80%Mn-13%Cu-5%Ni-2%Al). and Q37 (70%Mn-23%Cu-5%Ni-2%Al) all cracked in the early stages of rolling and alloy Q38 (85%Mn-9%Cu-5%Ni-1%Al) fell into pieces on casting. In all cases the brittleness could be connected with the presence of excessive amounts of βMn.

Although these alloys are of no practical use, it was thought worthwhile to solution treat samples and give then an ageing heat treatment at 400°C to determine if any significant influence was being exerted by Al on the $\gamma \rightarrow \gamma + \alpha$ reaction. The results obtained on all the alloys containing Al are shown in Figs. 92 and 93. The change in axial ratio with ageing time at 400°C was apparently conventional, but the hardness (H_V) values recorded for alloys Q36 (80%Mn-13%Cu-5%Ni-2%Al) and Q38 (85%Mn-9%Cu-5%Ni-1%Al) were irregular. Alloy Q36 (80%Mn-13%Cu-5%Ni-2%Al) contains 2%Al in conjunction with 80%Mn and Q38 (85%Mn-9%Cu-5%Ni-1%Al) contains 1%Al in conjunction with 85%Mn; it is likely therefore that these two alloys will be more prone to the formation of the βMn phase. It may then be possible that βMn or βMn + αMn is precipitating out of solid solution at 400°C in quantities too small to be detected by X-ray diffraction, and hence giving rise to the peculiarities



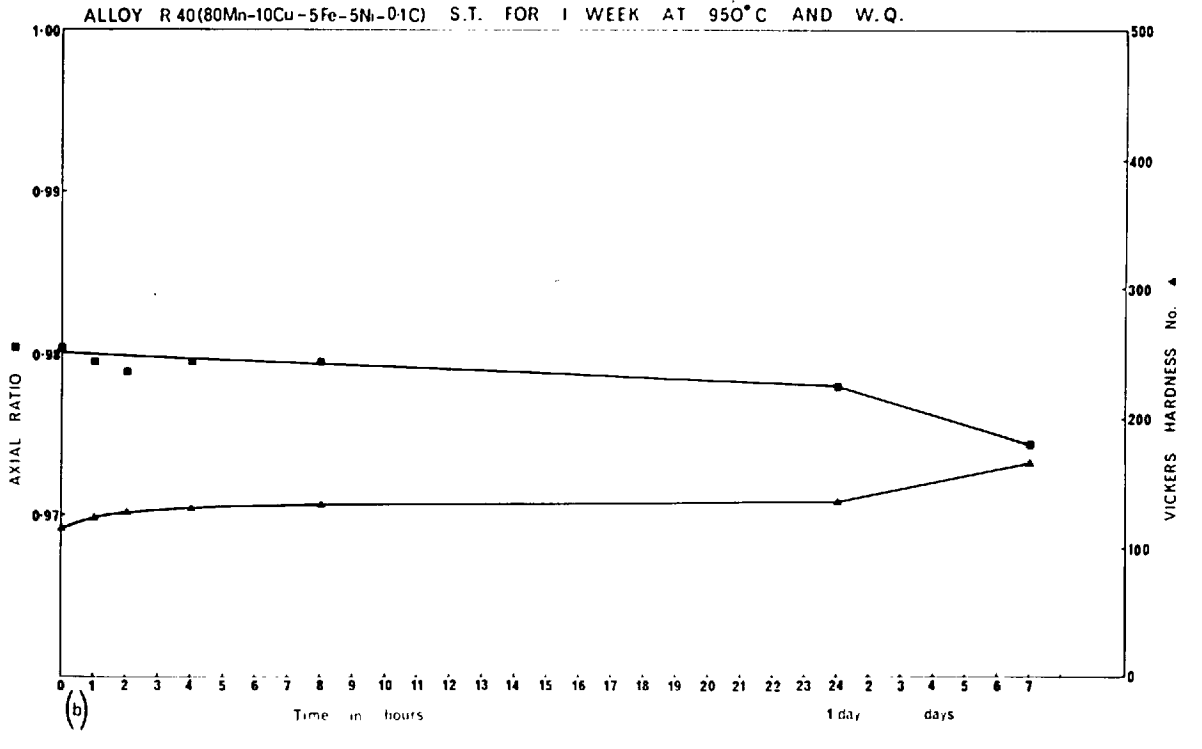


FIG. 94 CHANGE IN AXIAL RATIO AND HARDNESS (H_V), MEASURED AT ROOM TEMPERATURE, WITH THE HEAT TREATMENT TIME AT 400° C GIVEN TO ALLOYS Q 39 AND R 40

in the hardness (H_V) results. The fcc/fct transformation temperature of alloy Q38 (85%Mn-9%Cu-5%Ni-1%Al) was found to be about 110°C, showing that the replacement of 1%Cu by 1%Al in alloy T23 (85%Mn-10%Cu-5%Ni) has had a considerable effect in lowering the fcc/fct transformation temperature. As sound material could not be obtained in alloys with Al additions, it has not been possible to obtain damping results.

9.2.5 Alloy T20 (85%Mn-14%Ni-1%C), Q39 (80%Mn-10%Cu-5%Ni-5%Fe) and R40 (80%Mn-10%Cu-5%Ni-5%Fe-0.1%C).

It has been reported from the Admiralty Materials Laboratory[104] that the addition of small amounts of C to Mn-Cu alloys results in an appreciable reduction in damping properties. However, it has been claimed that in the "Sonoston" range of alloys, small additions of C improve the stress corrosion properties[102] In the first instance the 85%Mn-15%Ni alloy was chosen, because this represented the highest recorded fcc/fct temperature in this programme of work. The addition of 1%C was sufficient to completely prevent the fcc/fct transformation in the water quenched state, but tetragonality gradually developed after an ageing heat treatment. This is the only alloy containing more than 80%Mn which did not exhibit the fct structure at room temperature.

Alloy Q39 (80%Mn-10%Cu-5%Ni-5%Fe) and R40 (80%Mn-10%Cu-5%Ni-5%Fe - 0.1%C) were included in the programme because it was thought that the addition of Fe would allow the formation of a surface nitride layer, in a similar manner to the nitride layer that was formed in the earlier Mn-Fe alloys when they were heat treated in air. In view of the appreciable effect of 1%C upon the 85%Mn-15%Ni alloy, the opportunity was taken to add 0.1%C in alloy R40(80%Mn-10%Cu-5%Ni-5%Fe-0.1%C), so that a direct comparison between alloy R40 and Q39 and hence the effect of 0.1%C, could be made. Both alloys rolled satisfactorily and, after a solution treatment for 1 week at 950°C, responded to the ageing treatment at 400°C rather slowly, Fig. 94. The C addition of as low as 0.1% produced a detectable change in the

ageing characteristics, although the exact amount of C present, compared against that present in casts in which no intentional addition of C had been made, has not been determined.

The damping properties of alloys Q39 (80%Mn-10%Cu-5%Ni-5%Fe) and R40(80%Mn-10%Cu-5%Ni-5%Fe-0.1%C) were moderate when compared with other alloys based on 80%Mn, Fig. 88. They were, however, better than the damping results obtained from the binary 80%Mn-20%Ni alloy, Fig. 58. Both these alloys were designed with properties ancillary to damping capacity in mind and have been incorporated in this thesis to record the effect of C on their structural properties. Damping measurements on alloy T20 (84%Mn-15%Ni-1%C), given an ageing heat treatment of 24 hours at 550^{o}C, were very low, Table 7, confirming the conclusions derived from the X-ray work and the previous results of the Admiralty Materials Laboratory on Mn-Cu alloys[104].

Although the theme of the research programme has been the development of high damping capacity alloys, it is nevertheless interesting, when formulating possible mchanisms, to examine the role of elements which discourage the development of high damping properties, especially when they are as catastrophic in their effect as C.

It is unlikely that the correspondingly low damping properties are a result of interference with microtwin movement and an explanation based on interstitial C atoms, either stabilising the fcc γ structure or preventing the martensitic shearing transformation would seem more probable.

A number of neutron and X-ray diffraction experiments on Mn alloys containing C would probably lead to a much better understanding of the relationship between the antiferromagnetic properties and the fcc/fct transformation.

CHAPTER 10.

GENERAL DISCUSSION AND CONCLUSIONS.

10.1 THE DAMPING MECHANISM.

It now remains to re-assess the damping mechanism, which was developed from the study of Mn-Cu alloys in Sections 4.4 and 4.5, in the light of the results from the various elemental additions described in chapters 5 to 9. The detailed discussion has been included in each chapter and it is only necessary now to report general trends and emphasise any significant additional information relating to the interpretation of the results and the damping mechanism.

10.1.1 The effect of various additions on the $\gamma \rightarrow \gamma + \alpha$ reaction.

An examination of the way in which the axial ratio changes with ageing heat treatment time provides information on the progress of the $\gamma \rightarrow \gamma + \alpha$ reaction. However, it is not possible to unambiguously assign an order of relative importance to the effect of the various elemental additions on the $\gamma \rightarrow \gamma + \alpha$ ageing reaction. Some of the factors influencing the axial ratio have already been discussed in Section 4.3, especially the competing effect between the fct Mn-rich matrix and the Cu-rich zones which would otherwise revert to their stable fcc structure. It is now necessary to consider another uncertainty when attempting to compare the axial ratios of different alloy compositions after the same heat treatment. For instance, if the lattice parameters of quenched alloys in the Mn-Cu system are compared against those in the Mn-Cu-Zn system, Figs. 26 and 81, it will be seen that the axial ratiosof high Mn alloys in the Mn-Cu-Zn system are much lower than axial ratios of corresponding Mn concentrations in the Mn-Cu system. A situation could easily arise whereby a Mn-Cu alloy could develop a high Mn concentration during the $\gamma \rightarrow \gamma + \alpha$ ageing process, yet exhibit an axial ratio closer to 1 than a Mn-Cu-Zn alloy with a lower initial Mn concentration and yet a corresponding axial ratio much

ALL ALLOYS WERE S.T. FOR 5 DAYS AT 850 °C AND WATER QUENCHED.

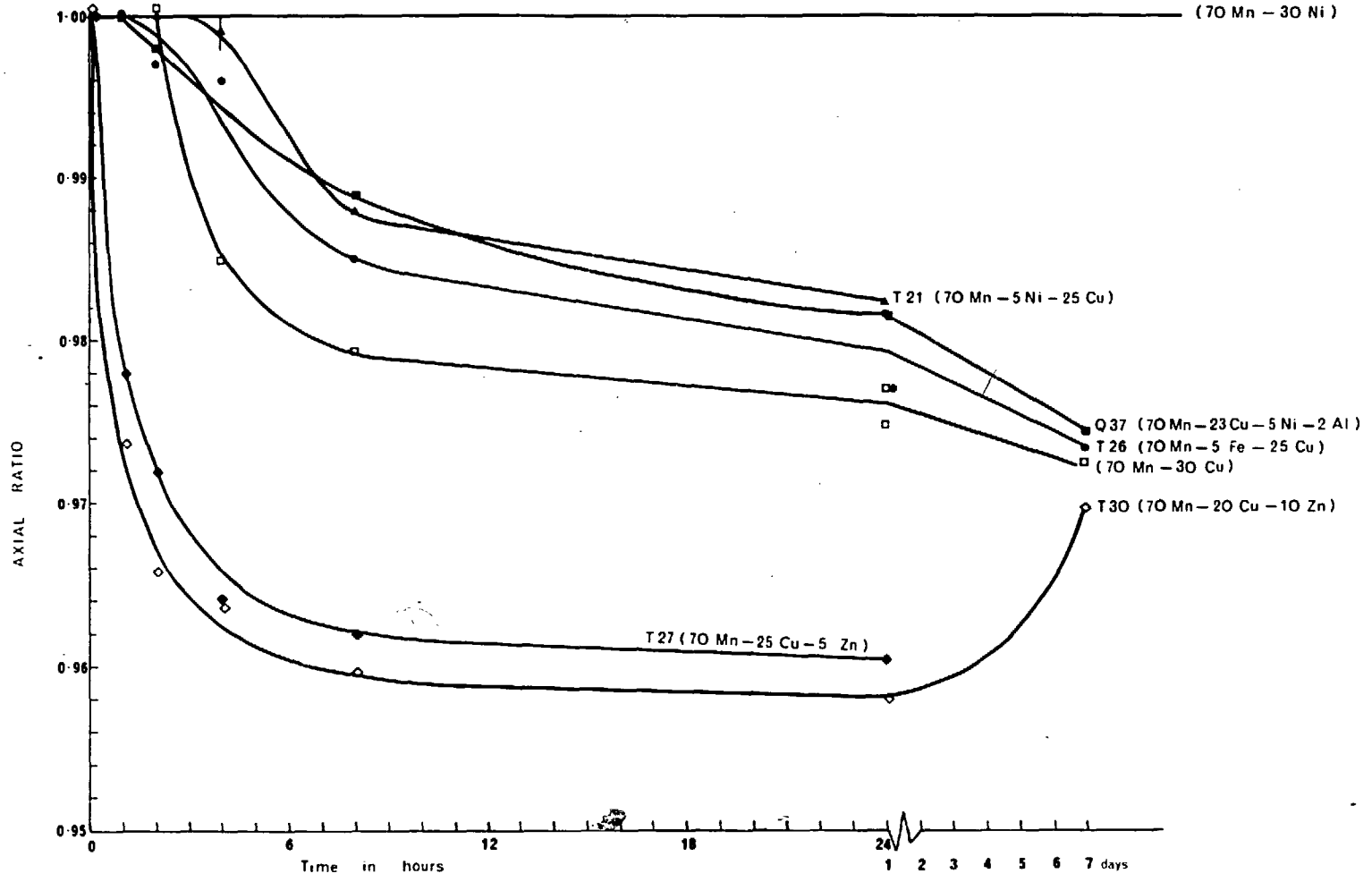


FIG. 95 THE CHANGE IN AXIAL RATIO, MEASURED AT ROOM TEMPERATURE, WITH HEAT TREATMENT TIME AT 400° C GIVEN TO VARIOUS ALLOYS BASED ON 70 % Mn.

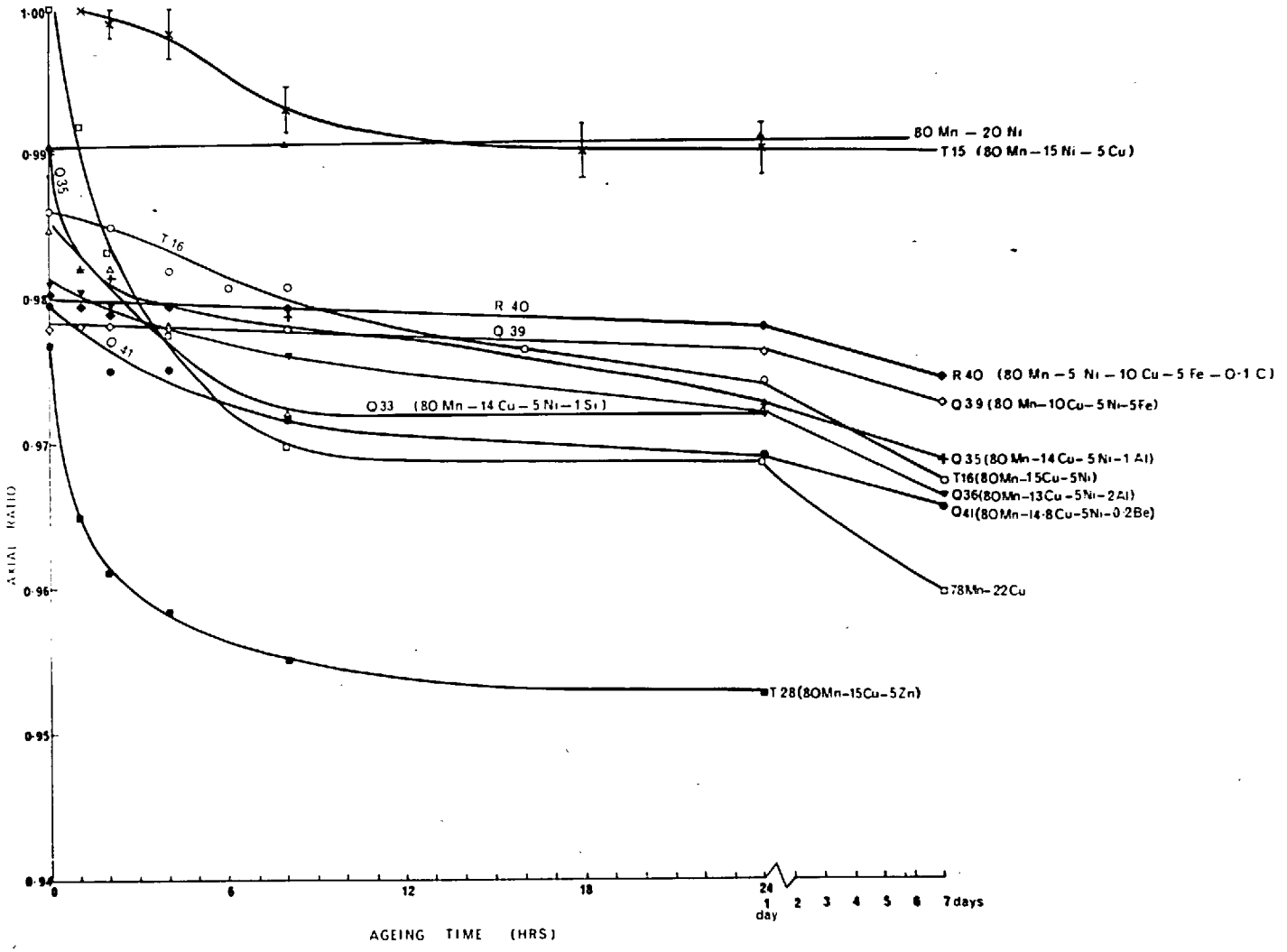


FIG. 96 THE CHANGE IN AXIAL RATIO, MEASURED AT ROOM TEMPERATURE, WITH HEAT TREATMENT TIME AT 400°C GIVEN TO VARIOUS ALLOYS BASED ON 80 % Mn.

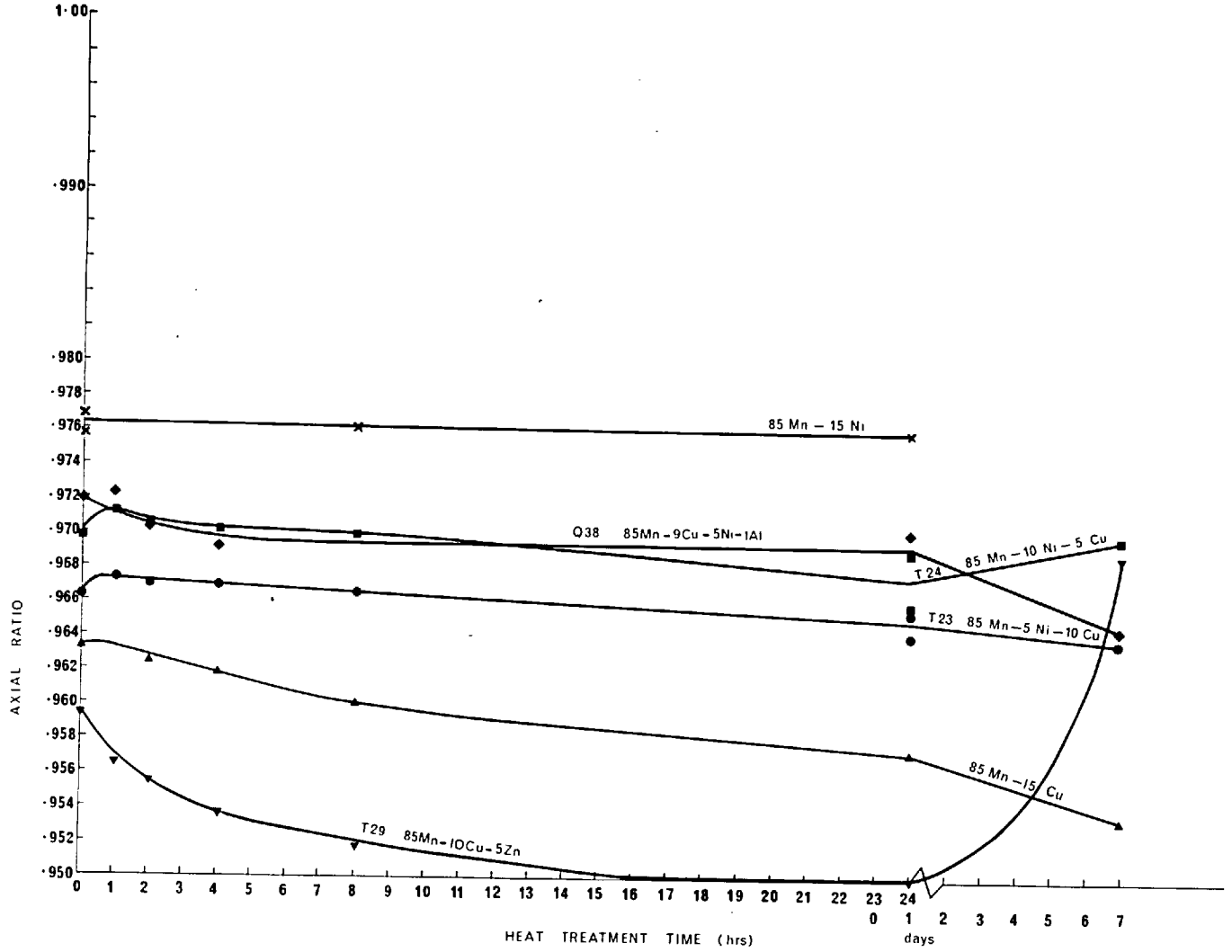


FIG. 97 THE CHANGE IN AXIAL RATIO MEASURED AT ROOM TEMPERATURE, WITH HEAT TREATMENT TIME AT 400°C GIVEN TO VARIOUS ALLOYS BASED ON 85 % Mn.

less than 1. If this effect were not taken into account, comparison of the two axial ratio values could lead to the false assumption that the Mn-Cu-Zn alloy had been given a longer heat treatment than the Mn-Cu sample. Another facet of the same problem involves the comparison of two different alloy compositions which have been given exactly the same heat treatment. For the same reasons as those outlined above, it cannot be assumed that the alloy which yields the lowest axial ratio responds most readily to the $\gamma \rightarrow \gamma + \alpha$ reaction.

A better criterion for assessing the progress of the $\gamma \rightarrow \gamma + \alpha$ reaction is the overall shape of the graph relating axial ratio to the ageing heat treatment. Useful reference could be made at this point to Figs. 95, 96 and 97 which record the change in axial ratio with heat treatment according to the Mn concentration of each alloy. Any confusion in detail in these graphs can be resolved by reference to the appropriate figure for the alloy concerned. A "knee" in the curve has already been correlated with the appearance of αMn precipitate particles in Mn-Cu alloys. If the addition of a particular element results in the movement of the "knee" to shorter heat treatment times, then that element can be said to have encouraged the $\gamma \rightarrow \gamma + \alpha$ reaction. Not all of the graphs show a pronounced "knee" and these are associated with alloys which show a poor response to the ageing process. When all factors are considered, including for instance optical microscopy and hardness measurements, it is possible to assign a tentative order of relative importance of the various elemental additions on the kinetics of the $\gamma \rightarrow \gamma + \alpha$ reaction. In order of decreasing influence on the reaction, these are Be, Zn, Cu, Si, Al, Fe, Ni and C. A similar order of decreasing influence on the $\gamma \rightarrow \gamma + \beta$ reaction would probably be Al, Si, Be, Fe, Zn, Ni, Cu and C. The significance of the order in these lists of elements is not immediately apparent, although the influence in promoting the stability of the various Mn phases must be

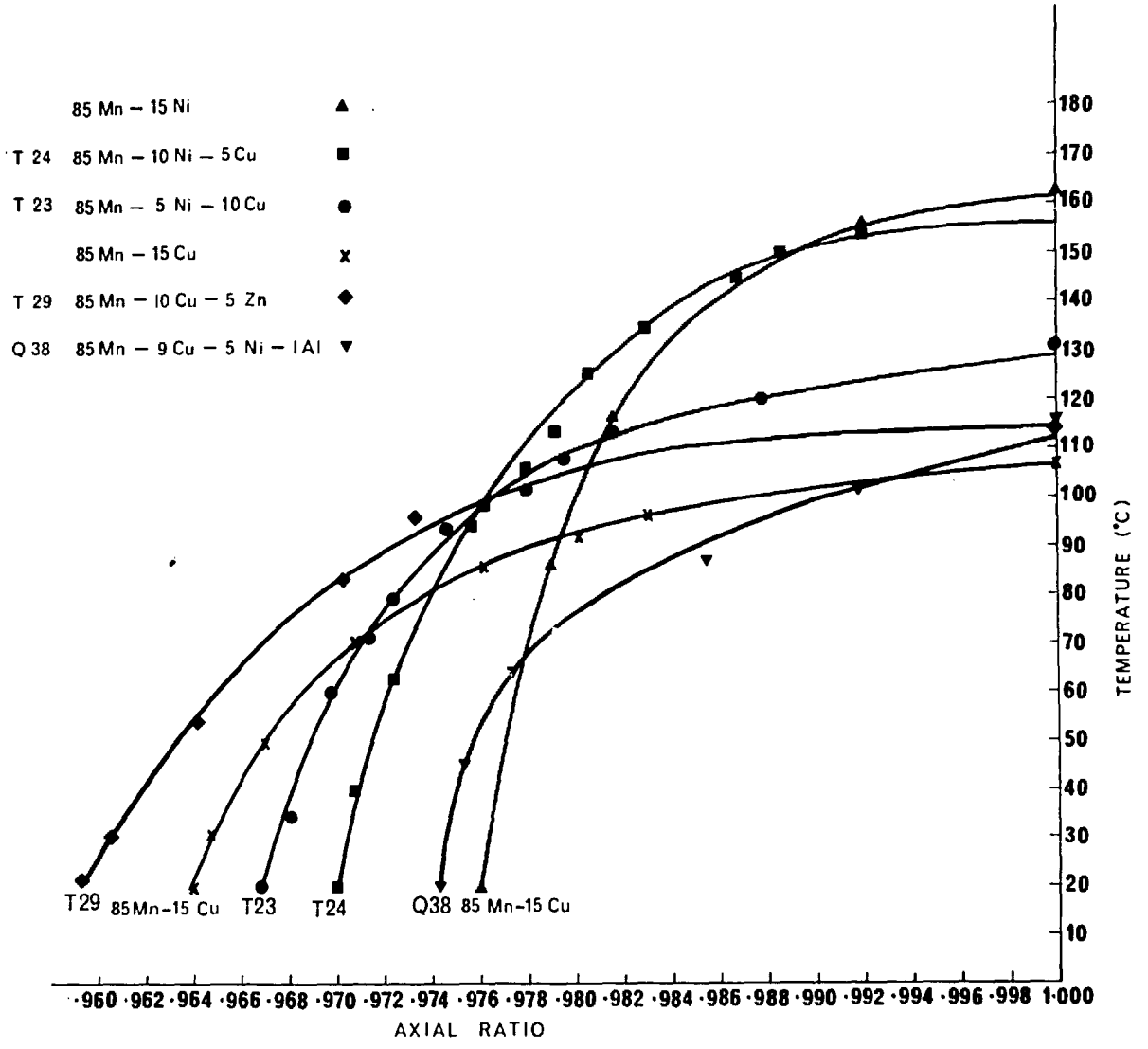


Fig. 98 The effect of temperature on the axial ratio of alloys based on 85 % Mn. All alloys have been solution treated and water quenched.

very important. The rate of diffusion of Mn atoms must also be a prime parameter. An empirical relationship is often quoted between the melting point of an alloy and the temperature at which diffusion becomes appreciable. An explanation along these lines may be proposed to explain why alloys with very high Mn contents do not respond to the ageing heat treatment so readily, when from a consideration of the relevent equilibrium diagrams it would be expected that αMn would precipitate out of solution more readily with increasing Mn content, because the Mn atoms would not then need to diffuse over such large distances.

10.1.2 The effect of the various additions on the fcc/fct transformation temperature.

Because of the different ageing response exhibited by Mn alloys, the absolute effect of a particular elemental addition on the fcc/fct transformation temperature can only be assessed when the alloy is in the solution treated and water quenched condition. Only alloys with 80%Mn or more can be considered because of this restriction. Furthermore, the axial ratios of water quenched alloys containing 80%Mn are usually close to 1 and the fcc/fct transformation temperature is close to room temperature. The effect of various additions on the fcc/fct transformation temperature can therefore best be established using alloys which contain 85% or more Mn and are in the solution treated and water quenched condition, Fig. 98. In those alloys which are based on Mn-Cu, Mn-Ni or Mn-Ni-Cu, a clear trend was established whereby a lower axial ratio measured at room temperature corresponded to a lower fcc/fct transformation temperature. This relationship turned out to be arbitrary and the results on alloys containing Zn and Al did not fit rigidly into this pattern.

There is a close correlation between the Néel temperature and the fcc/fct transformation temperature in Mn-Cu alloys[12,13,] Fig. 1 and a recent attempt has been made to directly relate

the degree of antiferromagnetic alignment with the axial ratio[105]. However, in Mn-Ni alloys, the fcc/fct transformation temperature at some Mn concentrations was appreciably lower than the Néel temperature, Fig. 41, so the theory[105] is not generally applicable to antiferromagnetic Mn alloys. There has been speculation in the scientific press[100] concerning the reasons for this disparity, but until detailed neutron diffraction measurements are undertaken on Mn-Ni and some of the other alloy compositions described in this thesis, a satisfactory explanation relating the intensity of antiferromagnetism and the degree of lattice distortion is not likely to arise. It is possible that the intensity of antiferromagnetic interaction needs to attain a critical value for each alloy composition before shear on the {110} will result. Such an approach however, would appear to be at variance with the prerequisite for high damping properties, namely easy shear on {110}.

10.1.3 Damping properties at room temperature.

Although several alloys have been developed which possess damping properties at room temperature comparable with the best damping properties obtained from the 60%Mn-40%Cu alloy, in no cases have better damping properties at room temperature been recorded. In general, the damping capacity of alloys containing 60%Mn increases with heat treatment at 400°C and passes through a maximum after a certain critical heat treatment. Alloys containing 70%Mn exhibit the same behaviour and shorter ageing times are required to produce similar high damping levels. Alloys containing 80%Mn exhibit a maximum in damping capacity in the quenched condition and further ageing heat treatment produces a fall in the damping properties. Alloys containing 85%Mn in general, have lower damping properties than alloys containing 60, 70 and 80%Mn and tend to be relatively insensitive to the ageing heat treatment; a notable exception is alloy T29 (87%Mn-3%Zn-10%Cu) which did respond to the ageing heat treatment, Fig. 97. It is not known if this general fall in

damping properties as the Mn content is increased is related to the ease of movement of the microtwins or is related to the state of the matrix through which the microtwin moves. The misorientation across microtwin boundaries increases as the Mn content of an alloy increases because of the change in axial ratio. If this were a significant factor, it could be argued that a quenched high Mn alloy should exhibit a maximum in the damping capacity as the temperature is increased, because there would then be an increase in axial ratio towards those values associated with lower Mn alloys and higher damping properties. This does not occur, so that an explanation biased towards the state of the matrix would seem more likely. The 60%Mn-40%Cu alloy develops very high damping properties in conjunction with the very fine substructure described in Section 4.5. Increasing the Mn content of an alloy would tend to decrease the volume percentage of Cu-rich zones developed during the $\gamma \rightarrow \gamma + \alpha$ reaction, yet decreasing the Mn content eventually leads to a situation where the fct structure does not develop during the ageing process. In the case of Mn-Cu it is therefore not surprising that maximum damping properties are developed in the 60%Mn-40%Cu alloy. An equivalent argument could be applied to other Mn alloys, in which case coherent zones of a composition equivalent to the terminal composition of the $\gamma \rightarrow \gamma + \alpha$ phase boundary would result.

10.1.4 Damping properties at elevated temperatures.

The structural and compositional requirements of an alloy exhibiting good damping properties at elevated temperatures are incompatible with the structural requirements of an alloy which is corrosion resistant and can easily be cast and fabricated. Al is the key element which confers ease of castibility and corrosion resistance. If Al is added to any alloy containing more than about 60%Mn, the brittle βMn phase forms, either during the casting process or during the subsequent heat treatment. Both ease of castability and corrosion resistance deteriorate

with increasing Mn content.

The prime requirement for good damping properties at elevated temperatures is a high Mn content in a stable γMn phase. It is possible then to adopt two different approaches in the search for a suitable high Mn alloy and these two approaches are exemplified by the alloys T23 (85%Mn-5%Ni-10%Cu) and T29 (87%Mn-3%Zn-10%Cu) which were finally selected. Theoretically, the best alloy for high damping capacities at elevated temperatures would have a composition approaching 100%Mn. The Néel temperature and the fcc/fct transformation temperature would then be at a maximum for an alloy based on Mn. Such an alloy would transform to one of the allotropic modifications, either αMn or βMn. It is therefore necessary to lower the Mn content by alloying. The selection of the alloying element has been shown to be very important. Ni is the best element to add to Mn to retain a high fcc/fct transformation temperature and 15%Ni is the minimum amount that can be added to ensure a γMn structure in the cast state. When the alloy is in the cast condition it is then possible to increase the Mn concentration further by the ageing heat treatment in which the $\gamma \rightarrow \gamma + \alpha$ reaction is utilised. It is necessary to prevent appreciable αMn precipitation or the mechanical properties will deteriorate. Unfortunately, in Mn-Ni binary alloys the reaction proceeds extremely slowly, even at temperatures up to 550^{o}C; above this temperature the $\gamma \rightarrow \gamma + \beta$ reaction is preferred. Heat treatments of several weeks are necessary to produce the very high damping properties at elevated temperatures, Fig. 59.

The fcc/fct transformation temperature decreases to a greater extent when Cu is added to Mn compared against an equivalent addition of Ni, Fig. 98. Cu does, however, discourage the formation of the brittle βMn phase during casting and tends to encourage the $\gamma \rightarrow \gamma + \alpha$ reaction. It is then a matter of weighing the disadvantages of the reduced fcc/fct transformation

temperature in the solution treated condition against the increase in fcc/fct transformation temperature which could result from an increased Mn concentration through a more ready response to the $\gamma \rightarrow \gamma + \alpha$ reaction. Such an approach led to the choice of alloy T23 (85%Mn-5%Ni-10%Cu).

The other approach for obtaining high damping properties at elevated temperatures involves the selection of an element which is particularly active in promoting the $\gamma \rightarrow \gamma + \alpha$ reaction and thereby leading to a high Mn concentration through the ageing process. It is unfortunate that an increasing propensity to encourage the $\gamma \rightarrow \gamma + \alpha$ reaction, appears to correspond to a decreasing fcc/fct transformation temperature. It is unlikely that this inverse relationship is coincidental, although an explanation for the connection is not immediately obvious. In this approach therefore, the damping properties are not expected to be particularly good at elevated temperatures when the alloy is in the solution treated condition, by virtue of the low fcc/fct transformation temperature. The aim is then to increase the Mn content and thereby increase the fcc/fct transformation temperature by means of a short ageing heat treatment at 400°C. Zn is an element which has a strong influence in promoting the $\gamma \rightarrow \gamma + \alpha$ reaction and alloy T29(87%Mn-3%Zn-10%Cu) typifies this approach. A drawback to be expected in this type of alloy is the tendency to precipitate αMn out of solid solution and the ageing heat treatment is therefore rather critical.

On the basis of these two approaches, it is likely that further compositional optimisation would yield even better damping properties at elevated temperatures without a significant loss in associated mechanical properties.

10.2 HAVE THE AIMS OF THE RESEARCH PROGRAMME BEEN MET?

The prime aim of the research programme has been the development of an alloy or alloys which exhibit damping properties at elevated temperatures, in contrast to the 60%Mn-40%Cu and 70%Mn-30%Cu alloys where the damping properties are lost at about

110°C. An approach was adopted which first involved identifying those physical features which were associated with the high damping condition and this was followed by a proposed mechanism to explain how these features arise and how they react under an external stress to give rise to the high damping properties. The proposed mechanism was then applied to the search for alternative systems and this led logically first to binary alloys and later to ternary and quaternary systems based on Mn. The research programme has been successful in identifying those requirements which are needed for alloys exhibiting good damping properties at elevated temperatures and certain alloy compositions have been identified and proved to possess these properties.

Adequate corrosion resistance to sea water can only be induced by the presence of Al and this element is inimical to the phase stability necessary for the development of damping properties in high Mn alloys.

There is an inverse relationship between damping properties and Young's modulus. Alloy compositions containing Be have been identified, which, with further development, could probably lead to higher strength alloys with improved Young's modulus and lower damping properties.

TABLE 1.

Chemical analysis of alloys used for structural analysis.

Position in billet. B=Bottom T=Top	Nominal Mn	Chemical Analysis (wt%) Mn	Cu	Fe	Si	C	N
	30	n.d	n.d	n.d	n.d	n.d	n.d
	40	n.d	n.d	n.d	n.d	n.d	n.d
B	50	50.76	49.03	n.d	n.d	n.d	n.d
T	50	50.76	49.03	0.02	0.01	0.005	0.01
B	60	57.13	42.61	n.d	n.d	n.d	n.d
T	60	56.97	42.88	0.02	0.02	0.005	0.01
	70	71.41	28.48	0.03	0.06	0.02	n.d
B	80	77.21	22.70	n.d	n.d	n.d	n.d
T	80	77.12	22.72	0.03	0.01	0.01	0.01
B	90	90.36	9.53	n.d	n.d	n.d	n.d
T	90	90.25	9.59	0.02	0.01	0.005	0.01
	95	n.d	n.d	n.d	n.d	n.d	n.d
Chemical analysis of alloys used for damping capacity determination.							
	60	60.42	39.45	0.03	0.02	0.08	n.d
	70	71.41	28.48	0.03	0.06	0.02	n.d

n.d = not determined.

TABLE 2.

Factors affecting the choice of a suitable X-radiation.

Target Material	Mo	Zn	Cu	Ni	Co	Fe	Mn	Cr
X-ray wavelength, λ	0.711	1.436	1.542	1.659	1.790	1.937	2.103	2.291
2θ position of (200)	21.8^{o}	45.0^{o}	48.4^{o}	52.4^{o}	56.8^{o}	62.0^{o}	68.2^{o}	75.0^{o}
2θ position of (002) with $\frac{c}{a} = 0.98$	22.2^{o}	46.0^{o}	49.6^{o}	53.6^{o}	58.2^{o}	63.6^{o}	69.8^{o}	77.0^{o}
Separation of (200) and (002)	0.4^{o}	1.0^{o}	1.2^{o}	1.2^{o}	1.4^{o}	1.6^{o}	1.6^{o}	2.0^{o}
Intensity of possible superlattice reflection								
Intensity of fundamental reflection	.006	.003	.001	.003	.006	.02	.01	.009
Severe fluorescence problems with	Zr	Ni	Co	Fe	Mn	Cr	V	Ti
	Y	Co	Fe	Mn	Cr	V	Ti	Sc
Readily available (R.A) Available only to special order (S.O)	R.A	S.O	R.A	S.O	R.A	R.A	S.O	R.A
Tube wattage. Not known (N.K)	1000	N.K	1000	N.K	350	350	N.K	300

TABLE 3.

Compositions of cast Mn-Fe alloys.

Nominal % Mn		Chemical analysis (wt%) Mn %	Fe %
85	T	84.4	15.29
	B	84.6	15.20
80	T	78.9	20.93
	B	78.6	20.88
75	T	74.8	25.06
	B	74.7	25.06
70	T	70.3	29.41
	B	70.5	29.33

Compositions of cast Mn-Ni alloys.

		Mn	Ni
95	T	n.d	5.17
	B	n.d	3.34
90	T	n.d	10.00
	B	n.d	10.30
85	T	84.7	15.06
	B	84.9	15.03
80	T	79.8	19.97
	B	79.7	19.97
70	T	70.2	29.48
	B	70.3	29.55
63	T	64.7	35.04
	B	64.6	35.09
60	T	59.6	39.98
	B	59.8	39.92

T = Top of Billet
B = Bottom of Billet
n.d = not determined.

TABLE 3 Cont.

Alloy No.	Nominal Composition									Chemical Analysis (wt%)								
	Mn	Cu	Ni	Fe	Zn	Al	Be	Si	C	Mn	Cu	Ni	Fe	Zn	Al	Be	Si	C
T1	70		10	20						66.9		9.66	23.44					
T2	75		5	20						74.33		5.12	20.55					
T3	80		10	10						79.10		9.63	10.27					
T4	75		20	5						75.23		20.46	5.31					
T5	75		10	15						75.04		9.82	15.14					
T6	75		15	10						74.48		15.06	10.46					
T7	65		15	20						65.07		15.02	19.91					
T8	80		15	5						80.1		14.8	5.10					
T9	60	20		20						59.78	20.56		19.66					
T10	60	10		30						60.17	10.05		29.78					
T11	70	20		10						69.54	20.3		10.16					
T12	45	45	10							45.28	44.92	9.8						
T13	55	35	10							54.76	34.98	10.26						
T14	65	25	10							64.82	25.08	10.10						
T15	80	5	15							79.80	5.08	15.11						
T16	80	15	5							79.97	14.99	5.03						
T20	85		14						1	n.d.	n.d	14.27						0.98
T21	70	25	5							70.06	24.79	5.04						
T22	60	35	5							60.06	35.31	4.99						

Cont.....

TABLE 3 Cont.

Alloy No.	Nominal Composition									Chemical Analysis (wt%)								
	Mn	Cu	Ni	Fe	Zn	Al	Be	Si	C	Mn	Cu	Ni	Fe	Zn	Al	Be	Si	C
T23	85	10	5							84.96	9.93	4.98						
T24	85	5	10							84.82	5.18	9.90						
T25	70	25		5						70.14	25.51		4.35					
T26	70	25		5						70.28	24.41		5.30					
T27	70	25			5					n.d	23.16			n.d				
T28	80	15			5					n.d	14.93			n.d				
T29(1)	85	10			5					n.d	10.26			n.d				
T29(2)	87	10			3					86.9	9.93			3.03				
T30	70	20			10					n.d	20.09			n.d				
Q31	80	14.4	5				0.6			n.d	14.44	4.82				n.d		
T32	60	38.4					1.6			n.d	38.10					n.d		
Q33	80	14	5					1		n.d	13.26	n.d					n.d	
Q35	80	14	5			1				n.d	14.07	4.91			n.d			
Q36	80	13	5			2				n.d	13.29	4.80			n.d			
Q37	70	23	5			2				n.d	22.40	5.00			n.d			
Q38	85	9	5			1				n.d	10.57	4.89			n.d			
Q39	80	10	5	5						n.d	10.25	4.84	n.d					
R40	80	10	5	5					0.1	n.d	10.44	4.89	n.d					n.d
Q41	80	14.8	5				0.2			n.d	14.55	4.90				n.d		

TABLE 4

Stress-dependence of the damping capacity of alloy T8 (80%Mn-5%Fe-15%Ni) which has been rolled and water quenched from 1000°C.

Surface Shear Stress p.s.i.	Damping Capacity (%)
1000	8
2000	9
3000	11
4000	13
5000	15

TABLE 5.

Stress-dependence of the damping capacity of alloy T15 (80%Mn-15%Ni-5%Cu) after various solution treatments at 1000°C.

Heat Treatment	Damping capacity (%) versus surface shear stress in p.s.i.				
	1000	2000	3000	4000	5000
Rolled and Water quenched from 1000°C	8.7	10.6	14.3	15.9	18.1
Solution treated for 1 week at 1000°C, and water quenched	11.5	14.2	16.1	20.3	24.6
Solution treated for 1 month at 1000°C and water quenched.	29.3	31.2	33.6	36.9	40.0

TABLE 6.

Stress-dependence of the damping capacity of Alloy T24 (85%Mn-10%Ni-5%Cu) which has been given a solution treatment for 1 week at 950°C and water quenched; before and after a further heat treatment for 4 weeks at 80°C.

Surface Shear Stress p.s.i.	Damping Capacity (%)	After a further 4 weeks at 80°C. Damping Capacity (%)
1000	19.1	17.3
2000	23.9	19.4
3000	27.0	22.7
4000	30.2	26.6
5000	34.7	27.6

Stress-dependence of the damping capacity of Alloy T24 (85%Mn-10%Ni-5%Cu) which has been given a solution treatment for 1 week at 950°C and water quenched and given a heat treatment for 24 hours at 400°C; before and after a further heat treatment for 4 weeks at 80°C.

Surface Shear Stress p.s.i.	Damping Capacity (%)	After a further 4 weeks at 80°C. Damping Capacity (%)
1000	15.6	13.7
2000	22.0	17.0
3000	26.7	20.0
4000	29.9	23.1
5000	33.7	24.6

TABLE 7.

Stress-dependence of the damping capacity of Alloy T20 (85%Mn-14%Ni-1%C) which has been rolled, water quenched and given an ageing heat treatment of 24 hours at 550°C.

Surface Shear Stress p.s.i.	Damping Capacity (%)
1000	2
2000	3
3000	4
4000	4.5
5000	5

REFERENCES.

1 Metallurgy Of The Rarer Metals-3,Manganese.
Editor A.F. Sully (1955) Butterworths.

2 A.E. Schwaneke and J.W. Jensen, J. Apply.Physics (1962), 33, 310S.

3 D. Birchon, D.E. Bromley and D. Healey, Metal Science J. (1968) 2.

4 J.A. Hedley, ibid p.129.

5 E.P. Butler and P.M. Kelly, Trans.Met.Soc. AIME (1968) 242, p.2105.

6 R.S. Dean, J.R. Long, T.R. Graham, E.V. Potter and E.T. Hayes. Trans.Amer.Soc.Metals (1945) 34, p.443.

7 E.M. Sokolovskaya, A.T. Grigorev and E.M. Smirnova, Russian J. Inorg.Chem. (1962) 7, p.1370.

8 R.J. Goodwin, Internal report (1966) Manganese Bronze Group Research (Ipswich).

9 Z.S. Basinski and J.W. Christian, J. Inst. of Metals (1951-1952) 80, p.659.

10 J.W. Jensen and D.F. Walsh, U.S. Bureau of Mines Bulletin, (1965), 624.

11 D. Meneghetti and S.S.Sidhu, Phys.Rev.(1957) 1, p.105.

12 G.E. Bacon, I.W. Dunmur, J.H. Smith and R. Street, Proc. Roy. Soc. (1957) 241, p.233.

13 R. Street, J. Appl. Physics (1960) 31, 310S.

14 L. Guttman, J. Metals (1950) Trans. AIME 188, p.1472.

15 J.S.Bowles, C.S.Barrett and L. Guttman, ibid p.1478.

16 M.W. Burkart and T.A. Read, J. Metals (1953) Trans.AIME p.1516.

17 Z.S. Basinski and J.W. Christian, Acta Met. (1954) 2, p.101.

18 Ibid, p.148.

19 A.S. Nowick, Progress in Metal Physics, Vol.4. Editor B.Chalmers (1953) Pergammon Press.

20 A. Granato and K. Lücke, J.Appl.Physics (1956) 27, 583.

21 G. Sumner and K.M. Entwhistle, J.Iron and Steel Inst. (1959) 192, p.238.

22 K.M. Entwhistle, The Physical Examination of Metals, Editors B.Chalmers and A.G. Quarrel (1960) Edward Arnold.

23 A.F. Siefert and F.T. Worrell, J.Appl.Physics (1951) 22, p.1257.

24 L.E. McCrary and B.A. Rogers, Metall.(1962) 16, p.1074.

25 B.W. Roberts, Acta Met.(1954) 2, p.597.

26 P.S. Rudman and B.L. Averbach, Acta Met.(1957) 5, 65.

27 V. Krasevec, P.Delavignette, S.Amelinckx. Mat.Res.Bulletin (1967) 2, p.775.

28 D.M. Jones and E.A. Owen, Proc.Phys.Soc. (1954) 67,4 p.297.

29 L.E. Tanner. Physica Status Solidi, (1968) 30.

30 R.W. James The optical principles of the diffraction of X-rays (1948) G. Bell and Sons.

31 R.J. Goodwin, Metal Science J. (1968) 2, p.121.

32 J.T. Norton, Trans.Amer.Inst.Min.Met.Eng. (1940) 137, p.49

33 E.P. Butler and P.M. Kelly, Sixth International Congress For Electron Microscopy, Kyoto (1966).

34 R. Gevers, P. Delavignette, H. Blank, J.Van Landuyt and S. Amelinckx, Physica Status Solidi (1964) 4, p.383

35 R. Gevers, P. Delavignette, H. Blank and S Amelinckx. Ibid. (1964) 5, p.595.

36 G. Remaut, R. Gevers, A. Lagasse and S. Amelinckx, Ibid (1965) 10, p.121.

37 R. Gevers, J. Van Landuyt and S. Amelinckx, Ibid (1965) 11,p.689.

38 G. Remaut, Ibid (1966) 13,p.125.

39 G. Kurdjumov and G. Sachs, Z.Physik (1930) 64, p.325.

40 L.E. Tanner, Phil. Mag. (1966) 14, p.111.

41 L.D. Ellsworth and F.C. Blake, J.Appl.Physics (1944) 15, p.507.

42 H.Blank and S.Amelinckx, Appl.Phys.Letters (1963) 2, p.236.

43 G. Remaut, A. Lagasse and S. Amelinckx, Phys.Stat.Sol.(1964) 7, p.497.

44 G. Remaut, P. Delavignette, A. Lagasse and S. Amelinckx, Phys.Stat.Sol (1965) 11, p.329.

45 R.E.Villagrana and G. Thomas, Phys.Stat.Sol.(1965) 9.p.499.

46 B.W. Batterman and C.S.Barrett, Phys.Rev.Letters (1964) 13, p.390.

47 H.W. King, F.H. Cocks and J.T.A. Pollock, Phys.Rev.Letters (1967) 24,p.315.

48 H.P. Klug and L.E. Alexander, X-Ray Diffraction Procedures (1962) John Wiley.

49 D. Birchon, Discussion,Physical Metallurgy of Alloys of High Damping Capacity, J.Inst.Metals 93,(1965) 546.

50 G.E. Bacon and N. Cowlam, J.Phys.C (1970) 3, p.675.

51 J.H.Smith and E.R. Vance, J.Applied Physics (1969) 40, p.4853.

52 J.H.Smith and E.R. Vance, J. Phys.C (1969) 2, 761.

53 E.R. Vance, J.H. Smith and T.M. Sabine, J.Phys.C (1970) No.1, 35S.

54 P.B. Hirsch, A. Howie, R.B. Nicholson, D.W. Pashley and M.J. Whelan, Electron Microscopy of Thin Crystals (1965) Butterworths.

55 L.E. Tanner. Communication to the author.

56 J.M. Cowley, Phys Rev.Letters (1950)77, p.669.

57 J.M. Cowley, J.Appl.Phys. (1950) 21, p.24.

58 J.M. Cowley, Phys.Rev.Letters (1960) 120, p.1048.

59 J. Crangle, Metallurgical Reviews (1962) 7, p.133.

60 C.G. Shull and M.K. Wilkinson, Reviews of Modern Physics (1953) 25.

61 G.E. Bacon, Acta Cryst. (1961) 14, p.823.

62 W.C. Koehler and R.M. Moon, Phys.Rev.(1966) No.2, 151.

63 L.M. Corliss, J.M. Hastings and R.J. Weiss, Phys.Rev.Letters (1959) 3, p.211.

64 A.W. Overhauser and A.Arnott, Phys.Rev.Letters (1960) No.5, 4.

65 E.W. Lee and M.A. Asgar, Phys.Rev.Letters (1969) 22, p.1436.

66 M. Shah, Phys.Rev. Letters (1969) No.9, 29.

67 E. Fawcett, Phys.Rev.Letters (1970) No.2, 32A, p.117.

68 R. Street. J. Appl. Physics (1960) 31, p.310S.

69 R. Street, Phil. Mag. (1956), 1, p.663.

70 M.J. Klein, J. Appl.Physics (1967), 38, p.819.

71 M.E. de Morton, Phys. Rev. Letters (1963) 10, p.208

72 R. Street, Phys. Rev. Letters (1963) 10, p.210.

73 M.J. Klein, A.H. Clauer, R.E. Maringer, J.Appl.Physics (1964) 35, p.1994.

74 B.C. Munday, A.R. Pepper, R.Street, Proceedings of the International Conference on Magnetism (1964) Inst. of Phys. and Phys. Soc, p.201.

75 A.E. Austin, E. Adelson, W.H. Cloud, J.Appl.Phys (1962) 33, p.1356.

76 J.H.Smith and P. Gaunt, Acta Met. (1961) 9, p.819.

77 G.E. Bacon, Proc. Phys.Soc. (1962) 79, 938.

78 A. Herpin, P. Meriel and A.J.P. Meyer, Compt.Rend.(1958), 246, p.3170.

79 A.J.P. Meyer and M.J. Besnus, Compt.Rend. (1961) 253, p.2651.

80 T. Ohoyama, J. Phys. Soc. Japan (1961) 16, p.1995.

81 J.S. Kasper and J.S. Kouvel, J. Phys. Chem. Solids (1959) 11, p.231.

82 E. Kren, E. Nagy, I Nagy, L. Pal and P. Szabo, J. Phys. Chem. Solids (1968) 29, p.101.

83 E. Raub and W. Mahler, Z. Metallk. (1954) 45, p.430.

84 J.S. Kouvel,C.C. Hartelius and L.M. Osika, J. Appl.Phys. (1963) 34, p.1095.

85 R. Lindsay, Phy.Rev.Letters (1951) 84, p.569.

86 J.M. Hastings, N. Elliott and L.M. Corliss, Phys.Rev.Letters (1959) 13, p.115.

87 K. Yasukochi, K. Kanematsu and T. Ohoyama, J. Phys.Soc. Japan (1961) 16, p.1123.

88 J.S. Kouvel and C.C. Hartelius, Phys.Rev.Letters (1961) 123,p.124.

89 E. Uchida, H. Kondoh and N. Fuknoka, J.Phys. Soc. Japan (1956) 11, p.27.

90 J.M. Hastings, N. Elliott and L.M. Corliss, Phys.Rev.Letters (1959) 13, p.115.

91 Y. Ishikawa and Y. Endoh. J. Phys. Soc. Japan (1967) 23, p.205.

92 C. Kimball, W.D. Gerber and A. Arrott, J. Appl. Physics (1963) 34, p.1046.

93 J.S. Kouvel and J.S. Kasper, J. Phys.Chem.Solids (1963) 24, p.529.

94 U. Zwicker, Z.Metallk. (1951) 42, p.246.

95 U. Zwicker, Z.Metallk. (1951) 42, p.331.

96 W.R. Patterson, Trans. Met. Soc. AIME (1965) 233, p.438.

97 M.P. Ravdel, G.A. Faivilevich, Phys. of Metals and Metallography (1961) 11, p.121.

98 Hansen, Constitution of Binary Alloys (1958) McGraw Hill.

99 Elliott,Constitution of Binary Alloys (1965) NcGraw Hill.

100 T.J. Hicks, A.R. Pepper and J.H.Smith, J. Phys. C (1968) 1, p.1683.

101 H. Uchishiba, T. Hori and Y. Nakagawa, J. Phys. Soc. Japan (1970) 28, p.792.

102 A.W.O.Webb and N. Bailey, Patent Specification 984, 870.

103 T.R. Graham, J.R. Long, C.E.Armantrout and A.H. Robertson, Trans.Amer.Inst.Min.Met.Eng. (1949) 185, p.675.

104 D. Birchon, Private Communication.

105 P. Makhurane and P.Gaunt, J. Phys.C (1969) 2, p.959.

ACKNOWLEDGEMENTS.

The author considers himself fortunate in having been able to discuss the work on Mn-Cu alloys with a number of leading metallurgists in the United Kingdom. In particular, thanks are due to Professor P.L. Pratt and Dr. I. Jenkins who have acted as supervisors, Professor G.E. Bacon and Dr. J. Crangle who kindly organised the experimental neutron diffraction work, Dr. K.D. Leaver for patiently explaining the theory of antiferromagnetism and Professors K.M. Entwhistle and R.B. Nicholson for useful discussions.

The author would like to gratefully acknowledge the assistance of a number of technical support staff, especially Messrs. M.A. Knights, R. Saunders, R. Bridgeman, M. Gale and P. King. Thanks are due to colleagues at Delta Metal Research for many useful discussions throughout the work and also many helpful suggestions and constructive criticism were offered by the staff at the Admiralty Materials Laboratory in the latter half of the programme.

Permission to submit this thesis has kindly been given by the Ministry of Defence (Navy) and the Directors of the Delta Metal Co. Ltd.

Finally special thanks are due to Miss J. Hartwell for drawing the line diagrams, Miss G. Williams for printing the photographs and Mrs. J.A. Hedley for typing the thesis in draft and final forms.